

Entrainment of the mammalian circadian clock by metabolism in the liver: a quantitative mathematical model



**Université
de Lille**

Aurore Woller

Université de Lille

Supervisors:

Bart Staels and Marc Lefranc

September 2016

“Sleep my little baby-oh
Sleep until you waken
When you wake you’ll see the world
If I’m not mistaken,

Kiss a lover
Dance a measure,
Find your name
And buried treasure,

Face your life
Its pain,
Its pleasure,
Leave no path untaken.”

Neil Gaiman, The Graveyard Book

Acknowledgements

First at all, I would like to thank my two supervisors, Marc Lefranc and Bart Staels for welcoming me in their lab and for allowing me to do a PhD on such an interesting topic. I am also grateful to H  l  ne Duez, in particular because she has brought to my attention many important experimental results. We have come a long and quite complicated way altogether but finally, something nice arose from our efforts and our numerous and engaging brainstorming sessions!

I would also like to acknowledge Benjamin Pfeuty and Quentin Thommen for their emotional support and for their valuable advice as well as Christophe Szwaj for kindly sharing his office with me. Thanks to Bruno, Eric, Nunzia and Denis for the pleasant lunchtimes.

Furthermore, I am thankful for the kindness of Didier Gonze and Odile Viltart's follow-up of my project. Moreover, I am very grateful to my current colleagues for their encouragements and the nice atmosphere of the lab. Last but not least, all this would not have been possible without the great people who surround me day by day.

Abstract

To anticipate daily changes in their environment, most living organisms have evolved a circadian clock, which is synchronized to the diurnal cycle and orchestrates numerous biological functions. At organismal level, daylight is the main signal driving the clock. In multicellular organisms, however, clocks in peripheral organs respond to other cues. For example, the liver clock is primarily synchronized by fasting/feeding cycles and variations in the cellular metabolic state, as reflected by the NAD⁺/NADH and ATP/AMP ratios. To better understand the entrainment of peripheral circadian clocks by metabolic cycles, we have constructed a mathematical model of the mammalian circadian clock incorporating the metabolic sensors SIRT1 and AMPK. This model reproduces accurately experimental clock gene expression data from mouse liver in vivo and predicts correctly the effect of SIRT1 or AMPK loss-of-function. We used our mathematical model to investigate the response of the liver clock to various temporal patterns of AMPK activation, mimicking the effect of a normal diet, of fasting and of a high-fat diet feeding. Our results predict significant changes in clock gene expression and NAD⁺ time profiles between these situations. They suggest that the night peak in NAD⁺ level is due to circadian rhythms in NAMPT expression, while the day peak results from transient AMPK activation. Finally, we find that the loss of amplitude in expression rhythms observed when AMPK is depressed may be pharmacologically rescued using a timed REV-ERB agonist administration, suggesting strategies to fight against high fat diet-induced obesity.

Table of contents

List of figures	xiii
List of tables	xxiii
1 Introduction	1
2 Interplay between the circadian clock and metabolism: important reminders	5
2.1 Biological rhythms	5
2.1.1 Rhythms arise on many time-scales in living systems	5
2.2 Circadian clocks	8
2.2.1 Fundamental properties of circadian systems	8
2.2.1.1 Circadian oscillations are self-sustained rhythms that can be entrained by external periodic cues	8
2.2.1.2 Temperature compensation	9
2.2.2 Circadian clocks allow fitness to changing environments	12
2.2.3 Organisation of the mammalian clock	15
2.2.3.1 Circadian rhythms are generated by the SCN	15
2.2.3.2 Circadian oscillations are cell autonomous	15
2.2.3.2.1 Transcriptional and translational feedback loops	15
2.2.3.2.2 Post-transcriptional and post-translational modi- fications	20
2.2.3.3 Secondary clocks in peripheral tissues	22
2.2.3.3.1 Clock genes are rhythmically expressed in mul- tiple tissues	22
2.2.3.3.2 Circadian gene expression is largely tissue-specific	24
2.2.3.4 Entrainment properties of peripheral clocks	25
2.2.3.4.1 The SCN drives peripheral clocks through neuro- endocrine cues	25

2.2.3.4.2	Food is the dominant zeitgeber for peripheral clocks	29
2.3	Clock and metabolism	32
2.3.1	Evidences for the coupling between clock and metabolism	33
2.3.1.1	Nuclear receptors are implicated in both clock and metabolic pathways	33
2.3.1.2	Defects in the clock lead to metabolic disorders	37
2.3.1.3	Disturbed feeding-fasting cycles lead to altered clock gene expression	38
2.3.2	Interplay between clock and metabolic pathways at the tissue-level	42
2.3.2.1	Energy producing processes: Cellular respiration	42
2.3.2.2	Energy consuming processes: Storage processes and gluconeogenesis	49
2.3.2.2.1	Glucose storage and gluconeogenesis	49
2.3.2.2.2	Fat storage	52
2.3.2.3	The nutrient sensors and their interactions with the clock	54
2.3.2.3.1	AMPK	54
2.3.2.3.1.1	AMPK as a nutrient sensor	54
2.3.2.3.1.2	AMPK and the clock	58
2.3.2.3.2	Sirtuins	58
2.3.2.3.2.1	Sirtuins as nutrient sensors	58
2.3.2.3.2.2	SIRT1 and the clock	61
2.3.2.3.2.3	SIRT3 and the clock	64
2.3.2.3.3	Crosstalks between AMPK and SIRT1	68
2.3.2.3.3.1	AMPK increases NAD ⁺ levels, thereby enhancing SIRT1 activity	68
2.3.2.3.3.2	SIRT1 deacetylates LKB1	69
2.3.3	Interplay between clock and metabolism at the level of the whole organism	70
2.4	Chronotherapy	73
2.4.1	Generalities about chronotherapy	73
2.4.2	Rev-Erb agonists	74
3	Mathematical modelling in biology	79
3.1	Roles of modelling in the study of circadian clocks.	79
3.2	Steps of a mathematical modelling process	81

3.2.1	Construction of a mathematical model: case of the Goodwin model and of a related clock model	84
3.2.1.1	The Goodwin model	84
3.2.1.2	A toy model for the mammalian clock	87
3.2.2	Considerations about parameter estimation methods	90
4	A detailed model describing entrainment of the liver clock by metabolism	93
4.1	Construction of the mathematical model	93
4.1.1	Model for the core clock	94
4.1.1.1	Equations	94
4.1.2	Addition of the action of the nutrient sensors AMPK and SIRT1 on the clock	98
4.1.2.1	Incorporation of the Nampt-NAD ⁺ -SIRT1 loop	98
4.1.2.2	Incorporation of AMPK and its interactions with the clock	101
4.1.2.3	Incorporation of PGC1- α	102
4.1.3	Summary of the construction of our model	104
4.2	Parameter estimation	104
4.2.1	Choice of experimental data	104
4.2.2	Reproduction of expression time profiles from wild-type animals .	106
4.2.3	Reproduction of knockout phenotypes	108
4.3	Effect of perturbations of AMPK rhythms on the clock	109
4.4	Targeting the clock to rescue physiological expression profiles	110
4.4.1	Rescue of clock oscillations amplitude in <i>Cry1</i> mutants following a dampening in AMPK rhythm	110
4.4.2	Pharmacological rescue of physiological expression profiles after disruption of AMPK rhythm	112
4.5	Conclusion	117
5	Preliminary results and Perspectives	119
5.1	Preliminary results	119
5.1.1	Relative importance of the different feedback loops	119
5.2	Perspectives	121
5.2.1	Improvement of our present model	121
5.2.1.1	Include the circadian variations of PGC1 α mRNA	121
5.2.1.2	Represent the positive feedback loop between AMPK and SIRT1	123

5.2.1.3	Consideration of the effect of neuro-endocrine cues from SCN on the liver clock: Effect of glucocorticoid signalling	124
5.2.2	Build a global model connecting our model to major metabolic pathways	125
5.2.2.1	Model A: glycolytic model	125
5.2.2.2	Model B: modelling of the switch between glycolysis and fatty acid oxidation	126
5.2.2.3	Model C: addition of storage processes and gluconeogenesis	127
5.2.2.4	Model D: taking into consideration the control of the feeding-fasting cycle by the SCN	128
6	Supplementary Information	131
6.1	Kinetic Equations	131
6.2	Forcing Function	135
6.3	List of Parameters	138
7	Résumé en français	145
7.1	Introduction: couplage entre horloge circadienne et métabolisme	145
7.1.1	Horloge circadienne	145
7.1.2	Horloge et métabolisme	146
7.2	Résultats: modèle mathématique décrivant l'entraînement de l'horloge du foie par le métabolisme	147
7.2.1	Construction du modèle	148
7.2.2	Estimation de paramètres	150
7.2.3	Effet des perturbations du rythme d'AMPK sur l'horloge	152
7.2.4	Approche pharmacologique: rétablissement du bon fonctionnement de l'horloge par l'administration d'un agoniste de l'horloge	154
7.3	Conclusions	156
	References	161

List of figures

1.1	Aims of the present work in three steps: first, we will model the physiological state (left panel); then, we will model the switch between the physiological and a pathological state (panel in the middle); finally, the administration of a clock agonist will be modelled (right panel).	2
2.1	Non exhaustive list of important biological rhythms. The asterisk indicates rhythms that occur at the cellular level [46].	6
2.2	Frequency-encoded information transmission in the NF- κ B signalling pathway. Left panel: a negative feedback loop between NF- κ B its partner I κ B α is at the core of the this network (Left panel) and enables the onset of an oscillatory behaviour. Right panel: the temporal pattern of the external stimulation (oscillation, constant level) determines the kind of gene transcription program that is triggered ([79]	8
2.3	Schematic plot of the locomotor activity rhythm of a typical nocturnal rodent under LD and DD conditions. Upper panel: in LD conditions, the rhythm of locomotor activity is entrained to the period T of the zeitgeber. Lower panel: in constant darkness, the free-running period τ slightly exceeds T [49].	10
2.4	Schematic view of the components of a circadian system: A) an input (the zeitgeber) informs the internal clock about the external local time. The clock itself drives several physiological processes (outputs). B): this scheme can be more complex with the input directly modulating the output. The latter can possibly feed back to the clock or even to the input device. [49].	11
2.5	Examples of compensation of the period length in cyanobacteria: the period of the oscillations only slightly varies upon changes in the ratio ADP/ATP (A) or in the temperature (B) [82].	13

2.6	Cultures mixed with several cyanobacteria strains (middle column) are placed either under a 11:11 LD (left column) pattern or under a 15:15 LD pattern (right column). After 27 days, the strain whose free-running period is the closest to the period of the LD cycle wins [130].	14
2.7	Recording of the firing rate for two individual cultured neurons. Both profiles are circadian but some phase heterogeneity is observed between the two time profiles [169].	16
2.8	Comparison of <i>Drosophila</i> 's eclosion rhythms (A) and locomotor activity (B) for WT, short-period, long-period and arrhythmic animals [92].	17
2.9	Circadian levels of <i>Per</i> mRNA in LD conditions. Comparison between WT and mutant(short and long-period mutants) profiles [64].	18
2.10	Schematic view of the main feedback loop at the core of most circadian systems: an activator complex (called positive element here) activates the transcription of negative elements (repressors). The latter repress the activity of the positive elements, thereby shutting down there own transcription. The degradation of the repressor proteins lead to the de-repression of the action of the positive elements and a new cycle of transcription can start. [13]. . .	19
2.11	Mammalian main transcriptional feedback loops: the activator complex, CLOCK-BMAL1, activates the transcription of the genes <i>Per</i> , <i>Cry</i> , <i>Rev-Erbα</i> and <i>Rora</i> . On the one hand, the repressor complex PER-CRY periodically inhibits the action of the activator complex CLOCK-BMAL1. On the other hand, the nuclear receptor REV-ERB α inhibits the transcription of <i>Bmal1</i> while ROR α activates it [13].	21
2.12	Scheme showing the sequential events at the promotor of a clock controlled gene during a cycle [90].	21
2.13	Effect of clock gene mutation on behavioural rhythms [39].	22
2.14	A given clock component (here PER) can be regulated at the transcriptional, post-transcriptional and post-translational level. Yellow panel: at the transcriptional level, <i>Per</i> expression is regulated by CLOCK-BMAL1. Green Panel: at the post-translational level, the stability of PER is regulated by the kinase CKI. Red panel: post-transcriptional modifications are the third possible layer of control [25].	23
2.15	Levels of mPer1 (blue curves), mPer2 (red curves) and mPer3 (green curves) oscillate in several peripheral tissues [183].	25
2.16	Comparison of the percentage of oscillating transcripts in 12 tissues [180]. . .	26
2.17	List of the transcripts cycling both in the liver and in the SCN [131].	26

2.18	Comparison of clock gene expression for an active (with Dox) and an inactive (without Dox) liver clock: clock gene expression is reduced when the liver clock is switched off except for <i>Per2</i> mRNA . (Dox is the abbreviation for the tetracycline analog doxycycline that is used to activate the liver clock)) [94].	27
2.19	The SCN periodically stimulates the adrenal gland through both endocrine cues (CRH and ACTH) and neuronal projections (ANS). This leads to the periodic secretion of glucocorticoids. Abbreviations are as follows: PVN, paraventricular nucleus of hypothalamus; PIT, pituitary gland; CRH, corticotropin-releasing hormone; ACTH, adrenocorticotrophic hormone [160].	28
2.20	A shift from nighttime (dotted line) to daytime feeding (solid line) inverts the phase of clock gene expression in liver [28].	29
2.21	The phase inversion observed in clock gene expression after a switch from nighttime feeding to daytime feeding occurs with different kinetics according to the tissue, the phase inversion being the fastest in the liver: time profiles of <i>Dbp</i> expression in different tissues are shown for animals fed A) during the night, B) during the day for 6 days, C) during the day for 3 days. Daytime feeding (B) inverts the phase of <i>mDbp</i> expression compared to nighttime feeding(A) [28].	30
2.22	Time profiles of glucocorticoid levels in animals fed A) during the night, B) during the day for one week, C) during the day for 1-2 days [117].	31
2.23	The SCN influences oscillations in peripheral clocks by driving food intake, body temperature cycles as well as neuro-endocrine cues (including glucocorticoid signalling) [119].	32
2.24	Schema of the link between clock and metabolism: periodicity in food intake gives rise to alternation between energy-consuming and energy-producing metabolic processes. The consequence of this is daily variations in the ratios of AMP/ATP and NAD ⁺ /NADH. This goes with a periodic activation of the nutrient sensors AMPK and SIRT1 which relay informations about the cellular nutrient status to the clock.	34
2.25	The clock partitions internal metabolic processes to appropriate phase with respect to external environmental variations [10].	35
2.26	Circadian expression profiles of several nuclear receptors in different metabolic tissues. Abbreviations are as follows: BAT, brown adipose tissue; WAT, white adipose tissue [174].	36
2.27	Mutations in clock genes lead to metabolic disorders [111].	37

2.28	Comparison of the levels of circulating metabolic markers (left column) and hypothalamic neuropeptides (right column) for normal chow (solid lines) and high fat diet (dotted lines) feeding conditions [89].	39
2.29	Comparison of hepatic clock gene expression for NCD (black curves) and HFD (orange curves) feeding: HFD feeding modifies clock gene expression [36].	40
2.30	Schematic comparison of four feeding patterns: animals are either fed on a normal chow (NA and NT) or on a high fat diet (FA and FT). In both groups, food access is either ad libitum (NA and FA) or restricted in time (NT and FT) [71].	41
2.31	Comparison of hepatic clock gene expression for the 4 feeding patterns. A: FA (pink curves) dampens decreases clock gene expression while FT (red curves) restores physiological amplitudes. B: clock gene expression is similar for NA (light blue curves) and NT (dark blue curves) conditions [71].	41
2.32	Schematic view of catabolic reactions [123].	42
2.33	Time profiles of the metabolites AMP and NAD ⁺ [71]	43
2.34	Five first steps of glycolysis [100].	44
2.35	Five last steps of glycolysis [100].	45
2.36	Fates of pyruvate in aerobic and anaerobic conditions [100].	46
2.37	Schematic view of the main steps in the TCA cycle followed by the respiratory chain [123].	48
2.38	Time profiles of several glycolytic intermediates [71]	49
2.39	Steps of fatty acid oxidation [100].	50
2.40	Effect of glucagon injection at different times for fasted animals [179] . . .	52
2.41	Steps of gluconeogenesis [100].	53
2.42	Scheme of AMPK activation mechanism. Under stress conditions, low AMP levels activate AMPK. AMPK then switches off anabolic energy consuming pathways and restores catabolic ATP producing pathways. This increases ATP levels which inactivates AMPK [60].	55
2.43	Schematic view of AMPK regulation by adenine nucleotides [56].	56
2.44	AMP promotes AMPK activation through three mechanisms: it enhances the effect of LKB1-mediated phosphorylation (A and B), it inhibits AMPK dephosphorylation by phosphatases (C) and it also activates AMPK on its allosteric sites (D) [56].	56
2.45	Roles of AMPK in four major metabolic tissues [107].	57

2.46	Effect of AICAR administration on clock gene expression: AICAR injection increases clock gene expression (red curve). Limiting the glucose in the culture medium also increases clock gene expression (grey curve). These effects are lost in AMPK mutants [97].	59
2.47	Circadian rhythms in the localization and in the activity of AMPK: (A) The expression of the AMPK β 2 subunit is circadian. (B) The accumulation of the catalytic subunit AMPK α 1 in the nucleus exhibit a circadian profile [97]	59
2.48	The knockout of the kinase LKB1 decreases clock gene expression in the liver [97].	60
2.49	Four different pathways can lead to NAD ⁺ synthesis: NAD ⁺ can be synthesized from tryptophan, nicotinic acid (NA), nicotinamide riboside (NR) and from nicotinamide (NAM) [170].	61
2.50	Nampt gene expression profile is circadian (A) while the time profiles of NAMPT protein and NAD ⁺ levels are bimodal (B and C). Curves with filled circles: WT mice; curves with open circles: Clock Δ ¹⁹ mutant mice) [141].	62
2.51	Effect of clock mutations on <i>Nampt</i> mRNA (A) and NAD ⁺ (B) levels: a knockout of elements of the positive limb of the clock (<i>Bmal1</i> ^{-/-}) decreases <i>Nampt</i> expression and NAD ⁺ levels while a knockout of elements of the negative limb increases <i>Nampt</i> and NAD ⁺ levels [141].	63
2.52	Sirt1 expression is constant (A) while the activity of SIRT1 protein is circadian (B) [124].	64
2.53	Clock gene expression (A) and NAD ⁺ levels (B) are increased in liver-specific <i>Sirt1</i> ^{Δex^{e4}} mice. [14].	65
2.54	SIRT1 knockdown decreases clock gene expression in MEFs with the exception of Rev-Erb α expression [7].	65
2.55	The expression of PGC1- α as well as those of its partners PGC1- β and PRC is circadian in the liver (A) and in the skeletal muscle (B). The accumulation of the proteins PGC1- α and PGC1- β is also rhythmic in liver nuclear extracts (C) [105].	66
2.56	PGC1- α activates <i>Bmal1</i> transcription in synergy with ROR- α [105].	66
2.57	In the liver, a knockdown of PGC1- α disturbs clock gene expression. WT mice: filled boxes. Pgc1- α null mice: empty boxes [105].	67
2.58	Summary of the different actions of SIRT1 on the clock: SIRT1 deacetylates BMAL1, PER2 and PGC1- α . Adapted from [8].	67

2.59	Schematic view of the sequential activation of the transcription factor PGC1- α : it is first phosphorylated by AMPK and then deacetylated by SIRT1 [22].	69
2.60	Our hypothesis to explain the bimodal profile in both NAMPT protein and NAD ⁺ levels: the peak around ZT14 is driven by the clock while the peak around ZT5 is due to the action of AMPK on NAMPT protein.	70
2.61	SIRT1-mediated activation of LKB1: SIRT1 deacetylates (A) and activates (B) LKB1 leading to the phosphorylation of LKB1 downstream targets (C). Conversely, SIRT1 inactivation or down-regulation decreases its activity [99].	71
2.62	Comparison of LKB1 activity in fed and fasted state in rats liver: in fasting conditions, LKB1 is deacetylated (A) and its consequent activation (B) promotes the phosphorylation of its targets (C) [99].	71
2.63	Schematic view of the SIRT1-mediated activation of LKB1 [99].	72
2.64	Most of the best sold drugs target target several cycling transcripts [180]. . .	74
2.65	Both REV-ERBs agonists SR9011 and SR9009 decrease <i>Bmal1</i> transcription in a dose dependent way [152].	75
2.66	Effect of agonist administration on locomotor activity and clock gene expression: In DD, agonist injection alters both locomotor activity (B) and clock gene expression (D) in SCN in DD but have less effect in LD (A and C) [152].	76
2.67	Agonist injection modifies the expression of clock genes (A) and metabolic genes (B) in liver [152].	76
2.68	Phase response curve for the injection of a REV-ERBa agonist: depending on the injection time, <i>Per2</i> expression peak can either be delayed (A) or advanced (B) [115].	77
3.1	Roles of mathematical modelling of biological systems [51].	81
3.2	Steps of the modelling process: after having summarized the data from the literature in order to obtain a global view of the interaction network (1), one can build the mathematical model based on this network (2). Once the model fits to experimental data profiles (3), the analysis of the dynamical properties of the system can begin (4). When the model is able to reproduce a reasonable number of experimentally observed phenotypes, it is can be used to make predictions and to design new experiments (5).	83
3.3	Scheme of the Goodwin model: the mRNA X is translated into the protein Y, that activates the repressor protein Z. Z inhibits the transcription of X. . . .	87

3.4	Dynamical behaviour of the Goodwin oscillator as a function of the kinetic parameter k_1 and n : the blue curve separates the steady state regime from the oscillator regime. The 3 bottom panels show the time series corresponding to point A, B, and C in the upper panel. When the value of Hill coefficient is lower or equal to 8, oscillations dampen out and finally reach a steady state (A and B).	88
3.5	Scheme of the successive steps for the construction of my toy model for the mammalian clock.	89
3.6	Agreement between experimental points (dotted lines) and simulation results (solid lines) for <i>Cry1</i> , <i>Bmal1</i> and <i>Rev-Erba</i> mRNA levels.	90
3.7	Main steps of a genetic algorithm. Each element of the population corresponds to a parameter set whose score function is evaluated. Each set is then replicated and slightly modified (mutated). Finally, the sets whose score function is the lowest will survive while the other die. A new cycle of evaluation can then start.	91
4.1	Scheme of our core clock model.	95
4.2	In vitro deacetylase activity of recombinant SIRT3 with acetylated SIRT3-selective target peptide in the presence of increasing concentrations of NAD ⁺ [133].	99
4.3	Scheme of the interactions of the NAD salvage pathway and SIRT1 with the clock.	102
4.4	Scheme of the interactions of AMPK with the clock and the NAD salvage pathway.	103
4.5	Scheme of the mathematical model coupling circadian clock to metabolism.	105
4.6	Time profiles for the mRNAs (left panel) and proteins (right panel) considered in our model.	105
4.7	Expression time profiles of the main clock actors obtained in mouse liver are accurately reproduced.	107
4.8	Our model reproduces the bimodal time profiles for AMPK, NAD ⁺ and NAMPT.	108
4.9	SIRT1 and AMPK loss-of-function phenotypes are qualitatively reproduced.	109
4.10	Fed state: effect of a dampening in AMPK activity (red curves) compared to a rhythmic activity of the nutrient sensor (blue curves) on clock gene expression.	111
4.11	Fasted state: effect of a high AMPK activity (green curves) compared to a rhythmic activity of the nutrient sensor (blue curves) on clock gene expression.	111

4.12	Rescue of clock oscillations amplitude in Cry1 mutants following a dampening in AMPK rhythm.	112
4.13	Rescue of oscillations in the Nampt (top) and Rev-Erb (bottom) expression profiles of cells subjected to dampened AMPK rhythms, using a REV-ERB agonist. In the A panel, the agonist pulse (top inset) is optimally timed around ZT 13.7, leading to restored profiles, unlike when the agonist pulse is shifted by 12 hours (B panel). The profiles corresponding to treated (resp., non treated) cells are shown in orange and red, respectively, and compared to those corresponding to WT cells under normal AMPK rhythms (dashed blue).	113
4.14	Effect of a Rev-Erb agonist treatment delivered at three different times of the day to cells subjected to dampened AMPK rhythms. The Nampt, NAMPT protein, and NAD ⁺ profiles corresponding to treated (resp., non treated) cells are shown in orange and red, respectively, and compared to those corresponding to WT cells under normal AMPK rhythms (blue). The optimal timing is shown in the middle column	114
4.15	Effect of a Rev-Erb agonist treatment delivered at three different times of the day to cells subjected to dampened AMPK rhythms. The Per, Cry, and Dbp profiles corresponding to treated (resp., non treated) cells are shown in orange and red, respectively, and compared to those corresponding to WT cells under normal AMPK rhythms (blue). The optimal timing is shown in the middle column.	115
4.16	Effect of a Rev-Erb agonist treatment delivered at three different times of the day to cells subjected to dampened AMPK rhythms. The Rev, Ror, and Bmal1 profiles corresponding to treated (resp., non treated) cells are shown in orange and red, respectively, and compared to those corresponding to WT cells under normal AMPK rhythms (blue). The optimal timing is shown in the middle column.	116
5.1	Illustration of the different interactions of AMPK with the clock that I have removed one by one.	120
5.2	Rev-Erb expression levels in WT (blue curves) and when the different interaction between AMPK and the clock are removed one by one (red curves).	121
5.3	Illustration of some possible improvement of our present model: (A) Addition of a positive feedback loop enabling oscillation in Pgc1 α mRNA. (B) Addition of a positive feedback loop between SIRT1 and AMPK	123

5.4	Metabolic (A) and temperature (B) compensation in cyanobacteria: the period of the oscillations only slightly varies upon changes in the ratio ADP/ATP or in the temperature [82].	124
5.5	Schema of an early metabolic model describing the glycolysis, the Krebs cycle and the electron transport chain [126].	126
5.6	Schema of Connection between our initial model and the metabolic model B	127
5.7	Schema of the interactions between circadian and metabolic networks in the whole body.	129
6.1	Structure of the pulse and meaning of the pulse parameters t_c , T_d , and T_w . A pulse function is shown in blue, which is essentially obtained as the difference between the two step functions shown in red, modified to be 24h-periodic.	137
7.1	Notre hypothèse pour expliquer le profil bimodal des niveaux de protéine NAMPT et de NAD ⁺ : le pic autour de ZT14 est sous le contrôle de l'horloge alors que le pic autour de ZT5 est causé par l'action de l'AMPK sur la protéine NAMPT. Données expérimentales de [141].	147
7.2	Le but du présent travail en trois étapes : d'abord nous allons modéliser l'entraînement de l'horloge par la nourriture en conditions physiologiques (panneau de gauche); ensuite, nous allons modéliser la transition entre un état physiologique et un état pathologique (panneau au centre); enfin, nous allons modéliser l'administration d'un agoniste de l'horloge (panneau de droite).	149
7.3	Schéma du modèle mathématique décrivant le couplage entre l'horloge et métabolisme.	151
7.4	Profils temporels pour les ARNm (panneau de gauche) et les protéines (panneau de droite) prises en compte dans notre modèle.	151
7.5	Les profils temporels décrivant l'expression des principaux gènes de l'horloge (phénotype sauvage) sont reproduits fidèlement.	152
7.6	Notre modèle reproduit fidèlement les profils bimodaux de l'AMPK, de NAD ⁺ et de NAMPT.	153
7.7	L'effet sur l'expression des gènes d'horloge d'une perte de fonction de SIRT1 (panneaux du haut) et de l'AMPK (panneaux du bas) est reproduit qualitativement.	153
7.8	État "rassasié": Effet sur l'expression des gènes d'horloge d'un amortissement de l'activité de l'AMPK (courbes en rouge) comparé à une activité rythmique normale du senseur nutritionnel (courbes en bleu).	155

-
- 7.9 État de jeûne: effet sur l'expression des gènes d'horloge d'une forte activité de l'AMPK (courbes en vert) comparé à une activité rythmique normale du senseur nutritionnel (courbes en bleu). 155
- 7.10 Rétablissement de l'amplitude des oscillations des gènes d'horloge (*Nampt*, *Per* et *Dbp*) pour des mutants *Cry* après un amortissement du rythme d'activité de l'AMPK (courbes oranges). Comparaison avec des cellules non mutantes soumises à un rythme d'AMPK normal (courbes bleues) ou amorti (courbes rouges). 156
- 7.11 Effet d'un traitement consistant à administrer un agoniste REV-ERB à trois moments différents de la journée pour des cellules avec un rythme d'AMPK amorti. Les profils de *Nampt*, de la protéine NAMPT et de NAD⁺ sont affichés en rouge quand le traitement a été administré, en orange sans traitement, et en bleu pour des cellules soumises à un rythme d'AMPK normal. Le timing optimal est affiché de la colonne du milieu. 157
- 7.12 Effet d'un traitement consistant à administrer un agoniste REV-ERB à trois moments différents de la journée pour des cellules avec un rythme d'AMPK amorti. Les profils de *Per*, *Cry* et de *Dbp* sont affichés en rouge quand le traitement a été administré, en orange sans traitement, et en bleu pour des cellules soumises à un rythme d'AMPK normal. Le timing optimal est affiché de la colonne du milieu. 157
- 7.13 Effet d'un traitement consistant à administrer un agoniste REV-ERB à trois moments différents de la journée pour des cellules avec un rythme d'AMPK amorti. Les profils de *Rev-Erb*, de *Ror* et de *Bmal1* sont affichés en rouge quand le traitement a été administré, en orange sans traitement, et en bleu pour des cellules soumises à un rythme d'AMPK normal. Le timing optimal est affiché de la colonne du milieu. 158

List of tables

6.1	List of variables of the mathematical model (Part 1). The time evolution of the variable is specified either by an ordinary differential equation (ODE), by a function of other variables, or by an externally imposed profile.	131
6.2	List of variables of the mathematical model (Part 2). The time evolution of the variable is specified either by an ordinary differential equation (ODE), by a function of other variables, or by an externally imposed profile.	132
6.3	Physical meaning of the arguments of our functions	139
6.4	mRNA and protein degradation rates (15 parameters)	139
6.5	complexation kinetic rates (4 parameters)	139
6.6	maximal transcription rates (7 parameters)	140
6.7	activation ratios (7 parameters)	140
6.8	Regulation thresholds (15 parameters)	141
6.9	Hill coefficients (15 parameters)	141
6.10	Translation rates (6 parameters)	142
6.11	Protein stability modulation constants (4 parameters)	142
6.12	NAD kinetics, Sirt1 and PGC1a activity (11 parameters)	142
6.13	Pulse parameters (12 parameters)	143
6.14	Miscellaneous constants used to describe perturbations	143

Chapter 1

Introduction

Circadian rhythms are biological processes that oscillate with a period of about 24 hours. These rhythms are ubiquitous, endogenous and can be entrained to other periods by external periodic events (such as light-dark cycle and feeding-fasting cycles) [13]. The mammalian circadian system is composed of multiple clocks [119]: at the central level, the suprachiasmatic nucleus (SCN) of the hypothalamus acts as a master pacemaker for organisms and drives secondary clocks located in peripheral tissues such as the liver, heart, skeletal muscles,... The SCN is entrained by light while peripheral clocks are primarily entrained by food cues [28].

The mammalian circadian system regulates many physiological processes from the cell cycle, the kidney functions and the immune system to heart functions, energy metabolism, the sleep-wake cycle, hormone secretion and many others [144]. In particular, there is a reciprocal link between clock and metabolism [140]. Perturbations of this coupling have important pathological consequences. Indeed, on the one hand, disruption of the clock leads to metabolic disorders [111]. On the other hand, disruption of the feeding-fasting cycle correlates with altered clock gene expression and metabolic troubles [89], [71], [36]. However, many aspects of these interactions are still unclear.

Data with high time resolution are now available for the mammalian transcriptome, which allows to combine mathematical modelling and lab experiments [78]. In particular, mathematical modelling allows to test rapidly the effects of defects in the studied regulation network and to evaluate those of novel pharmacological strategies [51]. Several detailed models for the mammalian clock have been developed but so far, none of them has taken into account the reciprocal coupling with metabolism [101], [40], [11], [118], [142]. Our aim is to build a model describing this coupling in the liver and to explore several conditions: we first want to describe how the feeding-fasting cycle entrains the clock in physiological conditions (healthy state). Then, we would like to use the model to see how our system goes from a healthy state to a pathological state (characterized by altered clock gene expression) when the

feeding-fasting cycle is disrupted. The final aim is to use our model to see if/how a well-timed administration of some clock agonist can restore the disturbed rhythms (pharmacological action).

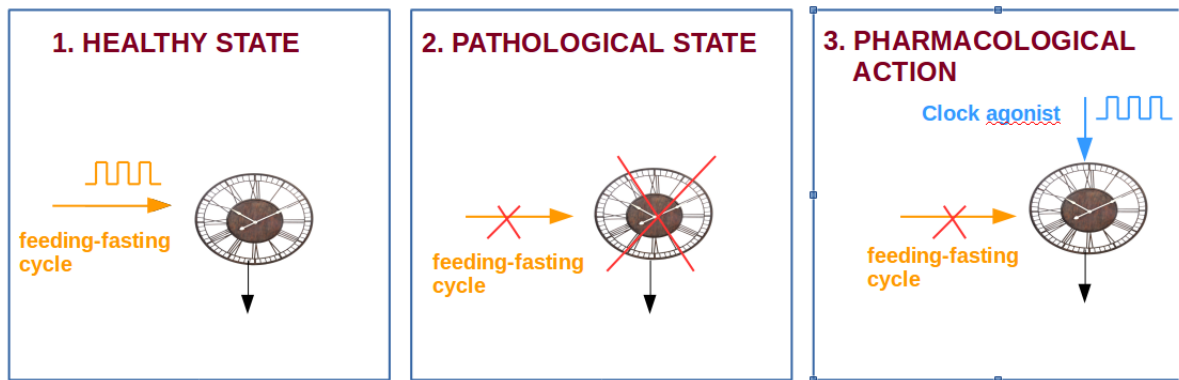


Fig. 1.1 Aims of the present work in three steps: first, we will model the physiological state (left panel); then, we will model the switch between the physiological and a pathological state (panel in the middle); finally, the administration of a clock agonist will be modelled (right panel).

The chapters are organized as follows: the first chapter summarises the data indicating a reciprocal link between clock and metabolism and highlights which aspects of this coupling are still poorly understood. It also presents the molecular knowledge that is needed to build the mathematical model. The next one presents the methods used in mathematical modelling. The third chapter describes our mathematical model. It is followed by an overview of the future developments of our model. This chapter also includes some preliminary results. The technical details (complete list of kinetic equations, parameter values,..) are described in the last chapter (supplementary information).

More specifically, the first chapter begins with a rapid overview of the three fundamental properties of circadian systems (self-sustained oscillations, entrainment and temperature compensation). I then focus on the mammalian circadian system whose pacemaker is located in the SCN. I recall that the cycling clock machinery is found not only in neurons of the SCN but also in many other cells throughout the body. This indicates the existence of local clocks in peripheral tissues. I then present experiments showing that many metabolic transcripts are cycling in these tissues and that food is the main zeitgeber for these clocks. This suggests that there are strong interactions between the core clock and metabolic pathways. The next section of the introduction is thus an overview of these interactions. First, I expose the evidences showing that the coupling between clock and metabolism is reciprocal. Then, I

describe how the alternation between energy-consuming and energy-producing metabolic pathways leads to daily variations in the metabolites AMP and NAD⁺ which periodically activate the nutrient sensors AMPK and SIRT1. I present the different interactions of these sensors with the clock and I also rapidly show how the clock can feed back on metabolic pathways. This introduction ends with a section emphasizing that the treatment of many diseases requires to take into account the timing of the drug administration.

The following chapter starts with an (non-exhaustive) overview of the roles and advantages of mathematical modelling in the field of circadian clocks. In the next section, I describe the steps that are generally followed by modellers to create and analyse a mathematical model. Then, in order to illustrate some important concepts of modelling in a simple way, I present an historical oscillator model: the Goodwin model.

The third chapter presents our mathematical model. First, I describe the construction of the model (hypothesis and equations). In the section about parameter estimation, I show that our model is able to reproduce experimental time profiles from normal and mutant mice. Our model is then used to see how disruption of the feeding-fasting cycles leads to altered clock gene expression. In the last section, I show how the well-timed administration of a clock agonist is able to rescue the clock.

This work is the result of a collaboration between physicists and biologist/pharmacist. Indeed, Marc Lefranc and myself are physicists and we did not know many things about metabolism before starting this work. Conversely, Bart Staels and Helene Duez are pharmacologists and biologists and their knowledge about mathematical modelling was quite limited. Therefore, I have tried to write this manuscript so that everyone can understand it irregardless of its background (modeller or experimenter). Accordingly, the first chapter will maybe seem relatively naive for biologists while the concepts exposed in the second Chapter could sound straightforward for modellers.

Chapter 2

Interplay between the circadian clock and metabolism: important reminders

2.1 Biological rhythms

Earth is a highly periodic environment. Indeed, Earth rotation around its axis and around the sun has important consequences including day-night alternations, succession of seasons and tidal movements. All these cyclic phenomena have a strong impact on life : some animals migrate; others hibernate while some marine species entirely adapted their metabolism to cope with tides. Human societies also have to cope with periodicity such seasonal variations in flu epidemics for example that strongly affects society's functioning. Rhythmicity is thus present in almost every aspects of life! Let's just think about heart beating, respiration, ovulation, about the cell cycle and sleep-wake cycles to name just a few. The next section constitutes a general overview of the main biological rhythms, about their roles and about some mechanisms that generate them.

2.1.1 Rhythms arise on many time-scales in living systems

Rhythmic processes are found in many species and can also appear on many time-scales with periods ranging from seconds to years (see Fig. 2.1) [46]. Circadian rhythms are among the most ubiquitous rhythms. Indeed, these 24-hour rhythms are found in eukaryotes as well as in bacteria. They control many physiological processes and will be the subject of this work. Rhythms with a period smaller than 24 h are called ultradian while rhythms with a period above 24 h are called infradian. Infradian rhythms include ovulation rhythms, reproduction rhythms, migration, hibernation, plant flowering rhythms,... But many rhythms are ultradian with periods from a fraction to several hours. For example, electrical rhythms such as neural

and cardiac rhythms have a small period from a fraction of to a few seconds. The period of cytosolic calcium oscillations ranges from seconds to minutes. Rhythm in the transport of the transcription factor Msn2 in and out the nucleus occur with a period of 6 min [80]. A segmentation clock has been shown to control somitogenesis. Its period is about 90 min [48]. The transcription factor NF- κ B, involved in the inflammatory response, can oscillate with a period of several hours, as well as the tumour suppressor p53 [103], [75]. Hormonal secretion can also be pulsatile with periods ranging from several minutes to 24 h when the process is controlled by the circadian clock [87] [48].



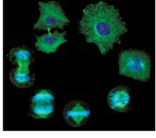
RHYTHM	PERIOD	
Neuronal rhythms *	0.01 to 10 s (and more?)	
Cardiac rhythms *	1 s	
Calcium oscillations *	1 s to several minutes	
Biochemical oscillations *	1 to 20 min	
Mitotic cycle *	10 min to 24h (or more)	
Hormonal rhythms *	10 min to several hours (also 24h)	
Circadian rhythms *	24 h	
Ovarian cycle	28 days (for humans)	
Annual rhythms	1 year	
Epidemiological and ecological oscillations	Years	

Fig. 2.1 Non exhaustive list of important biological rhythms. The asterisk indicates rhythms that occur at the cellular level [46].

All these examples of oscillatory behaviours may seem paradoxical. Indeed, the Second Law of thermodynamics tells us that the entropy of an isolated system can only increase [72]. That means that disorder will always increase and that the system will evolve to an equilibrium steady state. So, how is it possible for living systems to be highly organized in space and time? Indeed, oscillations are a form of temporal organization. This is because living systems such as cells for example, are not isolated systems. They are open systems that take energy from their environment to stay far away from the thermodynamical equilibrium. This has first been highlighted by Prigogine and his work about dissipative structures in the seventies [128]. Even open systems normally evolve to a stable steady state in course of time. But Prigogine and his co-workers have shown that this steady state can become unstable when the system evolve far from equilibrium and when it is nonlinear enough. It is what happens for living systems. Regulation of gene expression, nuclear-cytoplasmic transport as well as regulation of the activity of receptors, enzymes or ion channels associated with feedback mechanisms and/ or cooperativity give rise to instabilities and subsequent periodic behaviours [47]. In particular, it has been shown that the presence of a negative

feedback loop in a biochemical system is a necessary condition to generate self-sustained oscillations.

Indeed, most of the above mentioned cellular rhythms rely on a negative feedback loop. Interestingly, an oscillatory dynamics can have different functional roles. One of these roles is to enable frequency-encoded information transmission [48]: the temporal pattern of an input signal (high or low frequency pulses, constant level) determines which cellular response is triggered (see Fig. 2.2). The frequency encoded transmission is quite common and occurs inter alia in the case of calcium oscillations or p53 oscillations as well as in the NF- κ B pathway [48]. Frequency-encoded information transmission in the NF- κ B signalling pathway is described here for the sake of example. Ultradian oscillations have been observed in the activity of NF- κ B in the nucleus and these can be explained by a negative feedback loop between NF- κ B and its partner I κ B α [75]. Indeed, under unstimulated conditions, the binding between NF- κ B and I κ B α sequesters NF- κ B in the cytoplasm. Then, a stimulation of the cell by the tumour necrosis factor (TNF α) triggers a signalling cascade that activates the I κ B kinase (IKK). The latter promotes then the degradation of I κ B α . This enables NF- κ B to enter the nucleus where it activates the transcription of genes involved in the innate inflammatory response. Among them, I κ B α which sequesters once again NF- κ B in the cytoplasm which creates a negative feedback loop enabling an oscillatory behaviour [75]. Single-cell experiments have shown that the pattern (high frequency, low frequency or constant level) of the stimulation by an external signal (TNF α or LPS) results in a given dynamics of NF- κ B nuclear entry which determines the set of target genes that are activated [6], [158].

Frequency-encoded information transmission is not the only possible functional role of cellular oscillations. Indeed, in other biological rhythms such as circadian rhythms, the frequency is stable and an important functional role of circadian clocks seems to be to keep internal physiological processes in synchrony with the external periodic environment [132], [10]. As we will see just below, this is notably enabled by the three fundamental properties of circadian systems: these rhythms are endogenous (relying on a negative transcriptional feedback loop) but are entrainable by external periodic signals and their period is robust against temperature fluctuations [136]. From now on, we will only focus on the study of these fascinating clocks !

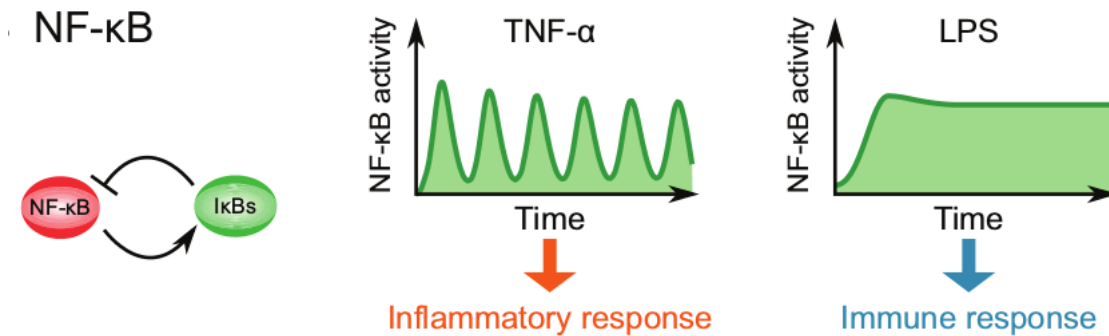


Fig. 2.2 Frequency-encoded information transmission in the NF- κ B signalling pathway. Left panel: a negative feedback loop between NF- κ B its partner I κ B α is at the core of this network (Left panel) and enables the onset of an oscillatory behaviour. Right panel: the temporal pattern of the external stimulation (oscillation, constant level) determines the kind of gene transcription program that is triggered ([79]).

2.2 Circadian clocks

2.2.1 Fundamental properties of circadian systems

2.2.1.1 Circadian oscillations are self-sustained rhythms that can be entrained by external periodic cues

The term circadian comes from the Latin, *circa* (around) and *diem* (a day). Circadian rhythms are thus rhythms with a period of approximately 24 h. The most obvious circadian rhythms are the sleep-wake cycles [70]. Locomotor activity is also an overt circadian rhythm for many animals, from *Drosophila* to rodents. Circadian rhythms were first observed in plants, many centuries ago. Indeed, in the middle of the eighteenth century, the french scientist de Mairan observed daily rhythms in the leaf movements of the plant *mimosa* [49]. He noticed that these daily leaf movements still persisted under constant darkness. In the first part of the twentieth century, researchers studied the locomotor activity of rodents [49]. Typically, animals were placed in a running wheel and their activity was recorded on an actogram. In natural conditions, that is under day-night alternation, animals display rhythmic activities of exactly 24 h. As for plant leaf movements, rhythms in animal locomotor activity persist under constant conditions Nevertheless, their period is slightly different from 24h. These rhythms are thus endogenous: they are generated by internal mechanisms with a free-running period that is close to 24 h (see Fig. 2.3) [49]. The exact duration of the free-running period depends on species and there is even some variability between “individuals” of the same species [146]. Furthermore, the free-running period is not totally the same in DD (constant darkness) and LL (constant light) conditions. Thus, these studies have highlighted two of the fundamental

properties of circadian rhythms [136]: they are self-sustained with a free-running period τ but can be entrained by an external periodic cue called *zeitgeber* ("time giver" in German) such as the light-dark cycle to a period T .

A circadian system is thus composed of three elements: an *input* device that is able to convey photic information about the local external time to the internal clock, an *internal clock* system generating self-sustained oscillations and driving rhythmic *outputs* resulting in overt circadian rhythms such as the locomotor activity rhythms but also rhythms in body temperature or hormone secretion (see Fig. 2.4.A). The scheme is of course a simplified view. Some circadian systems are more complex: the output rhythms can be driven by both the *zeitgeber* and the clock [49] and the output can also feedback on the clock or influence the effect of the *zeitgeber* on the clock (see Fig. 2.4.B) [49]. Moreover, as we will see later (in section 2.2.3.3.1), some organisms such as mammals have multiple clocks throughout the body [183].

The entrainment of internal clocks by *zeitgeber* cues informs organisms about the external local time and allows them to schedule their activities to an appropriate time of the day [10]. Entrainment not only implies that the period of the oscillator matches the one of the *zeitgeber*: it also entails a fixed phase relationship between the clock and the external cue. The latter depends on the amplitude and on the period of the *zeitgeber*, on the free running period and on the photoperiod, that is the illumination time [146]. The light-dark cycle is not the only *zeitgeber*; in particular, we will see (in section 2.2.3.4.2) that the feeding-fasting cycle is also an important *zeitgeber* [28].

2.2.1.2 Temperature compensation

A good timekeeping system must be robust against environmental fluctuations, notably to temperature fluctuations. This is the case for circadian systems whose period remain stable when they are facing temperature fluctuations. This property is quite amazing because in general, rate constants of biochemical reactions depend on temperature, according to Arrhenius law [26]

$$r = A \exp\left(\frac{-E_a}{RT}\right)$$

where E_a is the activation energy, T the temperature and R the gaz constant. This implies that chemical reactions will speed up when the temperature increases. But interestingly, it has long been recognized that the period of clock systems is relatively insensitive to temperature variations. In the eighteenth century, scientists had noticed that rhythms in leaf movements were independent of temperature fluctuations [49]. Around 1950, circadian rhythms were identified in *Drosophila* eclosion patterns [69]. The period of these rhythms

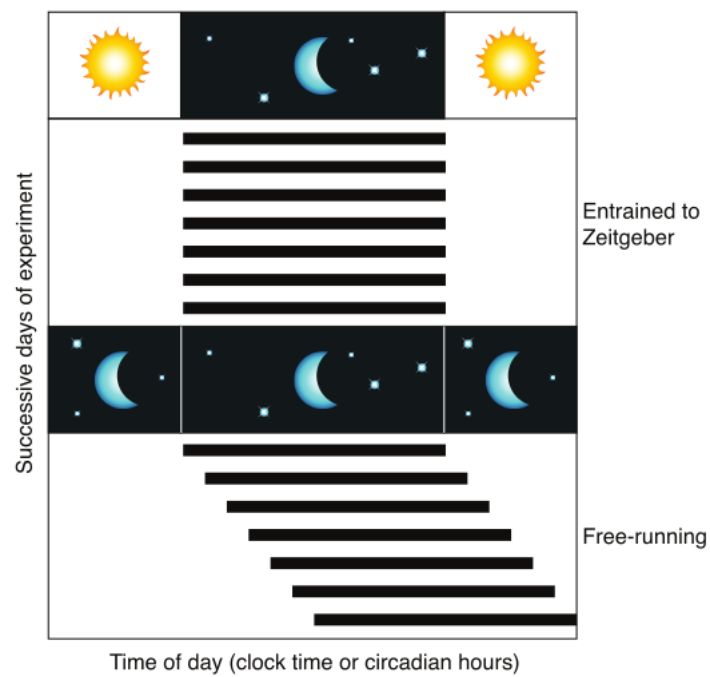


Fig. 2.3 Schematic plot of the locomotor activity rhythm of a typical nocturnal rodent under LD and DD conditions. Upper panel: in LD conditions, the rhythm of locomotor activity is entrained to the period T of the zeitgeber. Lower panel: in constant darkness, the free-running period τ slightly exceeds T [49].

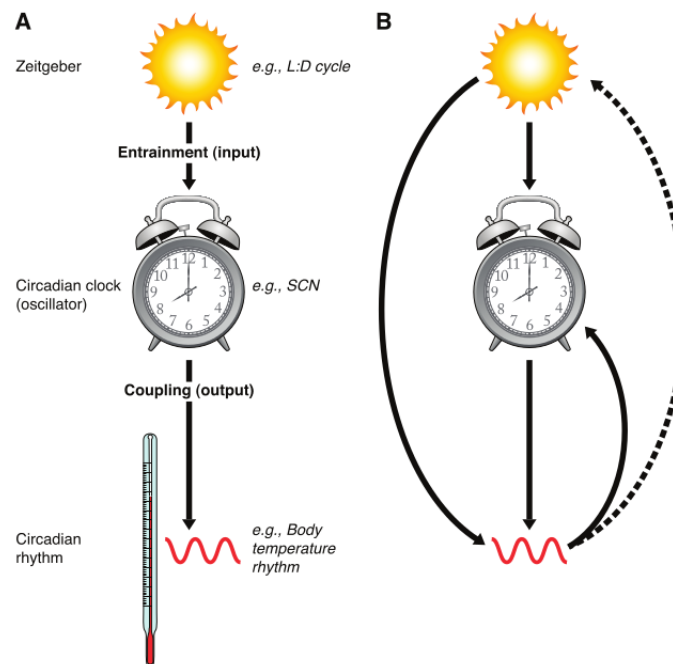


Fig. 2.4 Schematic view of the components of a circadian system: A) an input (the zeitgeber) informs the internal clock about the external local time. The clock itself drives several physiological processes (outputs). B): this scheme can be more complex with the input directly modulating the output. The latter can possibly feed back to the clock or even to the input device. [49].

was then evaluated under different temperatures (16, 22 and 26 degree Celsius) and in complete darkness. The period remained 24 h except for 16 degrees where it switched to 24.8 h. The temperature coefficient Q_{10} , that measures the rate of change of a biochemical reaction following a ten degrees temperature increase, is thus between 0.9 and 1.1 rather than 2 or 3 as usually. Absolute temperature independence would be associated to a Q_{10} equal to one. It is likely that individual reaction rates at the core of the clock are sensitive to temperature variations but that there is a compensation mechanism such that the overt period remains close to 24h. The precise mechanisms enabling temperature compensation are still unclear. This mechanism could be part of a more general mechanism called metabolic compensation. Indeed a precise clock is expected to be relatively insensitive not only to temperature fluctuations but also to external fluctuations in general such as metabolic fluctuations, pH variations,... In this vein, clocks of cyanobacteria have recently been shown to have compensation mechanisms for both variations in temperature and ATP concentration (see Fig. 2.5) [82].

2.2.2 Circadian clocks allow fitness to changing environments

Circadian rhythms are ubiquitous: they are found in bacteria as well as in eukaryotes. Indeed, organisms as varied as plants, fungi, insects, fishes, birds, mammals and so on exhibit circadian rhythms in diverse functions [13]. Furthermore, many traits of these circadian systems are conserved between organisms. This ubiquity suggests that circadian systems confer some important adaptive advantage. On the evolutive point of view, circadian systems have probably evolved in order to partition light-sensitive reactions to the dark phase [132]. This theory is called "escape-from-light" hypothesis.

Entrainment of the clock to external cues is thought to help organisms to anticipate the daily periodic changes of the environment. Species can thus anticipate dawn and dusk, food availability and avoid predators, which increases their survival. For example, flies have been shown to have circadian eclosion rhythms with a rhythmic emergence of the adult fly from the pupa [92]. Eclosion happens at dawn when the humidity is the highest, thereby probably increasing survival. Circadian systems also have mechanisms to measure the photoperiod (that is, the length of the day). This enables organisms to anticipate seasonal events such hibernation, reproduction or migration for birds [132].

A good way to test if a trait confers fitness to the environment, is to compare the reproduction fitness of wild-type versus mutant organisms. This was done with cyanobacteria strains [130]. The wild-type (WT) strain has a 25h free running period. Two mutants were characterized by a defect in the protein KaiC, which is important in the cyanobacteria clock [13]: the mutant SP22 is characterized by a 23h free running period while the mutant P28 has a 30h

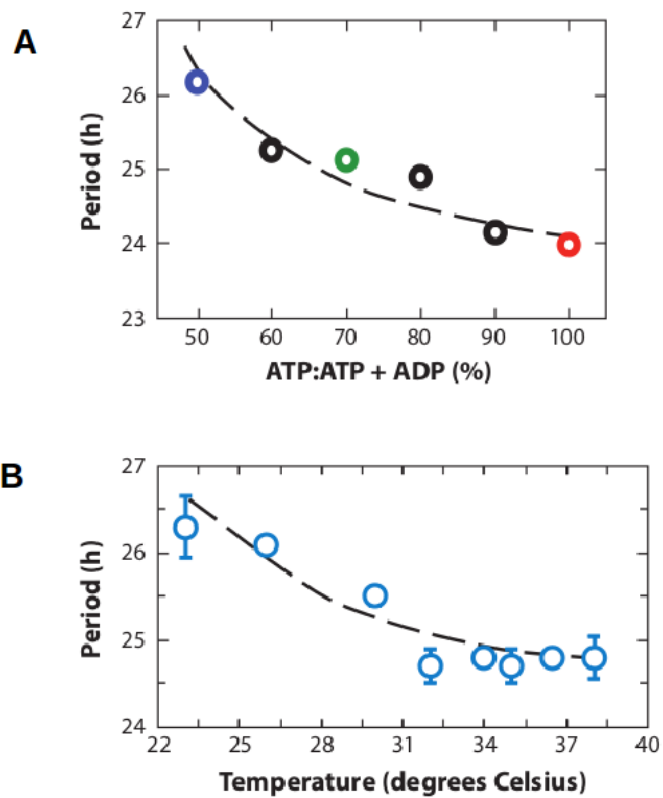


Fig. 2.5 Examples of compensation of the period length in cyanobacteria: the period of the oscillations only slightly varies upon changes in the ratio ADP/ATP (A) or in the temperature (B) [82].

free-running period. In pure cultures (that is, with only one strain), the growth rates of the different strains were approximately the same. Then, mixed cultures were created with two strains in competition. They were mixed in approximately equal densities in the beginning and the cultures were placed under different LD patterns: LD 11:11, LD 12:12, or LD 15:15. For example, a mixed culture with SP22 and WT cyanobacteria was placed under a 11:11 pattern. After several weeks, the culture contained mainly the SP22 strain, indicating that this strain grows faster under this condition. The results indicate that the strain that eliminates its competitor is the one whose free running period is the closest to the period of the LD cycle (see Fig. 2.6). This coincidence between the free running period and the period of the zeitgeber is called resonance by analogy with the phenomenon of resonance in physics [72]. Resonance between the free running period and the period of the LD cycle seems thus to constitute a selective advantage. Why? It could be because resonating strains exhibit an optimal phase relationship with the LD cycle. Indeed, experiments have shown that the phase relationship between the circadian clock and the LD cycle are different for resonating and non-resonating strain: the bioluminescence rhythm of cyanobacteria appear to peak at dusk for each resonating strain [175]. Thus, an important role of the clock is to schedule activities of organisms to an appropriate phase with respect to external cycles.

But organisms living under constant conditions such as fishes in caves for example, still have circadian rhythms suggesting that endogenous rhythms constitute an advantage per se. Indeed, the clock also enables to coordinate internal physiological processes: it helps to synchronize reactions that have to be performed simultaneously. Furthermore, it temporally separates incompatible processes [10].

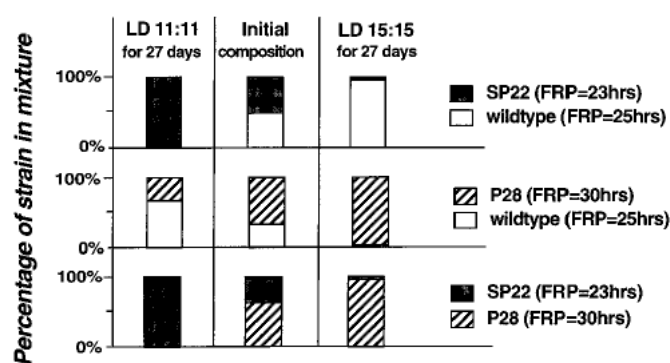


Fig. 2.6 Cultures mixed with several cyanobacteria strains (middle column) are placed either under a 11:11 LD (left column) pattern or under a 15:15 LD pattern (right column). After 27 days, the strain whose free-running period is the closest to the period of the LD cycle wins [130].

2.2.3 Organisation of the mammalian clock

2.2.3.1 Circadian rhythms are generated by the SCN

In mammals, the pacemaker is located in the suprachiasmatic nucleus (SCN), a paired nucleus in hypothalamus. Indeed, several pieces of evidence have led to this conclusion more than thirty years ago [161]. First, SCN displays an overt circadian rhythm in glucose utilization. Secondly, there is a direct connexion between the retina and the SCN through the retinohypothalamic tract (RHT) enabling the entrainment of the clock by the light-dark cycle. Thirdly, lesions of the SCN were shown to disturb circadian rhythms of locomotor activity, feeding behaviour, ovulation and hormone secretion, for both rodents and primates. Furthermore, transplantation of intact SCN tissue to SCN-lesioned animals restores circadian behavioural and activity rhythms with the period of the donor [139]. Indeed some rodents display a mutation (the tau mutation) characterized with a shorter circadian period (22h) in DD. Rats with a normal 24h period were SCN-lesioned and were then transplanted with SCN from tau-mutant animals. This restored locomotor rhythms with a period of 22h.

Experiments have also shown a circadian pattern in firing rates for SCN neuron populations. This raises the following question: do these rhythms persist at the level of the single cell ? Studies have shown that individual neurons still display daily rhythms in firing rate (see Fig. 2.7), but that there is an important heterogeneity in the firing period and that neurons firing with the same circadian period display different phases [169]. SCN neurons are thus single cell-autonomous oscillators!

As we will see in the next section, circadian oscillations at the cellular level are generated by so-called clock genes involved in a regulatory transcriptional network [13]. By recording clock gene expression and firing rates of isolated neurons, it was found that only 18% of them display robust circadian rhythms [168]. Indeed, 9% appear to be arrhythmic while in most of them, rhythms dampen after less than three days of culture. This indicates that most individual SCN neurons are unstable oscillators and that stable circadian rhythms at the level of the whole tissue are obtained through intercellular coupling between neurons which is in particular achieved through the action of neurotransmitters and neuropeptides [120].

2.2.3.2 Circadian oscillations are cell autonomous

2.2.3.2.1 Transcriptional and translational feedback loops

Circadian oscillations are thus cell-autonomous, but what is the mechanism generating them ? In the seventies, experiments on *Drosophila* have highlighted their genetic basis. *Drosophila* display notably daily rhythms in eclosion and locomotor activity. Researchers

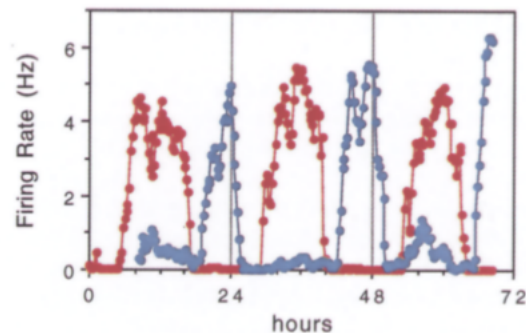


Fig. 2.7 Recording of the firing rate for two individual cultured neurons. Both profiles are circadian but some phase heterogeneity is observed between the two time profiles [169].

managed to obtain three clock mutants: one arrhythmic mutant (*Per0*), another short-period mutant (*PerS*, $\tau=19\text{h}$) and also a long period mutant (*PerL*, $\tau=28\text{h}$) [92]. Fig. 2.8 shows the effect of these three mutations on eclosion and locomotor rhythms. It was discovered that these three mutations involved the same gene located on X chromosome. This gene was later called the *Period* gene (*Per*). In the nineties, it was shown that both the level of PER mRNA and protein are cycling, with one peak a day (see Fig. 2.9) [64],[65]. Interestingly, the level of *Per* mRNA decreases when the level of protein increases. In addition, constitutive over-expression of the protein led to a strong decrease of *Per* mRNA levels. All together, these facts suggested the presence of a negative transcriptional feedback mechanism by which the protein PER inhibits the expression of its own gene.

Further progresses in molecular biology enabled to identify that negative transcriptional loops are at the core of most circadian systems [13]. But these feedback loops are often indirect: an activator complex (positive elements) activates the transcription of clock controlled genes. Among them, there are negative elements that repress the activity of the activator complex, thereby shutting down their own production. Degradation mechanisms then decrease the levels of these repressors, leading to a de-repression of the activity of the positive elements. And thus, the cycle starts again [13]. The mechanism is called transcriptional translational loop (TTL) and is responsible for oscillations at the cellular level in many organisms. Fig. 2.10 summarizes the positive and negative elements in model organisms in the realm of circadian biology. In the fungus *Neurospora crassa*, the negative element is the protein FRQ, while its positive complex is formed by the proteins WC-1 and WC-2 [108]. For the plant organism, *Arabidopsis thaliana*, TOC1 is the activator protein while CCA1 and LHY are the repressor proteins [167]. In *Drosophila*, PER and TIM form a complex re-

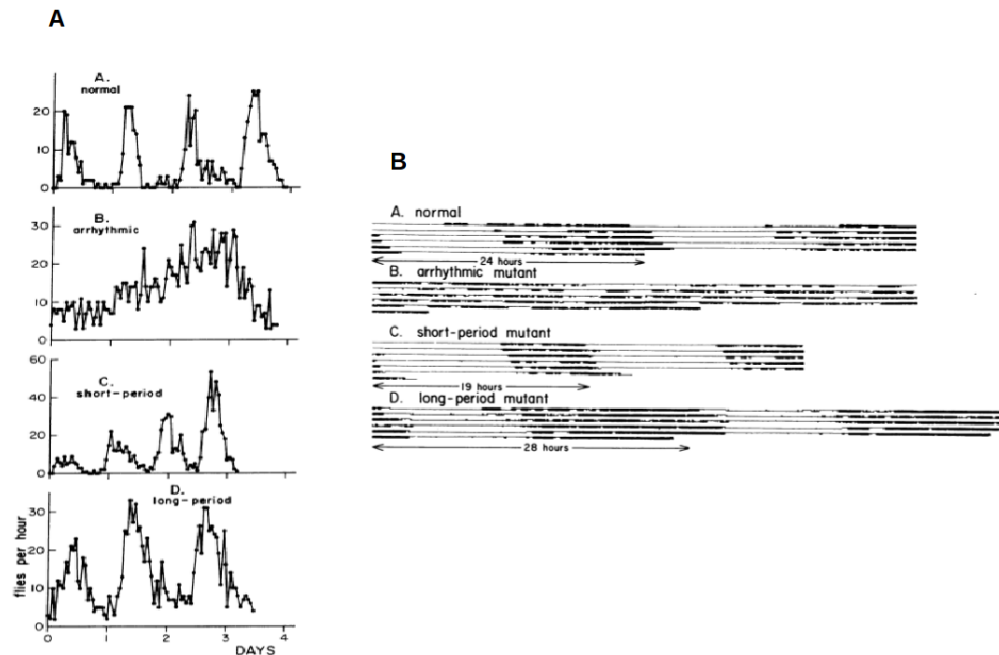


Fig. 2.8 Comparison of *Drosophila*'s eclosion rhythms (A) and locomotor activity (B) for WT, short-period, long-period and arrhythmic animals [92].

pressing the activity of the activator complex formed by the proteins CYC and CLK [44], [29].

Orthologs of *Drosophila* clock genes have been found in mammals: an activator complex composed of CLOCK (circadian locomotor output cycles kaput) and BMAL1 (brain and muscle ARNT-like 1) binds E-box sequences located on the promoter of clock-controlled genes (see Fig. 2.11) [86], [19]. Among these are the genes *Period* (*Per 1,2,3*) and *Cryptochrome* (*Cry1,2*) [95], [181]. After being translated, PERs and CRYs heterodimerize in the cytoplasm before being translocated into the nucleus. Once in the nucleus, the repressor complex inhibits the activity of the activator complex CLOCK-BMAL1. Once the negative complex has been degraded, a new cycle can start [88]. Besides this main negative feedback loops, additional transcriptional loops have been shown to include nuclear receptors: the retinoid-related orphan receptor alpha, beta, and gamma (ROR- α , β , γ) and the nuclear receptor reverse-erythroblastosis virus alpha and beta (REV-ERB and - β) [149], [137]. REV-ERBs and RORs are transcriptionally activated by CLOCK-BMAL1. In turn, they competitively bind to a ROR element in the *Bmal1* promoter where they respectively inhibit and activate *Bmal1* transcription. Mutations of these clock genes can modify both the period and the amplitude of oscillations (see Fig. 2.13). For example, the knockout of *Cry1* shortens the period while *Cry2* deletion lengthens the period [39]. Some mutations even totally suppress

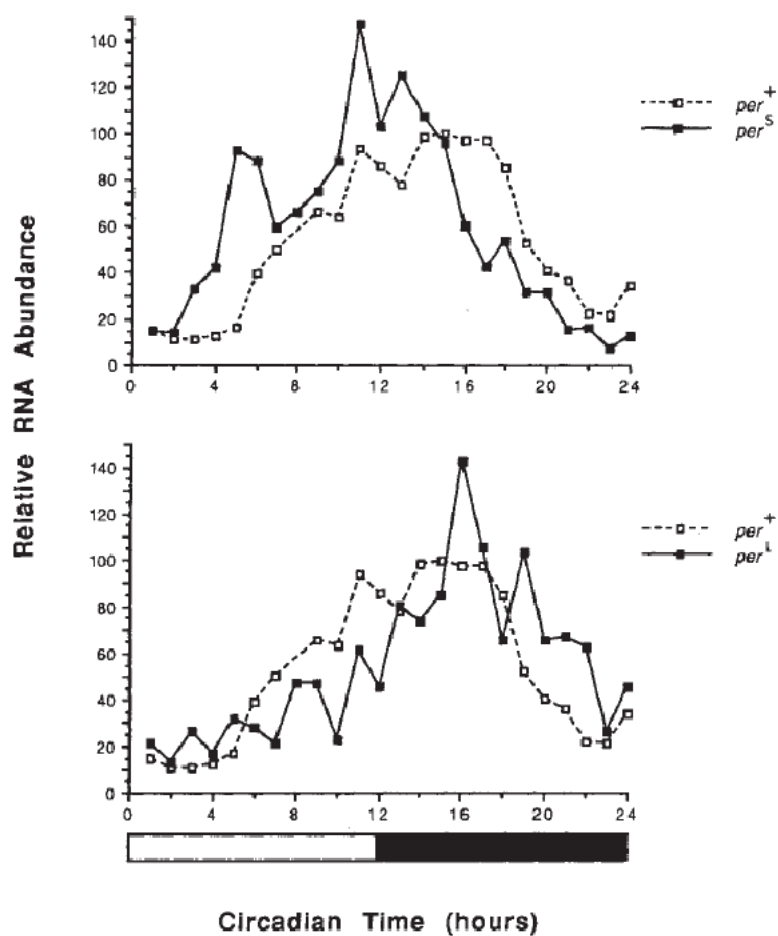


Fig. 2.9 Circadian levels of *Per* mRNA in LD conditions. Comparison between WT and mutant (short and long-period mutants) profiles [64].

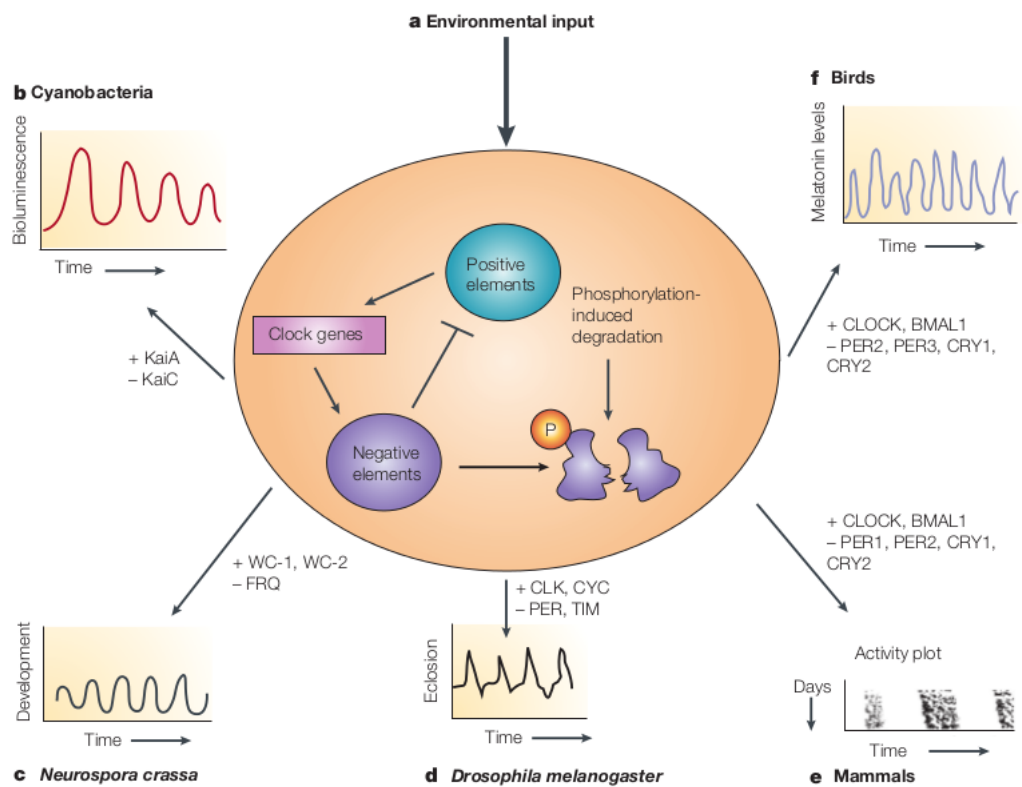


Fig. 2.10 Schematic view of the main feedback loop at the core of most circadian systems: an activator complex (called positive element here) activates the transcription of negative elements (repressors). The latter repress the activity of the positive elements, thereby shutting down their own transcription. The degradation of the repressor proteins leads to the derepression of the action of the positive elements and a new cycle of transcription can start. [13].

the oscillations. For instance, *Bmal1*^{-/-} mutants are arrhythmic. Animals deficient in both Rev-Erb- α and - β as well as other double knockout (*Cry1*^{-/-}*Cry2*^{-/-}, *Per1*^{-/-}*Per2*^{-/-}) are also arrhythmic [95], [181].

Lately, special attention has been paid to understand the exact sequence of molecular events leading to the alternation between transcriptionally active and repressive phases [90]. These studies have shown that at ZT0, both CLOCK-BMAL1 and the repressor CRY1 are bound to E-boxes on the promotor of clock-controlled genes. This state is called the poised state. Then, CRY1 concentration decreases and the arrival of chromatin activating markers such as the cofactor p300, establish a transcriptionally active state (see Fig. 2.12). This latter state is followed by the arrival of the repressor complex PER-CRY together with the decrease of CLOCK-BMAL1 presence on the promotor sequence. This state is the repressive one. The exact mechanisms leading to the transitions between these different states is still unclear. The protein CLOCK has been shown to have a histone acetyl transferase (HAT) activity and this is likely to play an important role in these transitions [66], [33], [74]. Indeed, CLOCK first acetylates the histone H3K9 which leads to the onset of the transcriptionally active state. Then it also acetylates its partner BMAL1 which favors the binding of the repressor complex PER-CRY .

2.2.3.2.2 Post-transcriptional and post-translational modifications

A recent study has investigated rhythmicity of the SCN proteome [24]. It indicates that only 13% of the SCN proteins oscillate. Among them, only 11% are circadian, the majority of them exhibiting ultradian oscillations: 6% oscillates with a 8h period and 14% with a period of 12h. Remarkably, proteins with 12 harmonics tend to peak at the transition periods, that is, dusk-dawn and dawn-dusk (for 12 hours photoperiods). This study also highlights the fact that cycling transcripts can give rise to non-rhythmic, circadian or ultradian proteins. Similarly, cycling proteins can result from transcripts that cycle with a different period or even do not cycle. Indeed, ultradian proteins often are not encoded by ultradian transcripts. This highlights the importance of post-transcriptional and post-translational modifications in the mammalian circadian system. Post-transcriptional regulation mechanisms include regulation at the level of mRNA maturation, degradation as well as at the level of translation. It is mediated by RNA binding proteins and micro RNAs. Post-translational regulation is an additional control layer (see Fig. 2.14). It includes modulations of protein stability, activity and localization. This can be achieved by modifications such as phosphorylation, acetylation, methylation, sumoylation, glycosylation and their reverse reactions. In particular,

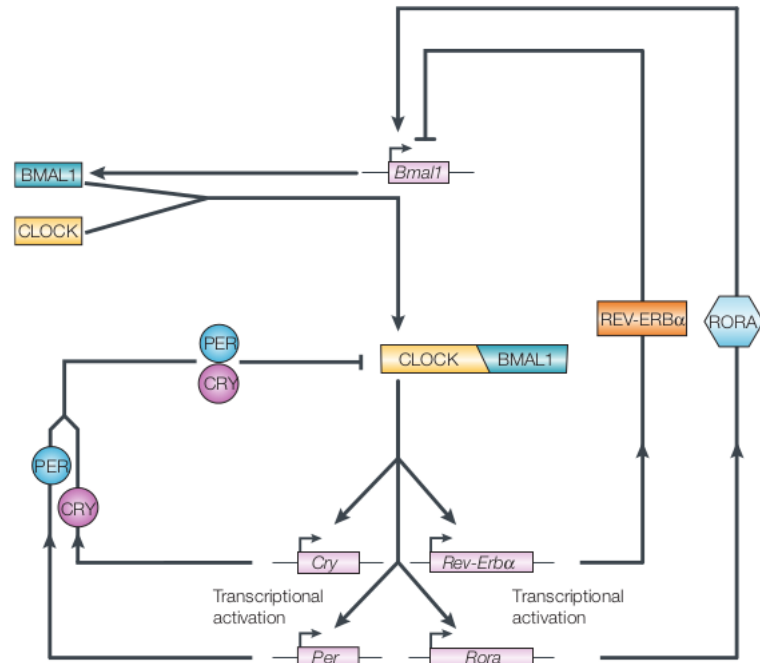


Fig. 2.11 Mammalian main transcriptional feedback loops: the activator complex, CLOCK-BMAL1, activates the transcription of the genes *Per*, *Cry*, *Rev-Erbα* and *Rora*. On the one hand, the repressor complex PER-CRY periodically inhibits the action of the activator complex CLOCK-BMAL1. On the other hand, the nuclear receptor REV-ERB α inhibits the transcription of *Bmal1* while ROR α activates it [13].

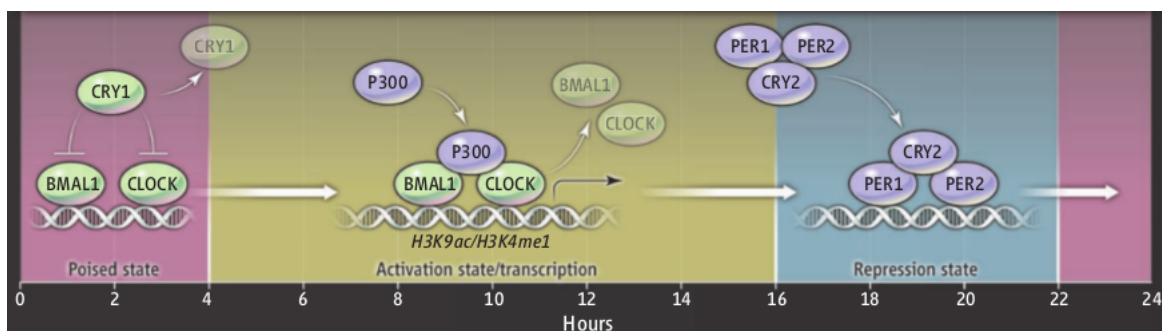


Fig. 2.12 Scheme showing the sequential events at the promoter of a clock controlled gene during a cycle [90].

Gene	Type	Behavioral Phenotype
<i>Clock</i>	Deletion	Long period to arrhythmic
<i>BMAL1</i>	Null	Arrhythmic
<i>Per1</i>	Null	Var. period to arrhythmic
<i>Per2</i>	Null	Var. period to arrhythmic
<i>Per3</i>	Null	Short period
<i>Per1/2</i>	Null/Null	Arrhythmic
<i>Cry1</i>	Null	Short period
<i>Cry2</i>	Null	Long period
<i>Cry1/2</i>	Null/Null	Arrhythmic
<i>CKIε</i>	Missense	Short period (<i>tau</i> hamster)
<i>CKIδ</i>	Not Done	Unknown

Fig. 2.13 Effect of clock gene mutation on behavioural rhythms [39].

the stability and the localization of the repressors PER and CRY are highly regulated: the degradation of CRY is controlled by the F-box and leucine-rich repeat protein 3 (FBXL3) and the degradation of PER is promoted by its phosphorylation by casein kinase I proteins (CKI δ/ϵ) [20], [2]. Furthermore, CKI ϵ also appears to modulate PER1 nuclear entry [157]. The kinase has thus multiple effects on the clock, some of them being still unclear. A loss of CKI functions is related to shortening of the cycle while an inhibition of FBXL3 activity increases the clock period. A recent interesting mathematical modelling work has clarified the role of these posttranslational modifications [81]: it suggests that CKI controls the phase of the PER-CRY repression while FBXL3 controls its duration [45], [150], [42]. One role of post-translational control is thus to ensure the proper timing of the different events during the cycle and to enable to achieve a 24h cycle. The presence of post-transcriptional and post-translational modifications also enables to integrate environmental and systemic cues. This enhances the flexibility in the circadian control of physiology and in particular, it enables tissue-specific control by the clocks [156].

2.2.3.3 Secondary clocks in peripheral tissues

2.2.3.3.1 Clock genes are rhythmically expressed in multiple tissues

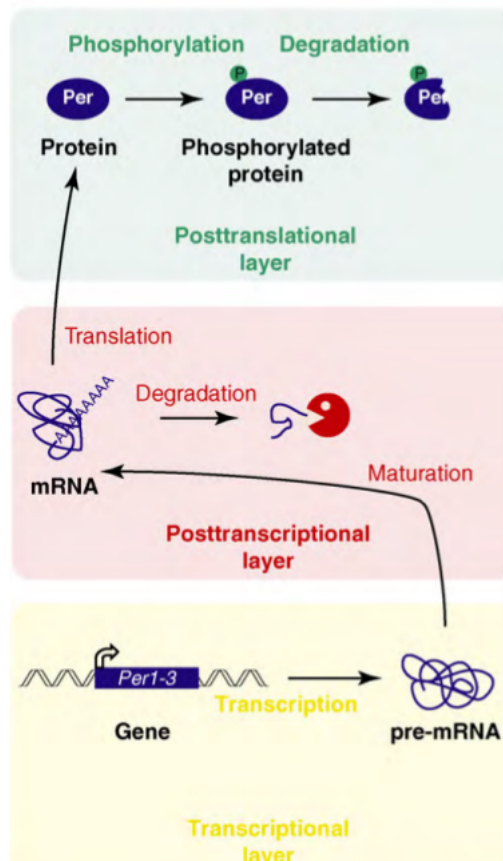


Fig. 2.14 A given clock component (here PER) can be regulated at the transcriptional, post-transcriptional and post-translational level. Yellow panel: at the transcriptional level, *Per* expression is regulated by CLOCK-BMAL1. Green Panel: at the post-translational level, the stability of PER is regulated by the kinase CKI. Red panel: post-transcriptional modifications are the third possible layer of control [25].

In the late nineties, experiments have highlighted circadian expression of *Per1,2,3* in several peripheral tissues: in liver, skeletal muscles and testis [183]. Thus, the clock machinery is also cycling in non-SCN cells with the peaks of expression being slightly delayed in peripheral clocks compared to the SCN (see Fig. 2.15). Since then, clocks have been discovered in many tissues including the liver, adrenal gland, aorta, brainstem, brown fat, cerebellum, heart, kidney, lung, skeletal muscle, white fat and hypothalamus (see, e.g. [180]). These core clock genes drive rhythmic expression of downstream genes involved in various physiological pathways. Consequently, almost 45 % of transcripts have been found to oscillate somewhere in the body and more are predicted to be discovered by sampling additional tissues [180]. Interestingly, circadianly expressed genes tend to cluster physically in the genome. Another important point is that many transcripts peak at zeitgeber transition periods, thus at dusk and dawn or even at both periods (bimodal expression profiles). Indeed, ultradian rhythms (with a period of 8 or 12 hours) in gene expression profiles of hundreds of transcripts have been discovered in liver but also in other peripheral tissues such as in the heart, the kidney and the lungs [78]. These rhythms whose period is an integer multiple of the 24 h are called harmonics of the circadian clock [78]. These ultradian rhythms appear to be implicated in many physiological pathways, including the cell cycle, lipid metabolism and in inflammatory pathways. Surprisingly, these harmonics are lost *in vitro*, indicating that they could be due to systemic cues and that synchronization techniques of cultured cells are thus not sufficient to reproduce this circulating cues *in vitro* [78]. Furthermore, *in vivo*, the amplitude of the peak during the subjective day and that of the one during the subjective night are in general not the same, suggesting that they could be driven by different signals, for example, one by the local clock and the other reinforced by some systemic cues such as food. Indeed, as we will see later, food is an important zeitgeber for peripheral clocks [28].

2.2.3.3.2 Circadian gene expression is largely tissue-specific

Circadian gene expression appears to be largely tissue-specific. Indeed, only 10 genes oscillate in all tissues: *Bmal1*, *Dbp*, *Rev-Erb α* , *Rev-Erb β* , *Per1*, *Per2*, *Per3*, *Usp2*, *Tsc22d3* and *Tspan4* [180]. The overlap is the highest between tissues that are related from a developmental point of view (such as kidney and liver, skeletal muscle and heart,...). Liver and kidney were found to have the most cycling genes while brain regions have the fewest. Let us consider the SCN and the most important nutrient distribution center, the liver. There is only few overlap between genes cycling in both tissues: 28 common circadian transcripts found in 2002 (see Fig. 2.17) [131]. The pacemaker drives circadian behavioural rhythms (locomotor activity, feeding, drinking behaviour,...) through neuro-endocrine cues. It is

thus not surprising that most of the cycling transcripts in SCN participate to the synthesis, processing or degradation of neuropeptides, neurotransmitters or hormones [131]. On the other hand, the liver major functions are the storage, redirection and utilization of fuel derived from nutrient. Accordingly, the majority of liver specific cycling genes are involved in different aspects of lipid and glucose metabolism. As it will be described in more detail later, there is a circadian control of rate limiting steps of glycolysis, gluconeogenesis, fatty acid oxidation, oxidative phosphorylation,... [131], [71]. Besides nutrient metabolism, cycling hepatic transcripts also appear to be involved in xenobiotic metabolism (that is the set of biochemical reactions that modify the structure of a foreign body (drug, poison) and lead to its excretion))[131]. All together, these data suggest a tight link between circadian and metabolic cycles in peripheral metabolic tissues [10].

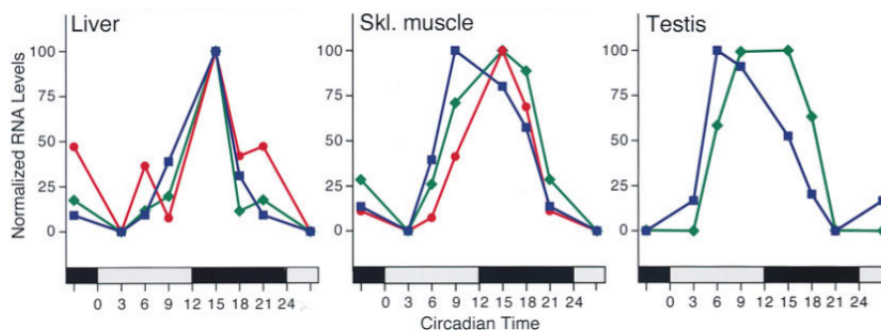


Fig. 2.15 Levels of mPer1 (blue curves), mPer2 (red curves) and mPer3 (green curves) oscillate in several peripheral tissues [183].

2.2.3.4 Entrainment properties of peripheral clocks

2.2.3.4.1 The SCN drives peripheral clocks through neuro-endocrine cues

As we have seen above, the existence of bimodal expression profiles suggests that gene transcription in peripheral tissues is under the control of both local clock and systemic cues. This raises several questions: what is the contribution of the local clock machinery to the oscillations in transcript levels and what is the proportion due to systemic cues controlled by the SCN? To answer these questions, a genetic construction has been designed where the liver clock can easily be switched on and off (by suppressing the circadian expression of *Bmal1*) [94]. These experiments have shown that the rhythmic expression of local core clock genes is lost when the hepatic clock is switched off except for *Per2* mRNA indicating that *Per2* is at least partially controlled by systemic cues (see Fig. 2.18). On the other hand, *Per2* expression also remains rhythmic *in vitro*, persisting thus in the absence of systemic

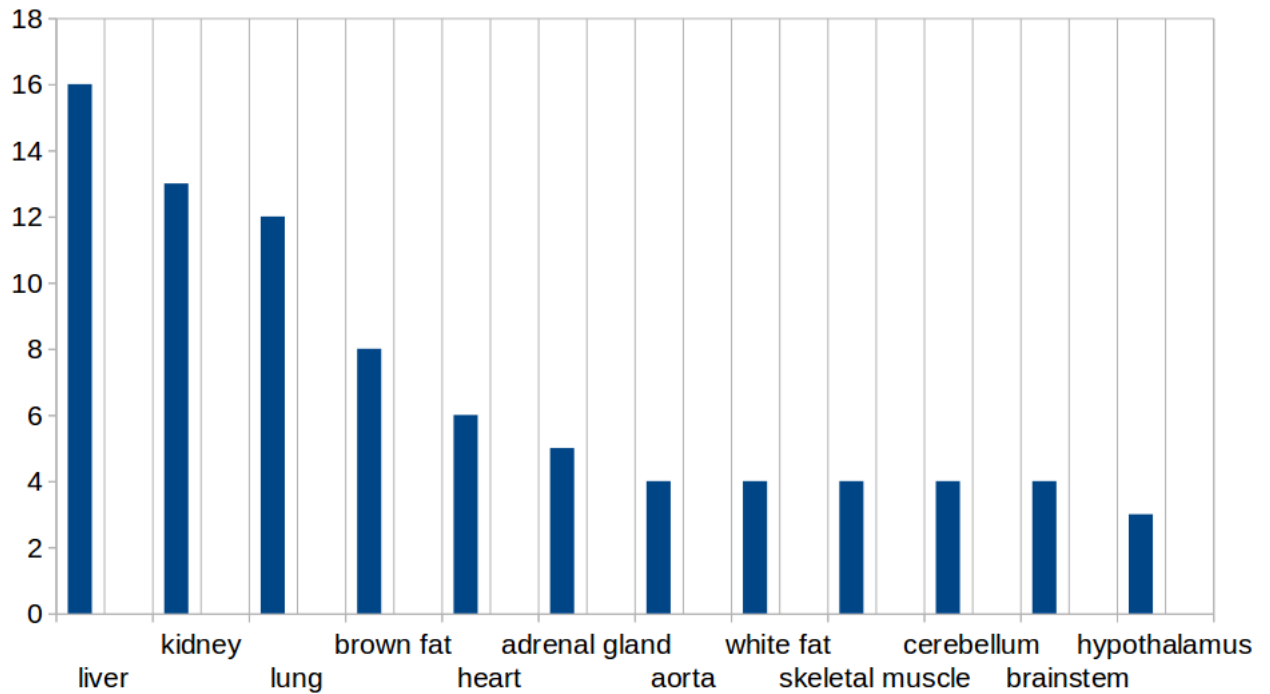


Fig. 2.16 Comparison of the percentage of oscillating transcripts in 12 tissues [180].



Fig. 2.17 List of the transcripts cycling both in the liver and in the SCN [131].

cues. This suggests that *Per2* could be an important convergence point for the integration of systemic cues by the local clocks.

Other experiments have highlighted the influence of the SCN on peripheral oscillations. Indeed, by using transgenic animals with luciferase under the control of *Per2* promoter, Yoo *et al* have observed robust circadian rhythms persisting in isolated peripheral tissues for more than 20 cycles when the SCN is intact [177]. Conversely, they have observed that SCN-lesioned animals show phase desynchronization between different tissues. This indicates that an important role of the SCN is to set appropriate phases in peripheral clocks that are otherwise out of synchronization.

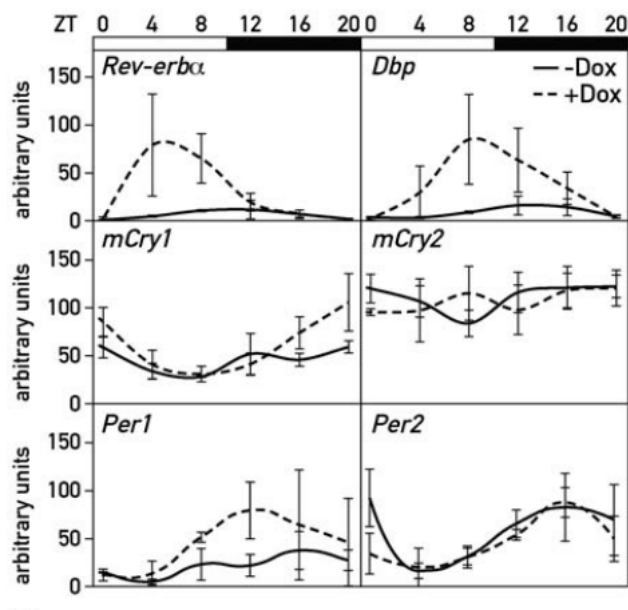


Fig. 2.18 Comparison of clock gene expression for an active (with Dox) and an inactive (without Dox) liver clock: clock gene expression is reduced when the liver clock is switched off except for *Per2* mRNA. (Dox is the abbreviation for the tetracycline analog doxycycline that is used to activate the liver clock) [94].

More specifically, it was shown that the SCN coordinates secondary clocks through both endocrine cues and neural projections. Indeed, the SCN projections reach several hypothalamic and thalamic brain areas including the amygdala (AMY), the arcuate nucleus (ARC), the paraventricular nucleus of hypothalamus (PVN) and the dorsomedial hypothalamus [4], [143]. Of particular interest is the PVN. Indeed, the SCN stimulates rhythmic release of two hormones from the PVN: corticotropin-releasing hormone (CRH) and vasopressin (AVP). In turn, AVP and CRH induce the release of the adrenocorticotropic hormone (ACTH) from the pituitary gland. Finally, the latter acts on the adrenal gland that releases glucocorticoids

(GC) [143]. But the SCN controls the glucocorticoid production not only by endocrine cues but also through neuronal projections. Indeed, sympathetic and parasympathetic projections from PVN also modulate GC release from the adrenal gland. Furthermore, the adrenal itself was found to be a local clock with cycling clock components that gate GC production [30]. It is thus not surprising that plasma glucocorticoid levels display overt circadian rhythms, with a peak at the beginning of the active phase of animals (see Fig. 2.19).

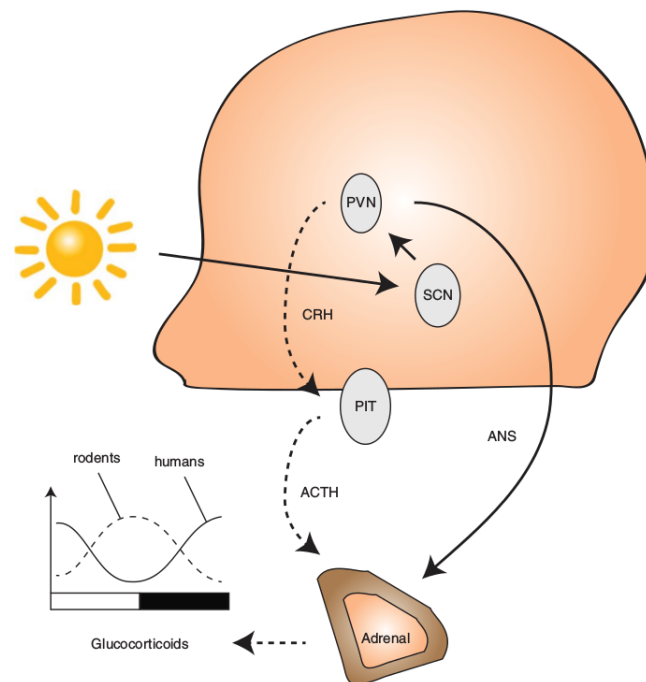


Fig. 2.19 The SCN periodically stimulates the adrenal gland through both endocrine cues (CRH and ACTH) and neuronal projections (ANS). This leads to the periodic secretion of glucocorticoids. Abbreviations are as follows: PVN, paraventricular nucleus of hypothalamus; PIT, pituitary gland; CRH, corticotropin-releasing hormone; ACTH, adrenocorticotropic hormone [160].

Glucocorticoids exert their effects on local clocks essentially by binding to glucocorticoid receptors (GR) that are expressed in many peripheral tissues [32]. Indeed, several clock genes (*Bmal1*, *Per1*, *Per2* and *Cry1*) have glucocorticoid-response elements (GRE) in their promoter. *Per1* has GRE in its promoter while *Per2* promoter includes an intronic domain. On the other hand, studies have shown that *Rev-Erb α* and *Ror α* have negative GRE in their promoter. Furthermore, both *CLOCK* and *CRY1* were shown to interact physically with GR [96]. Glucocorticoid signalling is thus likely one of the cues that enable the coordination of local clock by the SCN. This is coherent with experiments showing that clock gene expression

is shifted upon injections of dexamethasone (GC analog) at different times [9]. Nevertheless, the mutation of GR does not change the phase of local gene expression which indicates that GC can influence peripheral clocks but are not essential for their functioning.

2.2.3.4.2 Food is the dominant zeitgeber for peripheral clocks

To investigate the effect of food cues on clocks, Damiola and her collaborators have performed the following experiment: they have switched rodents from nighttime to daytime feeding [28]. They have observed a phase inversion of clock gene expression in the liver (see Fig. 2.20). Interestingly, this phase shift is observed in all tested peripheral tissues (pancreas, kidney, heart, liver) but not in the SCN. Indeed, the SCN phase remains unaffected by shifts in food access, both in LD and DD conditions. Daytime feeding can thus uncouple local peripheral clocks from the SCN master clock. It is also important to point out that the phase inversion in gene expression does not occur immediately after the shift in food access. It takes in general several days and different peripheral tissues appear to answer with different kinetics, the liver resetting faster than the other tissues (see Fig. 2.21). All together, these data indicate that food is thus the dominant zeitgeber in peripheral clocks. The action of the feeding fasting cycle on metabolic clock will be discussed more deeply in the following sections.

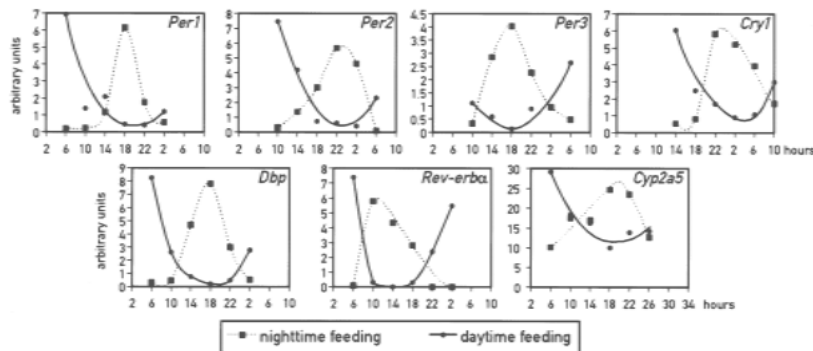


Fig. 2.20 A shift from nighttime (dotted line) to daytime feeding (solid line) inverts the phase of clock gene expression in liver [28].

Peripheral clocks are thus controlled by several cues including food intake and glucocorticoid signalling. This raises the following question: what is the influence of glucocorticoid signalling on the phase inversion dynamic? A study has compared the speed of the phase inversion in presence and in absence of the adrenal gland (adrenalectomy) in the liver [117]. The *Per2* mRNA normally peaks around ZT12 in liver. In the presence of intact GC signalling,

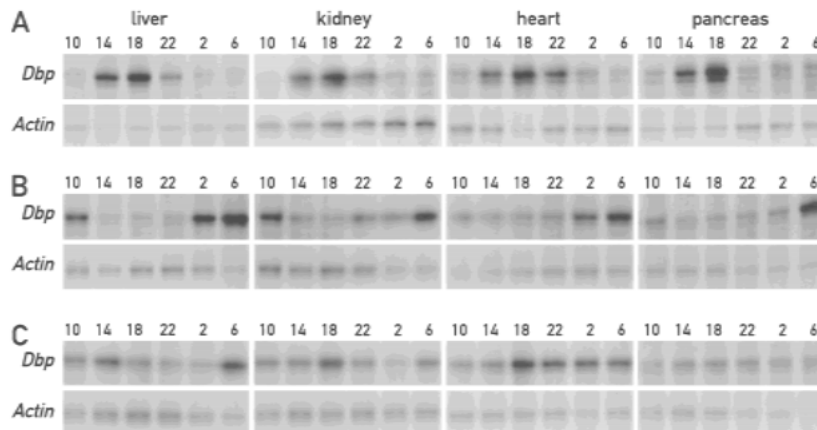


Fig. 2.21 The phase inversion observed in clock gene expression after a switch from nighttime feeding to daytime feeding occurs with different kinetics according to the tissue, the phase inversion being the fastest in the liver: time profiles of *Dbp* expression in different tissues are shown for animals fed A) during the night, B) during the day for 6 days, C) during the day for 3 days. Daytime feeding (B) inverts the phase of *mDbp* expression compared to nighttime feeding(A) [28].

it takes approximatively one week before a complete phase inversion. The dynamic is thus quite slow. Conversely, after an adrenalectomy, the phase is already almost inverted after one or two days. Similar results are obtained when the GR receptors are mutated (loss of function). These results thus indicate that glucocorticoid signalling impinges on the phase inversion during the switch from night-time to day-time feeding. It is interesting to observe the profile of GC levels during this inversion. During night-time feeding, GC levels peak around ZT12 while after the inversion, GC levels exhibit a bimodal profile with one peak around ZT12 and one around ZT0 (see Fig. 2.22). Finally, the dynamics of the switch from day-time feeding back to night-time feeding was also tested and appeared to be much faster than the opposite one in both the presence and the absence of GC signalling [117].

Besides glucocorticoids and food-related cues, we should note that peripheral oscillators are also influenced by temperature cycles driven by the SCN [18] (see Fig. 2.23). So, to summarize, the mammalian circadian system has its pacemaker located in the SCN and it drives secondary clocks located in peripheral tissues. The SCN is entrained by light while the feeding-fasting cycle is the dominant zeitgeber for peripheral clocks. The situation is quite complex as the SCN itself influences food intake [119]. The importance of food cues for peripheral clocks and the fact that many cycling genes are involved in metabolic pathways suggest a tight link between local clocks and energy metabolism which will be developed in the sections below.

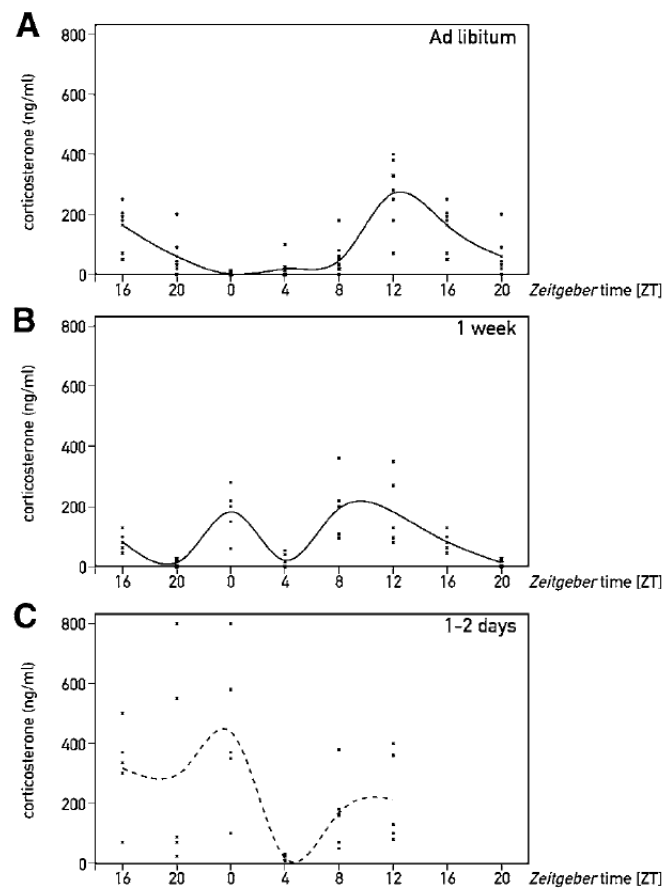


Fig. 2.22 Time profiles of glucocorticoid levels in animals fed A) during the night, B) during the day for one week, C) during the day for 1-2 days [117].

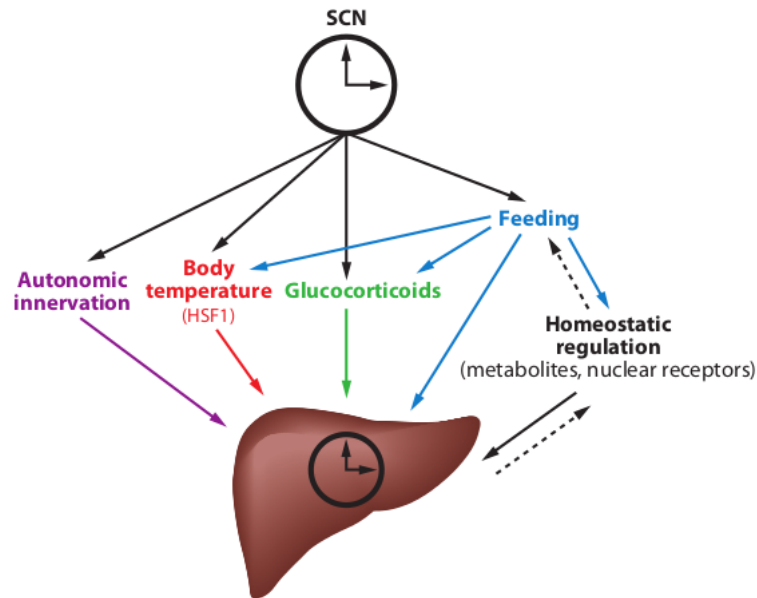


Fig. 2.23 The SCN influences oscillations in peripheral clocks by driving food intake, body temperature cycles as well as neuro-endocrine cues (including glucocorticoid signalling) [119].

2.3 Clock and metabolism

Glucose is the main fuel used to produce energy and some tissues such as the brain and the red blood cells absolutely require glucose to meet their energy needs [67]. The plasma glucose levels thus needs to remain nearly constant. However, glucose supply from meals is periodic. Therefore, several mechanisms have been developed to keep plasma glucose levels into a narrow range of concentrations despite that food is not available all the time. One of them is to create glycogen stores from glucose in excess after the ingestion of meals [100]. During short term fasting periods, the breakdown of glycogen into glucose enables to maintain almost constant levels of glucose in the blood stream. For longer fasting, when the glycogen stores are depleted, the kidney and the liver are able to synthesise glucose from other precursors. Thus, glucose-consuming and glucose-producing processes alternate during the feeding-fasting cycle in order to enable plasma glucose homeostasis.

Glucose-consuming reactions belong to the class of catabolic processes that provide energy from the oxidation of organic molecules. The energy produced by catabolic pathways is stored in energy carriers such as adenosine triphosphate (ATP) molecules. ATP is an energy carrier because some energy is stored in the covalent bond between the inorganic phosphate and ADP. Its hydrolysis into ADP or AMP and inorganic phosphates is thus energetically

favourable [3]. Metabolites such as NADH and NADPH are also used as energy carriers. The energy produced by catabolic processes is used by anabolic processes to build essential cell components.

The daily alternation between energy producing and energy consuming processes is responsible for variations in the ratios AMP/ATP and NAD⁺/NADH [3]. This periodically activates the nutrient sensors AMPK and SIRT1: AMPK is activated by high AMP levels while SIRT1 is activated by high NAD⁺ levels. As we will see below, these two nutrient sensors have several interactions with the clock (see Fig. 2.24) [97], [124], [12]. They are thus believed to relay information about the cellular nutrient status to the clock that, in turn, feeds back to metabolism to coordinate appropriate metabolic reactions with respect to external environmental conditions (see Fig. 2.25). Metabolic cycles are thus resulting from the combined action of local clocks and feeding-fasting cycles on metabolic pathways.

The reciprocal coupling between clock and metabolism is fundamental because it enables to keep internal physiological processes in synchrony with external variations of light and food availability [10]. As we will see below (section 2.3.1.2), clock disruption correlates with metabolic diseases [111].

First, I will present the main striking evidence of the bi-directional coupling between the clock and metabolic networks. Then, I will expose their interactions in more details with a special focus on the nutrient sensors AMPK and SIRT1 which are believed to be the nodal points between these two networks.

2.3.1 Evidences for the coupling between clock and metabolism

2.3.1.1 Nuclear receptors are implicated in both clock and metabolic pathways

As mentioned earlier, several core clock genes (RORs and Rev-Erbs) are nuclear hormone receptors. Nuclear receptors (NR) are transcription factors whose conformations and subsequent activities are changed after stimulation by a ligand. They are composed of several functional domains: an A/B domain for the binding of co-activator or co-repressors, a DNA binding domain (DBD) and a ligand binding domain (LBD). Some NR bind response elements in the promoter of their target genes as monomers while others act as homodimers or as heterodimers with the retinoid X receptors (RXR). For example, most steroid receptors tend to act as homodimers that cooperatively bind on a DNA response element while others like the peroxisome proliferator-activated receptors (PPARs) form heterodimers with RXR. Once the NRs are bound on the promoter of their target genes, co-regulators (co-activators or co-repressors) are recruited after ligand stimulation. For some of them, the ligand is still

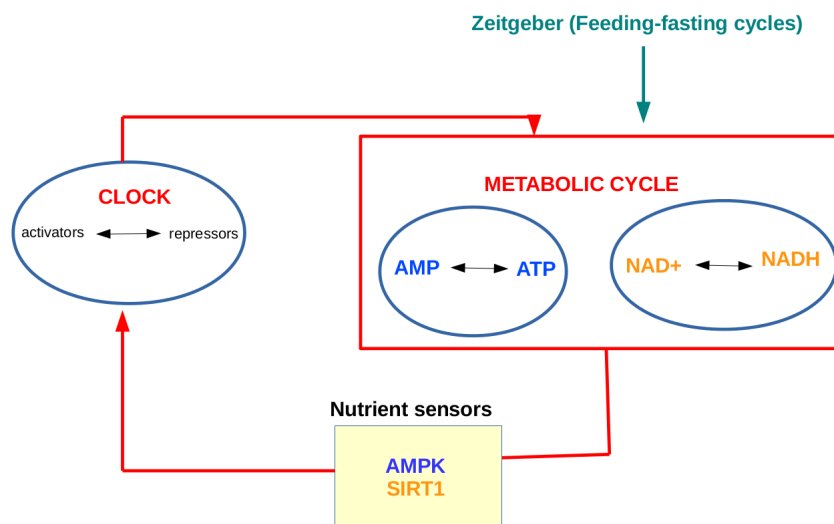


Fig. 2.24 Schema of the link between clock and metabolism: periodicity in food intake gives rise to alternation between energy-consuming and energy-producing metabolic processes. The consequence of this is daily variations in the ratios of AMP/ATP and NAD⁺/NADH. This goes with a periodic activation of the nutrient sensors AMPK and SIRT1 which relay informations about the cellular nutrient status to the clock.

unknown. These latter are called orphan receptors. 48 NRs have been found in humans (and 49 in mice) and are playing important roles in several metabolic pathways. Interestingly, half of the nuclear hormone receptors display circadian expression in the metabolic tissues (see Fig. 2.26) [174]. Furthermore, some of them are clearly involved in both clock and metabolic networks [34].

In particular, the clock proteins RORs and REV-ERBs are NRs involved in both glucose and lipid metabolism. Their ligands are sterols and haem respectively. REV-ERBs control several aspects of lipid metabolism. More particularly, REV-ERB controls bile metabolism as well as fatty acid and sterol metabolism through the sterol regulatory element-binding protein (SREBP) [34], [35]. Furthermore, REV-ERBs are also involved in glucose metabolism, in particular the control of gluconeogenesis [176], [91]. The knockdown of Rev-Erb α leads to elevated levels of triglycerides and plasma glucose while the opposite phenotype is observed for mice deficient in RORs. REV-ERBs and RORs are thus at the crossroads between the clock and metabolic network.

The peroxisome proliferator-activated receptors (PPARs) belong to a family of NRs that play an important role in the regulation of lipid metabolism. The family is composed of three members: PPAR- α , PPAR- γ and PPAR- β [125]. The binding of fatty acids and their

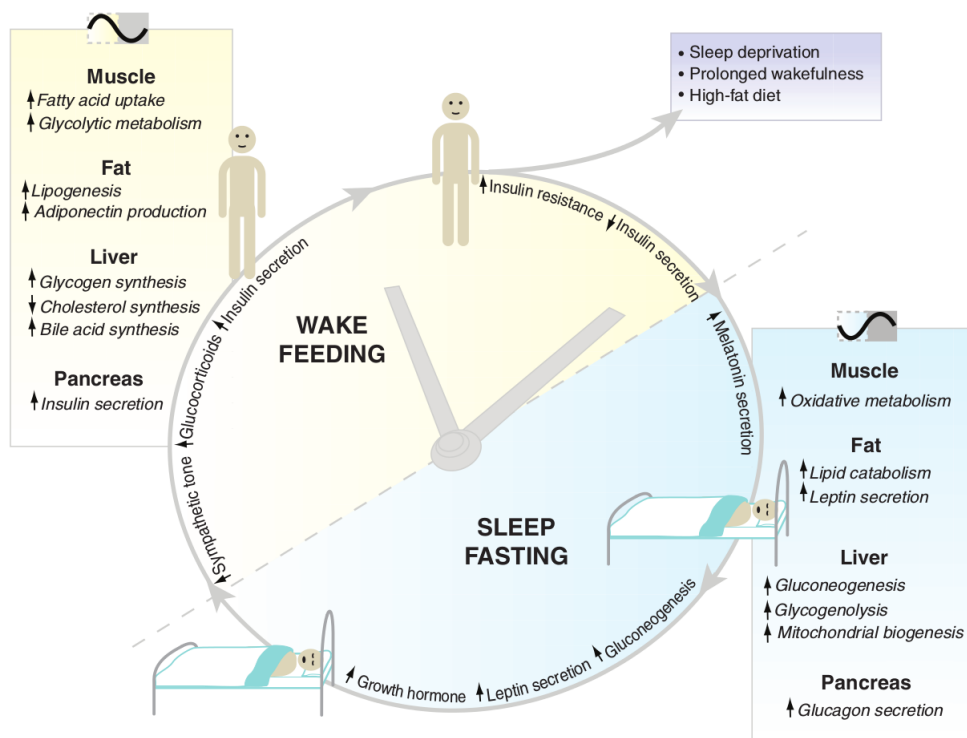


Fig. 2.25 The clock partitions internal metabolic processes to appropriate phase with respect to external environmental variations [10].

intermediates is required to activate the transcription of downstream genes. The three PPARs differ by their distribution in the body and their physiological functions [122]. PPAR- α is essentially found in the liver. During fasting periods, it mainly promotes fatty acid oxidation. PPAR- γ plays a predominant role in adipose tissue where it favors lipogenesis and fat storage during anabolic periods. It is also involved in the formation of adipocytes. PPAR- β has been less studied.

The expression of PPAR- α and PPAR- γ is circadian. In particular, PPAR- α is involved in a feedback loop with the clock. In particular, PPAR- α is involved in a feedback loop with the clock [21]. CLOCK-BMAL1 activates PPAR- α hepatic transcription thanks to an E-box on its promoter. This is consistent with the fact that *Bmal1* deletion strongly decreases *Ppar- α* expression. In turn, *Ppar- α* also appears to regulate *Bmal1* transcription as *Ppar- α* mutant animals have reduced *Bmal1* expression. Furthermore PPAR- α was also shown to modulate *Rev-Erba* transcription by binding to a DR2 element located on its promoter [43]. The interactions between PPAR- α and the clock components appear to be important in peripheral tissues but not in the SCN. In conclusion, the important role of several nuclear receptors in both the clock and metabolic pathways reinforces the idea that metabolic and circadian networks are intimately linked.

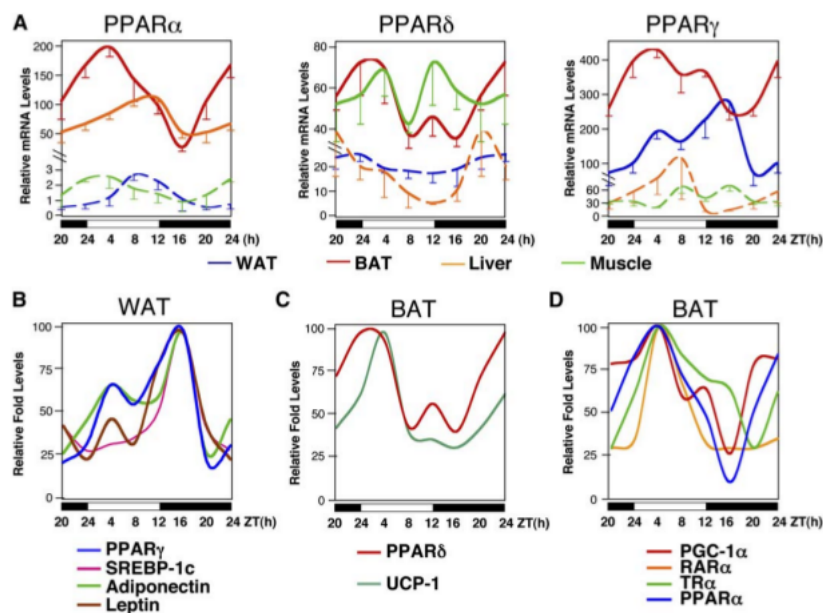


Fig. 2.26 Circadian expression profiles of several nuclear receptors in different metabolic tissues. Abbreviations are as follows: BAT, brown adipose tissue; WAT, white adipose tissue [174].

2.3.1.2 Defects in the clock lead to metabolic disorders

In agreement with the idea that clock and metabolism are coupled, clock mutations can lead to metabolic disorders. Indeed, *Clock* mutant animals have altered rhythms in locomotor activity and feeding behaviour [162]. More specifically, wild-type animals consume most of their food during the dark phase while the food intake is partially shifted to the light phase for mutant animals. And not only the timing of food intake is disturbed in *Clock* mutant but there is also an increase in the amount of total food intake. This is accompanied by disturbed metabolic rate and altered levels of circulating metabolic markers (such as ghrelin, leptin...). Consequently, mutants gain weight and exhibit several features of metabolic diseases such as hyperglycemia, hypertriglyceridemia and cholesterolemia. Mutation in clock genes seems thus to disturb the feeding centres in brain.

What is the effect of clock gene mutations in peripheral tissues? Interestingly, the effect of clock gene deletions on downstream metabolic targets appears to be tissue specific. In pancreas, a *Clock* mutation leads to altered expression of genes involved in insulin production. It was further shown that *Clock* and *Bmal1* mutants display reduced insulin secretion due to impaired β cell functioning which leads to metabolic troubles [112]. In liver, *L-Bmal1* deletion impairs the transcription of several genes involved in glucose metabolism, especially in gluconeogenesis and glycogenolysis [98]. In particular, *Bmal1* knockout mice loose rhythm in expression of the glucose transporter *Glut2* (which transports glucose between the liver and the blood). This leads to fasting hyperglycemia. Local clocks seem thus to be required for the proper coordination of local metabolic processes and disruption of clock genes correlates with numerous metabolic troubles that are summarized in Fig. 2.27.

Gene Disruption	Mutation	Circadian Phenotype	Metabolic Phenotype
<i>Clock</i>	Systemic dominant negative mutation	Arrhythmicity in DD	Hypertriglyceridemia, hypercholesterolemia, hyperglycemia, hyperleptinemia
<i>Bmal1</i>	Systemic KO	Arrhythmicity in DD	Impaired gluconeogenesis, adipogenesis, adipocyte differentiation; hyperlipidemia, glucose intolerance
<i>Per2</i>	Systemic KO	Shortening of period	Absent glucocorticoid rhythm, absent diurnal feeding rhythm, obesity, alternations in leptin-dependent bone density
<i>Cry1</i>	Systemic KO	Shortening of period in DD	
<i>Cry2</i>	Systemic KO	Lengthening of period in DD	
<i>Cry1/Cry2</i>	Systemic double KO	Arrhythmicity in DD	Impaired body growth; feminized patterns of growth hormone and metabolic genes in liver
Nocturnin	Systemic KO	WT	Resistance to diet-induced obesity, hepatic steatosis, impaired glucose tolerance, increased insulin sensitivity
<i>Bmal1</i>	Liver-specific KO	WT	Resting hypoglycemia, exaggerated glucose clearance

KO, knockout; DD, constant darkness.

Fig. 2.27 Mutations in clock genes lead to metabolic disorders [111].

2.3.1.3 Disturbed feeding-fasting cycles lead to altered clock gene expression

Mutations in clock genes have profound impact on metabolism. But is this link reciprocal? Does the metabolic state impact on clock functioning? We have seen that food is the dominant zeitgeber for peripheral clock. It is thus not surprising that disruptions of the feeding-fasting cycle perturb the proper functioning of the clock. A well-studied disruption of the feeding-fasting cycle is the high-fat diet feeding (HFD), which leads to diet-induced metabolic disorders [89], [71], [36]. Several studies have investigated its effects on the clock. In particular, an *ad libitum* HFD feeding was shown to increase animals free-running period [89]. Indeed, when placed in DD conditions, the mouse circadian period begins to increase after one week of HFD (thus, even before the beginning of gain in body weight). Animals on HFD also show disturbed food intake. Indeed, animals fed on a normal chow diet consume most of their food during the night while food consumption is partially shifted to the light phase for HFD feeding [89]. Accordingly, rhythms in circulating metabolic markers and in neuropeptides controlling the appetite appear to be strongly modified under a HFD. In particular, the rise in free fatty acids levels, which normally occurs during the light phase, is shifted to the dark phase and the levels of leptin (hormone that indicates that fat stores are full) are elevated during the major part of the cycle (see Fig. 2.28) [89].

Moreover, the expression levels of genes involved in both lipid and glucose metabolism are strongly perturbed. Indeed, under a HFD paradigm, the phase and the amplitude of many cycling transcripts are disturbed and some of them do even stop cycling [36]. In particular, a HFD modifies the expression of the core clock genes: a slight phase advance and amplitude reduction is observed compared to the normal chow diet (NCD) (see Fig. 2.29). A strong decrease in the expression of some clock controlled genes such as *Nampt* is also observed. This amplitude reduction can be linked to impaired recruitment of CLOCK-BMAL1 on the promoter of these genes. Normally, the major recruitment of CLOCK-BMAL1 on the promoter occurs between ZT4 and ZT12 [90]. However, expression levels of *Bmal1* are a little bit lower in a HFD feeding between ZT0 and ZT8, probably leading to less accumulation of CLOCK1-BMAL1 between ZT4-ZT12 [36].

Intriguingly, other transcripts only oscillate under HFD [36]. Many of them were shown to be targets of the sensor PPAR γ in the liver. Interestingly, PPAR γ nuclear localization strongly oscillates in HFD. A HFD has thus multiple effects on clock and metabolic pathways. Interestingly, the effect of an *ad libitum* HFD feeding on the clock genes and their outputs is even more marked in the adipose tissue than in the liver [71]. In conclusion, disturbed feeding pattern such as in a HFD thus strongly modify the functioning of local clocks through mechanisms that are still unclear.

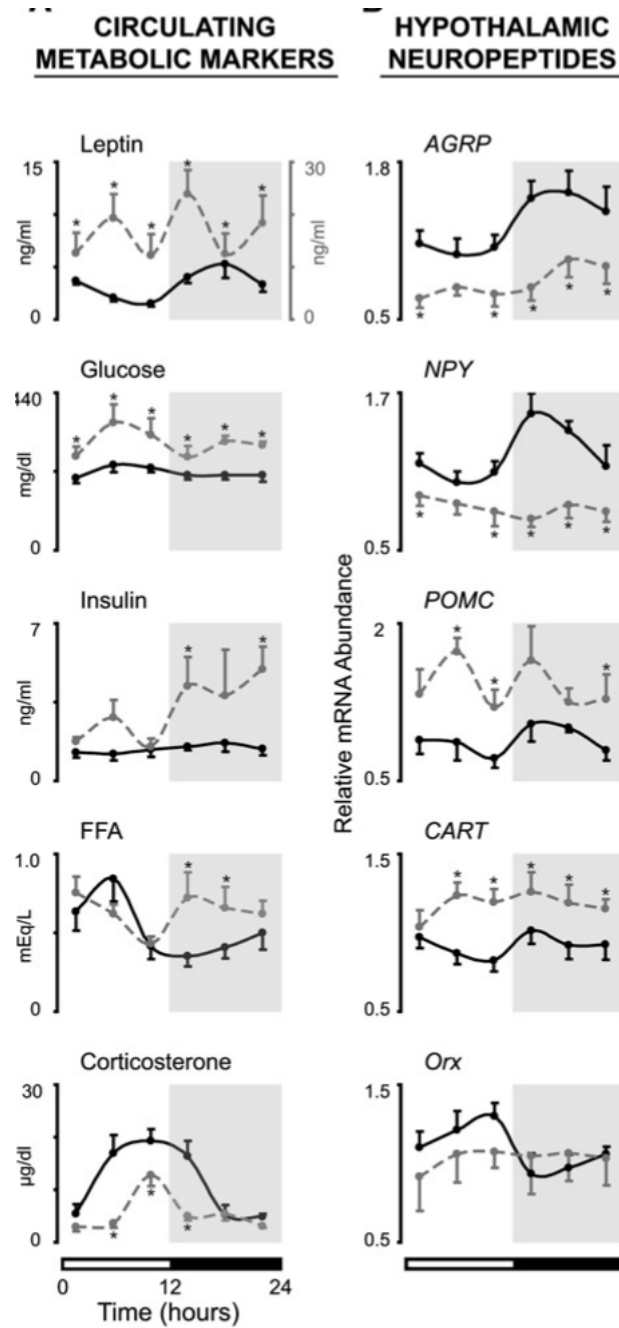


Fig. 2.28 Comparison of the levels of circulating metabolic markers (left column) and hypothalamic neuropeptides (right column) for normal chow (solid lines) and high fat diet (dotted lines) feeding conditions [89].

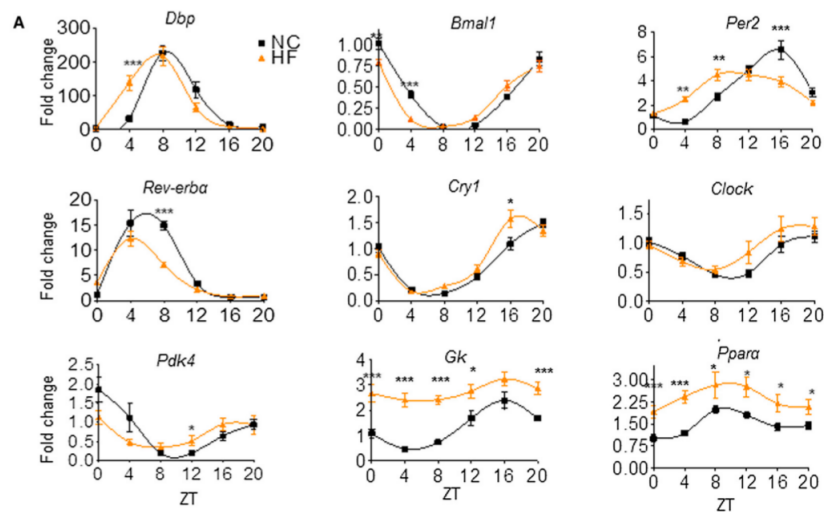


Fig. 2.29 Comparison of hepatic clock gene expression for NCD (black curves) and HFD (orange curves) feeding: HFD feeding modifies clock gene expression [36].

To deepen the understanding of the effect of disturbed feeding patterns on the clock, Panda *et al* carried the following experiment [71]: mice were fed either a HFD or a NCD. In both groups, food access was either *ad libitum* or restricted in time. They are thus four conditions: mice under *ad libitum* (NA) or time restricted (NT) normal chow and mice under *ad libitum* (FA) or time restricted (FT) high fat diet (see Fig. 2.30). Experiments were controlled so that the daily food intake (Kcal/mouse) is the same in the four cases. After several weeks, the mice of the FA group significantly gain weight and display metabolic troubles while the three other groups, including the FT one, remain healthy. Clock gene expression as well as the levels of several metabolites (including AMP and NAD⁺) are decreased for the FA mice. On the other hand, the FT feeding program is able to restore clock genes expression and metabolite levels to amplitude comparable to those of NA and NT animals despite that animals consume a HFD (see Fig. 2.31). This observation clearly points out that not only the quality of a diet but also the timing of food intake matters. A meticulous examination showed that FT condition correlates with increased energy expenditure. It also suggests a correlation between the rescue of clock gene amplitude and protection against diet-induced obesity. It would thus be interesting to test if a pharmacological rescue of clock gene expression after disruption of the feeding-fasting rhythm could cure diet-induced metabolic troubles.

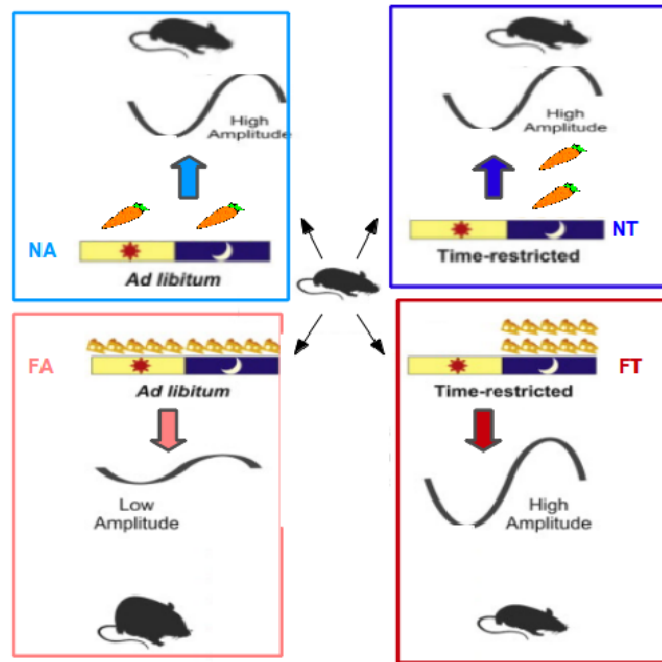


Fig. 2.30 Schematic comparison of four feeding patterns: animals are either fed on a normal chow (NA and NT) or on a high fat diet (FA and FT). In both groups, food access is either ad libitum (NA and FA) or restricted in time (NT and FT) [71].

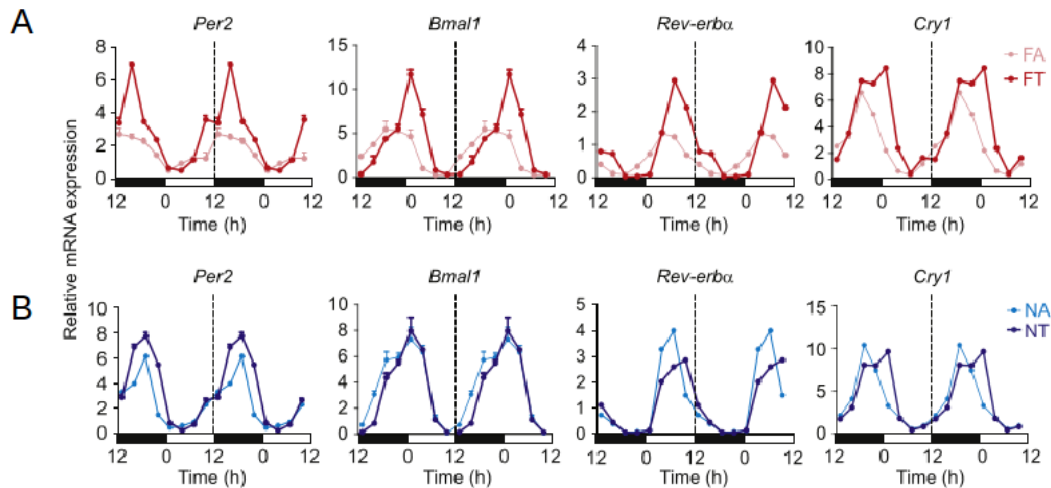


Fig. 2.31 Comparison of hepatic clock gene expression for the 4 feeding patterns. A: FA (pink curves) dampens decreases clock gene expression while FT (red curves) restores physiological amplitudes. B: clock gene expression is similar for NA (light blue curves) and NT (dark blue curves) conditions [71].

2.3.2 Interplay between clock and metabolic pathways at the tissue-level

2.3.2.1 Energy producing processes: Cellular respiration

Catabolic pathways begin with the breakdown of polysaccharides, lipids and proteins respectively into monosaccharides, fatty acids and amino acids. The products of the degradation of the latter (through processes such as glycolysis or fatty acid oxidation) are substrates for the tricarboxylic acid cycle (TCA) [100]. The TCA cycle is a set of oxidation reactions that leads to the reduction of NAD and FAD into NADH and FADH₂. These metabolites are then oxidized and the resulting electrons are transported in a protein complex chain (called electron transport chain) located in the inner membrane of mitochondria. This process is called oxidative phosphorylation and provides the energy needed to synthesise ATP (see Fig. 2.32). This ATP is then used by anabolic reactions to synthesise essential biomolecules. Therefore, the daily alternation between energy-producing and energy-consuming processes is accompanied by daily variations in the ratios AMP/ATP and NAD⁺/NADH. This is confirmed by experimental data showing daily variations in AMP and NAD⁺ time profiles (see Fig. 2.33). Surprisingly, these two profiles are bimodal with one peak in the middle of the rest/fasting phase and a second peak in the middle of the active phase. A possible explanation for the origin of this second peak will be given just below. Interestingly, the oscillations in these metabolites are strongly dampened during an ad libitum HFD feeding [71].

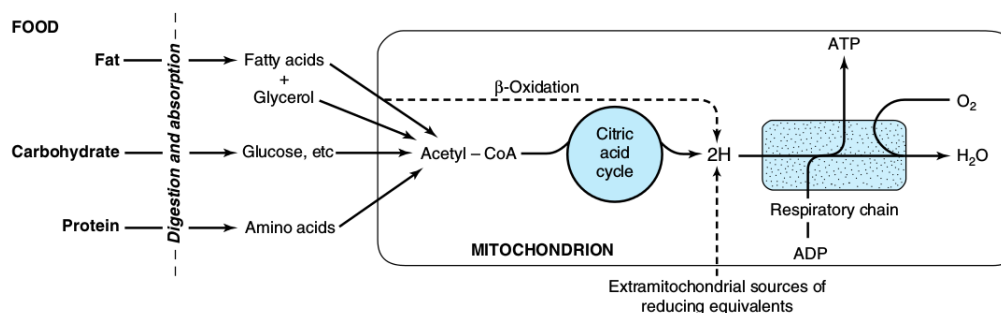


Fig. 2.32 Schematic view of catabolic reactions [123].

Glucose molecules from food are degraded into pyruvate by a mechanism called glycolysis. It occurs in the cytosol and leads to the production of pyruvate. More precisely, glycolysis

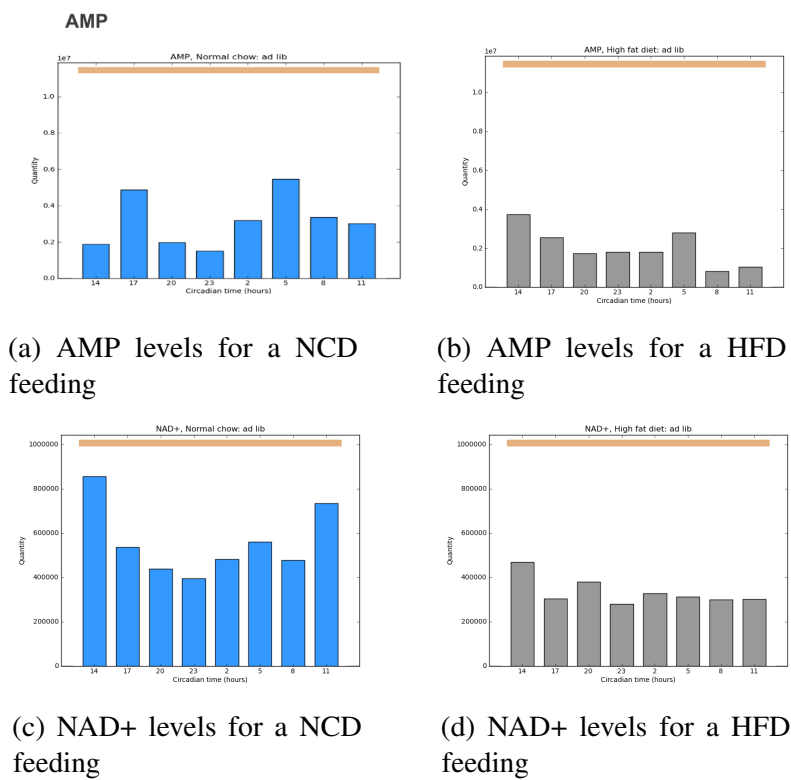


Fig. 2.33 Time profiles of the metabolites AMP and NAD+ [71]

consists in a set of ten reactions that are highly regulated (see Fig. 2.34 and 2.35). Three enzymes are particularly important: glucokinase, phosphofructokinase and pyruvate kinase [67]. Glucokinase catalyzes the transformation of glucose into glucose 6-P (in liver) that is then transformed in fructose 6-P. Phosphofructokinase catalyses the conversion of fructose 6-P into fructose 1,6-bis-P. The final step consists in the conversion of phosphoenolpyruvate in pyruvate and is catalysed by pyruvate kinase. These three enzymes are activated by high glucose condition (fed state) and inhibited during fasting state. In total, glycolysis uses two molecules of ATP and produces 2 NAD⁺, 4ATP and 2 molecules of pyruvate per molecule of glucose. The molecules of pyruvate can then enter the mitochondria to participate to the TCA cycle. Nevertheless, in anaerobic conditions, pyruvate is transformed in lactate and there is no net production of NADH (Fig. 2.36).

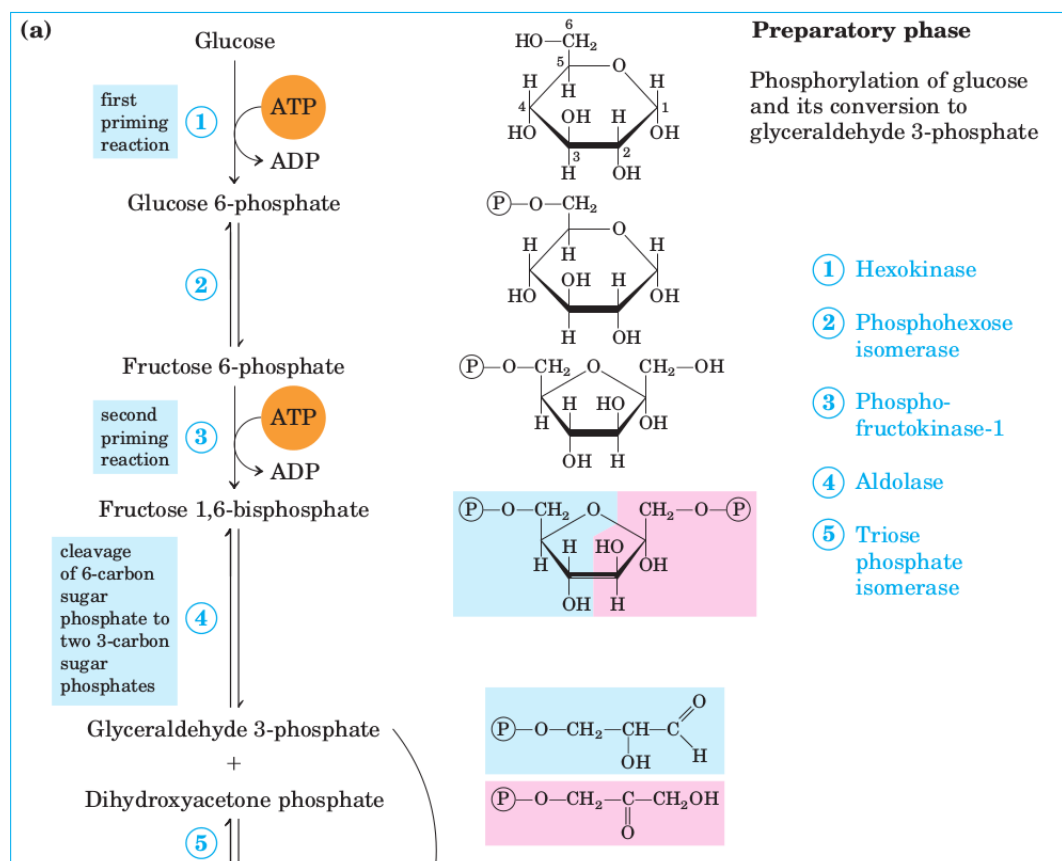


Fig. 2.34 Five first steps of glycolysis [100].

Glucose is the main substrate for cellular ATP production but fatty acids can also be used to generate ATP for the cell during food scarcity. This process is called fatty acid oxidation and corresponds to the degradation of fatty acids into acetyl CoA. For this, long fatty acid

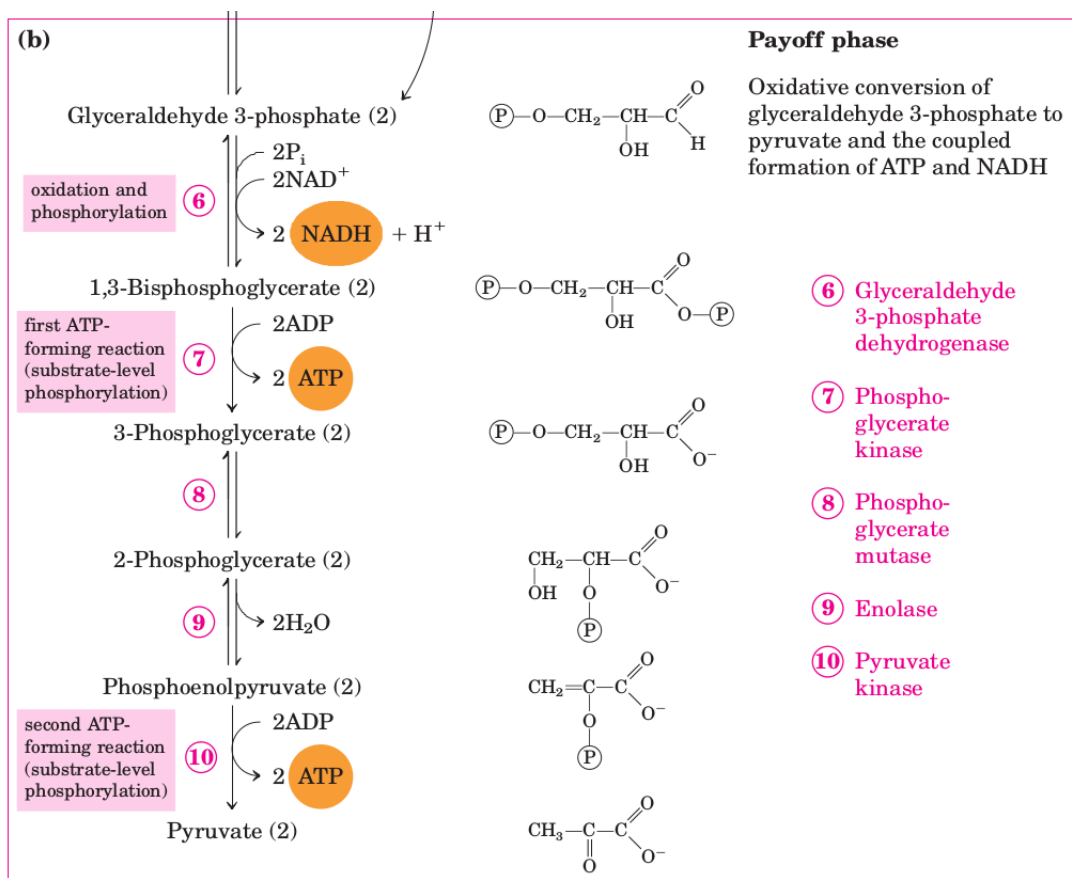


Fig. 2.35 Five last steps of glycolysis [100].

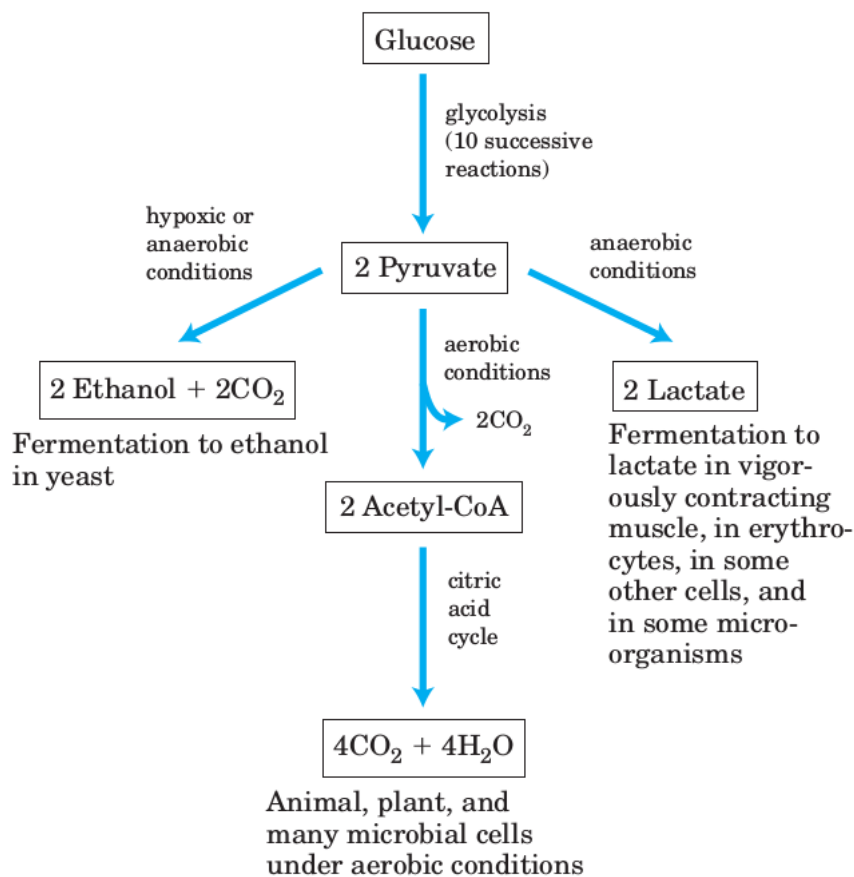


Fig. 2.36 Fates of pyruvate in aerobic and anaerobic conditions [100].

chains have to be translocated in the mitochondria by a carrier called carnitine. Carnitine is a molecule that can be obtained from food. Once in the mitochondrial matrix, the fatty acid chain is reduced in four steps: two oxidations, a hydration and a cleavage by thiolase [67]. This latter reaction releases the acetyl CoA molecule (Fig. 2.39). During these four reactions, molecules of NADH and FADH₂ are also produced. These can then be used to produce ATP by oxidative phosphorylation.

The TCA cycle is the place where the degradation of all carbon molecules from food converges [3]. In particular, pyruvate from glycolysis is converted into Acetyl CoA by a decarboxylation reaction. It is catalysed by the pyruvate dehydrogenase complex [67]. And fatty acids as well amino acids are also converted to Acetyl CoA. The TCA cycle consists in the oxidation of Acetyl CoA in two CO₂ molecules [67]. The complete oxidation of acetyl CoA may need several cycles. The first substrate of TCA cycle is oxaloacetate. Citrate is produced from the condensation reaction between oxaloacetate and Acetyl CoA (Fig. 2.37). At the end of the cycle, oxaloacetate is regenerated. The net gain of the TCA cycle is 3 molecules of NADH, 3 molecules of FADH₂ and one GDP.

These molecules of NADH and FADH₂ will serve to feed the electron transport chain. Indeed NADH and FADH₂ will be oxidized and transfer the electrons to protein complexes located in the inner membrane of the mitochondrion. This process is called electron transport chain. During their transport, electrons are transferred to more electronegative proteins. The final electron acceptor is O₂ that is reduced in H₂O. The energy lost by the electrons during their transport is then used to pump H⁺ ions from the mitochondrion matrix to the inter-membrane space, that is, against the electrochemical gradient. After that, the H⁺ ions spontaneously enter the membrane through H⁺ channels and this gradient constitutes an energy source used by ATP synthase to produce ATP (from ADP and P). On the one hand, more than 30 ATP are produced for the oxidation of one glucose molecule. On the other hand, the oxidation of a fatty acid produces more ATP than the one of a glucose molecule: indeed, for example, the oxidation of a 16 carbons chain such as palmitoyl CoA leads to the production of 129 molecules of ATP [67].

The levels of components involved in both glycolysis and fatty acid oxidation display daily variations. Figure 2.38 shows the time profiles of several glycolytic intermediates. Let us point out that these time profiles are also bimodal with a first peak at the beginning of the active phase (ZT14) and a second one at the end of the active phase (ZT20). Interestingly, the respiratory exchange ratio (RER) also displays a bimodal time profile [166]. The RER measures the ratio of O₂ consumed and CO₂ produced during cellular respiration

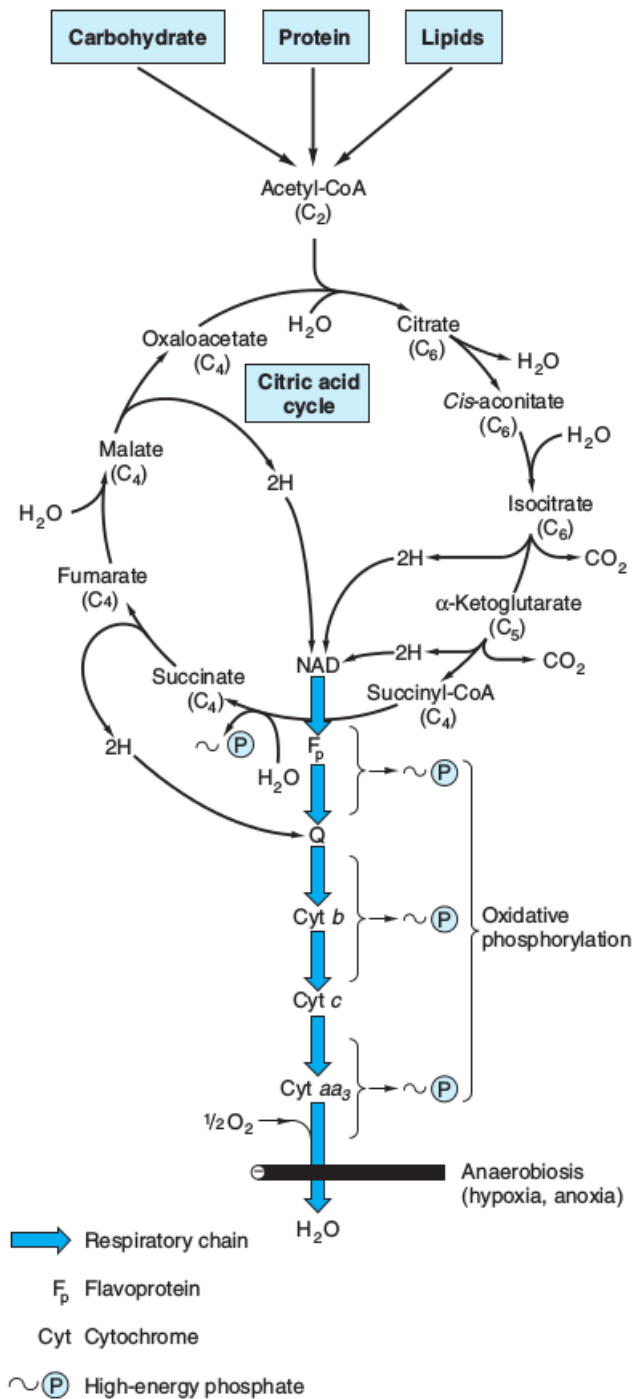


Fig. 2.37 Schematic view of the main steps in the TCA cycle followed by the respiratory chain [123].

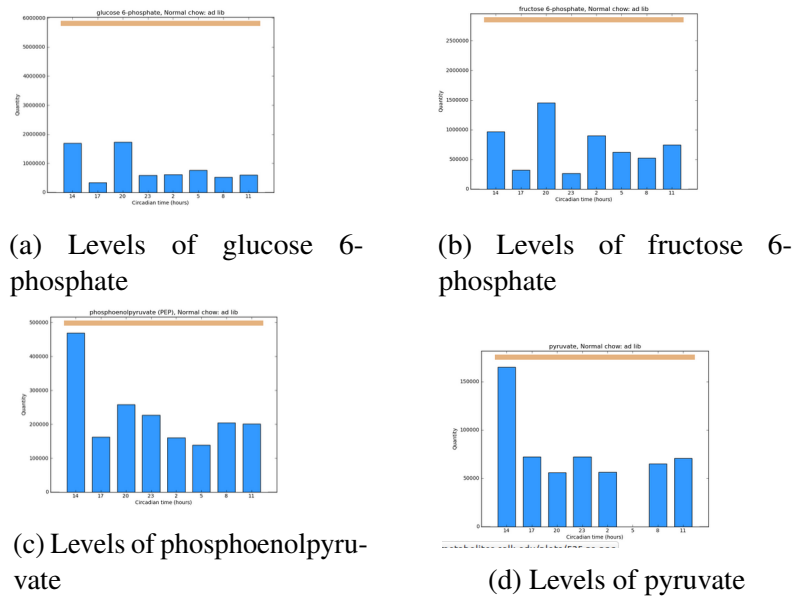


Fig. 2.38 Time profiles of several glycolytic intermediates [71]

and indicates thus which kind of fuel (fat or carbohydrate) is used. A RER around 0.7 indicates that the cell uses fatty acid oxidation to produce ATP while a RER around 1 indicates that cell uses carbohydrate fuel to meet its energy needs. In mice fed ad libitum, the RER displays 2 maxima during the active phase indicating two glycolytic phases during this period.

After a glycolytic period, the ATP production decreases leading to an increase of AMP levels and a resulting increase in the activity of AMPK [56]. This rise triggers fatty acid oxidation leading to ATP synthesis and resulting AMP decrease. As there are two glycolytic phases during the cycle (around ZT14 and ZT20), it logically leads to two AMP peaks a few hours later (ZT17 and ZT5). This could thus explain the bimodal time profile of AMP levels during a healthy feeding schedule (see Fig. 2.33). A healthy meal is composed of a balanced proportion between fat, carbohydrates and proteins while animals fed on a HFD consume a much higher proportion of fat than carbohydrates. Accordingly, the RER of animals fed on ad libitum HFD indicate that they are relying on fatty acid oxidation all day long [71]. This absence of alternation between glycolysis and fatty acid oxidation could explain the loss of rhythms in AMP levels during a HFD feeding (see Fig. 2.33).

2.3.2.2 Energy consuming processes: Storage processes and gluconeogenesis

2.3.2.2.1 Glucose storage and gluconeogenesis

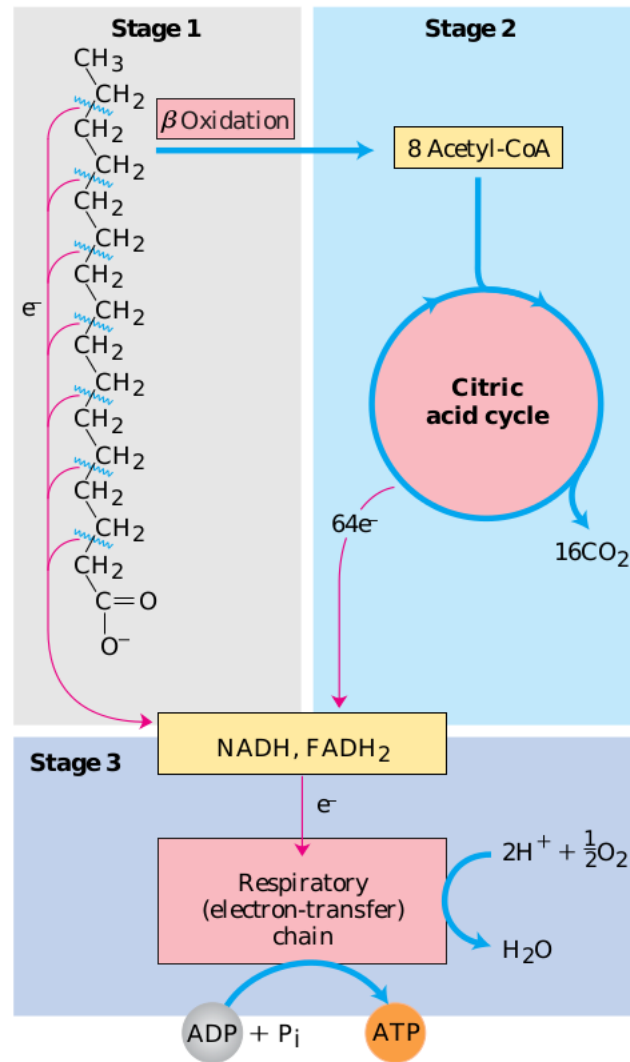


Fig. 2.39 Steps of fatty acid oxidation [100].

The post-absorptive state is an anabolic period where glycogen and fat stores are filled. Glycogen is a polysaccharide formed from alpha-D-glucose in the liver and in resting muscles. This process called glycogenesis occurs in the cytosol in several steps and requires energy in form of ATP and UTP (uridine triphosphate) [67]. It is catalysed by the enzyme glycogen synthase. These stores can be depleted through a process called glycogenolysis. Glycogenolysis is promoted by glycogen phosphorylase. Muscle stores are primarily depleted during exercise to meet muscle ATP needs. On the other hand, hepatic glycogen is mobilized during fasting periods and exported in the blood stream to maintain plasma glucose levels nearly constant.

Once hepatic glycogen stores are empty, the liver will rely on gluconeogenesis to synthesize and export glucose in the blood stream. Gluconeogenesis generates glucose from pyruvate by using several reactions common to glycolysis (in the opposite direction). However, glycolysis is not totally reversible. Indeed, only seven of the ten glycolytic reactions are reversible. Therefore, gluconeogenesis consists in seven reactions common to glycolysis plus four reactions unique to gluconeogenesis [67]. First, pyruvate is converted in oxaloacetate that is transported in the cytosol (see Fig. 2.41). There, it is converted in phosphoenolpyruvate. This step is regulated by the enzyme phosphoenolpyruvate carboxykinase (PEPCK) and is specific to gluconeogenesis. The next steps are just reversed glycolysis reactions. There are also two specific reactions at the end of the pathway: fructose 1,6 bis-phosphate is converted in fructose 6-P and this is catalysed by fructose 1,6 bis-phosphatase. And finally glucose 6-P is transformed in glucose by glucose 6-phosphatase. Gluconeogenesis can use several precursors. One of them is lactate produced by muscles during exercise that is reconverted in pyruvate. Furthermore, degradation of lipid stores releases glycerol that can be converted in an intermediate of gluconeogenesis. Finally, alpha-keto acids resulting from degradation of amino acids can be used to form oxaloacetate. Gluconeogenesis is an energy consuming process requiring 4ATP, 2GTP and 2 NAD⁺ for the production of one molecule of glucose. Glucagon, a pancreatic hormone secreted during fasting, promotes gluconeogenesis. In particular, the binding of glucagon to G-protein coupled receptors triggers an increase of intracellular cyclic adenosine monophosphate (cAMP). The production of this second messenger leads to the phosphorylation of cAMP response element-binding protein (CREB). In turn, the phosphorylated CREB activates the transcription of its gluconeogenic target genes. Those include *G6pc* and *Pck1* coding for the rate limiting enzymes glucose 6-phosphatase and PEPCK (Fig. 2.41) [67]. All this signalling cascade is gated by the clock. Indeed, a study has investigated the effect of the exogenous administration of glucagon at different times of the day for fasted mice: at ZT22-01 (transition active-inactive phase) and at ZT10-13 (transition inactive-active phase) [179]. It shows that glucagon can induce the phosphorylation of CREB

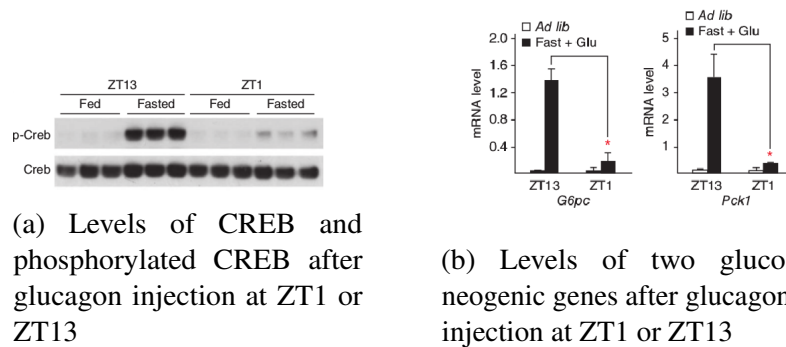


Fig. 2.40 Effect of glucagon injection at different times for fasted animals [179]

and the transcription of its gluconeogenic targets 40 folds better around ZT10-13 than around ZT22-01 suggesting that this process could be controlled by the clock (see Fig. 2.40). Further investigations have shown that the protein CRY1 periodically inhibits the cAMP signalling, thereby gating the cell sensitivity to glucagon to the appropriate time of the day (that is the transition inactive/active phase) [179]. This regulation of gluconeogenesis by the clock could explain the fasting hypoglycemia observed after a liver specific *Bmal1* knockdown [98]. Normally, CRY1 levels decrease at the beginning of the fasting period, thereby de-repressing the transcription of gluconeogenic genes and enabling the increase of glucose synthesis and its export. Nevertheless, Liver-specific *Bmal1* deficiency leads to constantly high *Cry1* expression which probably impinges gluconeogenesis and glucose export [98].

2.3.2.2.2 Fat storage

Lipids from meals are mainly triacylglycerol (TAG) which are esters formed by 3 fatty acids and a molecule of glycerol. During the post-absorptive period, TAG are stored in adipocytes as fat droplets. Furthermore, glucose and amino acids in excess after a rich meal can also be converted in fatty acids [67]. This energy-demanding process is called *de novo* fatty synthesis: long fatty acid chains are formed with carbons from Acetyl CoA [67]. The first step is the synthesis of Acetyl CoA from pyruvate in the mitochondrial matrix. Nevertheless, acetyl CoA is not able to cross the inner mitochondrion membrane. It is therefore converted into citrate, that is then exported to the cytosol where it is cleaved to form acetyl CoA. The rest of the *de novo* synthesis occurs in the cytosol. In the remaining steps, carbons from acetyl CoA are transferred to a growing fatty acid chain. The rate limiting step is the carboxylation of acetyl CoA to malonyl CoA. It is catalysed by acetyl CoA carboxylase 1 (ACC1). ACC is activated by the pancreatic hormone insulin after a rich meal and inhibited

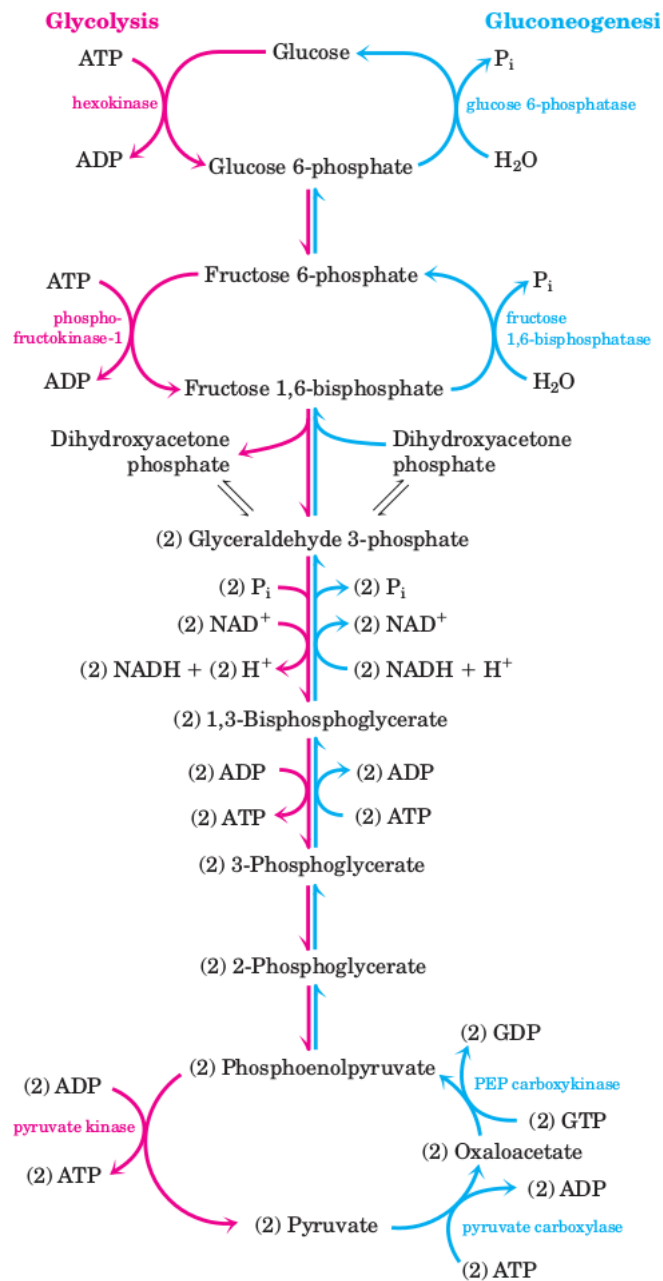


Fig. 2.41 Steps of gluconeogenesis [100].

by the nutrient sensor AMPK and glucagon during fasting periods. These newly formed fatty acids are finally converted into TAG. TAG are exported from the liver and delivered to other tissues as lipoproteins, and can be used to build cell membranes or be stored in the adipose tissue. During fasting periods, these TAG will be degraded to serve as energy source (fatty acid oxidation). During this low-energy phase, the nutrient sensor AMPK inactivates ACC to prevent fatty acid synthesis. Conversely, Malonyl CoA inhibits CPT-I during the feeding phase to prevent the entry of fatty acids into the mitochondria to be oxidized [67].

2.3.2.3 The nutrient sensors and their interactions with the clock

In order to enable a precise balance between energy intake, energy consumption and energy storage, the coordination between catabolic and anabolic processes is highly regulated. In particular, the pancreatic hormones insulin and glucagon play an important role by stimulating glucose-consuming and glucose-producing respectively to maintain blood glucose homeostasis. At the cellular level, the effect of these cues is often mediated by receptor binding which triggers signalling cascades involving second messengers (PIP3 for insulin, cAMP for glucagon) [67]. There, these cascades also interact with nutrient sensors regulating energy homeostasis at the cell-autonomous level [62]. After a rapid overview of the roles of nutrient sensors as metabolic actors, the next section will review their interplay with the clock machinery.

2.3.2.3.1 AMPK

2.3.2.3.1.1 AMPK as a nutrient sensor

AMPK is a kinase that is involved in nutrient sensing at the cellular level. AMPK is composed of several subunits: catalytic α subunits and regulatory subunits β and γ [63]. Seven genes are coding for AMPK subunits and there are thus several isoforms for each subunit. The γ subunits contain four adenine nucleotide-binding sites. Site 4 only binds AMP, sites 1 and 3 can competitively bind AMP, ADP and ATP while site 2 stays empty [63]. The binding of AMP increases the activity of the kinase when energy stores are depleted. The α subunits contain a serine/threonine kinase domain and AMPK can only be activated when a specific threonine residue (Thr 172 for humans) is phosphorylated by some kinases. The major kinase involved in this phosphorylation is the liver kinase B1 (LKB1) [61]. Early studies suggested that LKB1 is constitutively active but recent developments have shown that there is a deacetylation mechanism enhancing LKB1 activity (see below) [99]. Besides the

calmodulin-dependent protein kinase (CaMKKb), that is activated by Ca^{2+} release, can also phosphorylate AMPK in some cellular types (neurons) [61] and TAK1 also phosphorylates the threonine residue when induced by cytokines [61].

It is important for cells to keep high ATP levels to meet their energy needs. In particular, this is achieved thanks to the reaction $2\text{ADP} \rightleftharpoons \text{ATP} + \text{AMP}$ that is catalysed by adenylate kinase [61]. Indeed, when starvation or stress conditions disrupt catabolic ATP-producing pathways, this reaction is pushed to the right, which increases AMP levels. This activates AMPK which restores catabolic processes and shuts down anabolic ATP-consuming pathways.

The binding of AMP to AMPK increases the activity of the kinase through several mechanisms [56]. First, it enhances LKB1-mediated phosphorylation. Interestingly, it does not seem to promote CaMKKb-mediated phosphorylation. Secondly, AMP inhibits the dephosphorylation (and thus desactivation) of AMPK by phosphatases. Finally, as AMPK is an allosteric enzyme, AMP can also allosterically activate AMPK (see Fig. 2.44). These three mechanisms are summarized in Fig. 2.43. The comparison between the effect of AMP and ADP on the phosphorylation of AMPK have shown that AMP and not ADP is the true physiological activator of AMPK [56].

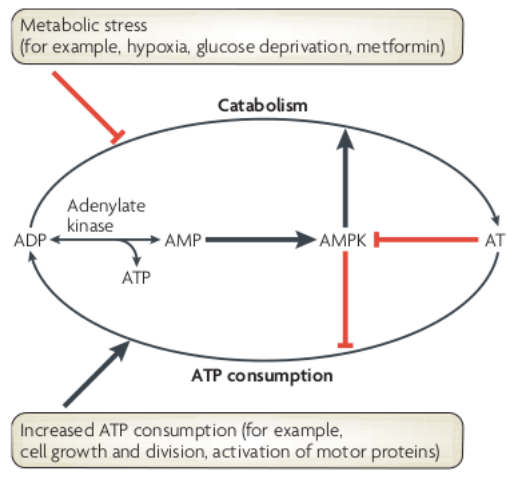


Fig. 2.42 Scheme of AMPK activation mechanism. Under stress conditions, low AMP levels activate AMPK. AMPK then switches off anabolic energy consuming pathways and restores catabolic ATP producing pathways. This increases ATP levels which inactivates AMPK [60].

AMPK activates energy-producing processes and inhibits energy-consuming ones during low energy periods [62]. In peripheral tissues such as the liver, it regulates both glucose and lipid metabolism (see Fig. 2.45). First, it favours glycolysis by activating 6-phosphofructo-2-kinase [178]. Furthermore, it inhibits both glycogen synthesis and gluconeogenesis. In

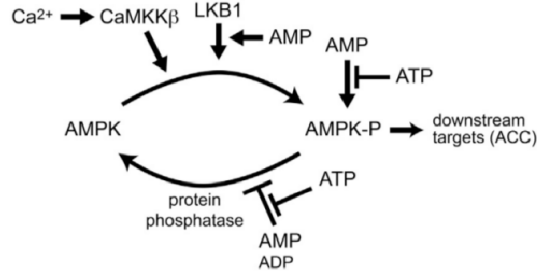


Fig. 2.43 Schematic view of AMPK regulation by adenine nucleotides [56].

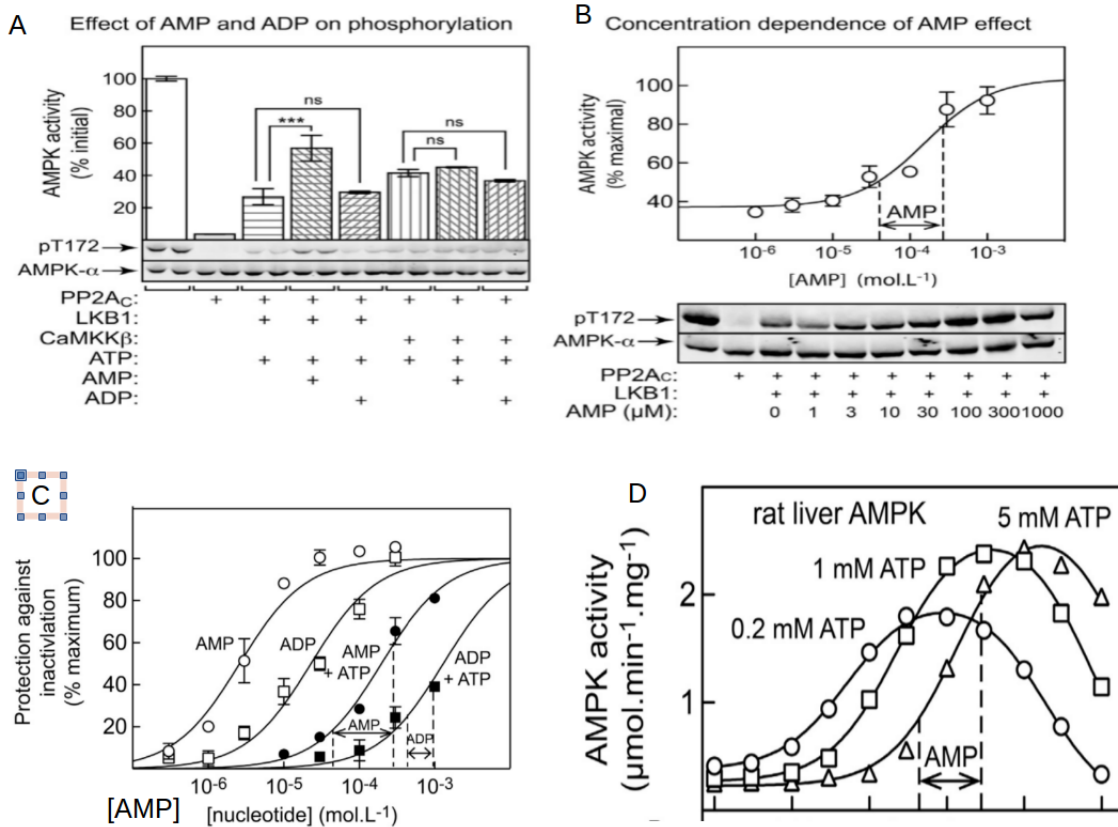


Fig. 2.44 AMP promotes AMPK activation through three mechanisms: it enhances the effect of LKB1-mediated phosphorylation (A and B), it inhibits AMPK dephosphorylation by phosphatases (C) and it also activates AMPK on its allosteric sites (D) [56].

skeletal muscle, it also promotes glucose uptake by the transporter GLUT4 [61]. Besides regulating glucose metabolism, AMPK also prevents fatty acid synthesis during fasting periods by inactivating one isoform of acetyl-CoA carboxylase (ACC1). Conversely, it induces fatty acid oxidation by the following mechanism: it prevents the synthesis of malonyl CoA (by inactivating ACC2) which leads to the activation of the enzyme CPT-I [178]. This enables the transport of long fatty acid chain from the cytosol to mitochondria and their subsequent oxidation in the TCA cycle [67]. Moreover, AMPK also limits cell proliferation: it inactivates the mTOR complex-1 (TORC1) that controls protein synthesis and thereby promotes cell growth. It leads to activation of the transcription factor Pgc1- α which in turn activates target genes involved in mitochondrial biogenesis [178].

The activity of AMPK itself is also regulated by several cues: for instance, the hormone adipokine, that is secreted by adipose tissue when energy stores are depleted, can activate hypothalamic AMPK, thereby inducing food intake [62].

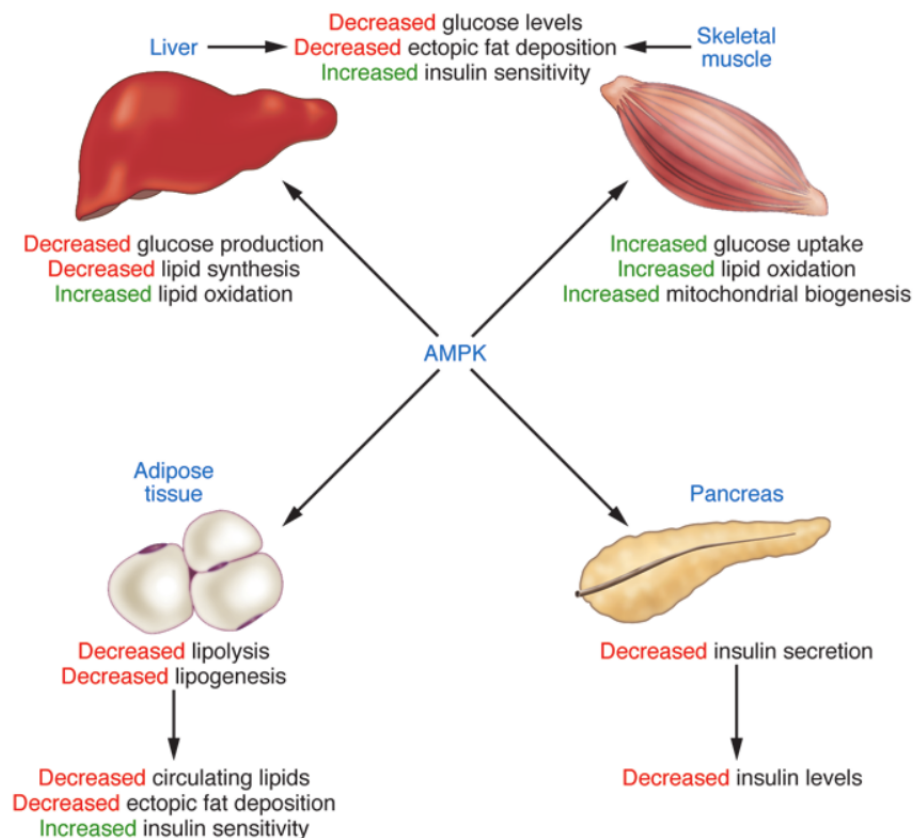


Fig. 2.45 Roles of AMPK in four major metabolic tissues [107].

2.3.2.3.1.2 AMPK and the clock

The nutrient sensor AMPK also has several crosstalks with the clock. More specifically, AMPK has been shown to destabilize the protein CRY1 by phosphorylation [83]. In fact, CRY1 possesses two serine sites (S71 and S280) and their phosphorylation mediated by AMPK promotes the interaction between CRY1 and the protein FBXL3. The binding between CRY1 and FBXL3 favours CRY1 degradation [97]. Experiments using MEFs show that administration of the pharmacological AMPK activator AICAR (5-aminoimidazole-4-carboxamide ribonucleoside) increases clock gene expression (see Fig. 2.46). This effect is lost in AMPK mutants. Limiting the availability of glucose in the culture medium has effects on clock gene expression that are similar to those of AICAR injection (see Fig. 2.46). This suggests that the effects of glucose limited availability on the clock are mediated through AMPK. This reinforces the idea that AMPK relays informations about nutrient availability to the clock [97].

As AMPK seems to be the mediator between the feeding-fasting cycle and the clock, it is thus not surprising that its activity and its localization are cycling. Not only AMP levels appear to be cycling but also the expression of AMPK β 2 subunit is circadian (see Fig. 2.47.A). As the β 2-subunit controls the kinase localization, it allows a time-dependent localization of AMPK. Furthermore, the accumulation of the catalytic subunits AMPK α 1 in the nucleus exhibits a circadian profile with a maximum accumulation around ZT8. This correlates with a minimum concentration of the protein CRY1 at this time (see Fig. 2.47.B). Interestingly, the effects of mutations of AMPK catalytic subunits appear to be highly tissue-specific [163]. Other studies have investigated the effect of the knockdown of LKB1 leading to a loss-of-function of AMPK: the liver-specific LKB1 knockdown decreases clock gene expression [97]. AMPK not only induces CRY1 degradation: it has also been shown that the kinase promotes PER degradation by phosphorylating CKI [164].

2.3.2.3.2 Sirtuins

2.3.2.3.2.1 Sirtuins as nutrient sensors

Sirtuins are also important sensors of cellular energy status. Mammalian sirtuins are a family of seven members. They are orthologs of the yeast protein Silent information regulator 2 (Sir2) that is involved in responses to caloric restriction and longevity. The seven mammalian sirtuins are different as regards their functions and their cellular localization. SIRT1, 6 and 7 are mainly located in the nucleus while SIRT3, 4 and 5 act in the mitochondria and SIRT2 in the cytoplasm. They can have different modes of action but most of them are

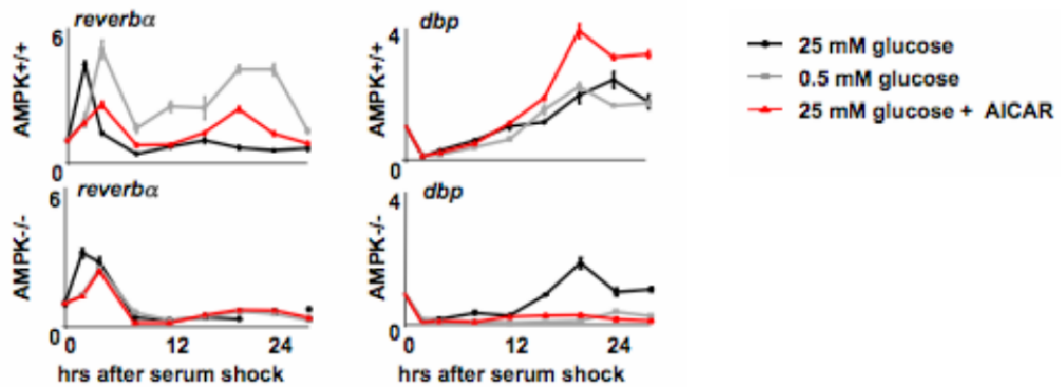


Fig. 2.46 Effect of AICAR administration on clock gene expression: AICAR injection increases clock gene expression (red curve). Limiting the glucose in the culture medium also increases clock gene expression (grey curve). These effects are lost in AMPK mutants [97].

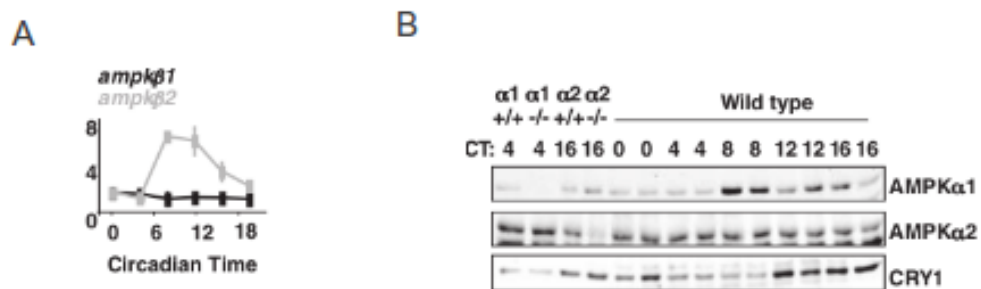


Fig. 2.47 Circadian rhythms in the localization and in the activity of AMPK: (A) The expression of the AMPK β 2 subunit is circadian. (B) The accumulation of the catalytic subunit AMPK α 1 in the nucleus exhibit a circadian profile [97]

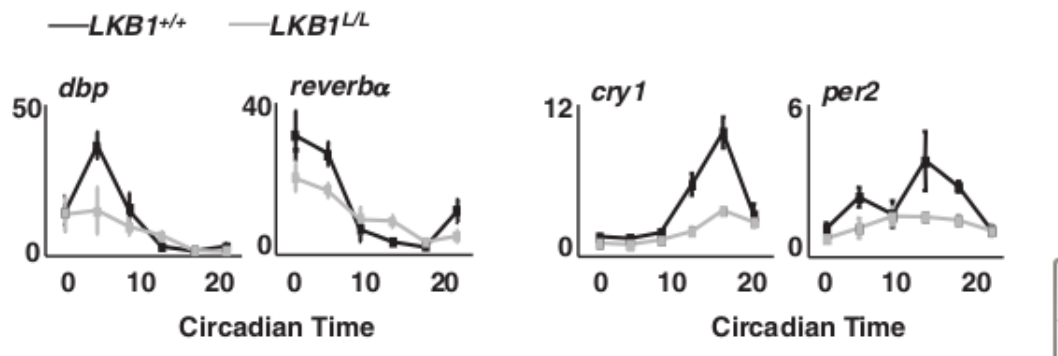


Fig. 2.48 The knockout of the kinase LKB1 decreases clock gene expression in the liver [97].

NAD⁺-dependent deacetylases: they deacetylate both histones and non-histone proteins in the presence of NAD⁺. The by-product of these deacetylation reactions are nicotinamide (NAM) and acetyl-ADP-ribose (resulting from the transfer of the acetyl group of the substrate target to the ADP-ribose group from NAD⁺) [37]. The activity of sirtuins is thus mainly regulated by NAD⁺ availability.

NAD⁺ can be synthesized through different pathways (see Fig. 2.49) [153]. In the NAD⁺ salvage pathway, NAD⁺ is obtained from nicotinamide (NAM) that is a by-product of vitamin B3: in the presence of the rate limiting enzyme NAMPT, NAM is converted into nicotinamide mononucleotide (NMN), which is in turn converted into NAD⁺ through adenylation by nicotinamide mononucleotide adenylyl transferase (NMNAT) [153]. Interestingly, high concentrations of NAM inhibit SIRT1 activity. Secondly, NAD⁺ can also be obtained from nicotinic acid (NA): an enzyme transforms NA into nicotinic acid mononucleotide (NaMN), which is then adenylated and amidated to obtain NAD⁺. Another route is the multi-step conversion of the amino acid tryptophan in NaMN, the latter being then adenylated and amidated such as in the NA pathway. Finally, nicotinamide riboside (NR) can also be converted into NMN by nicotinamide riboside kinase and the end of the pathway leading to NAD⁺ synthesis is similar to the salvage pathway.

SIRT1 is the most studied member of the sirtuin family. SIRT1 activity increases during fasting when NAD⁺ levels are high and it modulates both lipid and glucose metabolism [77]. More precisely, it enhances gluconeogenesis during long-term fasting: when glycogen stores are depleted, gluconeogenesis is first notably activated by CREB and its partner CRTC2. SIRT1 then deacetylates and thus deactivates CRTC2 which switches off the transcription of gluconeogenesis genes [23]. In parallel, SIRT1 activates the transcription factor PGC1 α which switches gluconeogenesis [23]. On the other hand, SIRT1 also increases fatty acid oxidation by activating the nuclear receptor PPAR α . Furthermore, it limits lipid and cholesterol synthesis as well as their storage. Inhibition of lipogenesis is achieved by

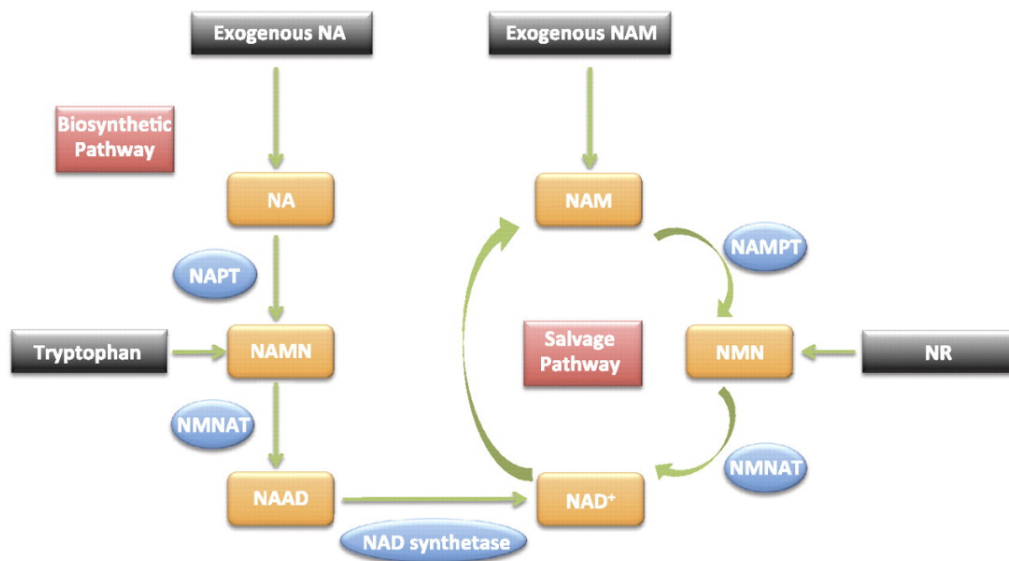


Fig. 2.49 Four different pathways can lead to NAD⁺ synthesis: NAD⁺ can be synthesized from tryptophan, nicotinic acid (NA), nicotinamide riboside (NR) and from nicotinamide (NAM) [170].

targeting SREBP1c and decreased lipid storage results from the SIRT1 mediated deactivation of the nuclear receptor PPAR γ . Another substrate of SIRT1 is the tumor suppressor protein p53 and overexpression of SIRT1 appears to stop tumour formation [23]. Last but not least, as NAD⁺ levels decrease with age, SIRT1 activity is likely to play a role in the ageing process.

2.3.2.3.2.2 SIRT1 and the clock

The NAD⁺ required for SIRT1 activity can be synthesized through several routes, one of them being the NAD⁺ salvage pathway whose rate limiting enzyme is NAMPT. Interestingly, the levels of *Nampt* mRNA are controlled by the clock: *Nampt* transcription is periodically activated by CLOCK-BMAL1 [141]. The mRNA is then translated into the protein NAMPT that periodically enhances the NAD⁺ salvage pathway (see Fig. 2.50). Accordingly, both *Nampt* and NAD⁺ levels are strongly decreased after a mutation of the positive arm of the clock (*Bmal1* KO) (see Fig. 2.51). On the other hand, mutations of the negative arm (*Cry1/Cry2* KO) increase *Nampt* and NAD⁺ levels [141]. We have to note that *Nampt* mRNA displays a circadian profile (one peak during the active phase) while NAMPT protein and NAD⁺ levels display a bimodal profile with one peak during the active phase (consistent with the one of *Nampt* mRNA) and one additional peak during the rest phase (see Fig. 2.50). We will propose an hypothesis to explain this second peak in section 2.3.2.3.3.1.

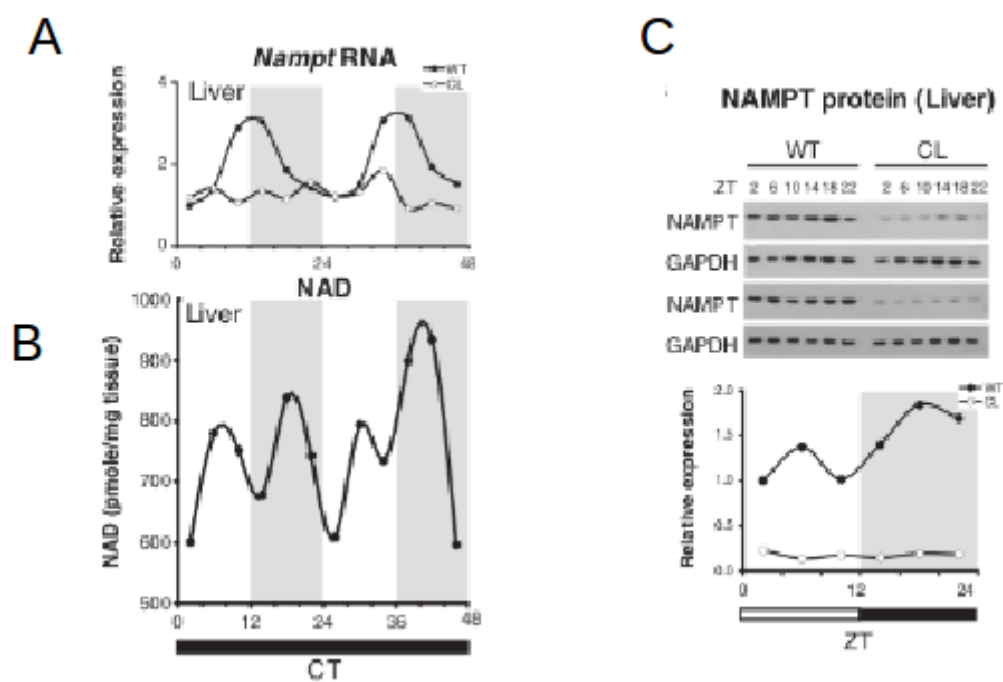


Fig. 2.50 *Nampt* gene expression profile is circadian (A) while the time profiles of NAMPT protein and NAD⁺ levels are bimodal (B and C). Curves with filled circles: WT mice; curves with open circles: *Clock*^{Δ19} mutant mice [141].

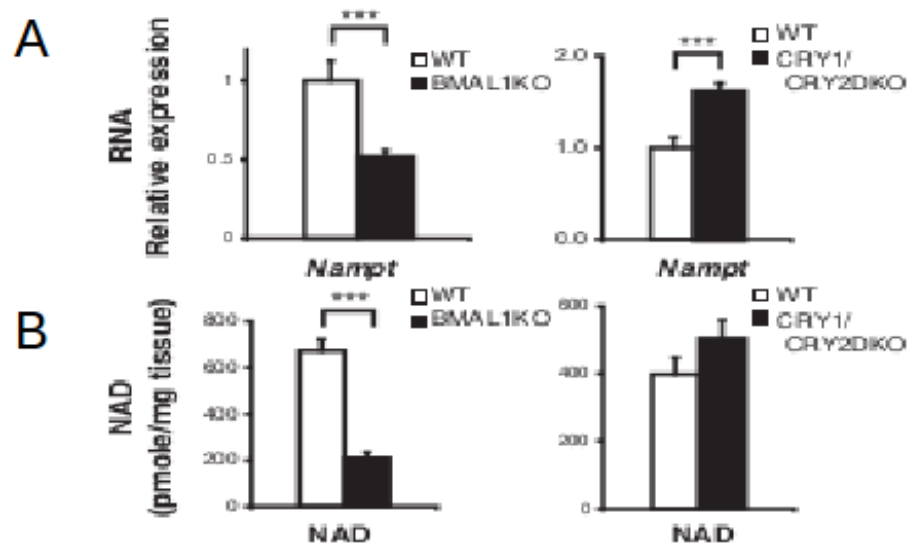


Fig. 2.51 Effect of clock mutations on *Nampt* mRNA (A) and NAD⁺ (B) levels: a knockout of elements of the positive limb of the clock (*Bmal1*^{-/-}) decreases *Nampt* expression and NAD⁺ levels while a knockout of elements of the negative limb increases *Nampt* and NAD⁺ levels [141].

As SIRT1 depends on NAD⁺ for its deacetylase activity, it is likely that SIRT1 activity is also cycling. Indeed, SIRT1 activity profile is circadian with a peak around ZT15, thus in the middle of the night [124]. This peak is consistent with the night peak in NAD⁺ time profile [141]. While activity of SIRT1 is cycling, its mRNA levels are constant (see Fig. 2.52). According to some experiments, its total protein levels are also cycling [7]. The effect of a SIRT1 knockout modifies clock gene expression but seems to be very tissue-dependent. On the one hand, in MEFs, a downregulation of SIRT1 leads to decreased clock gene expression (see Fig. 2.54) [7]. On the other hand, clock gene expression is increased after a knockout of *Sirt1* in the liver (see Fig. 2.53) [124]. This is in agreement with the fact that SIRT1 activators decrease clock gene expression while SIRT1 inhibitors (NAM and splitomicin) enhance clock gene expression in the liver [14].

SIRT1 has several actions on the clock: on the one hand, it deacetylates histones H3 [124]. Indeed, H3 acetylation levels vary periodically and these variations are lost for SIRT1^{-/-} mutants [124]. On the other hand, SIRT1 also deacetylates BMAL1 which is thought to favour the binding of the repressor complex PER-CRY on E-boxes, leading to the onset of a repressive state [12], [124]. The deacetylation activity of SIRT1 thus counteracts

CLOCK HAT (histone acetyltransferase) activity. Besides SIRT1 also appears to periodically deacetylate the protein PER2 thereby modifying its stability [7].

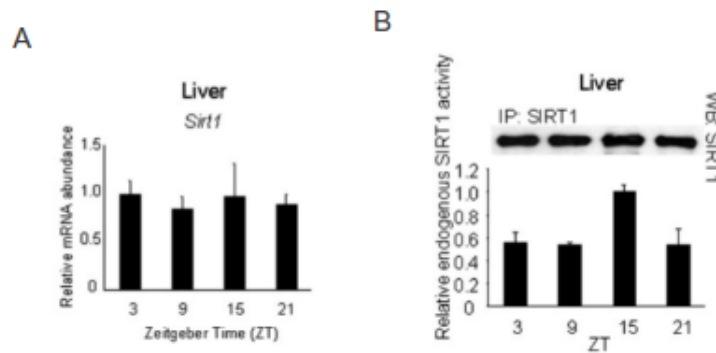


Fig. 2.52 Sirt1 expression is constant (A) while the activity of SIRT1 protein is circadian (B) [124].

Another important target of SIRT1 is the transcription factor Pgc1- α . To be active, Pgc1- α needs to be phosphorylated by AMPK and deacetylated by SIRT1 [127]. Interestingly, both its mRNA and its protein exhibit a circadian rhythm in expression (see Fig. 2.57) [105]. However, there are currently no data indicating that *Pgc1- α* transcription is under the direct control of the clock machinery. Rhythmicity in *Pgc1- α* expression is more likely due to periodic food intake [73]. Pgc1- α has multiple target genes including the clock gene *Bmal1* [105]: PGC1- α activates the transcription of *Bmal1* in synergy with ROR(α , γ) (see Fig. 2.55). Indeed, *Bmal1* transcription is enhanced in the presence of both ROR(α , γ) and PGC1- α while the knockout of PGC1- α decreases *Bmal1* expression levels (see Fig. 2.57). *Pgc1- α* null animals also exhibit an increased free running period and a disturbed body temperature profile [105]. PGC1- α probably activates *Bmal1* transcription by chromatin modifications: indeed, immunoprecipitation experiments indicate that PGC1- α induces histone H3 deacetylation leading to a transcriptionally active state [105].

2.3.2.3.2.3 SIRT3 and the clock

The role of CLOCK-BMAL1 in NAD⁺ biosynthesis suggests that metabolic cycles are not only driven by the feeding-fasting cycle but also by the clock. This is highlighted by the fact that rhythms in fatty acid oxidation and glycolysis persist in fasted animals [134]. Bass

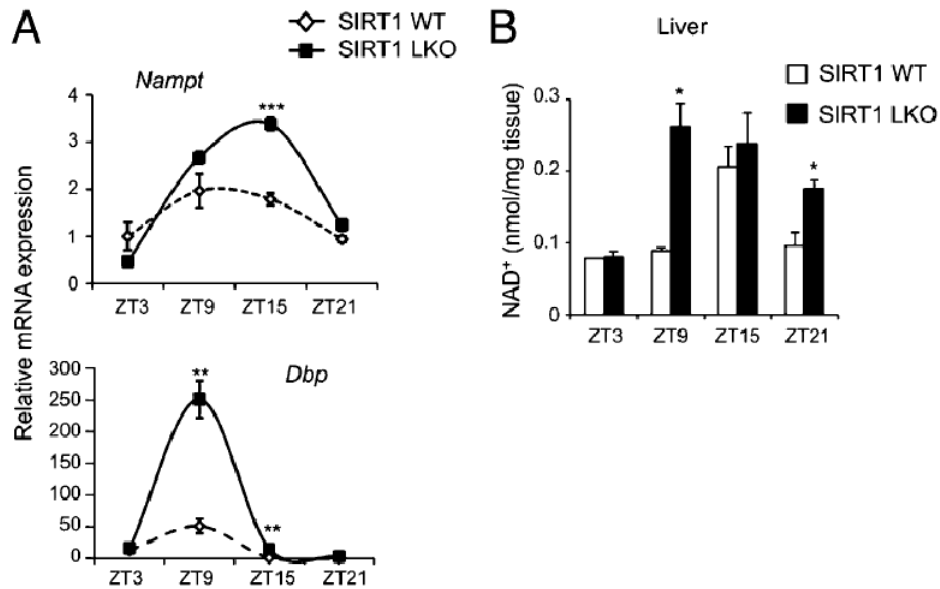


Fig. 2.53 Clock gene expression (A) and NAD⁺ levels (B) are increased in liver-specific *Sirt1*^{Δex4} mice. [14].

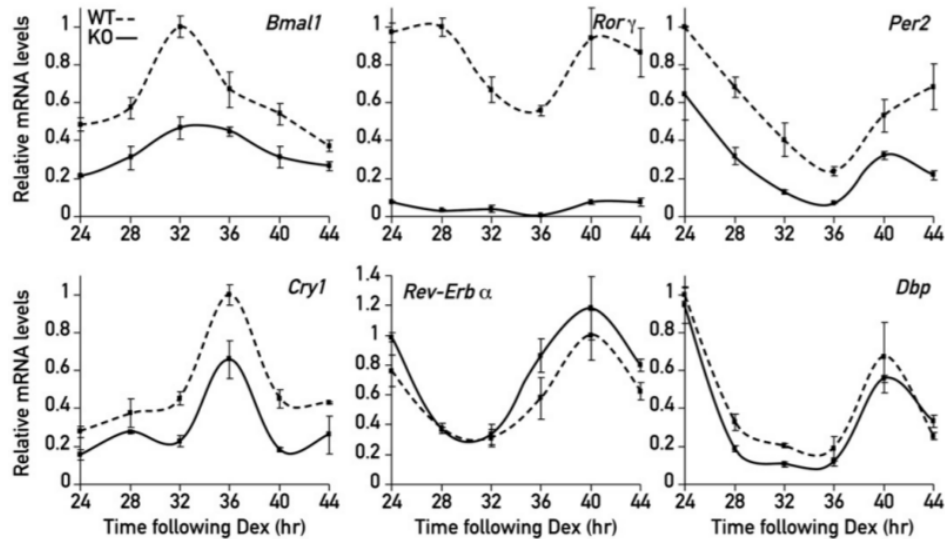


Fig. 2.54 SIRT1 knockdown decreases clock gene expression in MEFs with the exception of Rev-Erb α expression [7].

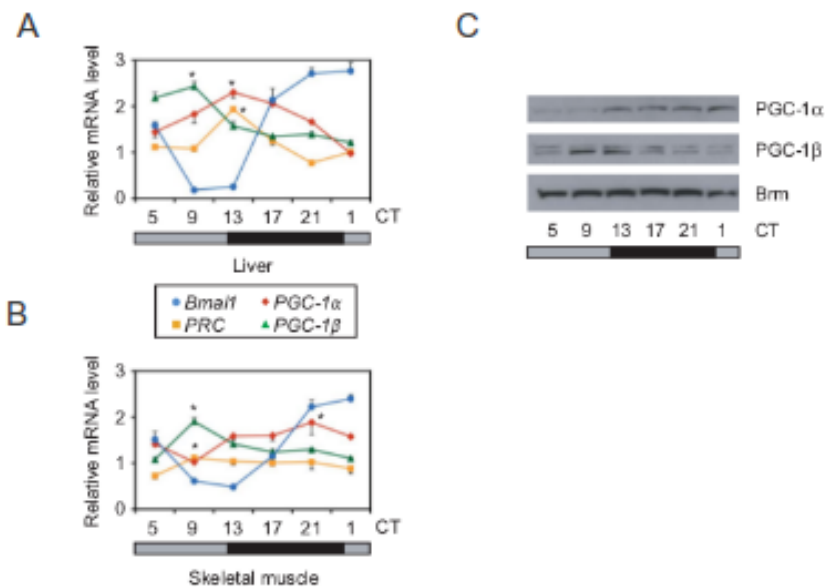


Fig. 2.55 The expression of PGC1- α as well as those of its partners PGC1- β and PRC is circadian in the liver (A) and in the skeletal muscle (B). The accumulation of the proteins PGC1- α and PGC1- β is also rhythmic in liver nuclear extracts (C) [105].

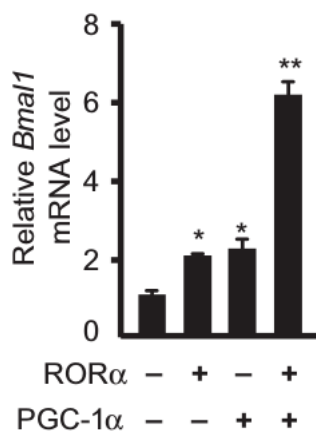


Fig. 2.56 PGC1- α activates *Bmal1* transcription in synergy with ROR- α [105].

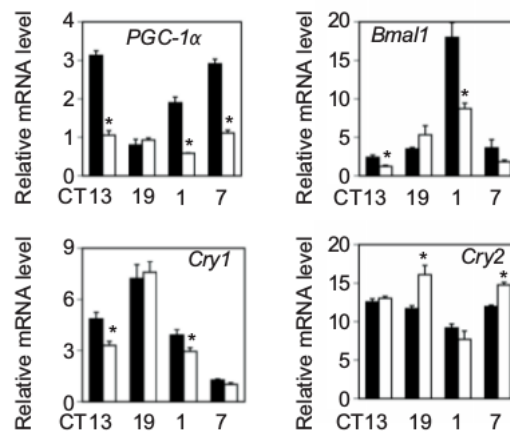


Fig. 2.57 In the liver, a knockdown of PGC-1 α disturbs clock gene expression. WT mice: filled boxes. Pgc1- α null mice: empty boxes [105].

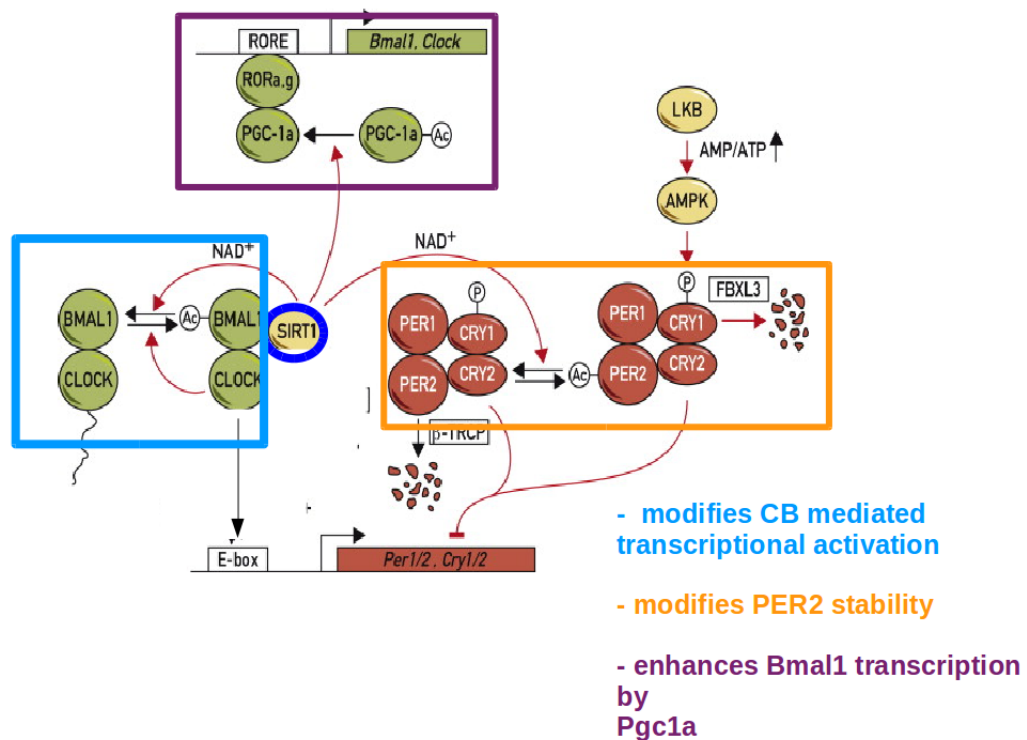


Fig. 2.58 Summary of the different actions of SIRT1 on the clock: SIRT1 deacetylates BMAL1, PER2 and PGC1- α . Adapted from [8].

et al have shown that a knockout of *Bmall* leads to decreased NAD⁺ levels and impaired fatty acid oxidation in the liver of fasted mice [134]. Injection of NMN (an intermediate of the NAD salvage pathway) can partially restore these levels. Furthermore, a liver-specific knockout of *Nampt* also decreases NAD⁺ levels and fatty acid oxidation. These experiments suggest that the clock controls metabolic cycles through the NAD⁺ salvage pathway, by periodically activating SIRT3. This is consistent with the fact that SIRT3 targets, which are involved in fatty acid metabolism, display a circadian pattern of activity. These activities are strongly reduced in *Bmall*^{-/-} mice and partially restored after NMN injection.

2.3.2.3.3 Crosstalks between AMPK and SIRT1

2.3.2.3.3.1 AMPK increases NAD⁺ levels, thereby enhancing SIRT1 activity

Interesting experiments have shown that AICAR administration in C2C12 myotubes induces PGC1- α deacetylation leading to the activation of its target genes [22]. Nevertheless, this effect is lost when cells are treated with the SIRT1 inhibitor, NAM, and after a SIRT1 knockdown. This suggests that AMPK promotes SIRT1 activity by increasing NAD⁺ levels. This raises the following question: does AMPK increase NAD⁺ levels by modulating the NAD⁺ salvage pathway or by converting NADH to NAD⁺? On the one hand, Canto *et al* have shown that AICAR administration increases NAD⁺/NADH levels and this is likely due to increased mitochondrial fatty acid oxidation as this effect is lost in the presence of the beta-oxidation inhibitor etomoxir [22]. On the other hand, Fulco *et al* have shown that AICAR administration as well as fasting or glucose restriction increases both *Nampt* mRNA levels and protein expression [41]. Later experiments have indicated that mutation of the AMPK α 2 subunit fails to increase NAMPT protein levels after AICAR injection but not *Nampt* mRNA [16]. Thus, how AMPK activation increases NAD⁺ levels and induces SIRT1 activity is still under debate.

However, a careful observation of experimental results leads us to hypothesize that AMPK probably interacts with the NAD⁺ salvage pathway by directly regulating the levels of NAMPT protein. Indeed, let us consider again the time profiles of *Nampt* mRNA and protein and NAD⁺ levels. *Nampt* mRNA peaks once during the active phase (ZT14) while NAMPT protein and NAD⁺ twice during the cycle: once during active phase (ZT14-15) and once during the rest phase (ZT5). The ZT14-15 peak is likely due to the clock (activation of

Nampt mRNA by CLOCK-BMAL1). The second resting peak in NAMPT protein and NAD⁺ profile is probably due to a post-transcriptional modification but its origin is unknown. We hypothesize that it is due to the action of AMPK on the levels of NAMPT protein (see Fig. 7.1). This seems consistent because AMPK is activated by a rise of AMP levels and the latter rise around ZT5 [71]. We will use our mathematical model to test the plausibility of our hypothesis.

AMPK has in fact two actions on PGC1- α activity: an indirect deacetylation action through SIRT1 and a phosphorylation action through AMPK [155], [84], [127]. It was shown that PGC1- α needs first to be phosphorylated before being deacetylated. Indeed, mutants in PGC1- α phosphorylation sites are not deacetylated (the possibility of a disturbed SIRT1 activity was ruled out by the fact that other targets of SIRT1 were properly deacetylated) [22].

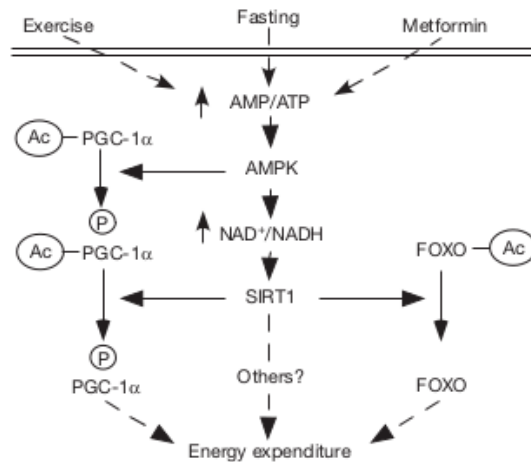


Fig. 2.59 Schematic view of the sequential activation of the transcription factor PGC1- α : it is first phosphorylated by AMPK and then deacetylated by SIRT1 [22].

2.3.2.3.3.2 SIRT1 deacetylates LKB1

As mentioned earlier, the kinase LKB1 targets downstream kinases including AMPK. Interestingly, LKB1 was found to be acetylated in both cultured cells and *in vivo* and this acetylation state is modulated by the deacetylase protein SIRT1 [99]. Indeed, LKB1 acetylation state decreases by 50 % in HEK293T cells in presence of SIRT1 (see Fig. 2.61). Conversely, catalytic inactivation as well as down-regulation of SIRT1 strongly increase LKB1 acetylation levels. It was shown that SIRT1 promotes LKB1 activation by deacetylating the LKB1-lysine at position 48 (Lys 48) [99]. This appears to favour the binding of LKB1 to its activator STRAD and its consequent transportation from nucleus to cytoplasm (after its translation, LKB1 is transported into the nucleus because it has a N-terminal nuclear localization signal).

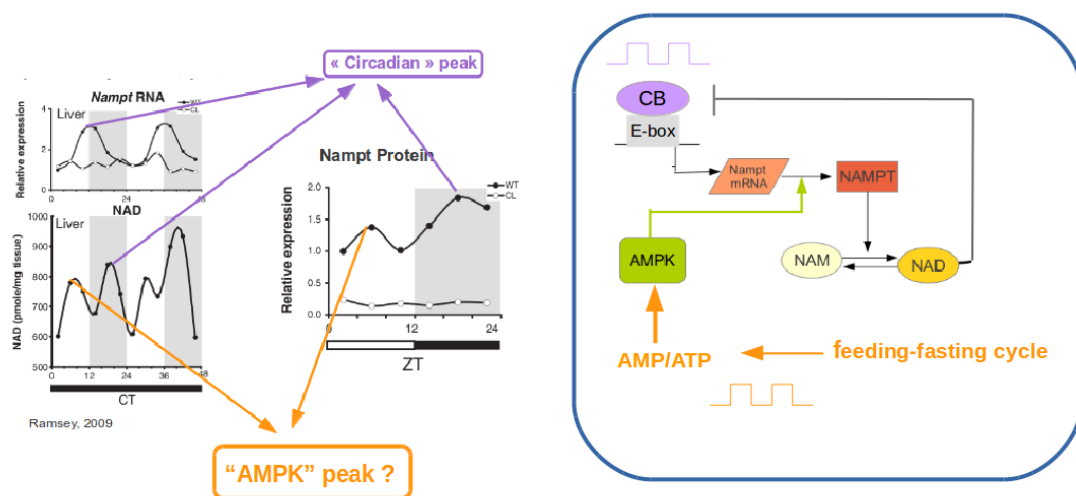


Fig. 2.60 Our hypothesis to explain the bimodal profile in both NAMPT protein and NAD⁺ levels: the peak around ZT14 is driven by the clock while the peak around ZT5 is due to the action of AMPK on NAMPT protein.

In the cytosol of HEK293T cells, LKB1 phosphorylates its downstream targets including AMPK and ACC and this effect is decreased when SIRT1 is down-regulated.

Moreover, LKB1 acetylation levels are decreased under starvation conditions in the liver and this correlates with its increased phosphorylation activity (see Fig. 2.62). All together, these data indicate a reciprocal link between AMPK and SIRT1. Indeed, under starvation conditions, AMPK is activated by increased AMP levels, which increases NAD⁺ levels and enhances SIRT1 deacetylase activity. In turn, SIRT1 activates LKB1 which enhances AMPK phosphorylation and consequent activity. In conclusion, the two nutrient sensors AMPK and SIRT1 are linked by a positive feedback loop enhancing their activities [76],[99].

2.3.3 Interplay between clock and metabolism at the level of the whole organism

A proper metabolic functioning implies a tight balance between food intake, its storage and its utilization. Therefore, the major metabolic tissues (pancreas, liver, adipose tissue, skeletal muscles) have to communicate properly about the body energy status. Furthermore, several brain areas also play a dominant role in keeping an appropriate energy balance. Indeed, food intake is under the control of the central nervous system (CNS)[171], [62]. In anticipation to daily meal absorption, oxyntic cells in the stomach secrete ghrelin. This hormone targets

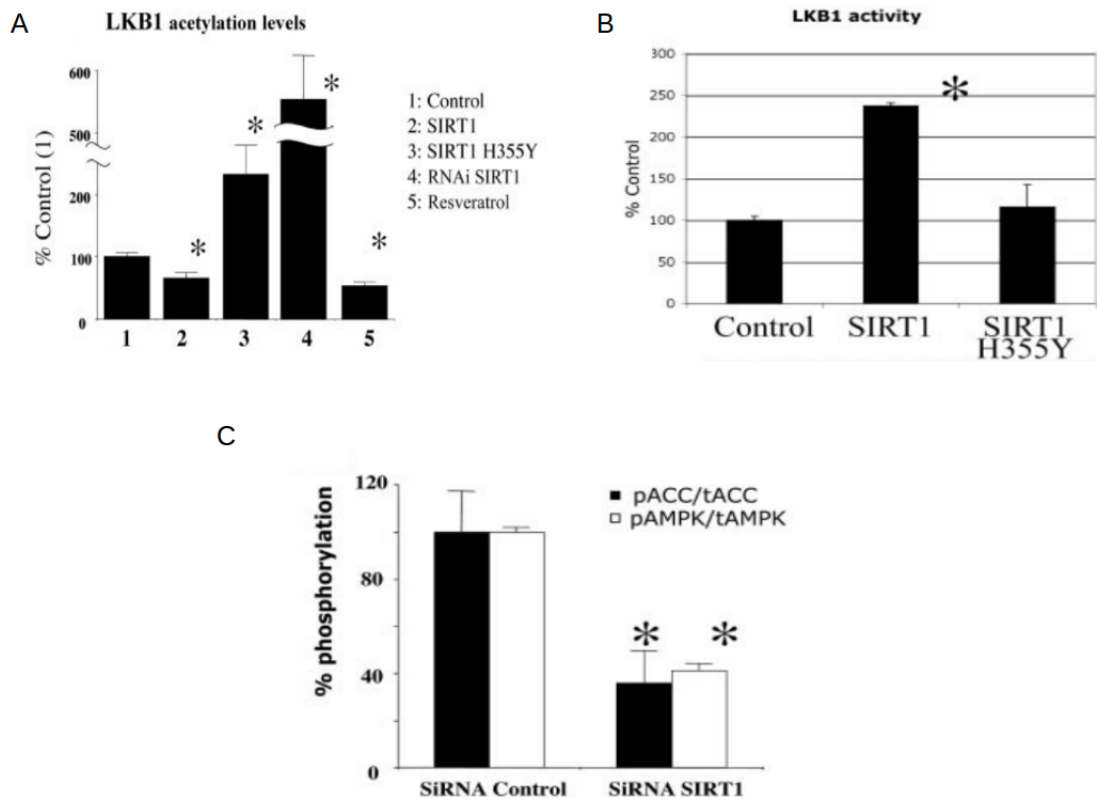


Fig. 2.61 SIRT1-mediated activation of LKB1: SIRT1 deacetylates (A) and activates (B) LKB1 leading to the phosphorylation of LKB1 downstream targets (C). Conversely, SIRT1 inactivation or down-regulation decreases its activity [99].

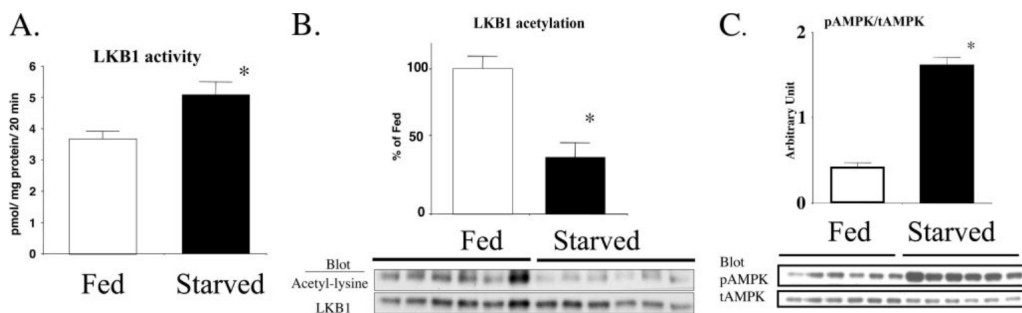


Fig. 2.62 Comparison of LKB1 activity in fed and fasted state in rats liver: in fasting conditions, LKB1 is deacetylated (A) and its consequent activation (B) promotes the phosphorylation of its targets (C) [99].

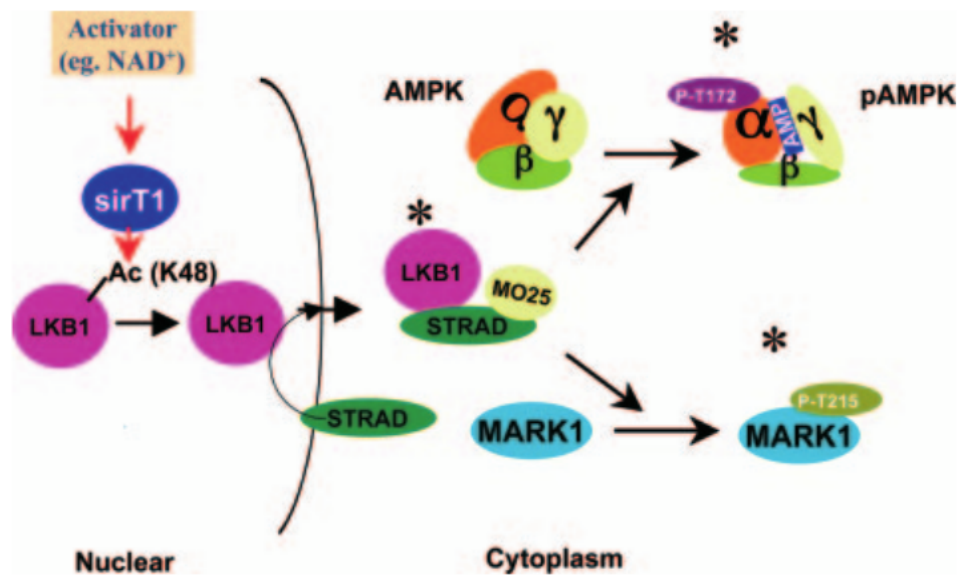


Fig. 2.63 Schematic view of the SIRT1-mediated activation of LKB1 [99].

specialized groups of neurons in the arcuate nucleus (ARC) thereby increasing the locomotor activity and promoting food intake [4]. The production of ghrelin appears to be under the control of the clock. Indeed, it was shown that oxyntic cells co-express ghrelin and the clock components *Per1,2* and that a mutation of the latter suppresses ghrelin expression [102]. Therefore, the stomach clock could be a food anticipatory oscillator preparing the organism to the imminent availability of food.

During the absorptive state, levels of blood glucose are high which triggers the release of insulin from the pancreas. This promotes hepatic glucose uptake that feeds glycolysis, the excess of glucose being converted into glycogen. Glycolysis produces pyruvate that is then converted into acetyl CoA. The latter has several fates. Some acetyl CoA enters the TCA cycle to produce ATP to meet hepatic energy needs. But acetyl CoA can also be used for fatty acid synthesis. The latter are packaged in lipoproteins and transported from the liver to the adipose tissue where they are stored [67]. The fed state is thus an anabolic period where glycogen and fat stores are replenished. Once fat stores are full, the white adipose tissue secretes leptin. Leptin is a hormone that favours satiety and reduces food intake, thereby counter-acting the effects of ghrelin [4]. In particular, leptin increases the sensitivity of the ARC neurons to the gut hormones (such as cholecystokinin) and peptides (such as PYY) that feed back to the CNS to reduce satiety after a meal ingestion. Similarly to its counter-regulatory hormone ghrelin, leptin production is regulated by the clock. Indeed, E-boxes have been found on the leptin promoter in adipose tissue: CLOCK-BMAL1 periodically

induces the *C/EBP α* -mediated leptin transcription [85]. The clock thus gates both ghrelin and leptin production to the proper phase of the cycle.

The rise of leptin levels marks the onset of a fasting phase. During this period, several tissues (liver, adipose tissue,..) rely on fatty acid oxidation to meet their energy needs. The remaining acetyl CoA is used for the creation of ketone bodies that will serve as fuel for other tissues, in particular for the muscles and even for the brain during long term fasting [67]. This process is called ketogenesis. This period is also characterized by increased glycogenolysis and gluconeogenesis which are also clock -controlled events as already mentioned earlier. This complex picture thus illustrates that the clock participates to the proper temporal coordination of major metabolic events throughout the day at the level of the whole organism.

2.4 Chronotherapy

2.4.1 Generalities about chronotherapy

As mentioned above (in section 2.2.3.3.1), almost 50 % of transcripts oscillate somewhere in the body indicating that most aspects of mammalian physiology are under the control of the clock, from major neurotransmitter systems such as the serotonergic, cholinergic or dopaminergic systems that display circadian variations at many levels, to circadian patterns in the secretion of hormones coordinating physiological processes between tissues. It is thus not surprising that most of the "top 100 most sold drugs" target some clock controlled factors (see Fig. 2.64) [180]. Furthermore, many aspects of drug metabolism depend on enzymes that exhibit daily variations in activity [27]. Indeed, the liver clock controls many steps of the xenobiotic detoxification process. Drug absorption also depends on gut motility that is itself rhythmic. Moreover, circadian variations of the gastric pH influence drug solubility. Finally, several important functions of the kidney (renal blood flow, glomerular filtration rate,...) are circadian and rhythmically influence drug elimination.

All together these facts highlights the fact that drug tolerance and efficacy vary during the day. This implies that the timing of drug administration should be carefully controlled. Among them are chrono-modulated drug delivery for cancer treatments [110]. However, nowadays the optimal administration time has only been studied in a few cases. One example is a treatment of bronchial asthma whose efficacy was shown to strongly depend on the time of the day [151]. Another argument in favour of the development of chrono-modulated treatments is that many diseases are linked with perturbation of the clock machinery. Indeed, as we have seen earlier, it is the case for cardio-metabolic diseases, cancer,.. Therefore, a well-timed

administration of clock agonists could constitute an interesting therapeutic strategy. In this line of thought, multiple clock agonists have been developed recently. Among them, CRY activator, CKI inhibitors and agonists of the nuclear receptors REV-ERBs and RORs. Targeting the latter seems an interesting approach, as nuclear receptors are at the crossroads between clock and metabolic networks.

Table 1. Drugs of the top-100 best-seller list that target circadian genes and have half-life < 6h

Rank	Sales, \$	Trade name	Indications	Circadian-gene targets	Organs in which targets oscillate
2	1.46 b	Nexium	Gastritis, GERD, Esophagitis	<i>Atp4a</i>	L
5	1.28 b	Advair Diskus	Asthma, Chronic obstructive pulmonary di...	<i>Serpina6, Pgr, Nr3c2, Adrb2, Pla2g4a</i>	Lu, H, L, K, S, A
11	794 m	Rituxan	Rheumatoid arthritis, Non-Hodgkin's lymph...	<i>Fcgr2b, Ms4a1, Fcgr3</i>	L, K, S
20	538 m	Diovan	Hypertension, Heart failure	<i>Slc22a6, Agtr1a, Slco1b2, Car4, Kcnma...</i>	H, AG, L, K, S
27	431 m	Vyvanse	Attention deficit hyperactivity disorder	<i>Adra1b</i>	L
32	392 m	Tamiflu	Influenza	<i>Neu2, Neu1, Ces1g, Slc22a8, Slc15a1, ...</i>	Lu, L, BF, K, C
33	383 m	Ritalin	Attention deficit hyperactivity disorder	<i>Slc6a4</i>	AG, K
37	348 m	AndroGel	Hypogonadism	<i>Slc22a4, Slc22a3, Ar, Cyp1a1, Cyp2b10...</i>	Lu, H, BS, WF, AG...
38	346 m	Lidoderm	Pain	<i>Slc22a5, Cyp2b10, Egfr, Abcb1a</i>	Lu, H, AG, BF, L,...
44	304 m	Seroquel XR	Bipolar disorder, Major depressive disor...	<i>Htr2c, Htr1b, Htr2a, Chrm2, Drd4, Adr...</i>	Lu, H, BS, WF, AG...
45	289 m	Viagra	Erectile dysfunction	<i>Cyp1a1, Pde6g, Abcc5, Abcc10, Pde5a, ...</i>	Lu, H, BS, WF, AG...
47	281 m	Niaspan	Hyperlipidemia	<i>Slco2b1, Slc22a5, Qprt, Slc16a1</i>	Lu, H, BS, AG, WF...
48	279 m	Humalog	Diabetes mellitus T2	<i>Igf1r</i>	K
49	274 m	Alimta	Mesothelioma, Nonsmall cell lung cancer	<i>Tyms, Atic, Gart, Slc29a1</i>	Lu, H, BS, BF, L,...
54	267 m	Combivent	Asthma, Chronic obstructive pulmonary di...	<i>Slc22a5, Slc22a4, Chrm2, Adrb1, Adrb2</i>	Lu, H, BS, BF, K,...
56	262 m	ProAir HFA	Asthma, Chronic obstructive pulmonary di...	<i>Adrb1, Adrb2</i>	Lu, K, S
62	240 m	Janumet	Diabetes mellitus T2	<i>Slc47a1, Slc22a2, Prkab1, Abcb1a, Dpp4</i>	H, BS, AG, Hy, L,...
66	236 m	Toprol XL	Hypertension, Heart failure	<i>Slc22a2, Adrb1, Adrb2, Abcb1a</i>	Lu, H, AG, BF, L,...
71	220 m	Vytorin	Hyperlipidemia	<i>Hmgcr, Cyp2b10, Soat1, Abcc2, Anpep, ...</i>	Lu, H, BS, AG, BF...
78	209 m	Aciphex	Gastritis, GERD, Esophagitis	<i>Cyp1a1, Atp4a, Abcg2</i>	Lu, H, BS, WF, L,...
90	189 m	Lunesta	Insomnia	<i>Ptgs1, Tspo, Gabra3</i>	Lu, H, AG, K
98	173 m	Prilosec	Gastritis, GERD, Esophagitis	<i>Cyp1a1, Atp4a, Abcg2, Cyp1b1, Abcb1a</i>	Lu, H, BS, WF, AG...
99	171 m	Focalin XR	Attention deficit hyperactivity disorder	<i>Slc6a4</i>	AG, K

Rank and sales are based on USA 2013 Q1 data from Drugs.com. A, aorta; AG, adrenal gland; BF, brown fat; BS, brainstem; C, cerebellum; H, heart; Hy, hypothalamus; K, kidney; L, liver; Lu, lung; S, skeletal muscle; WF, white fat.

Fig. 2.64 Most of the best sold drugs target target several cycling transcripts [180].

2.4.2 Rev-Erb agonists

Of particular interest are synthetic REV-ERB agonists. A few years ago, the natural agonist of REVERB, haem, has been identified [138]. This has led to the development of several pharmacological REV-ERBs agonists, among them, SR9011 and SR9009 [152]. Both decrease *Bmall* transcriptional activity in a dose dependent manner (see Fig. 2.65). In LD conditions, their administration at the middle of the day has only little effect on locomotor activity. Conversely, in DD conditions, agonist administration strongly disturbs locomotor rhythms during the subjective night. This is consistent with altered clock gene expression in hypothalamus following the agonist administration (see Fig. 2.66 A and B). Interestingly, *Per2* transcription is enhanced while rhythmic transcription of other genes such as *Cry2*

is lost in DD (see Fig. 2.66 D). Synthetic ligand injection also impacts peripheral clocks such as in the liver, muscle and WAT (white adipose tissue), but the effect appears to be tissue-dependent. In the liver, SR9011 treatment decreases expression of several genes involved in fatty acid, cholesterol and bile acid metabolism (see Fig. 2.67). Furthermore, a loss in animal body mass is observed for both SR9011 and SR9009 administration. Plasma levels of triglycerides, cholesterol and plasma leptin are also decreased. As the food intake is similar with and without treatment, this indicates that the agonists probably increase the metabolic rate. This suggests that administration of REV-ERB agonist could be an interesting strategy in the treatment of metabolic disorders. In particular, it could be really interesting to compare the benefits of different timings of agonist administration. Indeed, another study has investigated the effect of injections of another REV-ERB α agonist at different times of the cycle [115]. Depending on the administration time, the presence of the agonist either advances or delays the peak of both the negative (*Per2*) and the positive (*Bmal1*) limb of the clock (see Fig. 2.68). These phase shift and amplitude modulations are observed in both isolated fibroblasts and lung slices in rats after agonist injections. As we have seen earlier (in section 2.3.1.2), disruption of clock genes expression leads to metabolic disorders. This study suggests that it would be interesting to test if a specific timing of clock agonist injection could restore the amplitude and the phase of clock genes expression and thereby treat metabolic disorders.

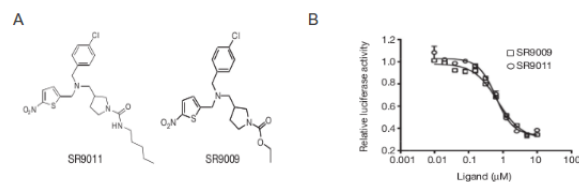


Fig. 2.65 Both REV-ERBs agonists SR9011 and SR9009 decrease *Bmal1* transcription in a dose dependent way [152].

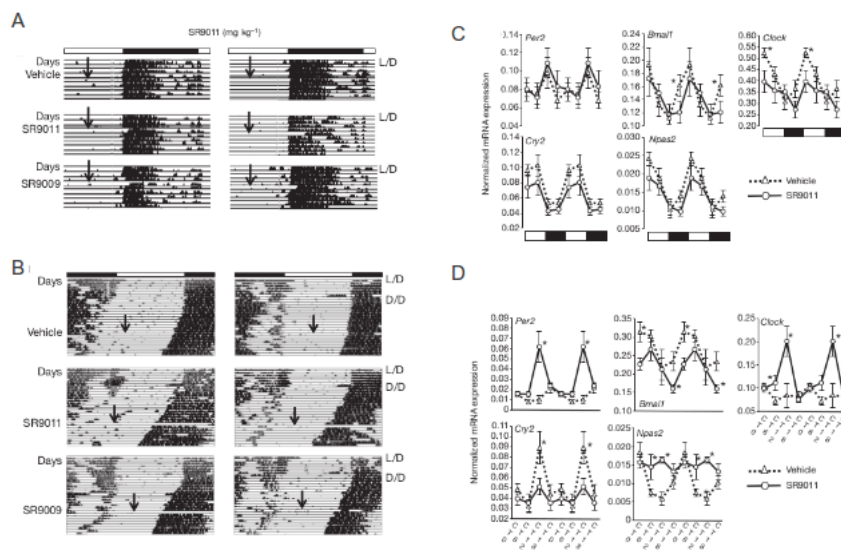


Fig. 2.66 Effect of agonist administration on locomotor activity and clock gene expression: In DD, agonist injection alters both locomotor activity (B) and clock gene expression (D) in SCN in DD but have less effect in LD (A and C) [152].

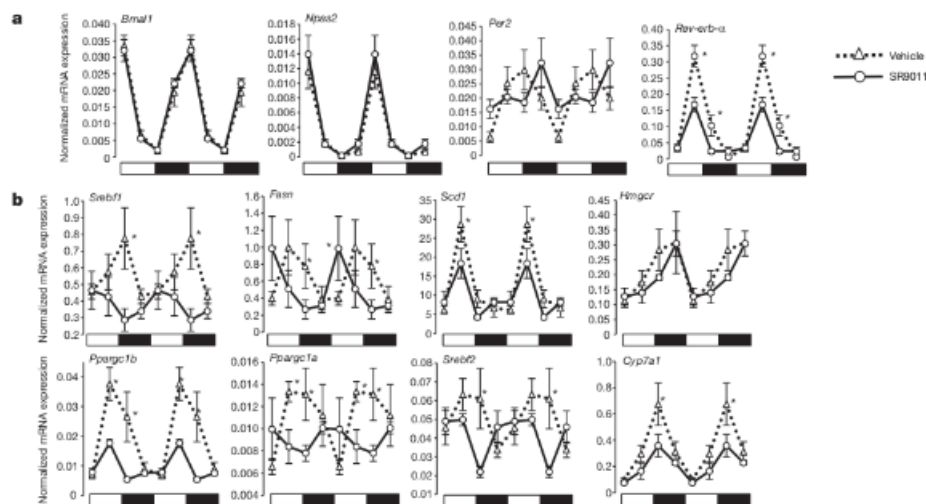


Fig. 2.67 Agonist injection modifies the expression of clock genes (A) and metabolic genes (B) in liver [152].

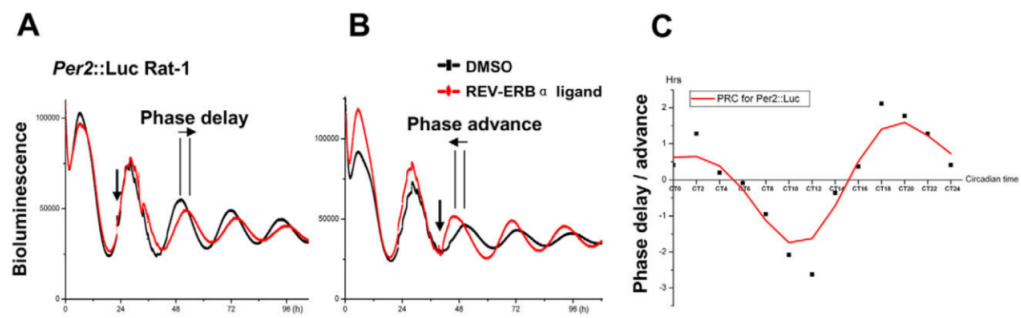


Fig. 2.68 Phase response curve for the injection of a REV-ERBa agonist: depending on the injection time, *Per2* expression peak can either be delayed (A) or advanced (B) [115].

Chapter 3

Mathematical modelling in biology

3.1 Roles of modelling in the study of circadian clocks.

The field of circadian rhythms is a really exciting and dynamic research area and many different kind of researchers are involved in it. Indeed, circadian clocks can be studied from many aspects: molecular biology, physiology, psychology, pharmacokinetics, as well as from a modelling perspective. Circadian clocks are composed of a complex network of transcriptional and posttranslational intertwined feedback loops that generate self-sustained oscillations, are temperature compensated and entrainable by external periodic cues. These complex and fascinating properties constitute thus a breeding ground for modelling approach of these systems. It is thus not surprising that multiple mathematical models have been developed for many years.

Models have been developed for various species from simple organisms such as cyanobacteria and algae to more complex ones such as flies, mammals or birds. Some of these models are very simple and do not consider the interactions between the clock components in detail. Such models only keep the essential features of the system and are thus called minimal models. These minimal models enable to study some generic properties of the clock. This is in particular the case for the Goodwin-like models that will be described a bit later in this Chapter. For example, Bernard *et al* have used a Goodwin-like model to study the synchronization properties of the cell autonomous oscillators that compose the SCN [53]. They have shown that a global neurotransmitter level is efficient to quickly synchronize a population of damped single cell oscillators. A minimal model that is able to reproduce the system behaviour despite its simplicity, gives us indications about the key interactions of the system.

On the other hand, other models are very detailed, describing precisely the molecular mechanism at the core of the clocks. Such models can be used to address questions that are difficult to approach experimentally. They can also serve to validate or invalidate some working hypothesis. The second situation occurred with Forger's detailed model for the mammalian circadian clock [40], [42]. This model takes into account several posttranslational modifications (phosphorylations,...) and was used to investigate the effect of a mutation of the kinase CKI on the clock.

Let us remind that this kinase has multiple effects on the clock. First, it promotes PER1 and PER2 degradation by phosphorylating them at multiple sites. Secondly, CKI was also shown to favour the binding of PER and CRY. Finally the kinase appears to modulate PER1 nuclear transport: it either increases or decreases PER1 translocation depending on the tissue. CKI_{ϵ}^{tau} is a mutation of CKI characterized by a shorter period: animals have a 20h period in DD conditions. *In vitro* experiments have shown that the mutation corresponds to a loss of function of the kinase activity, that is, less phosphorylation activity [109]. Accordingly, Forger *et al* first simulated the effect of CKI loss of function in the model by a 50 % decrease in PERs degradation rate. Surprisingly the simulation results led to a lengthening of the period in this case. They then tried to simulate CKI's loss of function by decreasing other parameters such as PER-CRY's binding rate, PERs' nuclear import rate,... But all combinations always led to longer period (more than 24h) for decreased phosphorylation. Furthermore, by testing other models they still obtained the same results. The modelling approach was thus suggesting that CKI_{ϵ}^{tau} could lead to a shorter period only if the mutation was characterized with a gain of function of the kinase leading to increased phosphorylation. But this was conflicting with *in vitro* results. They thus decided to test themselves the effects of a CKI mutation *in vivo* [42]: their experiments showed that CKI_{ϵ}^{tau} leads to increased PERs phosphorylation and consequent PERs degradation. The question is then: why were they conflicting results found *in vitro* ? It could be because CKI appears to phosphorylate non physiological sites *in vitro*. So this example shows a case where modelling has brought predictions conflicting with previous experimental data. These unexpected predictions have finally led to clarify the understanding of an important clock mechanism. This is a successful example of modelling that illustrates the power of mathematical modelling !

As the dynamics of the circadian network is complex, models can be used to investigate the role of the multiple positive and negative feedback loops lying at the core of most circadian systems. In particular, conceptual models (such as Goodwin-like models for example) enable to compare the dynamical properties of different alternative oscillator architecture (with and without positive feedback loops). In particular, recent studies have shown that positive loops make oscillations to occur with a lower degree of cooperativity and that they enhance the

robustness of the oscillations against noise [159], [5]. We can thus gain insight about the design principle of circadian clocks with computational models.

As mentioned in the first chapter, circadian clock controls many physiological pathways in animals such as the immune system, the cell cycle or metabolism. In the last decade, models describing how the clock regulates other important networks have emerged. In particular, recent models have described the coupling between the clock and the cell cycle [15], [38]. It enabled to test how perturbations in the clock network can lead to cell proliferation and cancer. Such models are thus particularly useful to explore in which conditions pathological behaviour (a pathological situation) can occur. Last but not least, as we have shown in chapter 1, treatments that target the clock are promising approaches for the treatment of some diseases. However, a given clock agonist should be tested at many different times of the day to determine the optimal administration time. This requires heavy experiments for the biologists with many sacrificed animals. A mathematical model-assisted approach would thus be very useful. The aim of a mathematical model is thus not only to fit experimental data: it has multiple advantages that are summarized in Figure 3.1

Roles and advantages of modeling

- Analyzing and understanding complex situations that are difficult to describe in verbal terms and for which sheer intuition becomes unreliable.
 - Rapid and systematic exploration of alternative mechanisms and large ranges of conditions.
 - Clarification and validation (or invalidation) of working hypotheses.
 - Identification of key interactions and parameters, and their qualitative or quantitative influence on the system's behaviour.
 - To determine precisely the conditions in which different behaviours will occur.
 - To address questions that are difficult or impossible to approach experimentally.
 - To provide testable predictions and suggestions for new experiments, and sometimes counterintuitive explanations that may corroborate or not conclusions drawn from experimental observations.
 - To provide a unified framework to account for the experimental observations and bring into light possible similarities between apparently unrelated processes.
-

Fig. 3.1 Roles of mathematical modelling of biological systems [51].

3.2 Steps of a mathematical modelling process

A mathematical modelling approach often begins with a series of questions from experimenters, which directs the attention of the modellers towards a specific biological system.

In order to build a mathematical model, the modellers have to be aware of the main actors playing a role in the system of interest. It thus implies to do an extensive literature search to be aware of all the interactions between the components of the selected network. Ideally, this literature search is accompanied by many discussions between modellers and experimenters. This step is crucial because it enables to have a clear and global view of the system that is essential to build the model. For example, in our case, we had to be aware about the key interactions between circadian and metabolic networks (the result of this literature search step corresponds to the first chapter of this manuscript).

The second step is the construction of the mathematical model (see Fig. 3.2). Depending on the system and the questions of interest, there are different types of models [182]. In particular, ordinary differential equations (ODE) are used to capture the dynamic of systems where space can be seen as homogeneous while partial differential equations (PDE) enable to take into account localization effects or gradient variations of some species. These are deterministic models (that is, models whose behaviour can be predicted from their initial conditions). On the other hand, stochastic models are used to take into account the effect of external and internal fluctuations on the system.

As we have seen in section 3.1, models can also differ in their level of details. Quantitative models as we use here are aimed to reproduce the functioning of the studied network as properly as possible. Therefore, it is important that simulation results fit to experimental data. However, as the values of most kinetic parameters of the model are unknown, parameter estimation methods are used to find the set of kinetic parameters that goes the best through experimental points [121]. This step of parameter values selection is quite important and will be discussed below (section 3.2.2).

Once the model is correctly constrained, simulations can finally be done to study the dynamical properties of our system. In particular, it is much faster to test the effect of local perturbations (such as the down-regulation or the activation of some specific component of the studied regulation network) with a mathematical model than in lab experiments. It is also easier to identify the master regulators of the network: this can be done thanks to the sensitivity analysis which tests how slight changes in parameter values impact on the properties of a system [182]. Other important contributions that can be obtained by *in silico* simulations are recapitulated in Fig. 3.1.

Once a model reproduces enough experimentally known phenotypes, it is validated and can be used to make some predictions. The latter can then be tested experimentally. Two cases are then possible: either lab experiments confirm the predictions or they are conflicting with the modelling results. The latter case can be due to a wrong working hypothesis. The model has then to be improved and a new cycle of the iterative process shown in Fig. 3.2 starts.

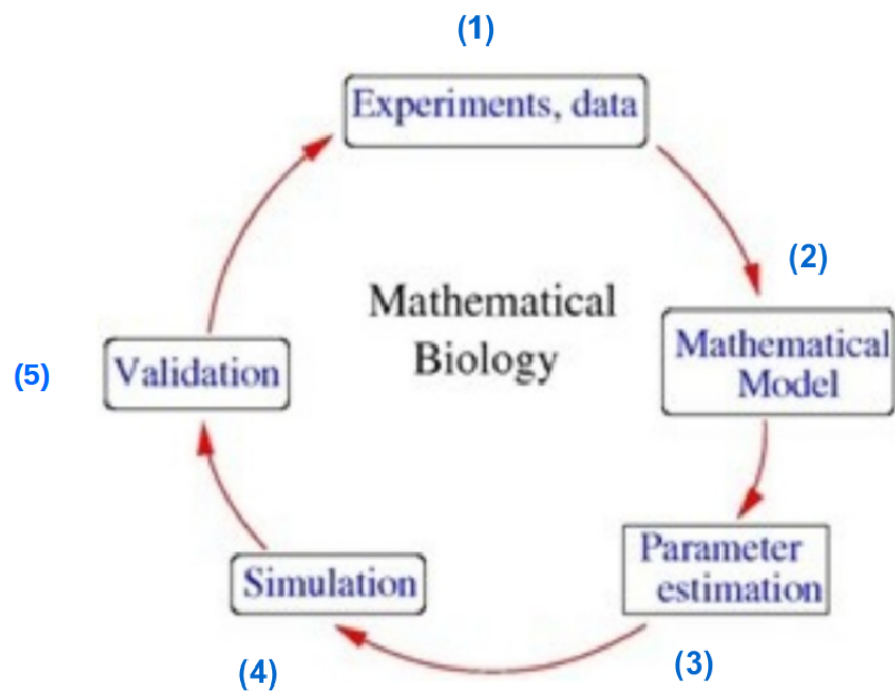


Fig. 3.2 Steps of the modelling process: after having summarized the data from the literature in order to obtain a global view of the interaction network (1), one can build the mathematical model based on this network (2). Once the model fits to experimental data profiles (3), the analysis of the dynamical properties of the system can begin (4). When the model is able to reproduce a reasonable number of experimentally observed phenotypes, it is can be used to make predictions and to design new experiments (5).

3.2.1 Construction of a mathematical model: case of the Goodwin model and of a related clock model

3.2.1.1 The Goodwin model

As mentioned in the first chapter (in section 2.1.1), the presence of a negative feedback is a necessary requirement to have self-sustained oscillations in a biochemical system. The Goodwin model is the first molecular oscillating model based on a negative feedback loop [54], [58]. This very simple clock model proposed more than forty years ago is still used to describe conceptually the negative feedback loop at the core of circadian systems. It describes the time evolution of the concentration of three hypothetical clock components: X (the mRNA of some clock gene), Y (the corresponding clock protein) and Z (a repressor protein activated by Y).

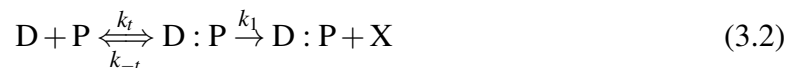
It is based on the following mechanism: after the clock gene transcription, the mRNA X is translated into the protein Y . The latter activates the repressor protein Z . In turn, the inhibitor Z repressed the transcription of X . As X , Y and Z are also subjected to degradation, the concentrations progressively decrease which leads to the de-repression of X transcription and a new cycle of transcription can then start (see Fig. 3.3).

This gives rise to the following set of reactions: when the repressor Z is present, it binds to a binding site, D , on the promoter of the clock gene and transcription is repressed. This can be written as



where the form $D:Z$ represents the complex between Z and D . The parameters k_i and k_{-i} are the binding and unbinding rates for $D:Z$.

When the repressor Z is not present, the RNA polymerase, P , can bind to the promoter of the gene, the latter being transcribed into the mRNA X , which gives



where the form $D:P$ represents the complex between P and D . The parameters k_t and k_{-t} are the binding and unbinding rates for $D:P$ and the parameter k_1 is the transcription rate.

Once X has been transcribed, it is translated into Y which leads to the activation of the repressor Z . These reactions are written as





where k_2 and k_3 are the production rates of the proteins Y and Z . The three following reactions describe the degradation of X , Y and Z :



where the parameters d_1 , d_2 and d_3 are the degradation rates of X , Y and Z respectively.

Using mass action kinetic, the kinetic equations describing the time evolution of the concentration of X , Y , Z and the complexes $D:Z$ and $D:P$ can be written as follows :

$$\left\{ \begin{array}{l} \frac{d([X])}{dt} = k_1 [D : P] - d_1 [X] \quad (a) \\ \frac{d([Y])}{dt} = k_2 [X] - d_2 [Y] \quad (b) \\ \frac{d([Z])}{dt} = k_3 [Y] - d_3 [Z] \quad (c) \\ \frac{d([D:Z])}{dt} = k_i [D] [Z] - k_{-i} [D : Z] \quad (d) \\ \frac{d([D:P])}{dt} = k_t [D] [P] - k_{-t} [D : P] \quad (e) \end{array} \right. \quad (3.8)$$

A conservation relation holds, indicating that the total concentration of binding sites is constant:

$$[D] + [D : P] + [D : Z] = \text{constant} \quad (3.9)$$

Several assumptions can be made about the timescales of the system. In particular, the binding rate of Z and P to the DNA binding site D is supposed to be much faster than the transcription and the translation rates. Therefore, we can assume that the reactions 3.1 and 3.2 are rapidly at equilibrium (that is, the quantity of binding events per unit of time is equal to the quantity of unbinding events per unit of time). This hypothesis is called the quasi

steady state assumption and implies that

$$\frac{d([D : Z])}{dt} = 0 = \frac{d([D : P])}{dt} \quad (3.10)$$

Another realistic assumption is that there is not only one but several DNA binding sites on the promoter of the clock genes and that the binding is cooperative. Cooperativity means that the binding of a molecule to one site facilitates the binding of the following molecules to the other sites. We suppose that it is the case here and the cooperative binding of the repressor protein Z to the binding sites D is characterized by a coefficient n , the Hill coefficient.

By combining the quasi-steady state assumption with the conservation relation and the cooperative binding hypothesis, Eq. 3.8.a can be re-written as

$$\frac{d([X])}{dt} \simeq \frac{k_1}{1 + \left(\frac{[Z]}{K}\right)^n} - d_1[X] \quad (3.11)$$

which implies that the system of ordinary differential equations (ODE) can be written

$$\left\{ \begin{array}{l} \frac{d([X])}{dt} = \frac{k_1}{1 + \left(\frac{[Z]}{K}\right)^n} - d_1[X] \quad (a) \\ \frac{d([Y])}{dt} = k_2[X] - d_2[Y] \quad (b) \\ \frac{d([Z])}{dt} = k_3[Y] - d_3[Z] \quad (c) \end{array} \right. \quad (3.12)$$

where the parameter K describes the inhibition rate of X transcription by Z and where n is the Hill coefficient that characterizes the degree of cooperativity.

Depending on the value of the kinetic parameters, the Goodwin model can generate either damped or self-sustained oscillations (see Fig. 3.4). The latter are also called limit cycle oscillations. More specifically, limit cycle oscillations are self-sustained oscillations characterized by a given amplitude and period which are independent of initial conditions [50]. In particular, analytical calculations have shown that limit cycle oscillations can only be obtained for an important degree of cooperativity, that is, if n is larger than 8 [58]. Interestingly, a two variable version of the model only shows damped oscillations indicating that there must be a sufficient delay in the feedback to generate self-sustained oscillations. All this indicates that a negative feedback, time delay and sufficient nonlinearities (here through cooperativity) are ingredients for the onset of oscillatory dynamics [129]. In many cases,

negative feedback loops are interlinked with positive feedback loops. Several studies have investigated the role of the latter. It was highlighted that networks with positive feedback loops exhibit oscillations for a larger range of kinetic parameters value than those with only a negative feedback loop [159]. More recently, it was shown that addition of positive loops to a network with a core negative feedback loop enables oscillations to occur with a lower degree of cooperativity [5].

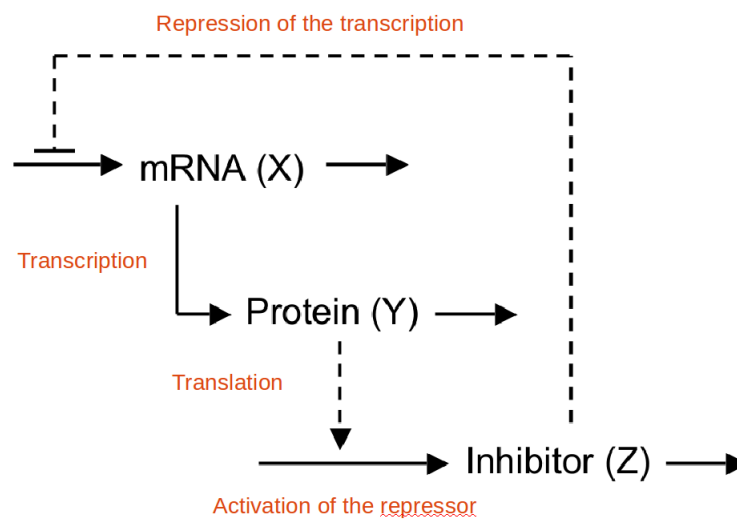


Fig. 3.3 Scheme of the Goodwin model: the mRNA X is translated into the protein Y , that activates the repressor protein Z . Z inhibits the transcription of X .

3.2.1.2 A toy model for the mammalian clock

The Goodwin model is still used nowadays both to study the conditions for the emergence of specific dynamical behaviours and for the qualitative modelling of some circadian systems [173], [172]. In particular, with my master lab in Brussels, we have modelled the avian circadian clock by two coupled and forced Goodwin-like oscillators [172]. During my thesis, I have also enjoyed myself in building a simple model for the mammalian clock starting from the Goodwin model. I have labelled it as "mammalian toy model" and will describe it here to illustrate how the Goodwin model can easily be extended to a realistic model for the mammalian clock.

I have started with a model whose equations were exactly the same as those of Goodwin model. I have considered that the variable X corresponds to the expression level of *Cry*, the variable y to the levels of CRY protein and the repressor variable z to the complex

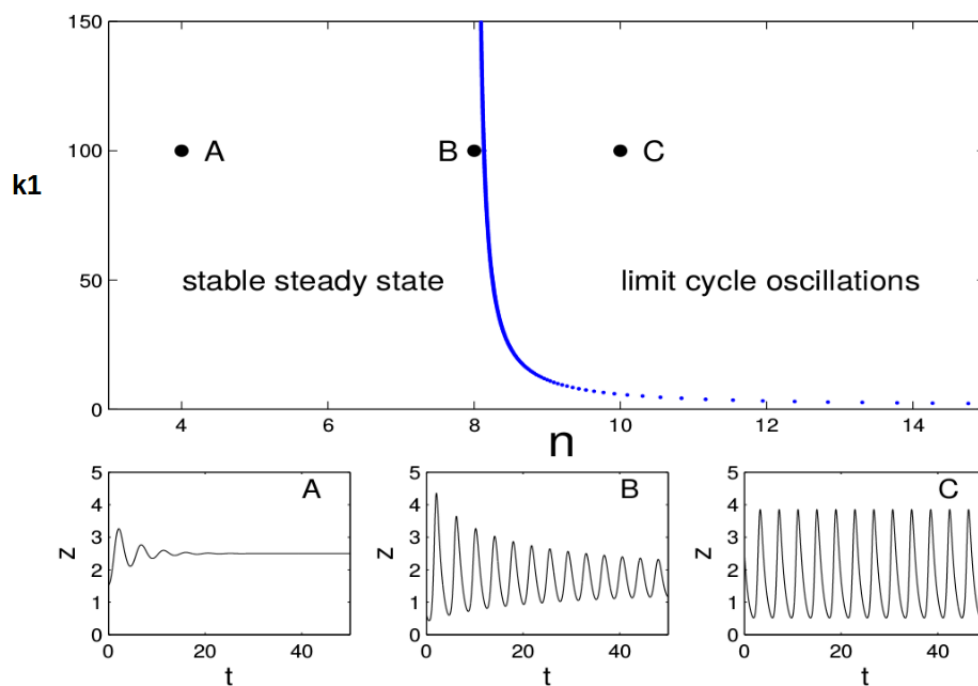


Fig. 3.4 Dynamical behaviour of the Goodwin oscillator as a function of the kinetic parameter k_1 and n : the blue curve separates the steady state regime from the oscillator regime. The 3 bottom panels show the time series corresponding to point A, B, and C in the upper panel. When the value of Hill coefficient is lower or equal to 8, oscillations dampen out and finally reach a steady state (A and B).

PER-CRY. The variables x and y could of course also represent the expression levels of *Per* and *PER*. Note that I do not make the difference between the isoforms of *Per* and *Cry* for the sake of simplicity. Let me also point out that an alternative formulation is possible where y corresponds to the cytoplasmic form of the protein CRY (or PER) and z to its nuclear form (that directly represses the gene transcription in this case).

I have then added the effect of the activator BMAL1 in the model. This implied to slightly modify the form of the *Cry* transcription function to take into account the dual effect of the inhibitor (PER-CRY) and the activator (see Chapter 5 for a similar formulation of clock gene transcription function). Finally, I have represented the action of REV-ERB in the clock. This last step is essential to have oscillations in *Bmal1* transcription (otherwise, *Bmal1* transcription would be constant). This gives rise to a 7 variable-model with 36 kinetic parameters. I have also tried to fit the model to the experiment mRNA expression profiles [78]. Surprisingly, it reproduces correctly experimental expression profiles in spite of its simplicity. Interestingly, I could not obtain the right phases for the three mRNA expression profiles (but only for two of them) until I added the repression of *Cry* transcription by REV-ERB. This suggests that this regulation is important to have a proper phase relationship between the different clock components.

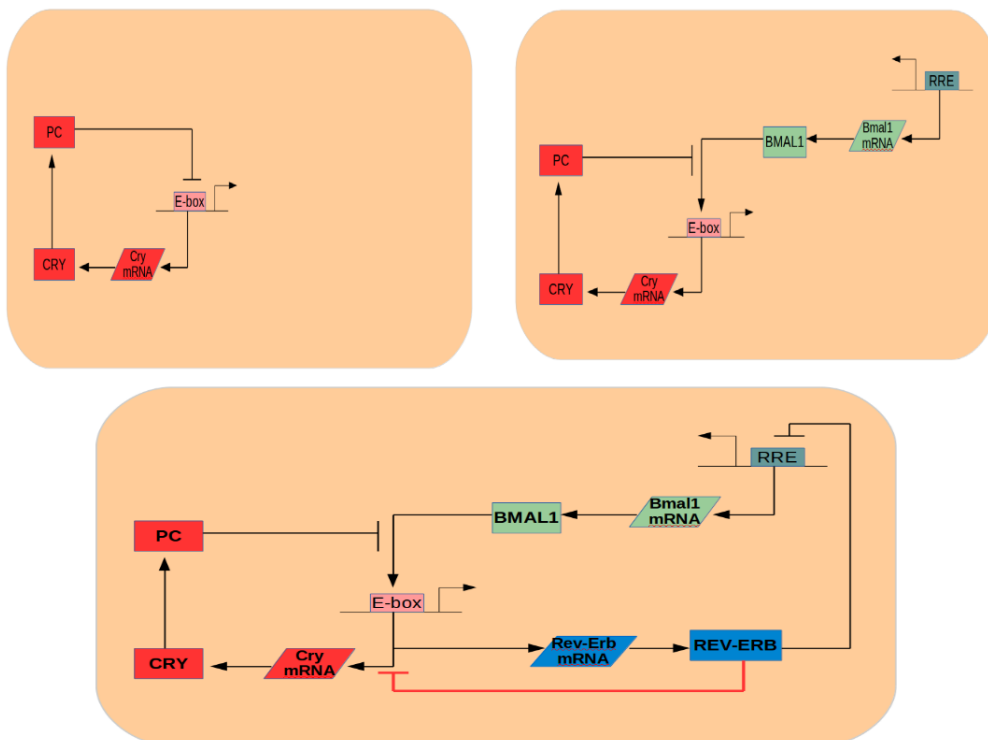


Fig. 3.5 Scheme of the successive steps for the construction of my toy model for the mammalian clock.

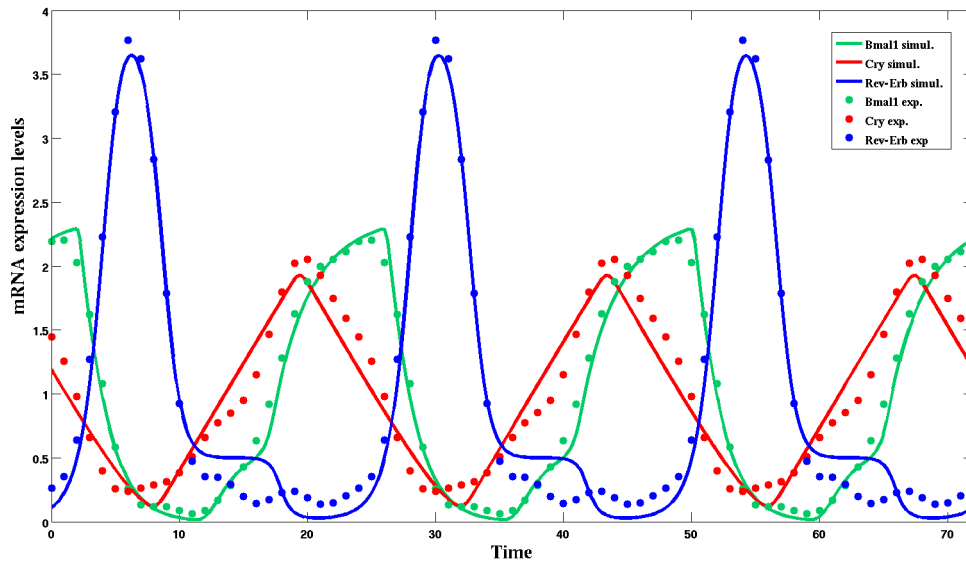


Fig. 3.6 Agreement between experimental points (dotted lines) and simulation results (solid lines) for *Cry1*, *Bmal1* and *Rev-Erba* mRNA levels.

3.2.2 Considerations about parameter estimation methods

At the core of every parameter estimation method is the objective function ϕ . The objective function (also called score function) measures the goodness of the fit, so basically it is a function of the distance (gap) between experimental data values and the corresponding numerical simulation values. An example is the function chi square defined as the weighted sum of the square of the distance between experimental and in silico data points [182].

As we want the fit to be as good as possible, parameter estimation methods try to find the set of parameters values that minimize the value of the objective function, thus, an optimum of ϕ by an iterative process [182]. But finding an optimum can be complicated because ϕ is a highly nonlinear function (that is, a function whose output is not directly proportional to its inputs). One simple parameter estimation method is the gradient descent method. It tries to find the minimum of an objective function by taking its gradient because the gradient of a function is locally the direction of deepest descent. This method is quite simple and several more complex variants have been developed. These techniques belong to the optimization methods requiring differentiable score functions. When the geometry of the objective function becomes more complicated, global optimization methods work better because they don't use derivatives to find ϕ_{min} . Several classes of optimization methods have been developed based on stochastic strategies [121]. Among them, the evolutionary

algorithms that imitate the process of natural selection (see Fig. 3.7). Here is how some simple case could work. It starts with N candidate parameter sets and the value of the score function is evaluated for each set. These N "parent" sets will then be replicated and each "offspring" set is submitted to a mutation. The fitness of these N offsprings is also evaluated. At this stage, the population is composed of $2N$ parameter sets (N parents and N offsprings). The N candidates with the highest score function will die while the N others will start a new cycle of mutation/evaluation. After many iterations, this algorithm will hopefully converge to an optimal parameter set (that is, with a minimal score function). This group of algorithms includes genetic algorithms, evolutionary programming and evolutionary strategies. Other well known global optimization classes are simulated annealing methods and meta-heuristic ones. The latter reproduce biological process based on food search strategies of ants colonies and so on. For example, they include the particle swarm method, that is based on the movement of fishes or bird flocks. It starts with several sets of candidate parameters, the particles. The particles movements in the parameter space will depend on their best solution and the best solution of the swarm, the goodness of a solution depending of course on the value of the score function. These methods don't require differentiable functions and are useful in case of noisy problems or for time-depending functions. They are less proved than deterministic methods to get stuck in a local optimum (because they perform a more exhaustive search in parameter space) but there is no guarantee of convergence.

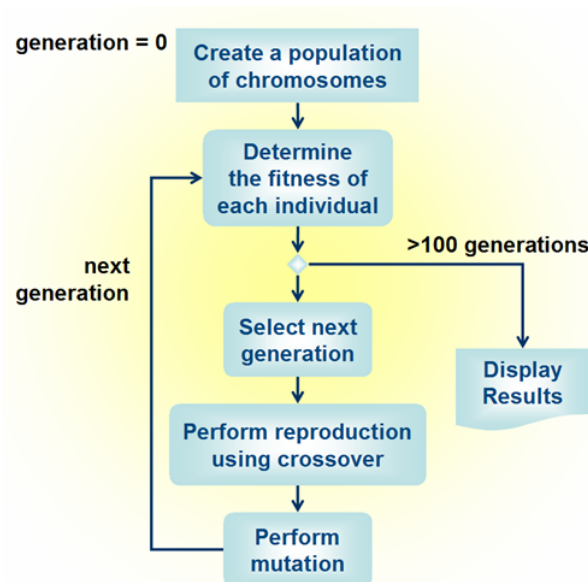


Fig. 3.7 Main steps of a genetic algorithm. Each element of the population corresponds to a parameter set whose score function is evaluated. Each set is then replicated and slightly modified (mutated). Finally, the sets whose score function is the lowest will survive while the other die. A new cycle of evaluation can then start.

Chapter 4

A detailed model describing entrainment of the liver clock by metabolism

4.1 Construction of the mathematical model

As indicated in the first chapter, our first goal was to build a mathematical model describing the coupling between clock and metabolism in order to understand how food entrains the clock. Several models describing the mammalian circadian clock can be found in the literature: most of them are representing the central clock and potentially how it is entrained by the light-dark cycle [101], [40], [11], [118], [142]. Conversely, there are very few models describing the clocks in peripheral tissues, which moreover do not consider the coupling with metabolism [93]. A full description of this coupling would require a model at the level of the whole organism. Indeed, both the brain areas controlling food intake and the major metabolic tissues (liver, adipose tissue, pancreas, muscle,..) should be represented as well as their interactions through endocrine cues (leptin, ghrelin, insulin, glucagon,..). Then, the clock machinery and the metabolic pathways should be modelled for each of those tissues, by taking into account the tissue-specific regulations. This is thus a quite complicated task! We have decided to start at a more basic level and to focus on one single peripheral tissue: the liver. We have chosen this major center of nutrient redistribution for several reasons. First, because the liver is particularly responsive to food cues. Indeed, the liver is the organ that adapts the fastest after a switch from a night-time to day-time feeding pattern [28]. This rapid "uncoupling" of the liver clock from the SCN influence also allows us to neglect the effect of the pacemaker as a first approximation. A second argument in favour of the liver is that there are much more experimental data (time profiles of clock and metabolic gene expression) available for the liver than for other tissues. Furthermore, experimental data

indicate that the liver clock is composed of well synchronized cells: indeed, phase coherence in clock gene expression persists between hepatocytes during several days in SCN-lesioned animals [148]. This allows us to model the liver as a single cell oscillator.

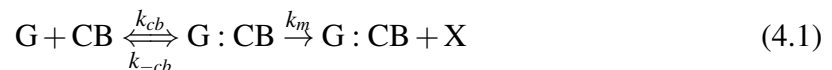
4.1.1 Model for the core clock

Before studying the interactions between clock and metabolism, we first needed to start with a model for the mammalian liver clock. We wanted a model of intermediate complexity: not too complicated to avoid over-fitting risk because of too many unknown parameter values but detailed enough to be realistic. Therefore, we have chosen not to represent the different isoforms of clock components. In our model, *Per1,2,3* are grouped as a single *Per* gene and the same holds true for the isoforms of the other core clock genes. Furthermore, we do not take into account post-transcriptional modifications (such as clock protein phosphorylation by the kinase CKI,..). Likewise, we do not take into account the nucleo-cytoplasmic transport and we thus do not make any difference between nuclear and cytoplasmic proteins.

The core of our clock model contains 12 species: the proteins PER, CRY, REV-ERB, ROR and BMAL1 and their mRNAs as well as the two complexes CLOCK-BMAL1 (CB) and PER-CRY (PC) (see Fig. 4.1). Our model takes into account the main feedback loops at the core of the mammalian circadian system: *Per* and *Cry* transcription is activated by the complex CB. The mRNAs are translated into the proteins PER and CRY that then form the repressor complex PC. PC inhibits the activity of the activator complex CB. Our model also takes into account the REV-ERB-ROR-BMAL1 axis: CB activates the transcription of *Rev-Erb* and *Ror*. The corresponding proteins REV-ERB and ROR then respectively inhibit and activate *Bmal1* transcription. Besides these components of the core clock, we have also represented the transcription of the clock controlled gene, *Dbp* [145]. This is useful because several experiments display the effect of the loss-of-function of the nutrient sensors SIRT1 and AMPK on *Dbp* expression profiles (see section 4.2.3).

4.1.1.1 Equations

We are modelling the interaction between the repressor and the activator complexes as follows: when CB is located on the promoter of a given clock-controlled gene *G*, the transcription is activated and leads to the synthesis the mRNA *X*. This can be written as:



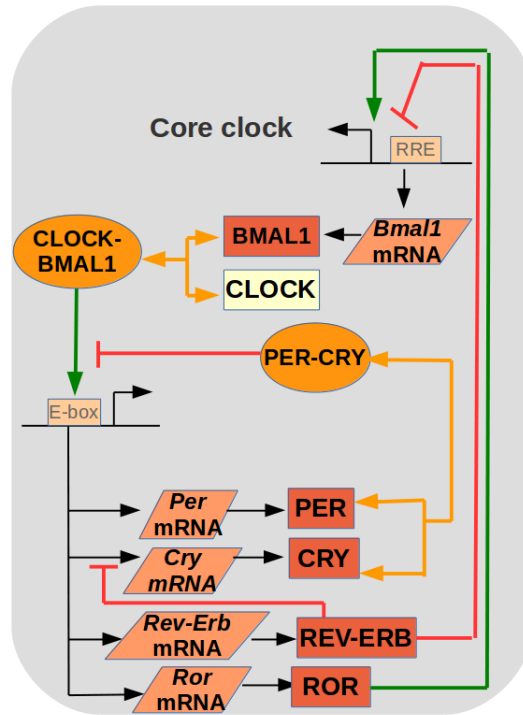


Fig. 4.1 Scheme of our core clock model.

The equation for the degradation of the mRNA at a rate d_m is

$$X \xrightarrow{d_m} \Phi \tag{4.2}$$

Once the repressor complex PC binds in turn to the E-box , the transcription of the gene is inhibited:



A conservation relation for the gene can also be written:

$$G + G : CB + G : CB : PC = cste \tag{4.4}$$

The above reaction scheme can be translated into ordinary differential equations by using the laws of mass action kinetics :

$$\left\{ \begin{array}{l} \frac{d[G:CB]}{dt} = k_{cb}[G][CB] - k_{-cb}[G : CB] \quad (a) \\ \frac{d[G:CB:PC]}{dt} = k_{pc}[G : CB][PC] - k_{-pc}[G : CB : PC] \quad (b) \\ \frac{d[X]}{dt} = k_m[G : CB] - d_m[X] \quad (c) \end{array} \right. \quad (4.5)$$

By doing the quasi-stationary approximation for Eqs. 4.5.a and 4.5.b and by using the conservation relation 4.4, the transcription rate of this gene can be written as

$$T = \left(\frac{\frac{[CB]}{K_{Acb}}}{1 + \frac{[CB]}{K_{Acb}} \left(1 + \frac{[PC]}{K_{Ipc}} \right)} \right)$$

(4.6)

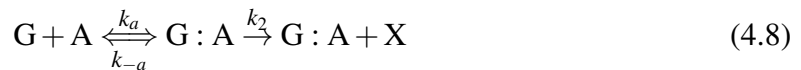
where $K_{Acb} = \frac{k_{-cb}}{k_{cb}}$ is the activation threshold and $K_{Ipc} = \frac{k_{-pc}}{k_{pc}}$ is the inhibition threshold for the transcription of the gene. The rate of change of the mRNA X can thus be written as

$$\frac{d[X]}{dt} = V_{max} \left(\frac{\frac{[CB]}{K_{Acb}}}{1 + \frac{[CB]}{K_{Acb}} \left(1 + \frac{[PC]}{K_{Ipc}} \right)} \right) - d_m[X]$$

(4.7)

where V_{max} is the maximal transcription rate.

On the other hand, ROR and REV-ERB competitively bind on the promoter of *Bmal1*. The binding of the activator A (that is, the protein ROR) on the promoter of *Bmal1* triggers its transcription and leads to the synthesis of *Bmal1* mRNA (labelled as X here):





where Eqs. 4.9 represents the degradation of *Bmal1* mRNA. When the repressor protein *I* (that is, the protein REV-ERB) binds to the promoter of *Bmal1*, the transcription is inhibited, which gives



with the conservation relation

$$G + G : A + G : I = cste \quad (4.11)$$

The kinetic equations corresponding to the above reaction scheme can be written as:

$$\begin{cases} \frac{d[G:A]}{dt} = k_a[G][A] - (k_{-a})[G : A] & (a) \\ \frac{d[G:I]}{dt} = k_i[G][I] - k_{-i}[G : I] & (b) \\ \frac{d_m[X]}{dt} = k_m[G : A] - d_m[X] & (c) \end{cases} \quad (4.12)$$

By doing quasi-stationary approximation for Eqs. 4.12.a and 4.12.b and by using the conservation relation 4.11, the transcription function can be written as

$$T = \left(\frac{\frac{[A]}{K_A}}{1 + \frac{[A]}{K_A} + \frac{[I]}{K_I}} \right)$$

(4.13)

where $K_A = \frac{k_{-a}}{k_a}$ is the activation threshold and $K_I = \frac{k_{-i}}{k_i}$ is the inhibition threshold. By replacing *A* by *ROR*, *I* by *REV-ERB* and *X* by *Bmal1* mRNA, the time evolution of *Bmal1* mRNA can be written as

$$\frac{d[Bmal1]}{dt} = \left(V_{max} \frac{\frac{[ROR]}{K_A}}{1 + \frac{[ROR]}{K_A} + \frac{[REV]}{K_I}} \right) - d_m [Bmal1] \quad (4.14)$$

where V_{max} is the maximal transcription rate and d_m the degradation rate.

The transcription functions 4.13 and 4.6 are similar to those of the Religio's model [142]. This is a model with 19 variables describing the time evolution of the main clock actors PER, CRY, REV-ERB, ROR and BMAL in the SCN. It also takes into account post-translational modifications such as PER-CRY phosphorylations and nuclear transport. As the parameters values of Religio's model were already carefully tuned to reproduce circadian rhythms in the SCN, we decided to start from this model as a basis. Compared to our above-described calculations, the model also takes into account basal transcription rates and cooperative binding to the promoter of clock genes (which is characterized by Hill coefficients). It also includes one additional regulation: the transcription of *Cry* is also inhibited by the protein REV-ERB [104]. Starting from Religio's set of equations and parameters value, we have reduced the model by eliminating progressively all the post-transcriptinal modifications (phosphorylation, translocation). We thus also had to modify the parameter values in order to keep appropriate phase relationships between clock components. We obtained a set of 12 differential ordinary differential equations (ODE) correctly describing the time evolution of clock gene expression in the liver.

4.1.2 Addition of the action of the nutrient sensors AMPK and SIRT1 on the clock

As we have seen in the first chapter, the alternation between food intake and fasting phases induces periodic variations in the levels of AMP and NAD⁺ and in the activities of the nutrient sensors AMPK and SIRT1. As a first step, it is reasonable to consider the variations in the activities of the nutrient sensors as a direct readout of the alternation between feeding and fasting phases. This avoids having to model the details of the metabolic pathways (glycolysis, fatty acid oxidation,..) linking food intake to the nutrient sensors activities. As we will see below, the metabolic input of our model is the activity of the nutrient sensor AMPK.

4.1.2.1 Incorporation of the Nampt-NAD⁺-SIRT1 loop

The first interaction between clock and metabolism that we have added is the negative feedback loop involving SIRT1 and the NAD⁺ salvage pathway [141], [124]. This involves the following reactions: the complexes CB and PC periodically bind to the promoter of the gene *Nampt*. This induces the periodic transcription and translation into the protein NAMPT. In turn, NAMPT periodically converts NAM into NAD⁺ which increases SIRT1 deacetylase

activity. The loop is closed when SIRT1 deacetylates BMAL1 and histone H3 (and PER2) leading to a repressive state. The deacetylation rate can be written as

$$V_{deac} = V_{max} \frac{NAD^+}{K + NAD^+} \quad (4.15)$$

Indeed, NAD⁺ induced SIRT1 activity corresponds in fact to a bi-substrate enzymatic reaction where SIRT1 uses NAD⁺ as a substrate to remove an acetyl group from a target protein. This yields to the formation of nicotinamide, 2' O-acetyl ADPR and the deacetylated product [37]. The relation (4.15) can be obtained by using two-substrate enzyme kinetics for the deacetylation reaction with some approximations. It is also coherent with experimental results depicting how another sirtuin (SIRT3) deacetylase activity is modulated by increasing concentrations of NAD⁺ in mitochondria [133].

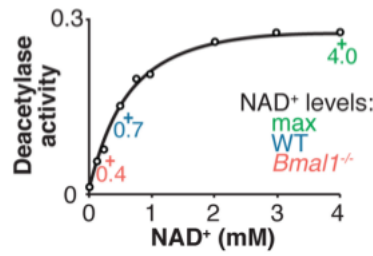
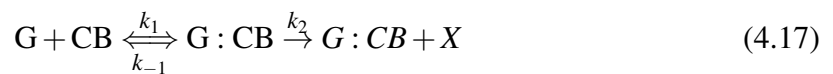


Fig. 4.2 In vitro deacetylase activity of recombinant SIRT3 with acetylated SIRT3- selective target peptide in the presence of increasing concentrations of NAD⁺ [133].

The repression of the transcription by SIRT1-mediated deacetylation is written as follows: we consider two forms of the complex CLOCK-BMAL1, CB and CB*, with BMAL1 being acetylated (CB) and deacetylated (CB*) respectively. SIRT1 shifts the equilibrium towards the form CB* with a rate V_{deac} . This form does not allow transcription to occur. This gives:



CB corresponds to the active form of the complex (with BMAL1 being acetylated). This form allows the transcription of clock controlled genes and leads to the synthesis of their mRNAs (X)





where Eqs. 4.18 represents the degradation dynamics of mRNA X and Eqs. 4.19 corresponds to the binding of the repressor complex PC on the promoter of the clock gene. We have once again a conservation relation for the total quantity of the gene:

$$G + G : CB + G : CB : PC = cste \quad (4.20)$$

The kinetic equations corresponding to the above reaction scheme can be written as:

$$\left\{ \begin{array}{l} \frac{d[G:CB]}{dt} = k_1[G][CB] - k_{-1}[G : CB] \quad (a) \\ \frac{d[G:CB:PC]}{dt} = k_3[G : CB][PC] - k_{-3}[G : CB : PC] \quad (b) \\ \frac{d_m[X]}{dt} = k_2[G : CB] - d_m[X] \quad (c) \\ \frac{d[CB]}{dt} = v_{ace}[CB^*] - v_{de}[CB] - k_1[G][CB] + k_{-1}[G : CB] \quad (d) \end{array} \right. \quad (4.21)$$

By applying the quasi-steady state approximation for the dynamics of the 2 complexes and by using the conservation relation for the gene (Eq. 4.20), we can rewrite Eq. 4.21.c as

$$\frac{d[X]}{dt} = k_2 \left(\frac{G_0 \left(\frac{[CB]}{K_A} \right)}{1 + \left(\frac{[CB]}{K_A} \right) \left(1 + \frac{[PC]}{K_I} \right)} \right) - d_m[X] \quad (4.22)$$

By applying the quasi-steady state approximation for Eq. 4.21a and by using the conservation relation for CB (that is $CB_{tot} = CB + CB^*$), Eq. 4.22 can be written as

$$\frac{d[X]}{dt} = \left(k_2 \frac{G_0 \left(\frac{[CB_{tot}]}{K_A(1 + \frac{v_{de}}{v_{ac}})} \right)}{1 + \left(\frac{[CB_{tot}]}{K_A(1 + \frac{v_{de}}{v_{ac}})} \right) \left(1 + \frac{[PC]}{K_I} \right)} \right) - d_m[X] \quad (4.23)$$

which means that the transcription rate of a given clock controlled gene translates into

$$T = \left(k_2 \frac{G_0 \left(\frac{[CB_{tot}]}{K_A \left(1 + c \left(\frac{[NAD]}{K + [NAD]} \right) \right)} \right)}{1 + \left(\frac{[CB_{tot}]}{K_A \left(1 + c \left(\frac{[NAD]}{K + [NAD]} \right) \right)} \right) \left(1 + \frac{[PC]}{K_I} \right)} \right)$$

(4.24)

In our model, we have thus considered that SIRT1 represses the transcription by increasing the threshold of the CB mediated-transcriptional activation (Eq. 4.24). Furthermore, SIRT1 also destabilizes the protein PER by increasing its degradation rate [7]. This regulation is also included in the model (see section 6.1 for the details). All the effects of SIRT1 activity on the clock are summarized in Fig. 4.3.

We have also made an important hypothesis about NAD⁺. As aforementioned, the variations in the levels of the metabolite NAD⁺ can be explained by several contributions: by the control of the NAD⁺ salvage pathway by the clock and by the interconversion of NADH and NAD⁺ during metabolic processes such as glycolysis and fatty acid oxidation. As a first approximation, we have decided to neglect this second contribution. For the sake of simplicity, the only metabolic input taken into account comes from the variations in AMP levels through AMPK (see section 4.1.2.2).

4.1.2.2 Incorporation of AMPK and its interactions with the clock

We also wanted to incorporate the interactions between the sensor AMPK and the clock machinery. As we have seen in the first Chapter (section 2.3.2.3.1.2), high AMP levels increase AMPK activity in several ways: in presence of active LKB1, AMP promotes AMPK phosphorylation at Thr172, inhibits its phosphorylation and also allosterically increases its activity. However, the relative importance of these different mechanisms is still unclear [56]. Therefore, we have decided not to model these reactions and to consider that AMPK activity is proportional to the variations in AMP levels. In our model, the activity of AMPK, *Act_AMPK*, is thus described by an external periodic forcing function. As the time profile of AMP variations is bimodal, this function is allowed to have several peaks per day (see section 6.2):

$$Act_AMPK \simeq \text{basal-rate} + A_1 \cdot \text{peak1} + A_2 \cdot \text{peak2}$$

The amplitudes A1 and A2, the phases and the width of the peaks will be selected during the parameter estimation process (see section 4.2.2).

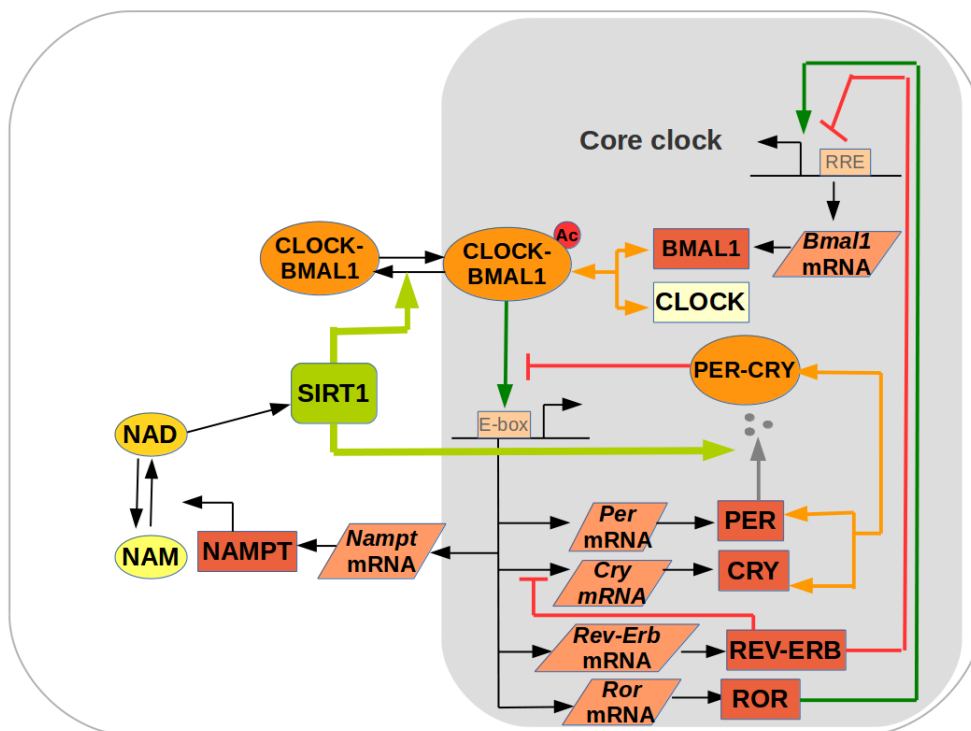
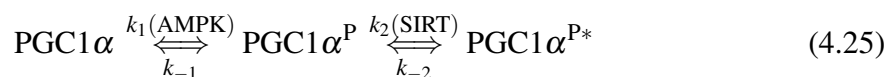


Fig. 4.3 Scheme of the interactions of the NAD salvage pathway and SIRT1 with the clock.

In agreement with data from the literature [97], [165], active AMPK destabilizes CRY and PER by increasing their degradation rate in our model. Furthermore, we have also considered that active AMPK increases NAD⁺ levels by directly enhancing NAMPT protein levels. Indeed, we have seen earlier (section 2.3.2.3.3.1) that it is unclear how AMPK increases NAD⁺ levels but the analysis of experimental data leads us to hypothesize that AMPK probably directly acts on the protein NAMPT. AMPK could increase NAMPT protein levels in two ways: either by increasing its translation rate or by decreasing its degradation rate. We have tested both options (and both are reproducing experimental data) but we have decided to keep the second solution (see Fig. 4.4).

4.1.2.3 Incorporation of PGC1- α

As we have seen before, both AMPK and SIRT1 induce Pgc1- α activation which in turn modulates *Bmal1* transcription [22], [105]. Indeed, AMPK phosphorylates the protein PGC1- α that can then be deacetylated by SIRT1. This can be written as



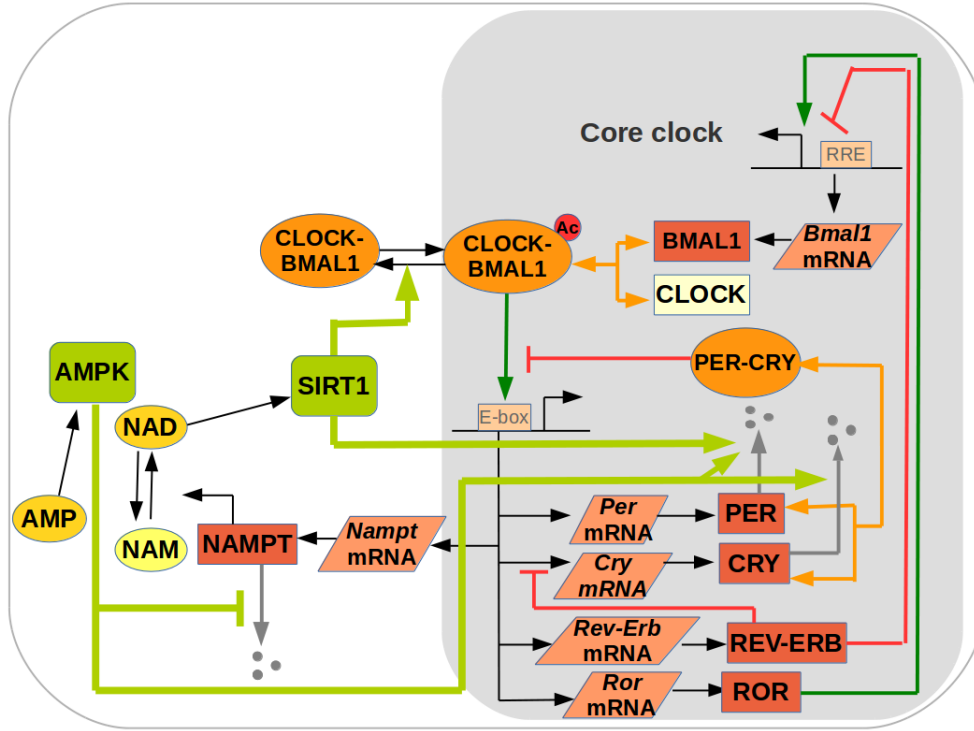


Fig. 4.4 Scheme of the interactions of AMPK with the clock and the NAD salvage pathway.

with the conservation relation for the total protein quantity

$$PGC1\alpha + PGC1\alpha^P + PGC1\alpha^{P*} = PGC1\alpha_{TOT} \quad (4.26)$$

where $PGC1-\alpha^P$ is the phosphorylated form of the protein and $PGC1-\alpha^{P*}$ the active form that has been phosphorylated and deacetylated. So, after developments similar to what has been done previously, the activity of $PGC1-\alpha$ can be written as

$$ACT_{PGC1\alpha} = \left(\frac{C \cdot (ACT_{AMPK}) \cdot (ACT_{SIRT}) \cdot [PGC1\alpha_{TOT}]}{1 + \frac{(ACT_{AMPK})}{K1} \cdot \left(1 + \frac{(ACT_{SIRT})}{K2}\right)} \right) \quad (4.27)$$

where $PGC1-\alpha_{TOT}$ is the total concentration of the protein $PGC1-\alpha$ and Act_{AMPK} and Act_{SIRT} the activities of the nutrient sensors. In our model, we consider that the active form of protein, represented by the quantity $ACT_{PGC1\alpha}$ enhances *Bmal1* transcription by increasing its transcription rate (see section 6.1).

Experimental time profiles show that both *Pgc1-α* mRNA levels and protein expression are circadian and that they are peaking during the night [105]. However as mentioned in the first chapter, there is no indication that *Pgc1-α* transcription is under the direct control of the clock. It is likely regulated by several systemic cues such as the cAMP response

element-binding protein (CREB)[73]. As the exact mechanism inducing circadian expression of *Pgc1- α* is not clear, we have decided not to take into account *Pgc1- α* transcription and to only reproduce the total protein concentration, $PGC1-\alpha_{TOT}$ by an external periodic function with parameter values (phase, amplitude,...) consistent with experimental data (see section 6.2).

4.1.3 Summary of the construction of our model

Using mass action kinetics, we have translated all the above described interactions into a mathematical form and we finally obtain a model featuring 16 variables and 103 parameters describing the interactions between the key nutrient sensors SIRT1 and AMPK and the clock components (see Fig. 4.25 and see section 6.1 for the complete system of differential equations). Our model contains a strong assumption: AMPK increases NAD⁺ by acting on NAMPT protein which could explain the presence of two peaks per day in NAMPT protein and NAD⁺ time profiles. Moreover, we have also made several simplifications: no posttranslational modifications and no direct contribution of the NAD/NADH variations (due to food intake) to the variations in NAD⁺ levels. However, it does not imply that food intake has no influence on NAD⁺ levels: indeed, here we incorporate the effect of periodic food intake through the variations in AMP levels (and thus AMPK), which directly impacts on NAD⁺ levels through the action of AMPK on NAMPT. Despite its simplicity, we will see that our model reproduces remarkably well experimental data (see section 4.2.2).

4.2 Parameter estimation

4.2.1 Choice of experimental data

To use our model to answer correctly relevant biological questions, we wanted to reproduce as accurately as possible the available experimental time profiles. The model contains many kinetic parameters and most of their values are unknown. We thus wanted to constrain their values by fitting *in silico* results to experimental time profiles. Nowadays, an increasing amount of circadian expression profiles are available and easily accessible in databases such as CircaDB. We decided to use mouse hepatic mRNA expression data, characterized by their high time resolution (one point every hour)[78]. When a model has many unknown parameters, it is important to constrain it with a large number of experimental points to reduce the risk of overfitting. More specifically, we have used mRNA time profiles for *Bmal1*, *Per2*,

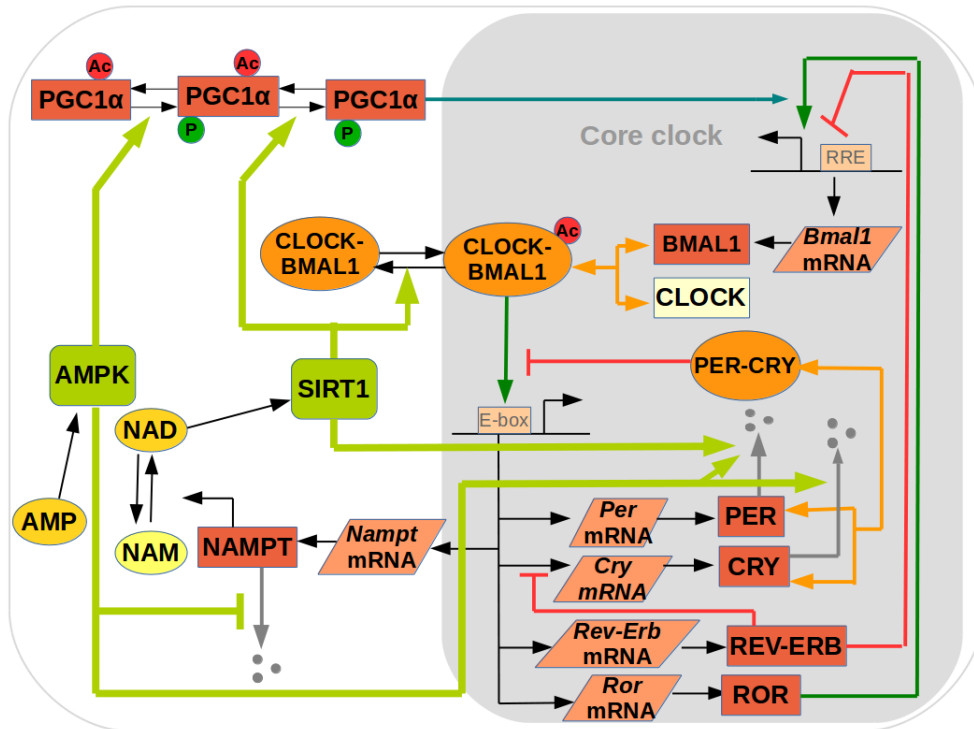


Fig. 4.5 Scheme of the mathematical model coupling circadian clock to metabolism.

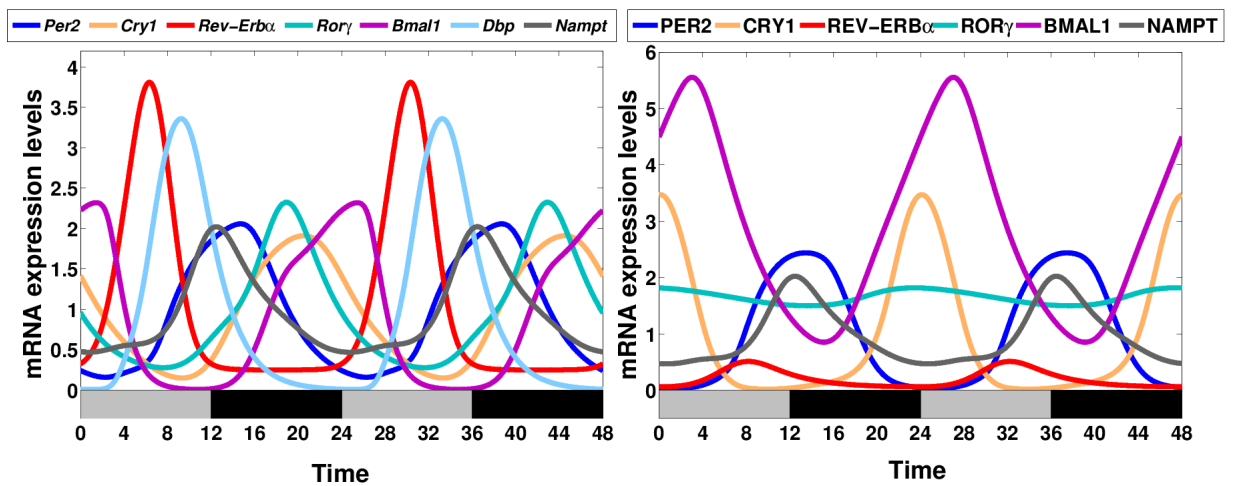


Fig. 4.6 Time profiles for the mRNAs (left panel) and proteins (right panel) considered in our model.

Cry1, *Rev-Erb*, *Ror α* and *Nampt*. These time profiles come from animals fed *ad libitum* and kept under constant darkness. These data are a bit noisy; therefore, the expression profiles have first been interpolated with Fourier series in order to make them periodic to facilitate the adjustment between data and the ODE system. Each data set $y(t)$ was thus adjusted to 4th order Fourier series $f(t)$ with

$$f(t) = a_0 + a_1 * \cos(t * \omega) + b_1 * \sin(t * \omega) + a_2 * \cos(2 * t * \omega) + b_2 * \sin(2 * t * \omega) + a_3 * \cos(3 * t * \omega) + b_3 * \sin(3 * t * \omega) + a_4 * \cos(4 * t * \omega) + b_4 * \sin(4 * t * \omega)$$

(4.28)

where the a_i and b_i are the Fourier coefficient and where $\omega=2\pi/\text{period}$. We have tried several periods and the one adjusting the best the data is 24h. We have also constrained the model by using the NAD+ time profile for the fitting (and the data are coming from animals fed *ad libitum* and entrained by the LD cycle [71]). Finally, we have not constrained the time evolution of our clock proteins because of the lack of high-resolution protein time profiles. Furthermore, most of the available protein time profiles correspond to the total protein concentration and we would have been more interested in their activity time profiles.

4.2.2 Reproduction of expression time profiles from wild-type animals

We have tested several parameter estimation methods: the Levenberg–Marquardt algorithm failed to find a good quality adjustment. Therefore we tried global optimization methods. Both the particle swarm and the Hookes and Jeeves methods worked quite well but we preferred the second one because we have noticed that the particle swarm algorithm tends to be stuck in local minima. [55]

As the values of our kinetic parameters have to be realistic, we allowed the parameter values to be chosen only in a range of physiological values [116]. However, sometimes, we were more permissive about the range of allowed values as for the Hill coefficients. As the latter are describing the cooperative binding of the protein complexes to E-boxes on the promoter of clock genes, it could seem not physiological to allow their value to be higher than 4 because it would correspond to multiple binding sites which is not realistic. Nevertheless a recent modelling work has shown that phosphorylation-dephosphorylation mechanisms can lead to sigmoidal dynamical equivalent to high Hill coefficients [52]. Therefore, we have allowed higher values for the Hill coefficients and this appeared to enhance our fitting.

We obtain an excellent adjustment between experimental data and simulation results. Not only the model reproduced accurately mRNA time expression profiles but also those of NAD⁺ levels (see Fig. 7.5). Furthermore, the parameters of the forcing function describing AMPK activity have been selected so that AMPK activity is bimodal with one high peak during the day (around ZT5) and one small peak during the night (around ZT17). The selected peaks of AMPK activity are thus totally consistent with those of AMP experimental levels. The action of AMPK on NAMPT protein is thus sufficient to reproduce the daily two peaks in NAMPT and NAD⁺ time profiles ((see Fig. 7.6). More precisely, the morning peak in NAMPT protein and NAD⁺ profiles is due to the action of AMPK on NAMPT levels while during the night, NAMPT protein levels increase because of the combined action of the circadian peak in mRNA *Nampt* and the smaller peak in AMPK activity rhythm.

In conclusion, the model shows that a periodic modulation of the rate limiting step in the NAD⁺ biosynthesis pathway by both the clock and the AMPK activity rhythm is sufficient to reproduce the daily variations in NAD⁺ levels without taking into account the effect of variations in the redox ratio NAD⁺/NADH. However it does not mean that variations of the redox ratio NAD⁺/NADH do not contribute to the NAD⁺ time profile but just that the contribution of the NAD⁺ biosynthesis pathway to the circadian variations in NAD⁺ is dominant compared to the NAD⁺/NADH ratio. This is agreement with the fact that a loss of the positive limb of the clock (*Bmal1* KO) leads to strongly decreased NAD⁺ levels [141].

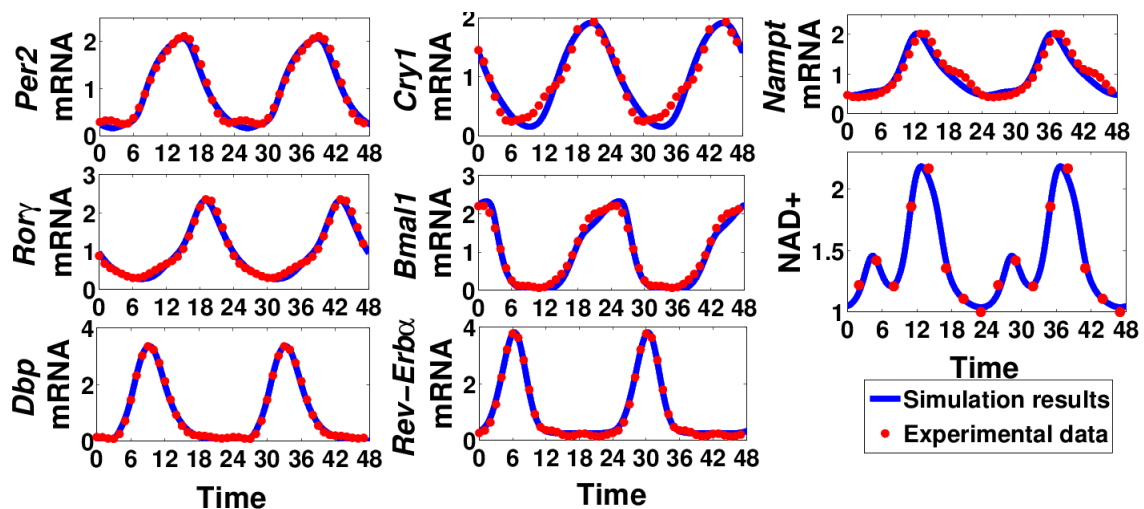


Fig. 4.7 Expression time profiles of the main clock actors obtained in mouse liver are accurately reproduced.

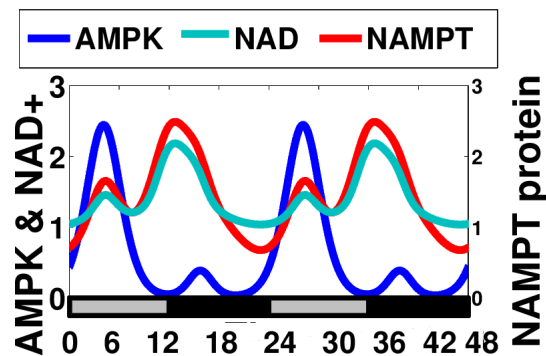


Fig. 4.8 Our model reproduces the bimodal time profiles for AMPK, NAD⁺ and NAMPT.

4.2.3 Reproduction of knockout phenotypes

We also aimed to reproduce *in silico* knockout experiments. In particular we wanted to reproduce the effect of SIRT1 and AMPK loss of function on clock gene expression in the liver. The knock-out of SIRT1 increases clock gene expression in the liver: in particular, it leads to a strong amplitude rise in *Nampt*, *Dbp* and NAD⁺ levels [14]. Conversely, available data indicate that the knock-out of LKB1 is responsible for decreased expression of *Rev-Erb α* , *Per2*, *Dbp* and *Cry1* mRNA in the liver [97]. A loss-of-function of LKB1 leads to a down-regulated AMPK activity. As LKB1 is not part of our model, the effect of its KO are represented by a strong dampening in the AMPK activity rhythm. However we still keep some residual rhythm because AMPK could still be activated by other kinases.

To reproduce the clock gene expression profiles from WT mice, we have used Hughes's very precise data (high time resolution) [78]. But Hughes did not carry out experiments on LKB1 or SIRT1 mutants. Unfortunately, the available LKB1 and SIRT1 knockout experiments were not conducted in the same conditions as the experiments of Hughes on WT animals [97], [14]: these knockout data can thus not be used directly to constrain the model. To bypass this issue, we have first calculated the changes in the relative amplitude of clock gene expression between the data from WT and mutant mice for these experiments. Then, we have applied this ratio to Hughes data (from WT animals) in order to obtain the "artificial" mutant time profiles corresponding to Hughes data. Thanks to this procedure, we were able to constrain parameter values to reproduce qualitatively the effect of SIRT1 and LKB1 loss-of-function on the clock (see Fig. 7.7).

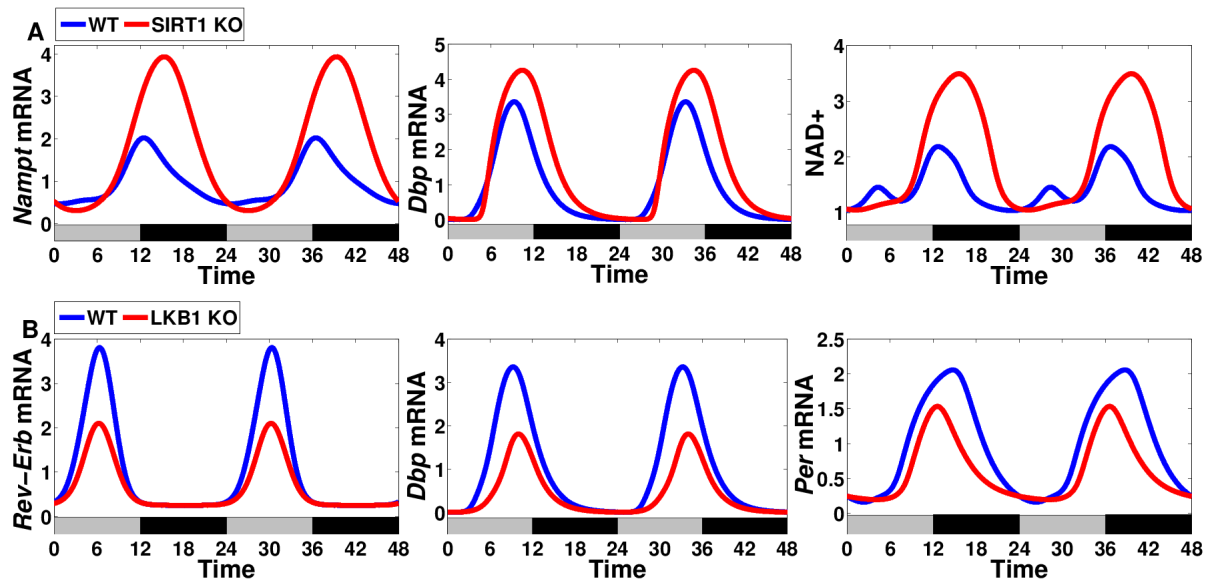


Fig. 4.9 SIRT1 and AMPK loss-of-function phenotypes are qualitatively reproduced.

4.3 Effect of perturbations of AMPK rhythms on the clock

Modern life style is characterized with a high flexibility in feeding behaviours and correlates with increasing metabolic disorders. Indeed irregular meal times and snacking are common and disturbed feeding patterns have been shown to lead to diet induced obesity and disturbed clock gene expression [71]. As, in our model, we have considered AMPK activity as a direct readout of the periodicity in food intake, we wanted to investigate the effect of perturbations in AMPK rhythms on clock gene expression. We have considered two conditions: the effect of a strongly dampened AMPK rhythm (see Fig. 7.8, first panel) and a state where the kinase activity is always high (see Fig. 7.9, first panel). On the one hand, the "very active AMPK" condition is similar to fasting conditions. On the other hand, a strongly dampening in AMPK rhythm can be compared to a situation where animals are eating most of the time and is thus termed "Fed State".

Let us notice that the activity of AMPK is not constitutively low or high but is still rhythmic for these two conditions. This is important because in physiological conditions, the liver clock is entrained by two zeitgebers: by the feeding fasting cycle (represented by the AMPK rhythm in our model) and through neuro-endocrine cues from the SCN (in particular, through glucocorticoid signalling). Thus, even if the rhythm in food intake is disturbed, the peripheral clocks are still indirectly driven through the SCN pacemaker. As we have not modelled the neuroendocrine forcing of the SCN, we always kept a residual rhythm in AMPK activity.

Otherwise the system would no longer be entrained and the phase of the oscillations would have had no longer signification.

We have compared the effect of these two disturbed activities to those of the normal AMPK rhythm. The model predicts that an enhanced AMPK activity increases Nampt (mRNA and proteins) and NAD⁺ levels. This is consistent with a fast-like state [134], [147]. Furthermore, the fasting-like state also increases the expression of some clock genes (see Fig. 7.9). Conversely, a dampening in AMPK activity rhythm reduces Nampt (mRNA and Protein) and NAD⁺ levels as well as clock gene expression ((see Fig. 7.8). This is thus very similar to what is observed with *ad libitum* high fat diet (HFD) feeding [36], [71]. Our model thus suggests that the amplitude reduction in clock gene expression and NAD⁺ levels under *ad libitum* HFD feeding is at least partially due to a dampening in AMPK activity rhythms. This is consistent with the fact that AMP levels are strongly depleted for animals fed on a *ad libitum* HFD [71]. It could also explain why a time restricted HFD feeding is able to restore physiological amplitudes in clock gene expression because it is expected that AMPK activity maintains a high amplitude in this case, as animals are not allowed to eat all the time. Furthermore, note that our simulations also show that the bimodal profile in NAD⁺ and NAMPT levels disappears in both the fasted-like and the fed-like state. This is in agreement with NAD⁺ uni-modal time profiles in both fasting and high-fat diet feeding conditions. Our model thus provides a simple way to understand these different phenotypes via changes in AMPK rhythm, even if other additional nutrient regulators such as mTOR and CREB are likely involved.

4.4 Targeting the clock to rescue physiological expression profiles

4.4.1 Rescue of clock oscillations amplitude in *Cry1* mutants following a dampening in AMPK rhythm

The work of Hatori *et al* suggests that there is a correlation between the rescue of physiological amplitude in gene expression and protection against obesity under high fat conditions [71]. Therefore, we were wondering if there are other ways than time restricted feeding to be protected against diet-induced obesity. Some experiments have demonstrated that, under a high fat diet, mice with a *Cry1* deletion are protected against diet-induced obesity while wild type animals gain weight [57]. In these experiments, the total food intake (number of kcal/day) between the wild-type and the mutant animals was similar as well as their total

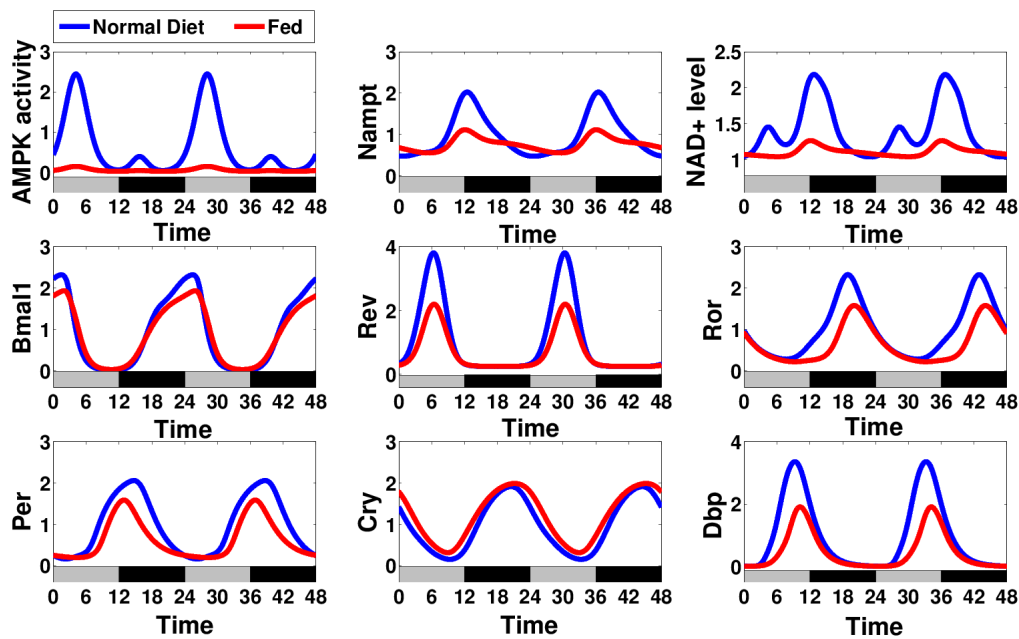


Fig. 4.10 Fed state: effect of a dampening in AMPK activity (red curves) compared to a rhythmic activity of the nutrient sensor (blue curves) on clock gene expression.

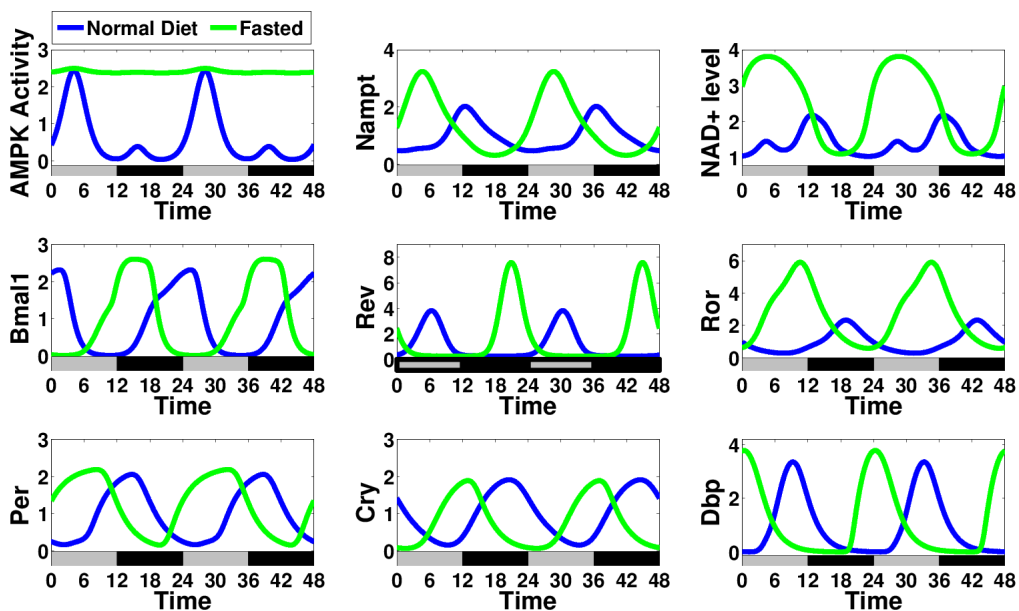


Fig. 4.11 Fasted state: effect of a high AMPK activity (green curves) compared to a rhythmic activity of the nutrient sensor (blue curves) on clock gene expression.

levels of plasma glucose, triacylglycerol and free fatty acids. This suggests that the reduced fat stores of mutant animals are likely due to an increase of energy expenditure even if the exact mechanism is unclear.

We have simulated the effect of this mutation after a dampening of the AMPK rhythm to mimic HFD feeding conditions. As in our model, a knockout of the gene *Cry* is equivalent to a double deletion of *Cry1* and *Cry2*, we have reduced the transcription rate of the gene *Cry* to represent a selective knockout of *Cry1*. As shown in Fig. 7.10, the amplitude of clock gene expression is then enhanced. Together with Panda's observation for time restricted high-fat diet feeding [71], this suggests a correlation between rescue of physiological levels in clock gene expression and protection against diet-induced obesity.

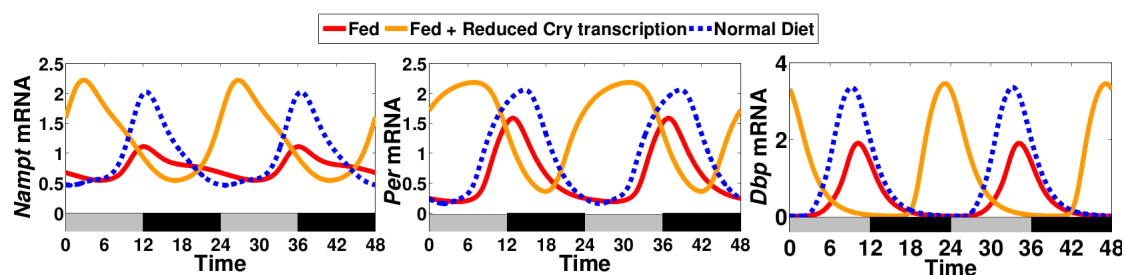


Fig. 4.12 Rescue of clock oscillations amplitude in *Cry1* mutants following a dampening in AMPK rhythm.

4.4.2 Pharmacological rescue of physiological expression profiles after disruption of AMPK rhythm

An interesting anti-obesity treatment could thus be to target the clock pharmacologically in order to restore physiological amplitudes of clock gene expression. This raises the following question: with our model, can we design the pharmacological rescue of physiological expression profiles after disruption (dampening) of AMPK activity rhythm? With regard to the choice of the clock target gene, REV-ERB seems a prime candidate as several synthetic REV-ERB agonists exist [152]. We have thus decided to model the periodic administration (once a day) of a synthetic REV-ERB agonist. The agonist concentration is therefore represented by a 24h-periodic function with a single peak, characterized by its amplitude, its width and its administration time. The amplitude is related to the dose of agonist that is administrated and the width to its half-life time. As the protein REV-ERB inhibits both *Bmal1* and *Cry1* transcription, we have considered that the agonist periodically increases the inhibition rate of *Bmal1* and *Cry1* transcription.

The model shows that it is possible to find an administration pattern that rescues the amplitude of most clock genes (see Figures 7.11, 7.12, 7.13). Interestingly, an appropriate phase of expression is obtained only for some administration times. Indeed, an agonist injection that is timed around ZT 13.7 leads to both optimal amplitudes and phases of clock gene expression (see Fig. 4.13, first column) unlike when the agonist pulse is shifted by 12 hours (see Fig. 4.13, second column). Two other timings, advanced and delayed by 8 hours are also shown for comparison in Figures 7.11, 7.12, 7.13. The model thus highlights that the effect of pharmacological administration of clock targets is strongly dependent on the administration time. More specifically, it suggests that physiological amplitude and phase of clock gene expression can be restored when the time of clock agonist administration is carefully chosen. However, although our model is quite detailed and is consistent with experimental data, we have neglected some interactions as the neuro-endocrine influence of the SCN. Therefore, we believe that we should not focus too much on the exact value of the optimal administration time but rather on elucidating the mechanism behind the amplitude and phase rescue (see section 5.1 for a more detailed analysis).

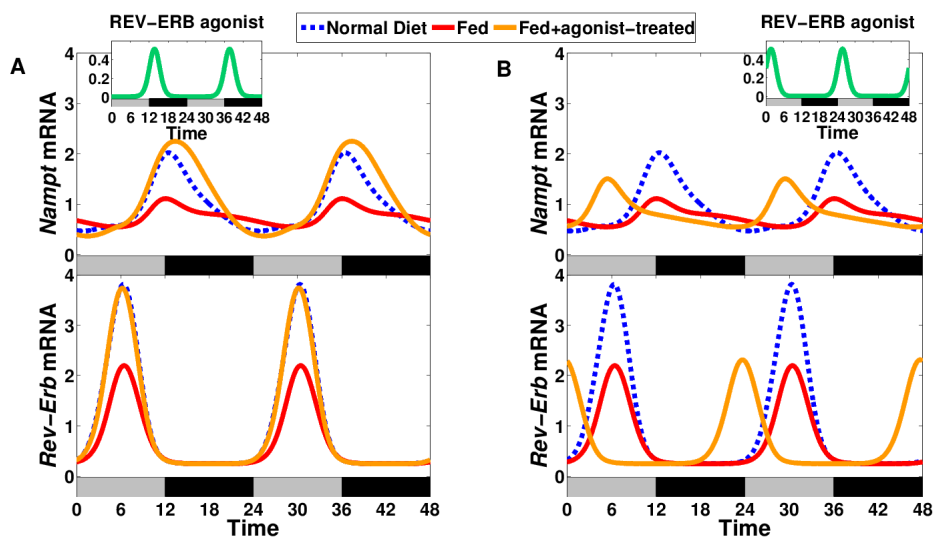


Fig. 4.13 Rescue of oscillations in the *Nampt* (top) and *Rev-Erb* (bottom) expression profiles of cells subjected to dampened AMPK rhythms, using a REV-ERB agonist. In the A panel, the agonist pulse (top inset) is optimally timed around ZT 13.7, leading to restored profiles, unlike when the agonist pulse is shifted by 12 hours (B panel). The profiles corresponding to treated (resp., non treated) cells are shown in orange and red, respectively, and compared to those corresponding to WT cells under normal AMPK rhythms (dashed blue).

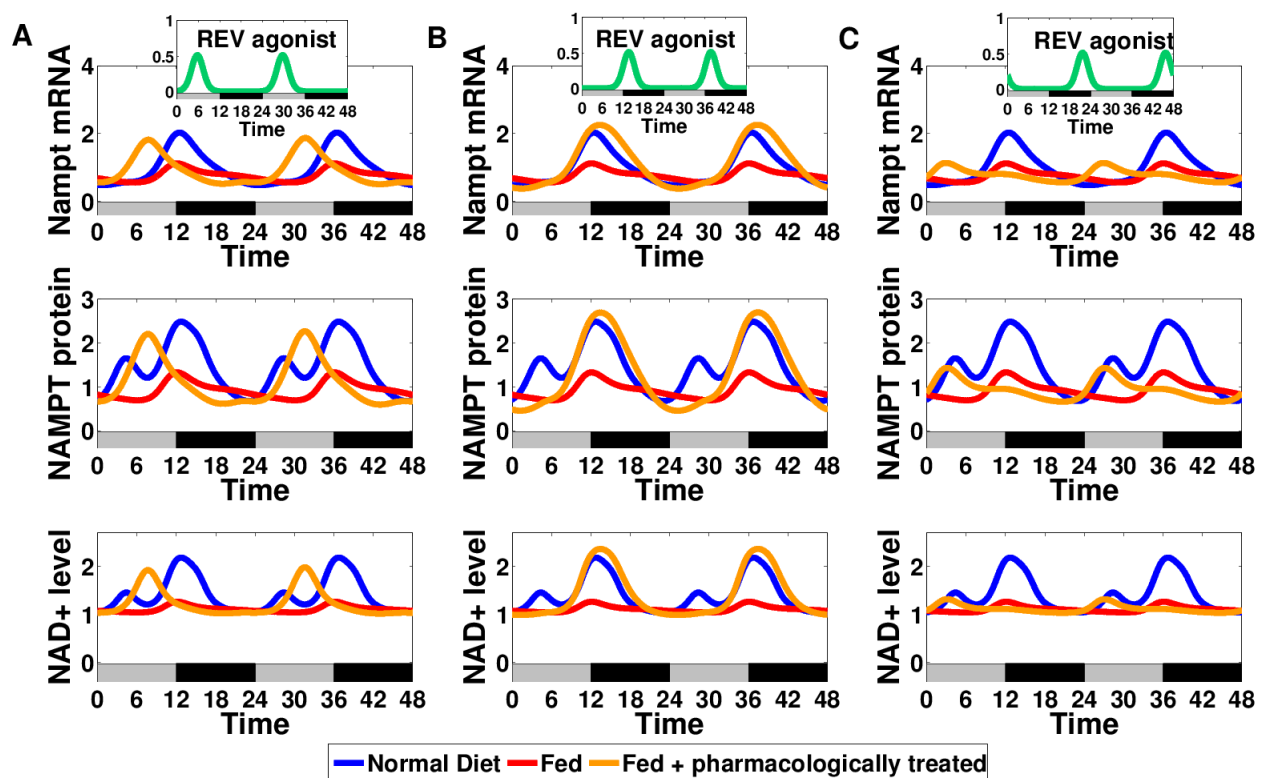


Fig. 4.14 Effect of a Rev-Erb agonist treatment delivered at three different times of the day to cells subjected to dampened AMPK rhythms. The Namp1, NAMPT protein, and NAD⁺ profiles corresponding to treated (resp., non treated) cells are shown in orange and red, respectively, and compared to those corresponding to WT cells under normal AMPK rhythms (blue). The optimal timing is shown in the middle column

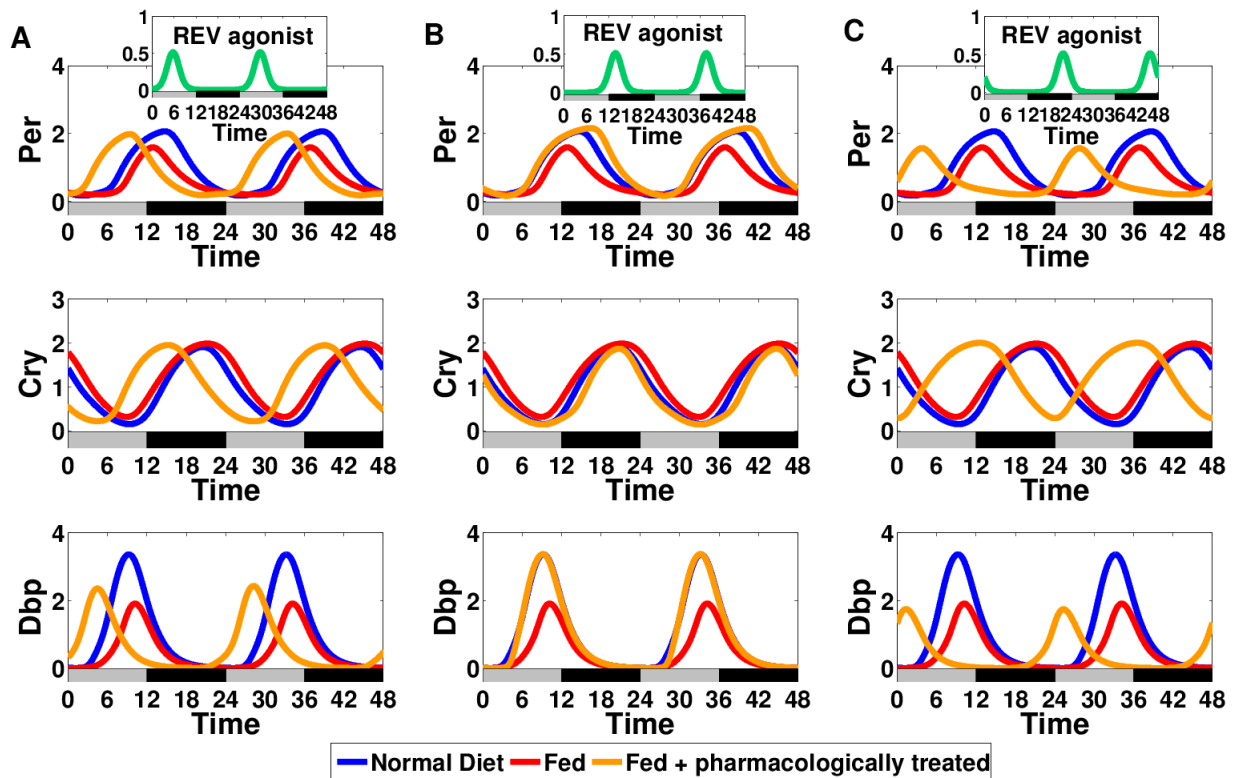


Fig. 4.15 Effect of a Rev-Erb agonist treatment delivered at three different times of the day to cells subjected to dampened AMPK rhythms. The *Per*, *Cry*, and *Dbp* profiles corresponding to treated (resp., non treated) cells are shown in orange and red, respectively, and compared to those corresponding to WT cells under normal AMPK rhythms (blue). The optimal timing is shown in the middle column.

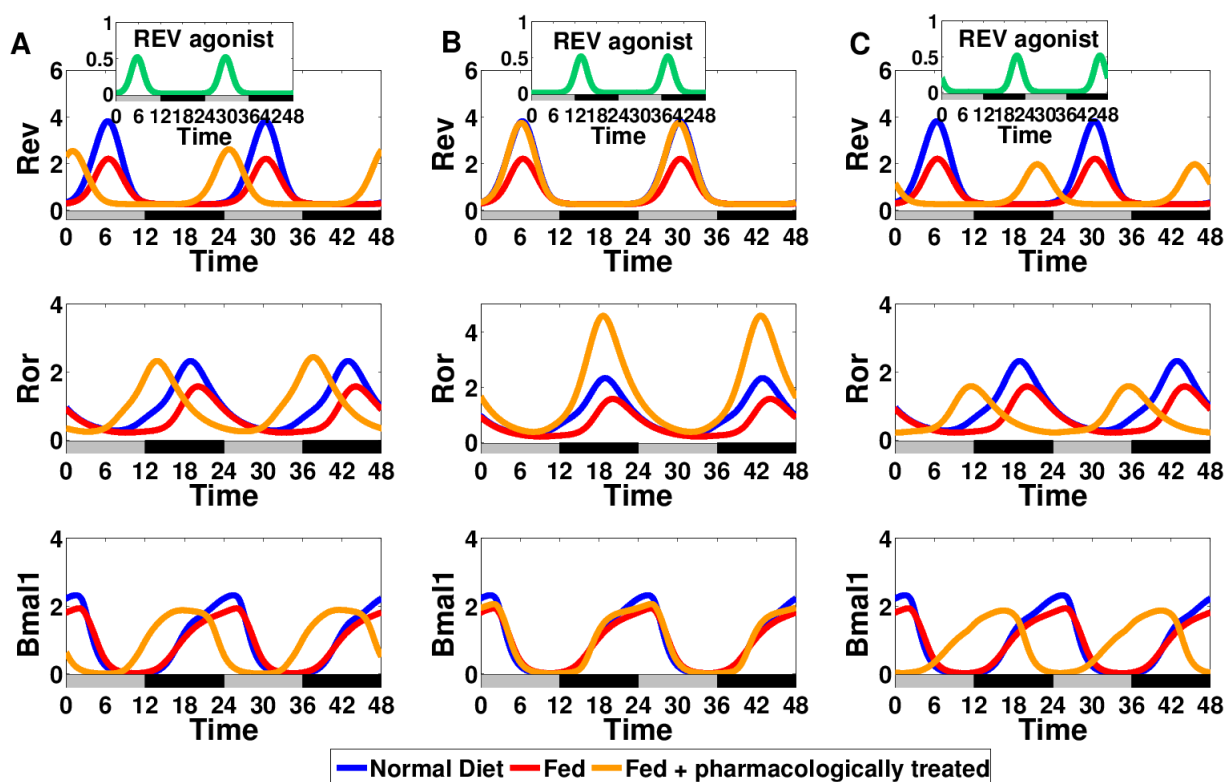


Fig. 4.16 Effect of a Rev-Erb agonist treatment delivered at three different times of the day to cells subjected to dampened AMPK rhythms. The Rev, Ror, and Bmal1 profiles corresponding to treated (resp., non treated) cells are shown in orange and red, respectively, and compared to those corresponding to WT cells under normal AMPK rhythms (blue). The optimal timing is shown in the middle column.

4.5 Conclusion

The circadian system enables to keep the internal physiological processes in synchrony with the external periodic cues such as the light-dark cycle but also the alternation between feeding and fasting phases. It is thus not surprising that peripheral clocks respond to food cues and are able to adjust metabolic processes (energy storage or utilization of different fuels) according to the cell nutrient status [135]. In order to investigate how the liver clock senses the metabolic status (or how food entrains the circadian clock), we have built a mathematical model coupling the circadian network to key metabolic actors. It includes the nutrient sensors SIRT1 and AMPK that are respectively sensitive to NAD⁺ and AMP levels. Variations in the levels of these two metabolites can be seen as a readout of alternation between feeding and fasting phases. Modification of SIRT1 activity upon fluctuations in NAD⁺ levels can arise from several mechanisms: either by variations of the redox ratio NAD⁺/NADH or through fluctuations in NAD⁺ biosynthesis, in particular in salvage pathway. Indeed, one of the rate limiting enzyme in NAD⁺ salvage pathway, NAMPT, is under the control of the clock [141]. In our model, we only took account of this last mechanism to explain NAD⁺ daily variations and it was sufficient to reproduce accurately the daily changes in NAD⁺ profiles. Moreover, active AMPK has been shown to increase NAD⁺ levels but it is still discussed whether it is a direct effect or an indirect one via the *Nampt* mRNA or via its protein. We have considered the last case and shown that it enables to explain the "mysterious" bimodal pattern in both NAMPT protein and NAD⁺ time profiles.

With so many kinetic parameters, one could argue that there is always a risk of over-fitting and ensued poor predictive power of the model. However, our model not only reproduces the right period, amplitude and phase of clock gene expression but accurately fits experimental mRNA data. Furthermore, we also reproduce qualitatively several knockdown phenotypes which constrains certain parameters values. It has been discussed that even if biological models are often sloppy with some poorly constrained parameters, valuable predictions can be made when a few parameters are well constrained. We should thus focus on our model predictions rather than on the set of selected values of kinetic parameters [17].

We used the model to see what happens following disturbance of AMPK rhythm. First, we have observed that the 12h harmonics in NAMPT protein and AMPK profiles are lost for both high and low AMPK activities, two conditions that can be assimilated to a fasted and to a constant fed state. Our simulation results thus reinforce the idea that some ultradian rhythms (here those in NAD⁺ and NAMPT protein profiles) are generated through the intersection between a local circadian rhythm and the feeding rhythm [78]. Another interesting result is the amplitude dampening in clock gene expression observed for the fed state. This suggests that the amplitude reduction in clock gene expression observed under a ad libitum high fat

diet feeding can at least partially be explained by the loss of AMPK rhythm that accompanies this disturbed feeding pattern.

Finally, several experiments have suggested that a rescue of clock gene amplitude after a high fat diet feeding protects animals against diet-induced obesity [71], [57]. Therefore, we have simulated the pharmacological administration of a clock agonist at different times. We have found that the amplitude of clock gene expression can be rescued only when the agonist is injected at certain moments of the day.

So, in summary, our work highlights the importance of the AMPK activity rhythm in the entrainment of the liver clock by food cues. Our model also indicates that the dampening of circadian rhythms associated with metabolic diseases and ageing could be treated by an optimally chosen circadian administration of clock agonists.

Chapter 5

Preliminary results and Perspectives

5.1 Preliminary results

5.1.1 Relative importance of the different feedback loops

Clock and metabolism are intimately linked. In particular, the two nutrient sensors AMPK and SIRT1 have several crosstalks with the clock. In our model, SIRT1 decreases the activation rate of CLOCK-BMAL1 but also promotes PER2 degradation and deacetylates PGC1 α . On the other hand, AMPK has also several actions on the clock. First, it destabilizes CRY1 and PER2. Secondly, it regulates the levels of protein NAMPT. Finally, it also phosphorylates PGC1 α . As seen in chapter3, the dampening of AMPK activity rhythm results in an amplitude reduction in clock genes expression. Therefore, it would be interesting to evaluate the relative contribution of the different actions of AMPK on this phenotype. More specifically, do all the interactions of AMPK with the clock play a role in this reduction of amplitude ? Or does one of these interactions play a predominant role ? To investigate this question, I have removed the different crosstalks one by one and evaluated the effect on the amplitude of gene expression (see Fig. 5.1). It shows that it is the axis AMPK-PGC1 α -*Bmal1* that is mainly responsible for the decrease in clock gene expression when the levels of AMPK are deprived (see Fig. 5.2). The same calculations will be done to see the relative importance of the different crosstalks between SIRT1 and the clock.

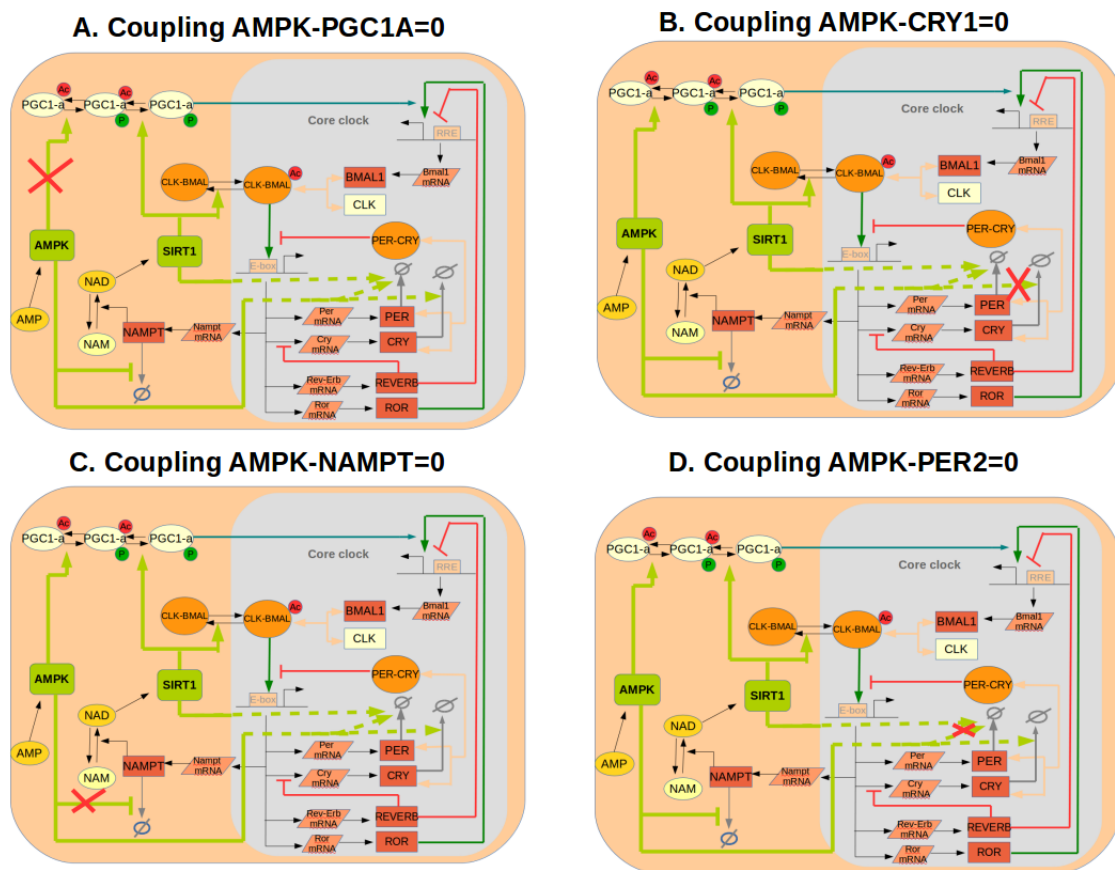


Fig. 5.1 Illustration of the different interactions of AMPK with the clock that I have removed one by one.

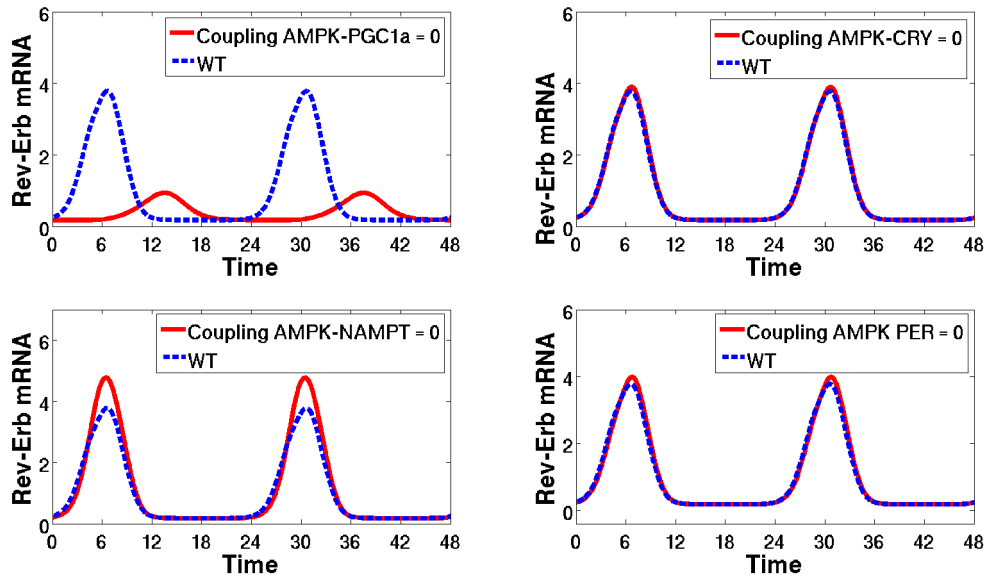


Fig. 5.2 Rev-Erb expression levels in WT (blue curves) and when the different interaction between AMPK and the clock are removed one by one (red curves).

5.2 Perspectives

5.2.1 Improvement of our present model

5.2.1.1 Include the circadian variations of $PGC1\alpha$ mRNA

Even if our present model reproduces properly the experimental data and also makes interesting predictions, it can still be improved. A first possible improvement concerns $PGC1\alpha$. As seen in Chapter 1, both $PGC1\alpha$ mRNA and protein time profiles are circadian. In particular, its mRNA peaks around ZT13 while immunoblotting data show that the total concentration of the protein, $PGC1\alpha_{TOT}$, is high between ZT13 and ZT1 in the liver [106]. In our model, an important quantity is the active form of $PGC1\alpha$. The latter depends on the activity of SIRT1 and AMPK and on the total concentration of the protein $PGC1\alpha_{TOT}$ (see Chapter 4, section 4.1.2.3 for the calculations). It is thus important to reproduce properly the time profile of $PGC1\alpha_{TOT}$ which depends, inter alia, on $Pgc1\alpha$ mRNA time profile. However, there is no indication that its mRNA is activated by the clock: oscillations in $Pgc1\alpha$ transcription may be due to the periodicity in food intake. Indeed, $Pgc1\alpha$ transcription is known to be activated by CREB, that is itself periodically phosphorylated (and thus activated) by glucagon [73]. In a first stage, we did not want to model this CREB signalling cascade. Therefore, we decided not to represent $Pgc1\alpha$ mRNA but only the total concentration of its protein, $PGC1\alpha_{TOT}$.

However, with this simplification, we did not manage to reproduce a time profile consistent with the experimental data for $PGC1\alpha_{TOT}$. Therefore, we decided to describe this quantity by a 24h external forcing function whose parameters are chosen to reproduce the oscillations observed in the immunoblotting data.

This means that our model includes 2 periodic inputs: the activity of AMPK and $PGC1\alpha_{TOT}$. This can become annoying in some situations, for example if we want to evaluate the effect of a phase shift in AMPK activity rhythm (which would reflect a phase shift in the feeding-fasting cycle). Indeed, a phase shift in food intake has probably an impact on the dynamic of $Pgc1\alpha$ mRNA and thus on $PGC1\alpha_{TOT}$: we should thus modify this second input too to make things properly but it is not clear how to do this because this input function is "artificial".

This is thus a problem: at this stage of our work (where we do not want to include the glucagon-CREB signalling cascade), it would be much more easier if $PGC1\alpha_{TOT}$ was just part of the regulation network and not an input. With this in mind, it is interesting to consider $Pgc1\alpha$ regulations in the muscle where $PGC1\alpha$ positively autoregulates its own promoter [22]: indeed, in myocytes, the transcription of $PGC1\alpha$ is activated by the calcium calmodulin-dependent protein kinase IV (CaMKIV) during exercise [59]. In turn, $PGC1\alpha$ activates a transcription factor, the myocyte enhancer factor 2 (MEF2) that then binds to $Pgc1\alpha$ promoter, thereby increasing its transcription. There is thus a positive feedback loop between $PGC1\alpha$ and this transcription factor in the muscle. There is no evidence of such a feedback loop in the liver. However, in a first approximation, it could be interesting to add such an hypothetical feedback loop to our hepatic model because this "trick" would enable to have oscillations in $Pgc1\alpha$ mRNA and so, we would probably be able to properly reproduce the experimental time profile for $PGC1\alpha_{TOT}$ oscillations without the introduction of the external forcing function. This would go as follows: the protein $PGC1\alpha$ is periodically activated (phosphorylated and deacetylated) by AMPK and SIRT1. In turn, this active form would activate an hypothetical transcription factor that would itself promote the transcription of $Pgc1\alpha$. This event would lead to a periodic translation of the mRNA into $PGC1\alpha$ protein that can then be activated again by AMPK and SIRT1 ((see Fig. 5.3). In a long term perspective (see below), we should of course build a big model that couples metabolic pathways (glycolysis, fatty acid oxidation,..) to the clock. Such a huge model could for example link variations in glucagon concentration to both AMP (and thus AMPK) levels and CREB (and thus $Pgc1\alpha$ transcription) activity.

Besides promoting *Bmal1* transcription in "collaboration" with ROR, $PGC1\alpha$ also works in synergy with the PPARs [125]. We have seen in the introduction that the latter are involved in a feedback loop with the clock. Another improvement of the model would be to add these loops. Nevertheless, these NR are activated by free fatty acids (FFA) whose levels vary with

the feeding-fasting cycles and a proper description of FFA time profiles would require a more global model taking into account lipid metabolism (fat storage, fatty acid oxidation,..)

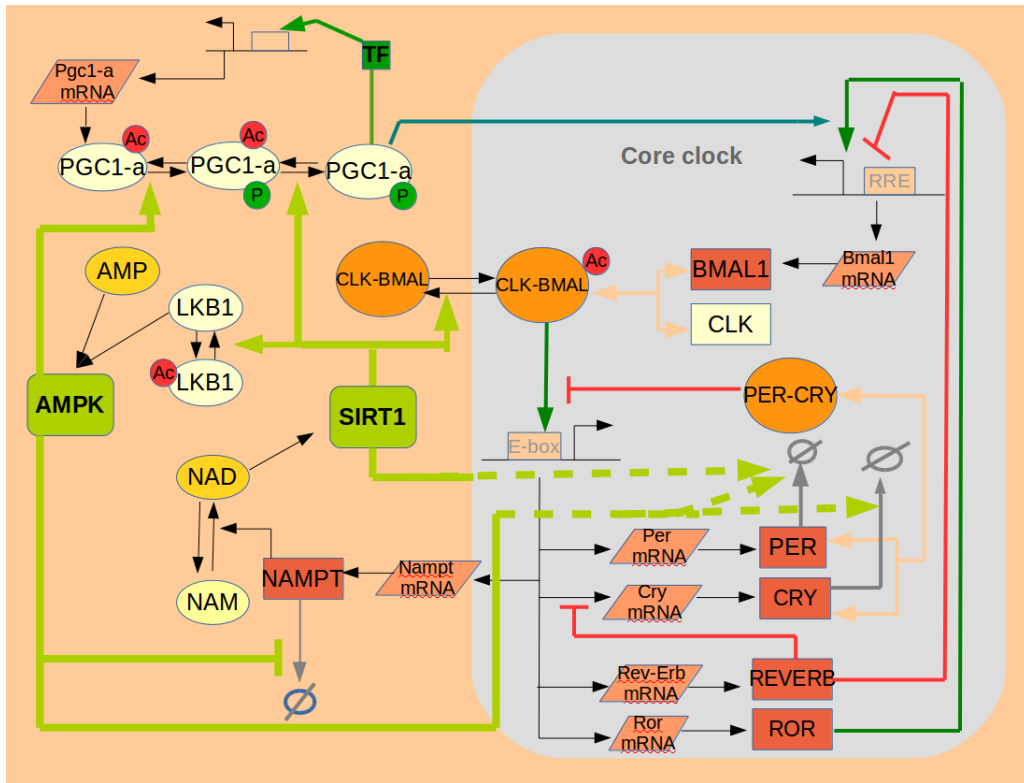


Fig. 5.3 Illustration of some possible improvement of our present model: (A) Addition of a positive feedback loop enabling oscillation in $Pgc1\alpha$ mRNA. (B) Addition of a positive feedback loop between SIRT1 and AMPK

5.2.1.2 Represent the positive feedback loop between AMPK and SIRT1

As mentioned in the introduction, AMPK needs to be phosphorylated by LKB1 to be active and this effect is increased by a rise in AMP levels. On the other hand, LKB1 needs to be deacetylated by SIRT1 to be activated. There is thus a positive feedback loop between AMPK and SIRT1 as AMPK also indirectly enhances SIRT1 activity through its interaction with the protein NAMPT. It would be interesting to include this positive loop in the model (see Fig. 5.3). This would require to write AMPK activity as a function of LKB1 activity and AMP levels. The main difficulty would be to write a function that takes into account the different mechanisms by which AMP increases AMPK activity (see Chapter 1).

5.2.1.3 Consideration of the effect of neuro-endocrine cues from SCN on the liver clock: Effect of glucocorticoid signalling

We have seen in the introduction that peripheral clocks are driven by the joined action of the feeding-fasting cycle and neuro-endocrine cues from the SCN. In particular, the SCN stimulates the periodic release of glucocorticoids by the adrenal gland [31]. The latter stimulates glucocorticoid receptors (GR) that bind on the promoter of some clock genes including *Per1* and *Per2* [31]. It would be interesting to take this effect into account in our model. This could be done in a simple way: we could add a 24h external forcing function (representing the SCN-driven variations in plasma glucocorticoid levels) that would periodically increase the transcription of the gene *Per*.

We would then have two periodic inputs in our model: the activity of AMPK (representing the effect of the feeding fasting cycle) and the glucocorticoid concentration (representing the effect of the SCN and thus of the light-dark cycle). It would then be interesting to see how our system reacts when these cues are conflicting as was done in Damiola's experiments [28].

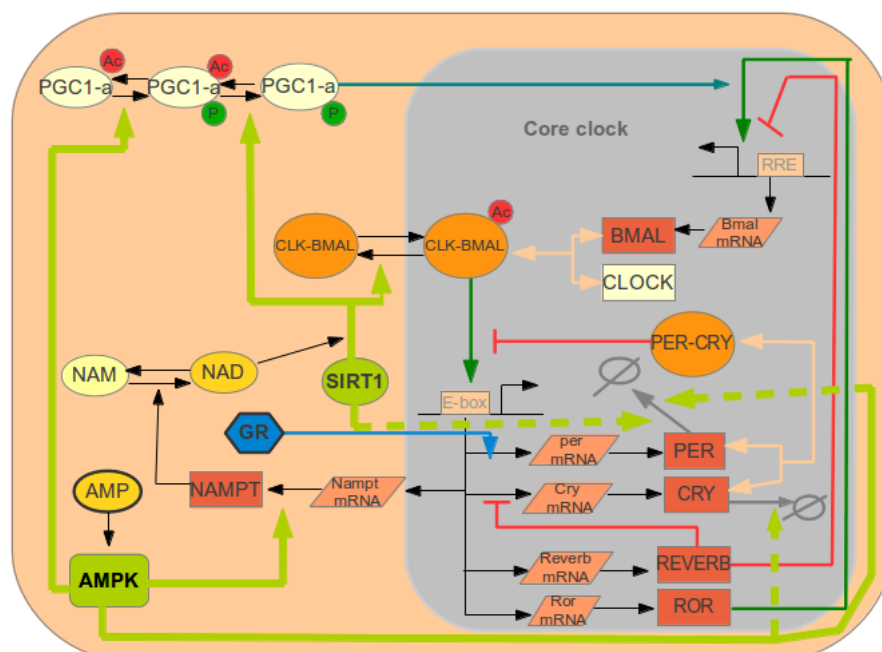


Fig. 5.4 Metabolic (A) and temperature (B) compensation in cyanobacteria: the period of the oscillations only slightly varies upon changes in the ratio ADP/ATP or in the temperature [82].

5.2.2 Build a global model connecting our model to major metabolic pathways

In our model, the entrainment of the clock by the feeding-fasting cycle is represented by the periodic variations in the activity of the nutrient sensor AMPK. This seems a reasonable approximation as the alternation between food intake and fasting periods leads to daily variations in the levels of AMP which periodically activates AMPK. Furthermore, as we have seen in the previous chapter, the AMPK time profile selected by the parameter estimation algorithm is completely consistent with the experimental time profile of AMP levels. However, the link between clock and metabolism is reciprocal and the clock thus feeds back on several metabolic processes. Let us just cite a few of them. In particular, as mentioned in the introduction, the protein CRY1 inhibits gluconeogenesis at the beginning of the fasting phase. Furthermore, the clock controls the NAD⁺ production, thereby periodically activating SIRT1 and SIRT3. In turn, SIRT3 activates fatty acid oxidation which is additional feedback of the clock on metabolism. Moreover, the clock proteins REV-ERB and ROR play a role in lipid metabolism. This suggests that it would be interesting to have a more global mathematical model connecting the clock to different metabolic pathways such as glycolysis, gluconeogenesis,.. This would of course require an important work and should be done in several steps.

5.2.2.1 Model A: glycolytic model

First, we should begin with a very simple model that describes the essential steps from food intake to ATP production: glycolysis, TCA cycle and electron transport chain (ETC). Such a model has been developed in the eighties and revisited (modified) in 2008 [126]. Glycolysis is described by three reactions: the first one lumps together the ATP consuming reactions and leads to the production of glyceraldehyde-3-phosphate. The second one corresponds the production of NADH and 1,3-diphosphoglycerate while the third one unites the ATP producing reactions and leads to synthesis of pyruvate (see Fig. 5.7). The model allows pyruvate to have different fates. Among them, pyruvate can lead to Acetyl-CoA synthesis with the production of one NADH. The TCA cycle is summarized by three reactions producing NADH. These molecules are then used by the electron transport chain summarized by one reaction converting NADH in NAD⁺ and leading to the production of ATP. The interesting point is thus that this model takes into account the conversion of AMP to ATP and NAD⁺ to NADH and vice versa during these processes. Nevertheless, as the glucose supply is constant in this model, the levels of AMP and NAD⁺ do not show any oscillations. I rapidly tried to impose a periodic glucose supply but it was not sufficient to lead to oscillations. This is

probably because the kinetic parameters are not correctly estimated. Therefore, it would be interesting to properly constrain these parameters by fitting the model to experimental time profiles for glycolytic intermediates. This should solve the problem and lead to an oscillatory behaviour for this glycolytic model (called model A).

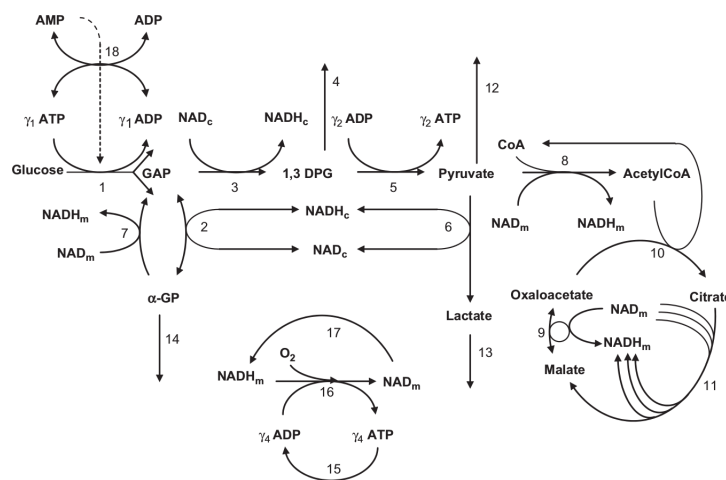


Fig. 5.5 Schema of an early metabolic model describing the glycolysis, the Krebs cycle and the electron transport chain [126].

5.2.2.2 Model B: modelling of the switch between glycolysis and fatty acid oxidation

Even if we succeed to obtain oscillations in the concentration of glycolytic intermediates, the model A would probably not reproduce the variations in AMP levels correctly. Indeed, in such a model, AMP levels would probably be high during the whole fasting period which is not what is observed experimentally: AMP levels begin to rise at the beginning of the fasting period, peak around ZT5 and then decrease. This decrease after ZT5 probably occurs for the following reason: the rise of AMP in the beginning of the fasting period activates fatty acid oxidation (through AMPK) which leads to ATP production and consecutive AMP drop. Therefore, I believe that a metabolic model describing the switch between glycolysis and fatty acid oxidation is needed to properly reproduce the experimental AMP time profiles. Let us call such a model "model B". The metabolic model B could then be connected to our initial model (see Fig. 5.6). The input of our model would thus directly be periodic food intake and not just the downstream AMPK variations.

Until now, I have essentially mentioned the AMP/ATP variations and not those of NAD⁺/NADH. How do these ratio vary due to these metabolic cycles ? Do the variations of NAD⁺/NADH also contribute to the daily (twice of day in fact) variations observed in NAD⁺ time profiles ?

Or are the latter mainly driven by the clock as suggested by our model ? The connection of model B to our clock model would enable to answer to such questions.

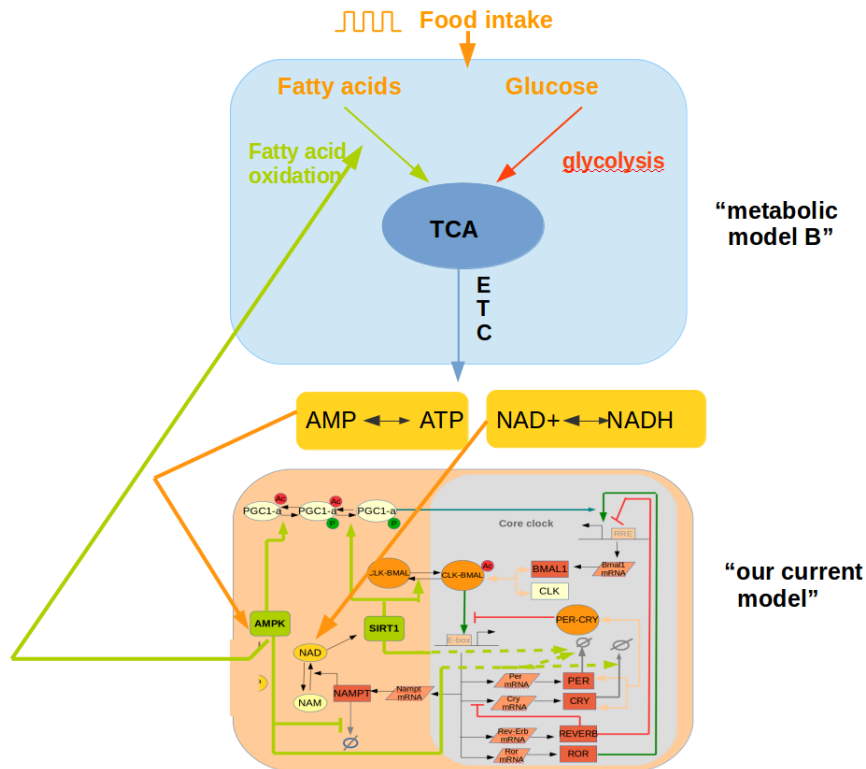


Fig. 5.6 Schema of Connection between our initial model and the metabolic model B

5.2.2.3 Model C: addition of storage processes and gluconeogenesis

The AMP levels periodically increase not only because animals stop eating during some periods but probably also because the post-absorptive state is in general an anabolic storage period. Indeed, processes like glycogen and fat storage require energy and are thus consuming ATP. It would thus be interesting to model such processes. We should also add gluconeogenesis that also an energy-requiring process. So, we would also be able represent the feedback of the clock on gluconeogenesis. Furthermore, the addition of fat storage processes would enable to describe correctly the dynamics of free fatty acids and their actions on PPARs (and thus on the clock).

Let us call such a huge single-cell model, "model C". At this stage, our "super" model would probably have many variables and require many computer resources. Therefore, it would probably be appropriate to reduce it to a more generic model that has qualitatively the same behaviour than the huge one. For example, the core clock network could be modelled by a

simpler such as the one that I have presented in Chapter 3 (section 3.2.1.2. Note that during such a reduction of the model size, attention must be given to keep the main properties of the network (such as important knockout phenotypes,...). Such a model reduction could be very useful for the next hypothetical step: represent the coupling between clock and metabolism at the level of whole organism.

5.2.2.4 Model D: taking into consideration the control of the feeding-fasting cycle by the SCN

As mentioned in the beginning of the Chapter "Results", a proper treatment of the crosstalk between clock and metabolism should integrate several tissues including brain areas. Indeed, informations about the body nutrient status not only go down for brain areas (such as the arcuate nucleus (ARC)) to peripheral tissues but also go back up to these areas and modulate food intake [4]: in particular, the hormones ghrelin and leptin promote and decrease food intake respectively, depending on the status of the energy stores (empty or full). And we have already seen that the secretion of these two hormones are also controlled by local clocks (in the stomach and in adipose tissue [154], [102]). We should thus represent these tissues in our huge model as well as the pancreas and the muscle that also contain clocks [180], [113]. The main modelling challenge would then be to take into account the tissue-specificities: indeed, the time profiles of cycling genes are in general not the same in every tissue [180], [?]. These differences could be due to differences in the relative importance of different metabolic pathways (no gluconeogenesis in the muscle, more fat storage in the adipose [68],...). Furthermore, neither is it impossible that there are also differences in the relative importance of the different feedback loops forming the core clock but few is known about this. In conclusion, all these elements should be taken into account in the construction and analysis of this huge model. Finally, we should also take into consideration that fact that the SCN projections also reach the arcuate nucleus [4]. This implies that the SCN indirectly controls food intake which makes that light and food cues are not totally uncorrelated zeitgebers.

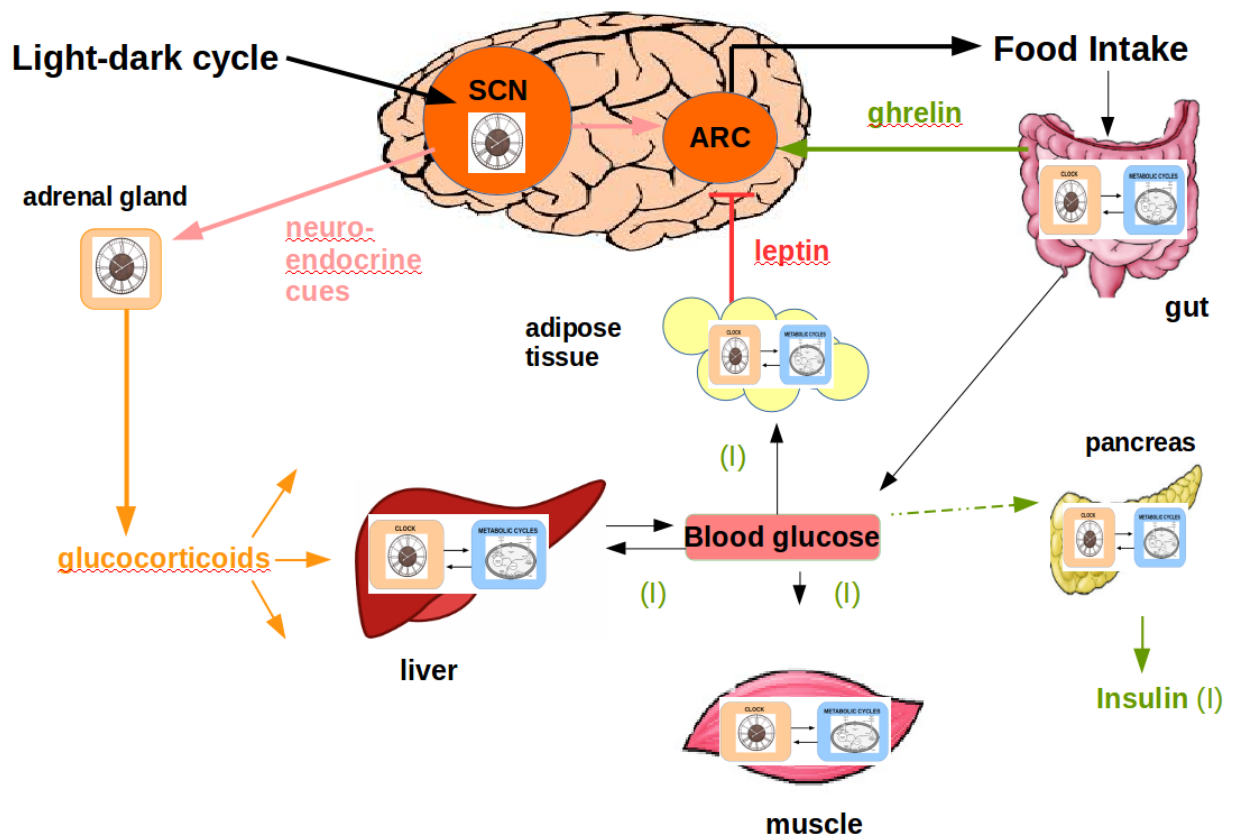


Fig. 5.7 Schema of the interactions between circadian and metabolic networks in the whole body.

Chapter 6

Supplementary Information

6.1 Kinetic Equations

Here we provide the mathematical expressions of the differential equations describing our mathematical model. Our model is composed of 16 ordinary differential equations (ODE) describing the time evolution of the concentrations of 16 species (7 mRNAs, 6 proteins, 2 complexes and 1 metabolite). In addition, three quantities are described by external forcing functions: the activity of AMPK, the total concentration of the protein PGC1 α and the concentration of the REV-ERB agonist. Some other quantities are written as a function of some of these species, such as SIRT1 that is a function of NAD⁺ levels. Similarly, the active form of the protein PGC1 α is a function of the activities of AMPK, SIRT1 and of the total concentration of the protein PGC1 α . The model has 103 constant parameters.

Variable name	Type	Description
[per]	ODE	Concentration of <i>Per</i> mRNA
[cry]	ODE	Concentration of <i>Cry</i> mRNA
[rev]	ODE	Concentration of <i>Rev-Erb</i> mRNA
[ror]	ODE	Concentration of <i>Ror</i> mRNA
[bmal]	ODE	Concentration of <i>Bmal1</i> mRNA

Table 6.1 **List of variables of the mathematical model (Part 1)**. The time evolution of the variable is specified either by an ordinary differential equation (ODE), by a function of other variables, or by an externally imposed profile.

Variable name	Type	Description
[Prot_per]	ODE	Concentration of PER protein
[Prot_cry]	ODE	Concentration of CRY protein
[Prot_rev]	ODE	Concentration of REV-ERB protein
[Prot_ror]	ODE	Concentration of ROR protein
[Prot_bmal]	ODE	Concentration of BMAL1 protein
[PC]	ODE	Concentration of PER-CRY protein complex
[CB]	ODE	Concentration of CLOCK-BMAL1 protein complex
[nampt]	ODE	Concentration of <i>Nampt</i> mRNA
[Prot_nampt]	ODE	Concentration of NAMPT protein
[dbp]	ODE	Concentration of <i>Dbp</i> mRNA
[NAD]	ODE	NAD level
Act_SIRT	function	Activity of SIRT1
Act_PGC1a	function	Activity of PGC1a
Act_AMPK	external	Activity of AMPK
Prot_PGC1a	external	Nuclear abundance of PGC1a
agonist_rev	external	Concentration of REV-ERB agonist

Table 6.2 **List of variables of the mathematical model (Part 2)**. The time evolution of the variable is specified either by an ordinary differential equation (ODE), by a function of other variables, or by an externally imposed profile.

$$\begin{aligned} \frac{d[\text{per}]}{dt} &= \left(\frac{V_{\text{max_per}} \cdot \left(1 + \text{fold_per} \cdot \left(\frac{[\text{CB}]}{K_{\text{a_per_cb}} \cdot (1 + \text{Act_SIRT})} \right)^{\text{hill_per_cb}} \right)}{1 + \left(\frac{[\text{CB}]}{K_{\text{a_per_cb}} \cdot (1 + \text{Act_SIRT})} \right)^{\text{hill_per_cb}} \cdot \left(1 + \left(\frac{[\text{PC}]}{K_{\text{i_per_pc}}} \right)^{\text{hill_per_pc}} \right)} \right) \\ &\quad - (\text{dm_per} \cdot [\text{per}]) \\ \\ \frac{d([\text{cry}])}{dt} &= \left(\frac{V_{\text{max_rev}} \cdot \left(1 + \text{fold_rev} \cdot \left(\frac{[\text{CB}]}{K_{\text{a_rev_cb}} \cdot (1 + \text{Act_SIRT})} \right)^{\text{hill_rev_cb}} \right)}{1 + \left(\frac{[\text{CB}]}{K_{\text{a_rev_cb}} \cdot (1 + \text{Act_SIRT})} \right)^{\text{hill_rev_cb}} \cdot \left(1 + \left(\frac{[\text{PC}]}{K_{\text{i_rev_pc}}} \right)^{\text{hill_rev_pc}} \right)} \right) \\ &\quad - (\text{dm_cry} \cdot [\text{cry}]) \\ \\ \frac{d([\text{rev}])}{dt} &= \left(\frac{V_{\text{max_rev}} \cdot \left(1 + \text{fold_rev} \cdot \left(\frac{[\text{CB}]}{K_{\text{a_rev_cb}} \cdot (1 + \text{Csirt} \cdot \text{Act_sirt})} \right)^{\text{hill_rev_cb}} \right)}{1 + \left(\frac{[\text{CB}]}{K_{\text{a_rev_cb}} \cdot (1 + \text{Csirt} \cdot \text{Act_sirt})} \right)^{\text{hill_rev_cb}} \cdot \left(1 + \left(\frac{[\text{PC}]}{K_{\text{i_rev_pc}}} \right)^{\text{hill_rev_pc}} \right)} \right) \\ &\quad - (\text{dm_rev} \cdot [\text{rev}]) \\ \\ \frac{d([\text{ror}])}{dt} &= \left(\frac{V_{\text{max_ror}} \cdot \left(1 + \text{fold_ror} \cdot \left(\frac{[\text{CB}]}{K_{\text{a_ror_cb}} \cdot (1 + \text{Act_SIRT})} \right)^{\text{hill_ror_cb}} \right)}{1 + \left(\frac{[\text{CB}]}{K_{\text{a_ror_cb}} \cdot (1 + \text{Act_SIRT})} \right)^{\text{hill_ror_cb}} \cdot \left(1 + \left(\frac{[\text{PC}]}{K_{\text{i_ror_pc}}} \right)^{\text{hill_ror_pc}} \right)} \right) \\ &\quad - (\text{dm_ror} \cdot [\text{ror}]) \end{aligned}$$

$$\begin{aligned}
\frac{d([bmal])}{dt} &= \left(\frac{V_{max_bmal} \cdot \left(1 + fold_bmal \cdot (1 + Act_PGC1a) \cdot \left(\frac{[Prot_ror]}{K_{a_bmal_ror}} \right)^{hill_bmal_ror} \right)}{1 + \left(\frac{[Prot_rev]}{K_{i_bmal_rev}} \right)^{hill_bmal_rev} + \left(\frac{[Prot_ror]}{K_{a_bmal_ror}} \right)^{hill_bmal_ror}} \right) \\
&\quad - (dm_bmal \cdot [bmal]) \\
\frac{d([Prot_per])}{dt} &= kp_per \cdot [per] \\
&\quad - (dp_per \cdot (1 + m_per_sirt \cdot Act_SIRT + m_per_ampk \cdot Act_AMPK) \cdot [Prot_per]) \\
&\quad - (kass_pc \cdot [Prot_cry] \cdot [Prot_per] - kdiss_pc \cdot [PC]) \\
\frac{d([Prot_cry])}{dt} &= (kp_cry \cdot [cry]) \\
&\quad - (dp_cry \cdot (1 + m_cry_ampk \cdot Act_AMPK) \cdot [Prot_cry]) \\
&\quad - (kass_pc \cdot [Prot_cry] \cdot [Prot_per] - kdiss_pc \cdot [PC]) \\
\frac{d([Prot_rev])}{dt} &= (kp_rev \cdot [rev]) \\
&\quad - (dp_rev \cdot [Prot_rev]) \\
\frac{d([Prot_ror])}{dt} &= (kp_rev \cdot [rev]) \\
&\quad - (dp_ror \cdot [Prot_ror]) \\
\frac{d([Prot_bmal])}{dt} &= (kp_bmal \cdot [bmal]) \\
&\quad - (dp_bmal \cdot [Prot_bmal]) \\
&\quad - (kass_cb \cdot [Prot_bmal] - kdiss_cb \cdot [CB]) \\
\frac{d([PC])}{dt} &= (kass_pc \cdot [Prot_cry] \cdot [Prot_per] - kdiss_pc \cdot [PC]) \\
&\quad - (d_pc \cdot [PC]) \\
\frac{d([CB])}{dt} &= (kass_cb \cdot [Prot_bmal] - kdiss_cb \cdot [CB]) \\
&\quad - (d_cb \cdot [CB])
\end{aligned}$$

$$\frac{d([nampt])}{dt} = \left(\frac{Vmax_nampt \cdot \left(1 + fold_nampt \cdot \left(\frac{[CB]}{Ka_nampt_cb \cdot (1 + Act_SIRT)} \right)^{hill_nampt_cb} \right)}{1 + \left(\frac{[CB]}{Ka_nampt_cb \cdot (1 + Act_SIRT)} \right)^{hill_nampt_cb} \cdot \left(1 + \left(\frac{[PC]}{Ki_nampt_pc} \right)^{hill_nampt_pc} \right)} \right) - (dm_nampt \cdot [nampt])$$

$$\frac{d([Prot_nampt])}{dt} = (kp_nampt \cdot [nampt]) - \left(\frac{dp_nampt \cdot [Prot_nampt]}{1 + m_nampt_ampk \cdot Act_AMPK} \right) - (dm_nampt \cdot [nampt])$$

$$\frac{d([NAD])}{dt} = \left(\frac{Vnad \cdot [Prot_nampt] \cdot (NAD_tot - [NAD])}{Knam + NAD_tot - [NAD]} \right) - \left(\frac{d_nad \cdot ([NAD] - NAD_basal)}{Knad + [NAD] - NAD_basal} \right)$$

$$\frac{d([Dbp])}{dt} = \left(\frac{Vmax_dbp \cdot \left(1 + fold_dbp \cdot \left(\frac{[CB]}{Ka_dbp_cb \cdot (1 + Act_SIRT)} \right)^{hill_dbp_cb} \right)}{1 + \left(\frac{[CB]}{Ka_dbp_cb \cdot (1 + Act_SIRT)} \right)^{hill_dbp_cb} \cdot \left(1 + \left(\frac{[PC]}{Ki_dbp_pc} \right)^{hill_dbp_pc} \right)} \right) - (dm_dbp \cdot [dbp])$$

with

$$Act_SIRT = \frac{Csirt \cdot Vsirt \cdot [NAD]}{Ksirt + [NAD]}$$

$$Act_PGC1a = \frac{Cpgc1 \cdot Vpg \cdot Act_AMPK \cdot Act_SIRT \cdot Prot_PGC1a}{1 + \frac{Act_AMPK}{Kpg1} \cdot \left(1 + \frac{Act_SIRT}{Kpg2} \right)}$$

$$Ki_bmal_rev = \frac{Ki_bmal_rev0}{1 + Crev \cdot agonist_rev}$$

$$Ki_cry_rev = \frac{Ki_cry_rev0}{1 + Crev \cdot agonist_rev}$$

6.2 Forcing Function

The activity of AMPK, the nuclear abundance of the protein PGC1a and the concentration of the agonist are described mathematically by a parametric forcing function that is able to

reproduce a large range of wave forms and that is easily encoded in SBML (the Systems Biology Markup Language is a common representation format convenient to store information about computational models). Our function has been adapted from [1]. The use of such a parametric function allows us to subject the AMPK, PGC1a and agonist profiles to parameter optimization without a priori knowledge of the profile shape. More precisely, we described the time evolution of a single pulse by the following function:

$$\begin{aligned} \text{Pulse}(\text{time}, t_c, T_d, T_r, \text{period}) = & ((\text{Step}(\text{time}, t_c - T_d/2, 0, T_r, \text{period}))) \\ & - ((\text{Step}(\text{time}, t_c - T_d/2, T_d, T_r, \text{period}))) \\ & + ((\text{Step}(\text{time}, t_c - T_d/2, T_c, T_r, \text{period}))) \\ & - ((\text{Step}(\text{time}, t_c - T_d/2, T_c + T_d, T_r, \text{period}))) \end{aligned}$$

with

$$\text{Step}(\text{time}, t_f, t_s, T_r, \text{period}) = 0.5 \cdot \left(1 + \tanh \left(\frac{\text{mod}(\text{time} - t_f, \text{period}) - t_s}{T_r} \right) \right)$$

and

$$\text{mod}(\text{time} - t_f, \text{period}) = (\text{time} - t_f) - \text{period} \cdot \text{floor} \left(\frac{(\text{time} - t_f)}{\text{period}} \right)$$

where the function $\tanh(x)$ corresponds to the hyperbolic tangent of x and where $\text{floor}(x)$ is the largest integer smaller than or equal to x . The physical meaning of the arguments of our functions is expressed in Table 6.3 and illustrated by Fig.6.1.

As mentioned above, the three quantities defined by external pulse functions are:

$$\begin{aligned} \text{Act_Ampk} = & (1 - \text{Campk}) \cdot \text{offs} + \text{Campk} \cdot (\text{amp1} \cdot \text{Pulse}(t, \text{tc1}, \text{Td1}, \text{Tr1}, 24)) \\ & + \text{Campk} \cdot (\text{amp2} \cdot \text{Pulse}(t, \text{tc2}, \text{Td2}, \text{Tr2}, 24)) \end{aligned}$$

$$\text{Prot_PGC1a} = \text{amp3} \cdot \text{Pulse}(t, \text{tc3}, \text{Td3}, \text{Tr3}, 24)$$

$$\text{agonist_rev} = \text{amp4} \cdot \text{Pulse}(t, \text{tc4}, \text{Td4}, \text{Tr4}, 24)$$

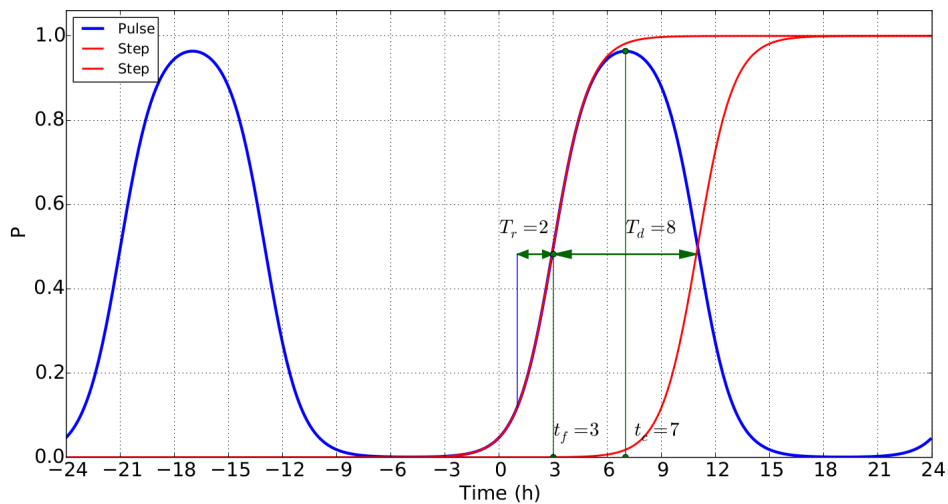


Fig. 6.1 Structure of the pulse and meaning of the pulse parameters t_c , T_d , and T_w . A pulse function is shown in blue, which is essentially obtained as the difference between the two step functions shown in red, modified to be 24h-periodic.

6.3 List of Parameters

Here, we provide the complete list of parameter values for our mathematical model. Many of these values are not uniquely determined, because there exist sets of parameters which may be changed in a coordinated way without degrading goodness of fit. As it has been discussed elsewhere [17], biological models are often sloppy with some poorly constrained parameters but valuable predictions can still be made when a few parameters are well constrained. We should thus focus on our model predictions rather than on the set of selected values of kinetic parameters. Parameter identification was carried out using the “Parameter estimation” module of the Copasi pathway simulator. This module tries to minimize an error function quantifying the discrepancies between the target profiles and the numerical solution for a given parameter set. We tested several of the algorithms proposed and found that the Hooke and Jeeves method yielded the best results. It is a derivative-free pattern search algorithm. Although it was relatively slow, this algorithm was much less prone to be blocked in a local minimum than others.

The value of some parameters changes depending on the condition. Indeed, the value of the parameters *Csirt*, *Campk* and *offs* is not the same in WT condition than in HFD, fasting or KO (SIRT1 or LKB1) state (see Table 6.14).

Parameter	Description
period	Period of the external cycles
T_d	Duration of the pulse
T_r	Time scale of the rising and decreasing fronts
t_c	Peak timing
$t_f = t_c - T_d/2$	Time location of the center of the step
t_s	Time shift

Table 6.3 Physical meaning of the arguments of our functions

Parameter	Value (h^{-1})	Description
dm_bmal	0.83722409429	<i>Bmal</i> mRNA degradation rate
dm_cry	0.360780034076	<i>Cry</i> mRNA degradation rate
dm_dbp	0.444112624528	<i>Dbp</i> mRNA degradation rate
dm_nampt	0.785562938814	<i>Nampt</i> mRNA degradation rate
dm_per	0.298478325434	<i>Per</i> mRNA degradation rate
dm_rev	3.87765089596	<i>Rev-Erb</i> mRNA degradation rate
dm_ror	0.248733351337	<i>Ror</i> mRNA degradation rate
dp_bmal	0.186413466797	BMAL protein degradation rate
dp_cry	0.735585028275	CRY protein degradation rate
dp_nampt	49.9365257011	NAMPT protein degradation rate
dp_per	6.72641260095	PER protein degradation rate
dp_rev	0.281564063057	REV-ERB protein degradation rate
dp_ror	0.0279543669837	ROR degradation rate
d_cb	0.188038524824	CLOCK-BMAL complex degradation rate
d_pc	0.56583376255	PER-CRY complex degradation rate

Table 6.4 mRNA and protein degradation rates (15 parameters)

Parameter	Value (h^{-1})	Description	
Parameter	Value	Unit	Description
kass_cb	0.016288166095	$nmol^{-1} \cdot l \cdot h^{-1}$	CLOCK-BMAL association rate
kass_pc	15.0415293295	$nmol^{-1} \cdot l \cdot h^{-1}$	PER-CRY association rate
kdiss_cb	0.0058093419285	h^{-1}	CLOCK-BMAL dissociation rate
kdiss_pc	0.00677798756031	h^{-1}	PER-CRY dissociation rate

Table 6.5 complexation kinetic rates (4 parameters)

Parameter	Value ($nmol \cdot l^{-1} \cdot h^{-1}$)	Description
Vmax_bmal	0.0876210969599	<i>Bmal</i> maximal transcription rate
Vmax_cry	0.790210123364	<i>Cry</i> maximal transcription rate
Vmax_dbp	0.0106454783875	<i>Dbp</i> maximal transcription rate
Vmax_nampt	3.59275282724	<i>Nampt</i> maximal transcription rate
Vmax_per	0.679649332349	<i>Per</i> maximal transcription rate
Vmax_rev	0.968348743692	<i>Rev-Erb</i> maximal transcription rate
Vmax_ror	7.546684801	<i>Ror</i> maximal transcription rate

Table 6.6 **maximal transcription rates** (7 parameters)

Parameter	Value (dimensionless)	Description
fold_bmal	15.767378716	activation ratio of <i>Bmal</i> by ROR
fold_cry	1.46890194306	activation ratio of <i>Cry</i> by CLOCK-BMAL
fold_dbp	210.934631172	activation ratio of <i>Dbp</i> by CLOCK-BMAL
fold_nampt	1.54764451481	activation ratio of <i>Nampt</i> by CLOCK-BMAL
fold_per	2.28164994985	activation ratio of <i>Per</i> by CLOCK-BMAL
fold_rev	72.0854248903	activation ratio of <i>Rev-Erb</i> by CLOCK-BMAL
fold_ror	265.446678507	activation ratio of <i>Ror</i> by CLOCK-BMAL

Table 6.7 **activation ratios** (7 parameters)

Parameter	Value ($nmol^{-1} \cdot l$)	Description
Ka_bmal_ror	0.00612521376364	Regulation threshold of <i>Bmal</i> by ROR
Ka_cry_cb	1.02504215499	Regulation threshold of <i>Cry</i> by CLOCK-BMAL
Ka_dbp_cb	0.179239014849	Regulation threshold of <i>Dbp</i> by CLOCK-BMAL
Ka_nampt_cb	3.3501356491	Regulation threshold of <i>Nampt</i> by CLOCK-BMAL
Ka_per_cb	1.92410288149	Regulation threshold of <i>Per</i> by CLOCK-BMAL
Ka_rev_cb	0.260846828116	Regulation threshold of <i>Rev-Erb</i> by CLOCK-BMAL
Ka_ror_cb	0.269355240074	Regulation threshold of <i>Ror</i> by CLOCK-BMAL
Ki_bmal_rev0	0.0106281082629	Regulation threshold of <i>Bmal</i> by REV-ERB
Ki_cry_rev0	0.265783177752	Regulation threshold of <i>Cry</i> by REV-ERB
Ki_cry_pc	0.00369879525409	Regulation threshold of <i>Cry</i> by PER-CRY
Ki_dbp_pc	2.98759559725	Regulation threshold of <i>Dbp</i> by PER-CRY
Ki_nampt_pc	0.0139623976236	Regulation threshold of <i>Nampt</i> by PER-CRY
Ki_per_pc	0.276913663213	Regulation threshold of <i>Per</i> by PER-CRY
Ki_rev_pc	106.094972455	Regulation threshold of <i>Rev-Erb</i> by PER-CRY
Ki_ror_pc	0.00790234946595	Regulation threshold of <i>Ror</i> by PER-CRY

Table 6.8 Regulation thresholds (15 parameters)

Parameter	Value (dimensionless)	Description
hill_bmal_rev	4.33262477046	Hill coeff., regulation of <i>Bmal</i> by REV-ERB
hill_bmal_ror	1.83992599578	Hill coeff., regulation of <i>Bmal</i> by ROR
hill_cry_cb	8.98314667872	Hill coeff., regulation of <i>Cry</i> by CLOCK-BMAL
hill_cry_pc	2.40163809608	Hill coeff., regulation of <i>Cry</i> by PER-CRY
hill_cry_rev	3.72151508117	Hill coeff., regulation of <i>Cry</i> by REV-ERB
hill_dbp_cb	9.52230932102	Hill coeff., regulation of <i>Dbp</i> by CLOCK-BMAL
hill_dbp_pc	11.9392784789	Hill coeff., regulation of <i>Dbp</i> by PER-CRY
hill_nampt_cb	1.97957210754	Hill coeff., regulation of <i>Nampt</i> by CLOCK-BMAL
hill_nampt_pc	1.35736883317	Hill coeff., regulation of <i>Nampt</i> by PER-CRY
hill_per_cb	8.90734525281	Hill coeff., regulation of <i>Per</i> by CLOCK-BMAL
hill_per_pc	8.62466105	Hill coeff., regulation of <i>Per</i> by PER-CRY
hill_rev_cb	9.3260229425	Hill coeff., regulation of <i>Rev-Erb</i> by CLOCK-BMAL
hill_rev_pc	2.24709629684	Hill coeff., regulation of <i>Rev-Erb</i> by PER-CRY
hill_ror_cb	9.40549778359	Hill coeff., regulation of <i>Ror</i> by CLOCK-BMAL
hill_ror_pc	1.84102439743	Hill coeff., regulation of <i>Ror</i> by PER-CRY

Table 6.9 Hill coefficients (15 parameters)

Parameter	Value (molecules per hour per mRNA)	Description
kp_bmal	0.623440064156	<i>Bmal</i> translation rate
kp_cry	3.74759559672	<i>Cry</i> translation rate
kp_nampt	58.9636945644	<i>Nampt</i> translation rate
kp_per	11.567711205	<i>Per</i> translation rate
kp_rev	0.056252697689	<i>Rev-Erb</i> translation rate
kp_ror	0.046692887989	<i>Ror</i> translation rate

Table 6.10 **Translation rates** (6 parameters)

Parameter	Value	Description
m_cry_ampk	0.218430240025	modulation of CRY stability by AMPK
m_nampt_ampk	0.624628800553	modulation of NAMPT stability by AMPK
m_per_ampk	0.00502446815924	modulation of PER stability by AMPK
m_per_sirt	0.348469409545	modulation of PER stability by SIRT

Table 6.11 **Protein stability modulation constants** (4 parameters)

Parameter	Value	Unit	Description
Vsirt	0.963939954171	N/A	Maximum SIRT1 activity
Ksirt	0.7501248	$nmol \cdot l^{-1}$	Value of [NAD] at which SIRT1 activity is half of maximum
d_nad	387.806117268	h^{-1}	Rate of transformation of NAD into NAM
Knad	0.321581717245	$nmol \cdot l^{-1}$	Value of [NAD] at which transformation into NAM is at half of maximum rate
NAD_basal	0.916571402867	$nmol \cdot l^{-1}$	Value of [NAD] below which transformation of NAD into NAM is inactivated
Vnad	294.403858466	molecule per hour per NAMPT protein	Maximum regeneration rate of NAD
NAD_tot	4.19511384268	$nmol \cdot l^{-1}$	Total concentration of NAD and NAM
Knam	2.75264507244	$nmol \cdot l^{-1}$	Value of NAM at which NAD salvage rate is half of maximum
Vpg	24.4255177746	$nmol^{-1} \cdot h$	Maximum activity of PGC1a
Kpg1	0.0532835320495	N/A	Michaelis-Menten constant for phosphorylation of PGC1a by AMPK
Kpg2	13.2432679016	N/A	Michaelis-Menten constant for deacetylation of PGC1a by SIRT1

Table 6.12 **NAD kinetics, Sirt1 and PGC1a activity** (11 parameters)

Parameter	Value	Unit	Description
tc1	4.125	<i>h</i>	Timing of the first AMPK pulse
tc2	15.75	<i>h</i>	Timing of the second AMPK pulse
tc3	18.875	<i>h</i>	Time of maximal nuclear PGC1a abundance
Td1	2.25	<i>h</i>	Duration of the first AMPK pulse
Td2	1.5	<i>h</i>	Duration of the first AMPK pulse
Td3	15.25	<i>h</i>	Duration of the nuclear PGC1a presence
Tr1	2.6	<i>h</i>	Rise time of the first AMPK pulse
Tr2	1.8	<i>h</i>	Rise time of the second AMPK pulse
Tr3	0.5	<i>h</i>	Rise time of nuclear PGC1a
amp1	6.0	N/A	Amplitude of the first AMPK pulse
amp2	0.9778008	N/A	Amplitude of the second AMPK pulse
amp3	0.803062	<i>nmol⁻¹ · l</i>	Amplitude of the nuclear PGC1a abundance pulse

Table 6.13 **Pulse parameters** (12 parameters)

Name	WT	SIRT1 KO	LKB1 KO	HFD	fasting
Csirt	1	0	1	1	1
Campk	1	1	0.0375	0.05	0.05
offs	0.02	0.02	0.02	0.02	2.5

Table 6.14 **Miscellaneous constants used to describe perturbations**

Chapter 7

Résumé en français

7.1 Introduction: couplage entre horloge circadienne et métabolisme

7.1.1 Horloge circadienne

Les rythmes circadiens sont des processus biologiques qui oscillent avec une période d'environ 24h. Ces rythmes d'origine endogène sont entrainables par des signaux périodiques externes tels que l'alternance jour-nuit ou le rythme de prise alimentaire [13]: les horloges circadiennes permettent ainsi aux organismes de synchroniser leurs processus physiologiques avec les variations périodiques de leur environnement [10]. Chez les mammifères, ces rythmes sont générés au niveau des noyaux suprachiasmatiques (SCN) de l'hypothalamus. En effet, il a été montré qu'une ablation du SCN élimine le rythme d'activité locomotrice chez les rongeurs mais que celui peut être restauré suite à une transplantation du SCN [161], [139]. De plus, il existe une connexion directe entre le SCN et la rétine, ce qui permet l'entraînement de l'horloge par la lumière.

Ces rythmes persistent également au niveau des cellules individuelles du SCN où ils sont générés par un mécanisme de rétroaction négative au niveau de la transcription [13]. Plus spécifiquement, un complexe protéique activateur, CLOCK-BMAL1 (CB) active la transcription des gènes d'horloge. Parmi eux, les represseurs Period (*Per 1,2,3*) et Cryptochrome (*Cry 1,2*) dont les protéines vont réprimer l'action du complexe CB. En plus de cette boucle de rétroaction négative, l'horloge comprend également les récepteurs nucléaires REV-ERB- α et β et ROR- α , β et γ dont la transcription est sous le contrôle de CB et qui inhibent et activent respectivement la transcription du gène *Bmal1* [161].

Il y a une vingtaine d'années, on a découvert que l'expression des gènes d'horloge n'oscillait

pas uniquement dans le SCN mais également dans d'autres tissus périphériques tels que le foie, les muscles, les reins, le coeur,..indiquant l'existence d'horloges dans ces tissus périphériques [183],[180]. Alors que l'horloge centrale du SCN est entraînée par le cycle jour-nuit, les horloges périphériques sont d'abord entraînées par la nourriture: chez les rongeurs, lors du passage d'une prise alimentaire nocturne à une prise alimentaire diurne, le profil d'expression des gènes d'horloge dans les tissus périphériques s'inverse progressivement pour être en phase avec les signaux de nourriture [28]. Par contraste, les profils de l'horloge centrale restent en phase avec le cycle jour-nuit.

7.1.2 Horloge et métabolisme

L'horloge des mammifères régule de nombreux processus physiologiques tels que le cycle veille-sommeil, le cycle cellulaire, la réponse immunitaire, la sécrétion hormonale,...En particulier, le fonctionnement de l'horloge et du métabolisme énergétique sont intimement liés [135]. En effet, l'alternance entre phase de prise alimentaire et jeûne provoque des variations des ratios AMP/ATP et NAD⁺/NADH [67]. Ceci active périodiquement les senseurs nutritionnels AMPK et SIRT1: AMPK est activé par des niveaux élevés d'AMP et SIRT1 par une augmentation des niveaux de NAD⁺. Ces deux senseurs ont plusieurs interactions avec les composants de l'horloge et pourraient donc être des points névralgiques du couplage entre horloge et métabolisme [12],[124],[97],[165].

La sirtuine SIRT1 est une deacetylase dont l'activité dépend de la présence de son cofacteur NAD⁺ [37]. Or l'une des voies de biosynthèse du NAD⁺ (nommée le salvage pathway) est sous le contrôle de l'horloge [141]: la conversion du nicotinamide en NAD⁺ se fait en présence de l'enzyme NAMPT dont la transcription est activée par le complexe CB. Il agit d'une boucle de rétroaction négative car une fois que SIRT1 a été activé par NAD⁺, la sirtuine inhibe l'activité du complexe CB en le déacétylant [124]. Par ailleurs, SIRT1 déacétyle également la protéine PER2 ainsi que le facteur de transcription PGC1 α qui est lui-même un co-activateur de *Bmal1* [12],[7],[105]. Avant de poursuivre, arrêtons-nous un instant sur un fait étonnant: le profil d'expression de l'ARN de *Nampt* présente un pic d'expression vers ZT12 alors que les profils temporels des variations de la protéine NAMPT et de NAD⁺ sont bimodaux avec un pic durant la journée (autour de ZT5) et un pic durant la nuit (autour de ZT14-15) (voir Fig.7.1). Le pic en début de nuit provient du contrôle de l'expression de l'ARN de *Nampt* par l'horloge mais l'origine du pic diurne (absent du profil de l'ARN de *Nampt*) demeure inconnue. Nous y reviendrons un peu plus loin !

La kinase AMPK, qui est activée quand les niveaux du métabolite AMP augmente, a elle aussi plusieurs actions sur l'horloge. Premièrement, elle déstabilise les protéines PER2 et CRY1 [97],[165]. Ensuite, elle augmente aussi les niveaux de NAD⁺ et interagit donc avec la

boucle de feedback reliant SIRT1 à l'horloge [22]. Certains travaux suggèrent que l'AMPK module la conversion de NADH en NAD⁺ [22] tandis que d'autres auteurs pensent que l'AMPK agirait plutôt au niveau du salvage pathway, soit au niveau de l'ARN de *Nampt* [41] soit au niveau de sa protéine [16]: le débat est donc toujours ouvert!

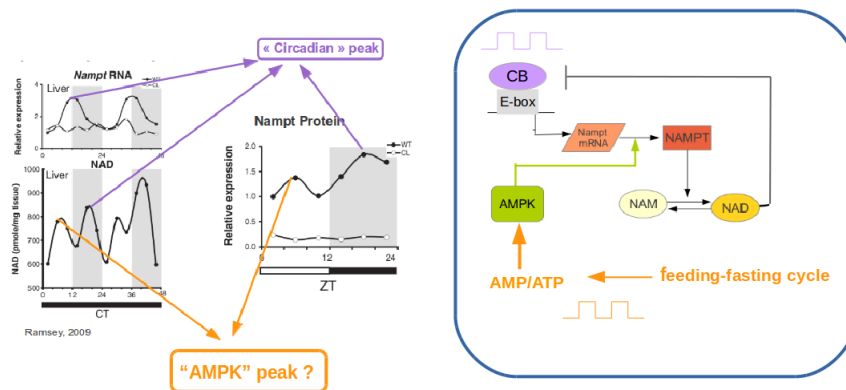


Fig. 7.1 Notre hypothèse pour expliquer le profil bimodal des niveaux de protéine NAMPT et de NAD⁺: le pic autour de ZT14 est sous le contrôle de l'horloge alors que le pic autour de ZT5 est causé par l'action de l'AMPK sur la protéine NAMPT. Données expérimentales de [141].

7.2 Résultats: modèle mathématique décrivant l'entraînement de l'horloge du foie par le métabolisme

Comme nous l'avons vu dans la section précédente, le réseau métabolique et celui de l'horloge sont intimement connectés et perturber ce couplage peut donner lieu à diverses pathologies. En effet, les données expérimentales montrent que d'une part, perturber l'expression des gènes d'horloges donne lieu à des maladies métaboliques [114] et que d'autre part, des perturbations dans le rythme de prise alimentaire sont corrélées avec des modifications de l'expression des gènes d'horloge et des troubles métaboliques [71]. Néanmoins, plusieurs aspects de ce couplage demeurent toujours incompris. L'amélioration de la résolution temporelle des données transcriptomiques permet d'associer les approches expérimentales à la modélisation mathématique. En particulier, la modélisation mathématique permet tester rapidement l'effet de dérèglements dans le système de régulation considéré ainsi que d'évaluer l'effet de nouvelles stratégies pharmacologiques.

C'est pourquoi nous avons décidé de construire un modèle décrivant le couplage entre

horloge et métabolisme chez les mammifères et d'explorer trois conditions (voir Fig.7.2): tout d'abord, comment le cycle de prise alimentaire/jeune entraîne l'horloge en condition physiologique. Ensuite, nous aimerions utiliser le modèle pour voir comment ce système passe d'un fonctionnement physiologique à un fonctionnement pathologique (caractérisé par une altération de l'expression des gènes d'horloge) lorsque le cycle de prise alimentaire est perturbé. Enfin, nous aimerions nous servir du modèle pour voir s'il existe une heure optimale d'administration d'un agoniste de l'horloge qui permette de restaurer le bon fonctionnement de l'horloge.

Une description complète de ce problème nécessiterait un modèle à l'échelle de l'organisme entier. En effet, il faudrait considérer tant l'horloge centrale qui contrôle la prise alimentaire que les horloges des tissus métaboliques majeurs (foie, tissu adipeux, muscle, pancreas) et les signaux endocriniens (leptine, ghréline, insuline, glucagon,...) via lesquels tous ces tissus interagissent [4]. Ce serait donc un tâche colossale. Afin de simplifier un peu les choses, nous avons décidé de nous focaliser sur les interactions entre horloge et métabolisme dans un tissu uniquement: le foie. Nous avons choisi ce tissu pour plusieurs raisons. Premièrement, parce que le foie est particulièrement sensible aux signaux de nourriture: en effet, le foie est l'organe qui s'adapte le plus vite lors d'un passage d'une prise alimentaire nocturne à une prise alimentaire diurne [28]. Ceci indique que l'horloge du foie se découple facilement de l'influence du SCN et cela nous autorise à négliger l'influence du forçage par horloge centrale en première approximation et à ne considérer que l'effet du forçage par la nourriture. Un second argument en faveur du foie est qu'il existe beaucoup plus de données expérimentales disponibles (profils d'expression des gènes métaboliques et d'horloges) pour ce tissu que pour d'autres. Enfin, des résultats expérimentaux indiquent que le foie est composé de cellules bien synchronisées entre elles: en effet, même les animaux avec des lésions au niveau du SCN présentent une cohérence de phase entre hépatocytes dans l'expression des gènes d'horloge [148]. Cette observation nous permet de modéliser le foie comme un seul oscillateur plutôt que comme une population d'oscillateurs cellulaires.

7.2.1 Construction du modèle

Nous démarré avec un modèle décrivant le fonctionnement de l'horloge dans le foie et nous avons progressivement rajouté les interactions de celle-ci avec plusieurs acteurs métaboliques clés. Nous avons fait plusieurs hypothèses afin d'avoir un modèle de complexité intermédiaire: tout d'abord, pour la partie horloge, nous avons choisi de ne pas représenter chaque isoforme des composants de l'horloge. Ainsi, par exemple, les gènes *Per1,2,3* sont représentés sous la forme d'un seul gène *Per* et ainsi de suite. Ensuite, nous avons décidé de ne prendre en compte ni les diverses modifications posttraductionnelles (telles que la phosphorylation

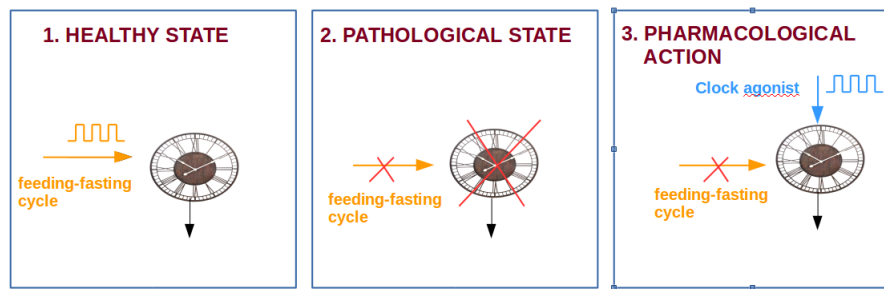


Fig. 7.2 Le but du présent travail en trois étapes : d'abord nous allons modéliser l'entraînement de l'horloge par la nourriture en conditions physiologiques (panneau de gauche); ensuite, nous allons modéliser la transition entre un état physiologique et un état pathologique (panneau au centre); enfin, nous allons modéliser l'administration d'un agoniste de l'horloge (panneau de droite).

des protéines de l'horloge,...) ni le transport nucléo-cytoplasmique. Donc, notre modèle ne fait pas la distinction entre la forme cytoplasmique et nucléaire des protéines. La partie horloge du modèle contient 12 espèces: les protéines PER, CRY, BMAL1, REV-ERB et ROR, les ARNm correspondants ainsi que deux complexes protéiques: PER-CRY (PC) et CLOCK-BMAL1 (CB).

Comme nous l'avons mentionné plus haut, l'alternance entre phases de prise alimentaire et jeûne induit des variations périodiques des niveaux des métabolites AMP et NAD⁺ ainsi que de l'activité des senseurs nutritionnels AMPK et SIRT1. En première approximation, nous avons considéré les variations périodiques de l'activité d'AMPK (et de SIRT1) comme une mesure directe de l'alternance entre jeûne et prise alimentaire. Ceci nous permet d'éviter de devoir modéliser en détail toutes les voies métaboliques comprises entre la prise alimentaire et l'activation des senseurs nutritionnels. Nous avons tout d'abord incorporé le premier senseur nutritionnel SIRT1 au modèle et plus précisément, la boucle de rétroaction négative comprenant l'ARN et la protéine Nampt, NAD⁺ et SIRT1. Pour rappel, l'horloge active la transcription de Nampt via CLOCK-BMAL1 (CB); puis la protéine NAMPT favorise la biosynthèse de NAD⁺, ce qui promeut l'activité de deacetylase de SIRT1 [141]. A son tour, SIRT1 inhibe l'activité de CB et déstabilise la protéine PER2 [12],[124]. Nous avons incorporé toutes ces interactions dans notre modèle.

La seconde étape a été d'ajouter les actions du second senseur nutritionnel, AMPK sur l'horloge. Nous avons choisi de décrire l'activité de l'AMPK par une fonction périodique externe qui représente les variations d'AMPK sous l'effet du cycle de prise alimentaire. Notre AMPK déstabilise les protéines CRY et PER en augmentant leur taux de dégradation [97],[165]. Par ailleurs, on sait que l'AMPK augmente également les niveaux de NAD⁺ [22] mais le mécanisme exacte n'est toujours pas clair: on ne sait pas si c'est direct ou indirecte

(via l'ARN ou la protéine *Nampt* [41],[16]). Néanmoins, un examen approfondi des données expérimentales nous a menés à faire l'hypothèse que l'AMPK augmente directement les niveaux de la protéine NAMPT: en effet, le profil temporel des niveaux d'AMP présente un pic diurne autour de ZT5, qui coïncide avec le mystérieux pic diurne dans les profils de la protéine NAMPT et de NAD⁺ (voir Fig.7.1). Comme ce pic est présent au niveau de la protéine NAMPT mais pas de son ARN, nous avons émis l'hypothèse que l'AMPK (qui est activée par l'AMP) régule les niveaux de la protéine NAMPT. Une seconde hypothèse importante concerne les variations des niveaux de NAD⁺. Celles-ci pourraient s'expliquer par plusieurs contributions: tout d'abord, de par le contrôle de la biosynthèse de NAD⁺ par l'horloge (via *Nampt*) et ensuite, de par l'inter-conversion NADH-NAD⁺ durant le cycle de prise alimentaire. Nous avons décidé de négliger la seconde contribution. Cela ne signifie pas que la nourriture n'a pas d'effet sur les niveaux de NAD⁺ mais plutôt que dans notre modèle, cet effet se manifeste par la voie AMPK-NAMPT-NAD⁺. Donc, dans notre modèle, l'input de la nourriture sur l'horloge se fait via l'AMPK. Finalement, le dernier acteur métabolique que nous avons incorporé est le facteur de transcription PGC1 α qui est activé à la fois par l'AMPK (par phosphorylation) et par SIRT1 (par déacétylation)[59]. Une fois activé, PGC1 α co-active la transcription du gène d'horloge *Bmal1* en collaboration avec la protéine ROR [105].

En utilisant la loi d'action de masse, nous avons traduit toutes ces interactions entre horloge et acteurs métaboliques sous forme mathématique, ce qui mène à un système de 16 équations différentielles décrivant le couplage entre horloge et métabolisme (voir Fig.7.3). Comme nous allons le voir ci-contre, malgré sa simplicité, ce modèle reproduit fidèlement de nombreuses données expérimentales.

7.2.2 Estimation de paramètres

Afin d'obtenir un modèle mathématique qui puisse répondre de manière pertinente à des questions biologiques, il faut que celui-ci reproduise le mieux possible les données expérimentales. Comme notre modèle contient 103 paramètres cinétiques et que les valeurs de ceux-ci sont généralement inconnues, nous avons décidé de contraindre celles-ci en ajustant nos résultats *in silico* aux données expérimentales. Les profils temporels que nous utilisons pour le fitting sont des profils d'expression des principaux gènes d'horloge et de *Nampt* et sont caractérisés par leur haute résolution temporelle (un point par heure). Ils proviennent de foie de souris placées en obscurité constante et nourries *ad libitum* [78]. Nous avons également utilisé des profils temporels pour le métabolite NAD⁺ [71]. La méthode d'estimation de paramètre que nous avons appliquée est une méthode d'optimisation globale nommée Hookes and Jeeves: nous avons constaté qu'elle présente l'avantage d'éviter que l'algorithme reste coincé dans

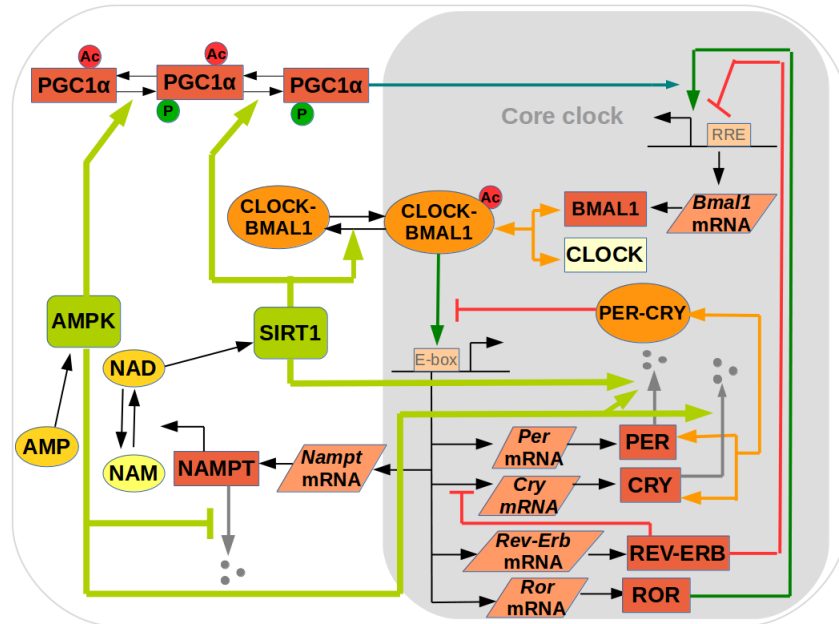


Fig. 7.3 Schéma du modèle mathématique décrivant le couplage entre l'horloge et métabolisme.

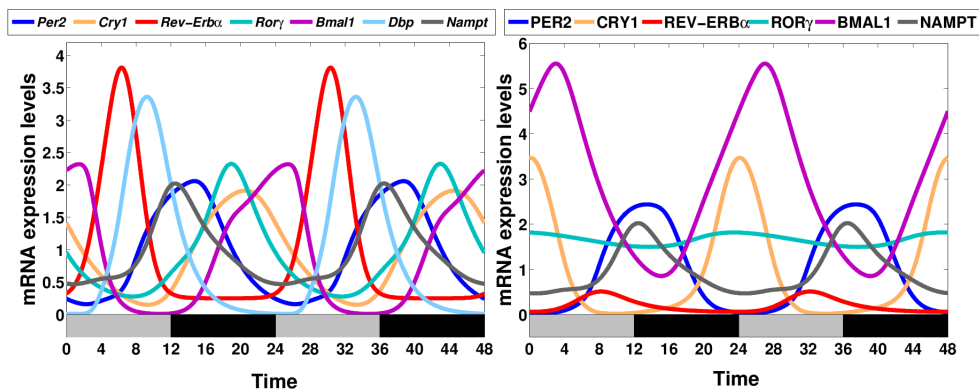


Fig. 7.4 Profils temporels pour les ARNm (panneau de gauche) et les protéines (panneau de droite) prises en compte dans notre modèle.

des minima locaux. Afin de rester réalistes, nous n'avons autorisé l'algorithme qu'à tester des valeurs de paramètre physiologiquement acceptables [116].

Cette procédure d'optimisation nous a permis d'obtenir un excellent ajustement entre résultats numériques et données expérimentales: nous avons pu reproduire précisément tant les données d'expression d'ARN que les niveaux de NAD⁺ (voir Fig.7.5). De plus, le profil d'AMPK qui été sélectionné par l'estimation de paramètre est en cohérence parfaite avec les niveaux expérimentaux d'AMP [71]: un pic durant la journée (autour de ZT5) et un pic pendant la nuit (autour de ZT14). Notre hypothèse concernant l'action de l'AMPK sur la protéine NAMPT permet donc de reproduire le mystérieux profil bimodal de NAD⁺ et de la protéine NAMPT (voir Fig.7.6). En plus du phénotype sauvage, nous avons aussi pu contraindre notre modèle afin de reproduire l'effet de certaines mutations importantes (voir Fig.7.7). En particulier, il reproduit correctement l'effet d'une perte d'activité de SIRT1 (augmentation de l'expression des gènes d'horloges) et de l'AMPK (diminution de l'expression des gènes d'horloge) [14],[97].

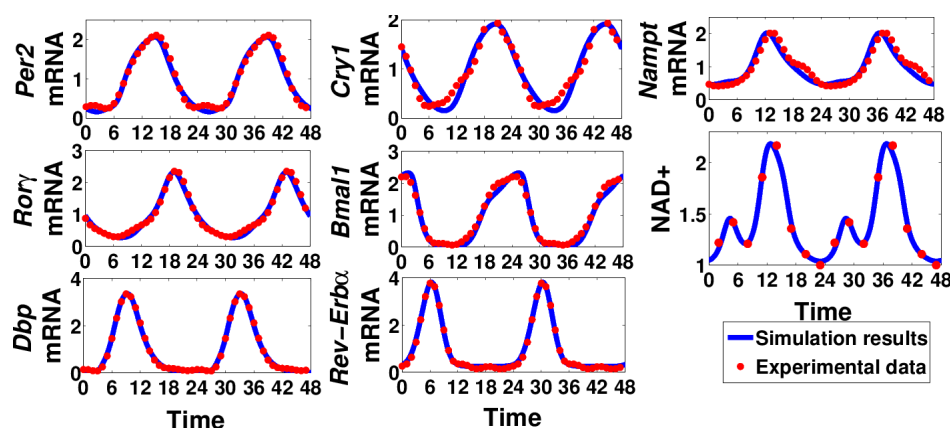


Fig. 7.5 Les profils temporels décrivant l'expression des principaux gènes de l'horloge (phénotype sauvage) sont reproduits fidèlement.

7.2.3 Effet des perturbations du rythme d'AMPK sur l'horloge

Notre style de vie moderne est caractérisé par une grande flexibilité au niveau des comportements alimentaires (heure des repas variable, grignotage, alimentation grasse) et cela est corrélé avec une forte augmentation de l'incidence des maladies métaboliques accompagnée de dérèglements de l'horloge. En particulier, les régimes alimentaires riches en graisse entraînant de l'obésité sont associés à une importante perte d'amplitude des gènes d'horloge mais les mécanismes sous-jacents demeurent peu compris [71],[36]. Nous nous sommes particulièrement intéressés à une expérience réalisée dans le groupe de S.Panda [71]: soit 4

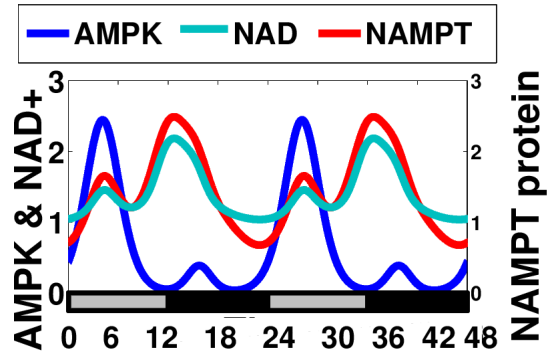


Fig. 7.6 Notre modèle reproduit fidèlement les profils bimodaux de l'AMPK, de NAD+ et de NAMPT.

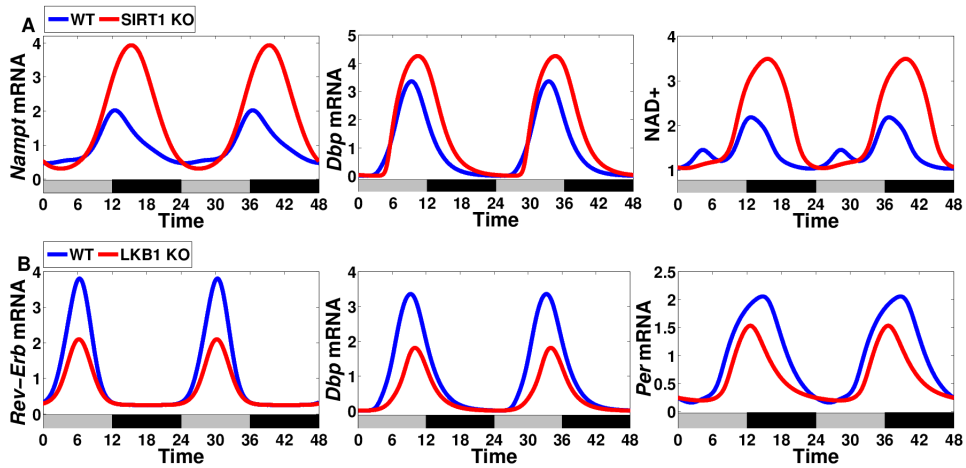


Fig. 7.7 L'effet sur l'expression des gènes d'horloge d'une perte de fonction de SIRT1 (panneaux du haut) et de l'AMPK (panneaux du bas) est reproduit qualitativement.

groupes de souris. Deux de ces groupes n'ont accès à la nourriture qu'au moment des repas ("time restricted feeding") tandis que les 2 autres peuvent grignoter tout au long de la journée ("ad libitum feeding"). Néanmoins, l'expérience a été contrôlée de telle sorte que la quantité totale de nourriture ingérée soit la même dans tous les cas. Dans chacun des sous-groupes, il y a un ensemble de souris qui mangent sainement ("normal diet feeding") tandis que l'autre ensemble mange très gras ("high-fat diet feeding"). Après quelques semaines, on constate que 3 groupes de souris sont en pleine santé tandis que les souris du 4ème groupe (celui en ad libitum high-fat diet feeding) développent des problèmes métaboliques (obésité) et le fonctionnement de leur horloge est complètement perturbé. Le point intéressant, c'est que les souris qui ne mangent gras mais qu'au moment des repas (time-restricted high-fat diet feeding) n'ont aucun soucis de santé, ce qui indique l'importance du timing de prise alimentaire.

Comme dans notre modèle, l'AMPK est considérée comme une mesure directe de l'alternance entre phases de jeûne et de prise alimentaire, nous nous sommes intéressés à l'effet de perturbations du rythme d'AMPK sur l'expression des gènes d'horloge. Plus précisément, nous avons testé deux conditions: tout d'abord, l'effet d'un important amortissement dans le rythme d'AMPK et ensuite, le cas d'une activité d'AMPK toujours haute. Le premier cas correspond à une situation où les rongeurs mangent tout le temps tandis que le second cas est très similaire aux conditions de jeûne. Le modèle prédit qu'un accroissement de l'activité de l'AMPK augmente les niveaux de Nampt (ARN et protéine) et de NAD+, ce qui concorde avec l'état de jeûne [134]. De plus, l'expression de plusieurs gènes d'horloge augmente également dans cette condition (voir Fig.7.9).

Par ailleurs, un amortissement de l'activité de l'AMPK réduit l'amplitude d'expression des gènes d'horloge, de *Nampt* ainsi que les niveaux de NAD+ (voir Fig.7.8). De façon intéressante, ceci est très similaire à ce qu'on observe en régime "high fat ad libitum" [71],[36]. Notre modèle suggère donc que les dérèglements de l'horloge observés dans ces conditions peuvent en bonne partie être expliqués par l'amortissement de l'activité de l'AMPK. Ceci est cohérent avec le fait que les niveaux d'AMP sont fortement diminués chez les rongeurs soumis à ce type de régime alimentaire [71].

7.2.4 Approche pharmacologique: rétablissement du bon fonctionnement de l'horloge par l'administration d'un agoniste de l'horloge

Les travaux de S.Panda suggèrent qu'il existe une corrélation entre rétablissement des amplitudes physiologiques pour l'expression des gènes d'horloge et protection contre l'obésité

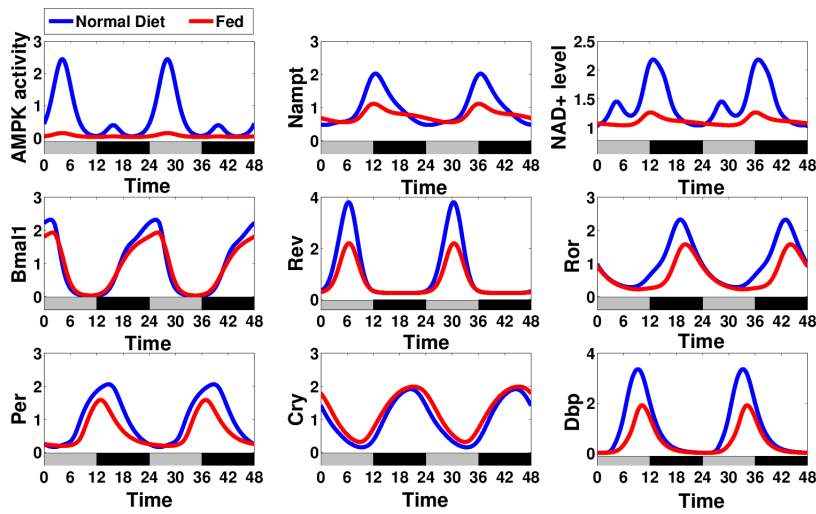


Fig. 7.8 État "rassasié": Effet sur l'expression des gènes d'horloge d'un amortissement de l'activité de l'AMPK (courbes en rouge) comparé à une activité rythmique normale du senseur nutritionnel (courbes en bleu).

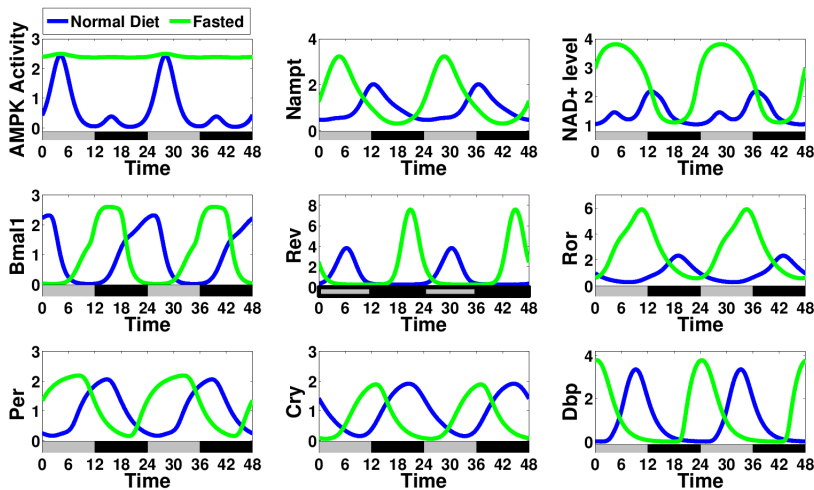


Fig. 7.9 État de jeûne: effet sur l'expression des gènes d'horloge d'une forte activité de l'AMPK (courbes en vert) comparé à une activité rythmique normale du senseur nutritionnel (courbes en bleu).

induite par un régime riche en graisse [71]. Une autre étude a montré qu'une double délétion du gène *Cry* protégeait également contre des troubles métaboliques en dépit d'une alimentation riche en graisse [57]. Nous avons simulé cette expérience (KO de *Cry* et AMPK amorti afin d'être en conditions similaires à un "high fat ad libitum") avec notre modèle et montré que l'expression des gènes d'horloge est ré-augmentée lors de cette mutation (voir Figs.7.10). Toutes ces observations indiquent donc une corrélation entre restauration de l'amplitude des gènes d'horloge et protection contre l'obésité en régime "high fat".

L'administration d'un traitement pharmacologique restaurant le bon fonctionnement de l'horloge pourrait donc constituer un bon traitement anti-obésité. Récemment, des agonistes synthétiques des composants de l'horloge ont été développés, en particulier, deux agonistes du récepteur nucléaire REV-ERB (SR9011 et SR9009) [152]. Il a d'ailleurs été montré que l'effet de leur administration sur les gènes d'horloge dépend fortement du moment d'administration [115]. Nous avons modélisé l'administration périodique d'un agoniste de REV-ERB pour voir s'il était possible de restaurer des profils d'expression physiologiques (phases et amplitudes correctes) après amortissement du rythme d'AMPK. Nous avons simulé des administrations d'agoniste à différents moments de la journée. Nos résultats montrent que l'amplitude et la phase de la plupart des gènes d'horloge ainsi que celle de *Nampt* et *NAD+* peuvent être restaurées mais uniquement si l'agoniste est injecté à un moment précis de la journée (voir Figs.7.11,7.12,7.13).

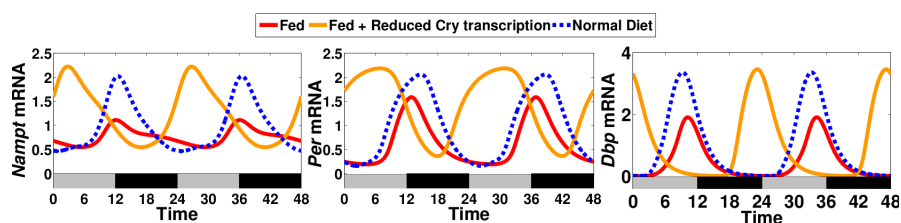


Fig. 7.10 Rétablissement de l'amplitude des oscillations des gènes d'horloge (*Nampt*, *Per* et *Dbp*) pour des mutants *Cry* après un amortissement du rythme d'activité de l'AMPK (courbes oranges). Comparaison avec des cellules non mutantes soumises à un rythme d'AMPK normal (courbes bleues) ou amorti (courbes rouges).

7.3 Conclusions

L'horloge circadienne permet aux organismes de synchroniser leurs processus physiologiques avec les signaux environnementaux périodiques tels que le cycle jours-nuit mais également le cycle de prise alimentaire-jeûne. Il n'est donc pas surprenant que les horloges périphériques répondent au rythme de nourriture et qu'elles soient capables d'ajuster les

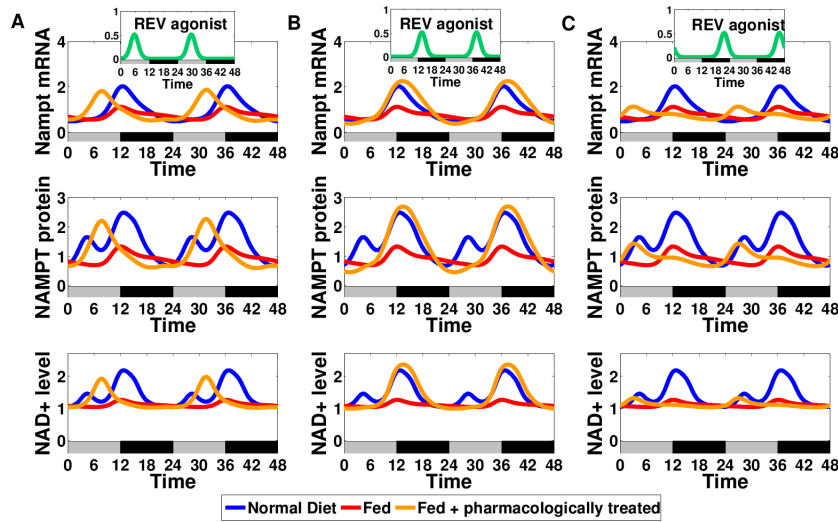


Fig. 7.11 Effet d'un traitement consistant à administrer un agoniste REV-ERB à trois moments différents de la journée pour des cellules avec un rythme d'AMPK amorti. Les profils de *Nampt*, de la protéine NAMPT et de NAD⁺ sont affichés en rouge quand le traitement a été administré, en orange sans traitement, et en bleu pour des cellules soumises à un rythme d'AMPK normal. Le timing optimal est affiché de la colonne du milieu.

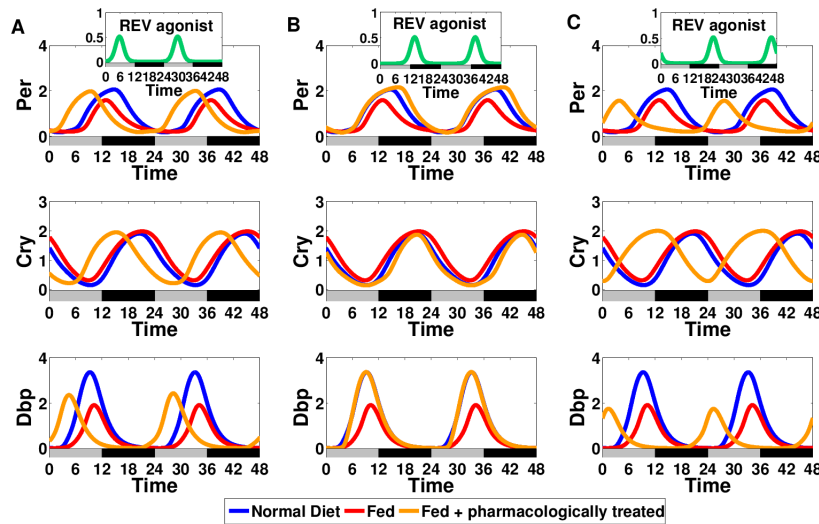


Fig. 7.12 Effet d'un traitement consistant à administrer un agoniste REV-ERB à trois moments différents de la journée pour des cellules avec un rythme d'AMPK amorti. Les profils de *Per*, *Cry* et de *Dbp* sont affichés en rouge quand le traitement a été administré, en orange sans traitement, et en bleu pour des cellules soumises à un rythme d'AMPK normal. Le timing optimal est affiché de la colonne du milieu.

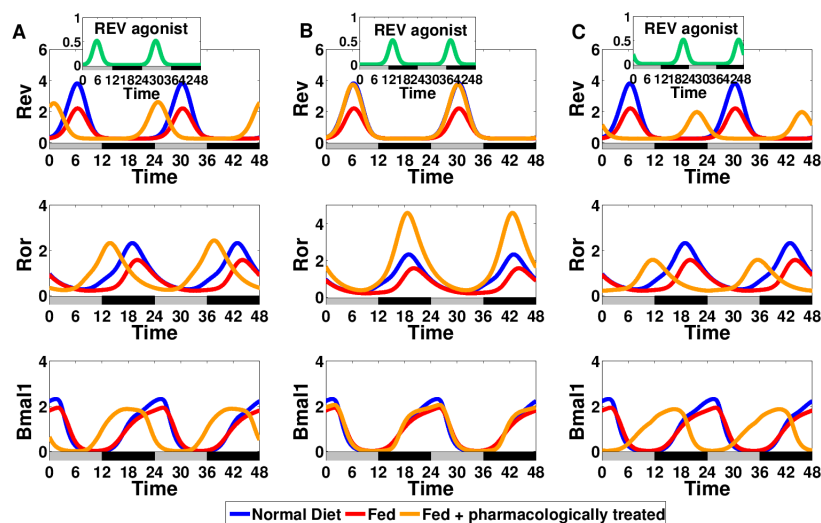


Fig. 7.13 Effet d'un traitement consistant à administrer un agoniste REV-ERB à trois moments différents de la journée pour des cellules avec un rythme d'AMPK amorti. Les profils de *Rev-Erb*, de *Ror* et de *Bmal1* sont affichés en rouge quand le traitement a été administré, en orange sans traitement, et en bleu pour des cellules soumises à un rythme d'AMPK normal. Le timing optimal est affiché de la colonne du milieu..

processus métaboliques (tels que le stockage ou l'utilisation de différentes sources d'énergie) en fonction de l'état nutritionnel de la cellule. Afin de déterminer comment l'horloge du foie est entraînée par le cycle de prise alimentaire-jeûne, nous avons construit un modèle mathématique couplant le réseau circadien aux acteurs clé du métabolisme. Il inclut les senseurs nutritionnel SIRT1 et AMPK qui sont respectivement sensibles aux niveaux de NAD⁺ et d'AMP. Les variations des niveaux de ces deux métabolites peuvent être interprétées comme un indicateur de l'alternance entre les phases de jeûne et de prise alimentaire. Les activités des deux senseurs ne sont pas totalement indépendantes. En effet, divers travaux ont montré que l'activité de l'AMPK augmente les niveaux de NAD⁺ mais ils ne s'accordent toujours pas entre eux par rapport au mécanisme exacte (action de l'AMPK au niveau de la conversion de NADH en NAD⁺ ou sur l'ARN ou la protéine Nampt): nous avons testé cette dernière hypothèse et avons montré qu'elle permet d'expliquer le mystérieux motif bimodal dans les profils temporels de la protéine NAMPT et de NAD⁺. Nos simulations renforcent donc l'idée que qu'une partie des rythmes ultradiens observés expérimentalement sont générés par l'intersection d'un rythme circadien local et du rythme de prise de nourriture [78]. Par ailleurs, les modifications de l'activité de SIRT1 sous l'effet des fluctuations du niveau de NAD⁺ peuvent être causées par différent mécanismes : soit par la conversion périodique de NADH en NAD⁺ soit par les fluctuations de la biosynthèse de NAD⁺ contrôlée par NAMPT. Dans notre modèle, pour des raisons de simplicité, nous n'avons pris en compte que ce

dernier mécanisme pour expliquer les variations quotidiennes de NAD⁺ et cela fût suffisant pour reproduire fidèlement le changement dans les profils journaliers de NAD⁺ [141]. Ceci suggère que la périodicité observée dans le niveau de NAD⁺ proviendrait principalement des oscillations dans la voie de biosynthèse de NAD⁺, ce qui est en accord avec les résultats expérimentaux: en effet, les mutants de l'horloge (Bmal1 KO) présentent des niveaux de NAD⁺ fortement réduits.

Notre modèle comprend 16 variables et une centaine de constantes cinétiques. Avec tant de paramètres, on pourrait envisager un risque d'over-fitting et par conséquent un faible pouvoir prédictif de ce dernier. Cependant, notre modèle ne reproduit pas uniquement la période, les phases et les amplitudes correctes pour l'expression des gènes d'horloge, mais il colle très précisément également aux données expérimentales pour l'ARNm. De plus, nous avons également reproduit quantitativement plusieurs phénotypes mutants, ce qui a contraint encore davantage certaines valeurs de paramètres. Il a d'ailleurs été montré que même si les modèles biologiques contiennent souvent des paramètres mal contraints, on peut faire des prédictions utiles dès que quelques paramètres clés sont bien contraints [17]. Nous devrions donc nous concentrer sur les prédictions de notre modèle plutôt que sur l'échantillon des valeurs sélectionnées pour les constantes cinétiques.

Nous avons utilisé le modèle pour étudier l'effet de perturbations dans le rythme d'activité de l'AMPK. Tout d'abord, nous avons observé que le petit pic du profil bimodal de la protéine NAMPT et de l'AMPK disparaît tant lors d'une forte augmentation que lors d'une forte baisse de l'activité de l'AMPK, deux conditions qui peuvent être assimilés à un état de jeûne et de prise de nourriture continue respectivement. Un autre point intéressant est l'amortissement de l'amplitude de l'expression des gènes d'horloge observé lors de l'amortissement de l'activité de l'AMPK. Ce résultat suggère que la réduction de l'amplitude de l'expression des gènes d'horloge observée lors d'un régime gras ad libitum peut être au moins partiellement expliquée par la perte du rythme d'AMPK qui accompagne ce régime alimentaire, ce qui n'exclut pas que d'autres senseurs tels que mTOR ou CREB influencent également l'expression des gènes d'horloge. Enfin, plusieurs expériences suggèrent qu'un rétablissement de l'amplitude d'expression des gènes d'horloge constituerait une protection contre l'obésité induite par une alimentation riche en graisse [71], [57]. De ce fait, nous avons simulé l'administration pharmacologique d'un agoniste de l'horloge à différents moments du cycle. Notre modèle montre que les amplitudes et les phases d'expression des gènes d'horloge ne peuvent être restaurées que lorsque l'agoniste est administré à certains moments spécifiques de la journée. Donc, en conclusion, notre travail souligne l'importance du rythme d'activité de l'AMPK dans l'entraînement de l'horloge du foie par la nourriture. Notre modèle suggère également que l'amortissement des rythmes circadien associé avec

certaines maladies métaboliques et le vieillissement pourrait être traitées par l'administration d'agonistes de l'horloge à une heure optimale de la journée.

References

- [1] Adams, R. R., Tsorman, N., Stratford, K., Akman, O. E., Gilmore, S., Juty, N., Le Novère, N., Millar, A. J., and Millar, A. J. (2012). The Input Signal Step Function (ISSF), a standard method to encode input signals in SBML models with software support, applied to circadian clock models. *Journal of Biological Rhythms*, 27(4):328–332.
- [2] Akashi, M., Tsuchiya, Y., Yoshino, T., and Nishida, E. (2002). Control of intracellular dynamics of mammalian period proteins by casein kinase I epsilon (CKIepsilon) and CKIdelta in cultured cells. *Molecular and Cellular Biology*, 22(6):1693–1703.
- [3] Alberts, B., editor (2002). *Molecular biology of the cell*. Garland Science, New York, 4th ed edition.
- [4] Albrecht, U. (2012). Timing to Perfection: The Biology of Central and Peripheral Circadian Clocks. *Neuron*, 74(2):246–260.
- [5] Ananthasubramaniam, B. and Herzog, H. (2014). Positive Feedback Promotes Oscillations in Negative Feedback Loops. *PLoS ONE*, 9(8):e104761.
- [6] Ashall, L., Horton, C. A., Nelson, D. E., Paszek, P., Harper, C. V., Sillitoe, K., Ryan, S., Spiller, D. G., Unitt, J. F., Broomhead, D. S., Kell, D. B., Rand, D. A., Sée, V., and White, M. R. H. (2009). Pulsatile stimulation determines timing and specificity of NF-kappaB-dependent transcription. *Science (New York, N.Y.)*, 324(5924):242–246.
- [7] Asher, G., Gatfield, D., Stratmann, M., Reinke, H., Dibner, C., Kreppel, F., Mostoslavsky, R., Alt, F. W., and Schibler, U. (2008). SIRT1 regulates circadian clock gene expression through PER2 deacetylation. *Cell*, 134(2):317–328.
- [8] Asher, G. and Schibler, U. (2011). Crosstalk between Components of Circadian and Metabolic Cycles in Mammals. *Cell Metabolism*, 13(2):125–137.
- [9] Balsalobre, A., Brown, S. A., Marcacci, L., Tronche, F., Kellendonk, C., Reichardt, H. M., Schütz, G., and Schibler, U. (2000). Resetting of circadian time in peripheral tissues by glucocorticoid signaling. *Science (New York, N.Y.)*, 289(5488):2344–2347.
- [10] Bass, J. and Takahashi, J. S. (2010). Circadian integration of metabolism and energetics. *Science (New York, N.Y.)*, 330(6009):1349–1354.
- [11] Becker-Weimann, S., Wolf, J., Kramer, A., and Herzog, H. (2004). A model of the mammalian circadian oscillator including the REV-ERBalpha module. *Genome Informatics. International Conference on Genome Informatics*, 15(1):3–12.

- [12] Belden, W. J. and Dunlap, J. C. (2008). SIRT1 Is a Circadian Deacetylase for Core Clock Components. *Cell*, 134(2):212–214.
- [13] Bell-Pedersen, D., Cassone, V. M., Earnest, D. J., Golden, S. S., Hardin, P. E., Thomas, T. L., and Zoran, M. J. (2005). Circadian rhythms from multiple oscillators: lessons from diverse organisms. *Nature Reviews Genetics*, 6(7):544–556.
- [14] Bellet, M. M., Nakahata, Y., Boudjelal, M., Watts, E., Mossakowska, D. E., Edwards, K. A., Cervantes, M., Astarita, G., Loh, C., Ellis, J. L., Vlasuk, G. P., and Sassone-Corsi, P. (2013). Pharmacological modulation of circadian rhythms by synthetic activators of the deacetylase SIRT1. *Proceedings of the National Academy of Sciences of the United States of America*, 110(9):3333–3338.
- [15] Bieler, J., Cannavo, R., Gustafson, K., Gobet, C., Gatfield, D., and Naef, F. (2014). Robust synchronization of coupled circadian and cell cycle oscillators in single mammalian cells. *Molecular Systems Biology*, 10:739.
- [16] Brandauer, J., Vienberg, S. G., Andersen, M. A., Ringholm, S., Risis, S., Larsen, P. S., Kristensen, J. M., Frøsig, C., Leick, L., Fentz, J., Jørgensen, S., Kiens, B., Wojtaszewski, J. F. P., Richter, E. A., Zierath, J. R., Goodyear, L. J., Pilegaard, H., and Treebak, J. T. (2013). AMP-activated protein kinase regulates nicotinamide phosphoribosyl transferase expression in skeletal muscle. *The Journal of Physiology*, 591(Pt 20):5207–5220.
- [17] Brown, K. S., Hill, C. C., Calero, G. A., Myers, C. R., Lee, K. H., Sethna, J. P., and Cerione, R. A. (2004). The statistical mechanics of complex signaling networks: nerve growth factor signaling. *Physical Biology*, 1(3-4):184–195.
- [18] Brown, S. A., Zimbrunn, G., Fleury-Olela, F., Preitner, N., and Schibler, U. (2002). Rhythms of mammalian body temperature can sustain peripheral circadian clocks. *Current biology: CB*, 12(18):1574–1583.
- [19] Bunger, M. K., Wilsbacher, L. D., Moran, S. M., Clendenin, C., Radcliffe, L. A., Hogenesch, J. B., Simon, M. C., Takahashi, J. S., and Bradfield, C. A. (2000). Mop3 is an essential component of the master circadian pacemaker in mammals. *Cell*, 103(7):1009–1017.
- [20] Busino, L., Bassermann, F., Maiolica, A., Lee, C., Nolan, P. M., Godinho, S. I. H., Draetta, G. F., and Pagano, M. (2007). SCFFbx13 Controls the Oscillation of the Circadian Clock by Directing the Degradation of Cryptochrome Proteins. *Science*, 316(5826):900–904.
- [21] Canaple, L., Rambaud, J., Dkhissi-Benyahya, O., Rayet, B., Tan, N. S., Michalik, L., Delaunay, F., Wahli, W., and Laudet, V. (2006). Reciprocal Regulation of Brain and Muscle Arnt-Like Protein 1 and Peroxisome Proliferator-Activated Receptor Defines a Novel Positive Feedback Loop in the Rodent Liver Circadian Clock. *Molecular Endocrinology*, 20(8):1715–1727.
- [22] Cantó, C., Gerhart-Hines, Z., Feige, J. N., Lagouge, M., Noriega, L., Milne, J. C., Elliott, P. J., Puigserver, P., and Auwerx, J. (2009). AMPK regulates energy expenditure by modulating NAD⁺ metabolism and SIRT1 activity. *Nature*, 458(7241):1056–1060.

- [23] Chang, H.-C. and Guarente, L. (2014). SIRT1 and other sirtuins in metabolism. *Trends in endocrinology and metabolism: TEM*, 25(3):138–145.
- [24] Chiang, C.-K., Mehta, N., Patel, A., Zhang, P., Ning, Z., Mayne, J., Sun, W. Y. L., Cheng, H.-Y. M., and Figeys, D. (2014). The Proteomic Landscape of the Suprachiasmatic Nucleus Clock Reveals Large-Scale Coordination of Key Biological Processes. *PLoS Genet*, 10(10):e1004695.
- [25] Cibois, M., Gautier-Courteille, C., Legagneux, V., and Paillard, L. (2010). Post-transcriptional controls - adding a new layer of regulation to clock gene expression. *Trends in Cell Biology*, 20(9):533–541.
- [26] Connors, K. A. (1990). *Chemical kinetics: the study of reaction rates in solution*. Wiley-VCH, New York, NJ, nachdr. edition.
- [27] Dallmann, R., Brown, S. A., and Gachon, F. (2014). Chronopharmacology: New Insights and Therapeutic Implications. *Annual Review of Pharmacology and Toxicology*, 54(1):339–361.
- [28] Damiola, F., Le Minh, N., Preitner, N., Kornmann, B., Fleury-Olela, F., and Schibler, U. (2000). Restricted feeding uncouples circadian oscillators in peripheral tissues from the central pacemaker in the suprachiasmatic nucleus. *Genes & Development*, 14(23):2950–2961.
- [29] Darlington, T. K., Wager-Smith, K., Ceriani, M. F., Staknis, D., Gekakis, N., Steeves, T. D., Weitz, C. J., Takahashi, J. S., and Kay, S. A. (1998). Closing the circadian loop: CLOCK-induced transcription of its own inhibitors per and tim. *Science (New York, N.Y.)*, 280(5369):1599–1603.
- [30] Dickmeis, T. (2009a). Glucocorticoids and the circadian clock. *The Journal of Endocrinology*, 200(1):3–22.
- [31] Dickmeis, T. (2009b). Glucocorticoids and the circadian clock. *The Journal of Endocrinology*, 200(1):3–22.
- [32] Dickmeis, T., Weger, B. D., and Weger, M. (2013). The circadian clock and glucocorticoids—interactions across many time scales. *Molecular and Cellular Endocrinology*, 380(1-2):2–15.
- [33] Doi, M., Hirayama, J., and Sassone-Corsi, P. (2006). Circadian regulator CLOCK is a histone acetyltransferase. *Cell*, 125(3):497–508.
- [34] Duez, H. and Staels, B. (2009). Rev-erb-alpha: an integrator of circadian rhythms and metabolism. *Journal of Applied Physiology (Bethesda, Md.: 1985)*, 107(6):1972–1980.
- [35] Duez, H., van der Veen, J. N., Duhem, C., Pourcet, B., Touvier, T., Fontaine, C., Derudas, B., Baugé, E., Havinga, R., Bloks, V. W., Wolters, H., van der Sluijs, F. H., Vennström, B., Kuipers, F., and Staels, B. (2008). Regulation of bile acid synthesis by the nuclear receptor Rev-erbalpha. *Gastroenterology*, 135(2):689–698.

- [36] Eckel-Mahan, K. L., Patel, V. R., de Mateo, S., Orozco-Solis, R., Ceglia, N. J., Sahar, S., Dilag-Penilla, S. A., Dyar, K. A., Baldi, P., and Sassone-Corsi, P. (2013). Reprogramming of the circadian clock by nutritional challenge. *Cell*, 155(7):1464–1478.
- [37] Feige, J. N. and Auwerx, J. (2008). Transcriptional targets of sirtuins in the coordination of mammalian physiology. *Current Opinion in Cell Biology*, 20(3):303–309.
- [38] Feillet, C., Krusche, P., Tamanini, F., Janssens, R. C., Downey, M. J., Martin, P., Teboul, M., Saito, S., Lévi, F. A., Bretschneider, T., van der Horst, G. T. J., Delaunay, F., and Rand, D. A. (2014). Phase locking and multiple oscillating attractors for the coupled mammalian clock and cell cycle. *Proceedings of the National Academy of Sciences of the United States of America*, 111(27):9828–9833.
- [39] Forger, D. B., Dean, D. A., Gurdziel, K., Leloup, J.-C., Lee, C., Von Gall, C., Etchegaray, J.-P., Kronauer, R. E., Goldbeter, A., Peskin, C. S., Jewett, M. E., and Weaver, D. R. (2003). Development and validation of computational models for mammalian circadian oscillators. *OmicS: A Journal of Integrative Biology*, 7(4):387–400.
- [40] Forger, D. B. and Peskin, C. S. (2003). A detailed predictive model of the mammalian circadian clock. *Proceedings of the National Academy of Sciences*, 100(25):14806–14811.
- [41] Fulco, M., Cen, Y., Zhao, P., Hoffman, E. P., McBurney, M. W., Sauve, A. A., and Sartorelli, V. (2008). Glucose restriction inhibits skeletal myoblast differentiation by activating SIRT1 through AMPK-mediated regulation of Nampt. *Developmental Cell*, 14(5):661–673.
- [42] Gallego, M., Eide, E. J., Woolf, M. F., Virshup, D. M., and Forger, D. B. (2006). An opposite role for tau in circadian rhythms revealed by mathematical modeling. *Proceedings of the National Academy of Sciences of the United States of America*, 103(28):10618–10623.
- [43] Gervois, P., Chopin-Delannoy, S., Fadel, A., Dubois, G., Kosykh, V., Fruchart, J.-C., Najib, J., Laudet, V., and Staels, B. (1999). Fibrates Increase Human REV-ERB Expression in Liver via a Novel Peroxisome Proliferator-Activated Receptor Response Element. *Molecular Endocrinology*, 13(3):400–409.
- [44] Glossop, N. R., Lyons, L. C., and Hardin, P. E. (1999). Interlocked feedback loops within the *Drosophila* circadian oscillator. *Science (New York, N.Y.)*, 286(5440):766–768.
- [45] Godinho, S. I. H., Maywood, E. S., Shaw, L., Tucci, V., Barnard, A. R., Busino, L., Pagano, M., Kendall, R., Quwailid, M. M., Romero, M. R., O’neill, J., Chesham, J. E., Brooker, D., Lallane, Z., Hastings, M. H., and Nolan, P. M. (2007). The after-hours mutant reveals a role for Fbxl3 in determining mammalian circadian period. *Science (New York, N.Y.)*, 316(5826):897–900.
- [46] Goldbeter, A. (2004). *Biochemical oscillations and cellular rhythms: the molecular bases of periodic and chaotic behaviour*. Cambridge University Press, Cambridge, transferred to digital print edition.
- [47] Goldbeter, A. (2007). Biological Rhythms as Temporal Dissipative Structures. In Rice, S. A., editor, *Advances in Chemical Physics*, volume 135, pages 253–295. John Wiley & Sons, Inc., Hoboken, NJ, USA.

- [48] Goldbeter, A., Gérard, C., Gonze, D., Leloup, J.-C., and Dupont, G. (2012). Systems biology of cellular rhythms. *FEBS letters*, 586(18):2955–2965.
- [49] Golombek, D. A. and Rosenstein, R. E. (2010). Physiology of Circadian Entrainment. *Physiological Reviews*, 90(3):1063–1102.
- [50] Gonze, D. (2011a). Modeling circadian clocks: From equations to oscillations. *Open Life Sciences*, 6(5).
- [51] Gonze, D. (2011b). Modeling circadian clocks: Roles, advantages, and limitations. *Central European Journal of Biology*, 6(5):712–729.
- [52] Gonze, D. and Abou-Jaoudé, W. (2013). The Goodwin model: behind the Hill function. *PLoS One*, 8(8):e69573.
- [53] Gonze, D., Bernard, S., Waltermann, C., Kramer, A., and Herzel, H. (2005). Spontaneous Synchronization of Coupled Circadian Oscillators. *Biophysical Journal*, 89(1):120–129.
- [54] Goodwin, B. C. (1965). Oscillatory behavior in enzymatic control processes. *Advances in Enzyme Regulation*, 3:425–438.
- [55] Gottfried, B. S. and Weisman, J. (1973). *Introduction to optimization theory*. Prentice-Hall international series in industrial and systems engineering. Prentice-Hall, Englewood Cliffs, N.J.
- [56] Gowans, G., Hawley, S., Ross, F., and Hardie, D. G. (2013). AMP Is a True Physiological Regulator of AMP-Activated Protein Kinase by Both Allosteric Activation and Enhancing Net Phosphorylation. *Cell Metabolism*, 18(4):556–566.
- [57] Griebel, G., Ravinet-Trillou, C., Beeské, S., Avenet, P., and Pichat, P. (2014). Mice deficient in cryptochrome 1 (*cry1 (-/-)*) exhibit resistance to obesity induced by a high-fat diet. *Frontiers in Endocrinology*, 5:49.
- [58] Griffith, J. S. (1968). Mathematics of cellular control processes. I. Negative feedback to one gene. *Journal of Theoretical Biology*, 20(2):202–208.
- [59] Handschin, C., Rhee, J., Lin, J., Tarr, P. T., and Spiegelman, B. M. (2003). An autoregulatory loop controls peroxisome proliferator-activated receptor coactivator 1 expression in muscle. *Proceedings of the National Academy of Sciences*, 100(12):7111–7116.
- [60] Hardie, D. G. (2007). AMP-activated/SNF1 protein kinases: conserved guardians of cellular energy. *Nature Reviews Molecular Cell Biology*, 8(10):774–785.
- [61] Hardie, D. G. (2011). AMP-activated protein kinase: an energy sensor that regulates all aspects of cell function. *Genes & Development*, 25(18):1895–1908.
- [62] Hardie, D. G. (2012). Organismal carbohydrate and lipid homeostasis. *Cold Spring Harbor Perspectives in Biology*, 4(5).

- [63] Hardie, D. G., Ross, F. A., and Hawley, S. A. (2012). AMPK: a nutrient and energy sensor that maintains energy homeostasis. *Nature Reviews Molecular Cell Biology*, 13(4):251–262.
- [64] Hardin, P. E., Hall, J. C., and Rosbash, M. (1990). Feedback of the *Drosophila* period gene product on circadian cycling of its messenger RNA levels. *Nature*, 343(6258):536–540.
- [65] Hardin, P. E., Hall, J. C., and Rosbash, M. (1992). Circadian oscillations in period gene mRNA levels are transcriptionally regulated. *Proceedings of the National Academy of Sciences of the United States of America*, 89(24):11711–11715.
- [66] Hardin, P. E. and Yu, W. (2006). Circadian transcription: passing the HAT to CLOCK. *Cell*, 125(3):424–426.
- [67] Harvey, R. A. and Ferrier, D. R. (2011a). *Lippincott's illustrated reviews: Biochemistry*. Wolters Kluwer Health, Philadelphia, 5th ed edition.
- [68] Harvey, R. A. and Ferrier, D. R. (2011b). *Lippincott's illustrated reviews: Biochemistry*. Wolters Kluwer Health, Philadelphia, 5th ed edition.
- [69] Hastings, J. W. and Sweeney, B. M. (1957). ON THE MECHANISM OF TEMPERATURE INDEPENDENCE IN A BIOLOGICAL CLOCK. *Proceedings of the National Academy of Sciences of the United States of America*, 43(9):804–811.
- [70] Hastings, M. H., Reddy, A. B., and Maywood, E. S. (2003). A clockwork web: circadian timing in brain and periphery, in health and disease. *Nature Reviews Neuroscience*, 4(8):649–661.
- [71] Hatori, M., Vollmers, C., Zarrinpar, A., DiTacchio, L., Bushong, E. A., Gill, S., Leblanc, M., Chaix, A., Joens, M., Fitzpatrick, J. A. J., Ellisman, M. H., and Panda, S. (2012). Time-restricted feeding without reducing caloric intake prevents metabolic diseases in mice fed a high-fat diet. *Cell Metabolism*, 15(6):848–860.
- [72] Hecht, E. and Martin, J. (1999). *Physique*. DeBoeck Univ, Paris.
- [73] Herzig, S., Long, F., Jhala, U. S., Hedrick, S., Quinn, R., Bauer, A., Rudolph, D., Schutz, G., Yoon, C., Puigserver, P., Spiegelman, B., and Montminy, M. (2001). CREB regulates hepatic gluconeogenesis through the coactivator PGC-1. *Nature*, 413(6852):179–183.
- [74] Hirayama, J., Sahar, S., Grimaldi, B., Tamaru, T., Takamatsu, K., Nakahata, Y., and Sassone-Corsi, P. (2007). CLOCK-mediated acetylation of BMAL1 controls circadian function. *Nature*, 450(7172):1086–1090.
- [75] Hoffmann, A., Levchenko, A., Scott, M. L., and Baltimore, D. (2002). The IkappaB-NF-kappaB signaling module: temporal control and selective gene activation. *Science (New York, N.Y.)*, 298(5596):1241–1245.
- [76] Hou, X., Xu, S., Maitland-Toolan, K. A., Sato, K., Jiang, B., Ido, Y., Lan, F., Walsh, K., Wierzbicki, M., Verbeuren, T. J., Cohen, R. A., and Zang, M. (2008). SIRT1 Regulates Hepatocyte Lipid Metabolism through Activating AMP-activated Protein Kinase. *Journal of Biological Chemistry*, 283(29):20015–20026.

- [77] Houtkooper, R. H., Pirinen, E., and Auwerx, J. (2012). Sirtuins as regulators of metabolism and healthspan. *Nature Reviews. Molecular Cell Biology*, 13(4):225–238.
- [78] Hughes, M. E., DiTacchio, L., Hayes, K. R., Vollmers, C., Pulivarthy, S., Baggs, J. E., Panda, S., and Hogenesch, J. B. (2009). Harmonics of Circadian Gene Transcription in Mammals. *PLoS Genet*, 5(4):e1000442.
- [79] Isomura, A. and Kageyama, R. (2014). Ultradian oscillations and pulses: coordinating cellular responses and cell fate decisions. *Development (Cambridge, England)*, 141(19):3627–3636.
- [80] Jacquet, M., Renault, G., Lallet, S., De Mey, J., and Goldbeter, A. (2003). Oscillatory nucleocytoplasmic shuttling of the general stress response transcriptional activators Msn2 and Msn4 in *Saccharomyces cerevisiae*. *The Journal of Cell Biology*, 161(3):497–505.
- [81] John, P. C. S., Hirota, T., Kay, S. A., and Doyle, F. J. (2014). Spatiotemporal separation of PER and CRY posttranslational regulation in the mammalian circadian clock. *Proceedings of the National Academy of Sciences*, 111(5):2040–2045.
- [82] Johnson, C. H. and Egli, M. (2014). Metabolic compensation and circadian resilience in prokaryotic cyanobacteria. *Annual Review of Biochemistry*, 83:221–247.
- [83] Jordan, S. D. and Lamia, K. A. (2013). AMPK at the crossroads of circadian clocks and metabolism. *Molecular and Cellular Endocrinology*, 366(2):163–169.
- [84] Jäger, S., Handschin, C., St.-Pierre, J., and Spiegelman, B. M. (2007). AMP-activated protein kinase (AMPK) action in skeletal muscle via direct phosphorylation of PGC-1. *Proceedings of the National Academy of Sciences*, 104(29):12017–12022.
- [85] Kettner, N., Mayo, S., Hua, J., Lee, C., Moore, D., and Fu, L. (2015). Circadian Dysfunction Induces Leptin Resistance in Mice. *Cell Metabolism*, 22(3):448–459.
- [86] King, D. P., Zhao, Y., Sangoram, A. M., Wilsbacher, L. D., Tanaka, M., Antoch, M. P., Steeves, T. D. L., Vitaterna, M. H., Kornhauser, J. M., Lowrey, P. L., Turek, F. W., and Takahashi, J. S. (1997). Positional Cloning of the Mouse Circadian Clock Gene. *Cell*, 89(4):641–653.
- [87] Knobil, E. (1981). Patterns of hormonal signals and hormone action. *The New England Journal of Medicine*, 305(26):1582–1583.
- [88] Ko, C. H. and Takahashi, J. S. (2006). Molecular components of the mammalian circadian clock. *Human Molecular Genetics*, 15(suppl 2):R271–R277.
- [89] Kohsaka, A., Laposky, A. D., Ramsey, K. M., Estrada, C., Joshu, C., Kobayashi, Y., Turek, F. W., and Bass, J. (2007). High-fat diet disrupts behavioral and molecular circadian rhythms in mice. *Cell Metabolism*, 6(5):414–421.
- [90] Koike, N., Yoo, S.-H., Huang, H.-C., Kumar, V., Lee, C., Kim, T.-K., and Takahashi, J. S. (2012). Transcriptional architecture and chromatin landscape of the core circadian clock in mammals. *Science (New York, N.Y.)*, 338(6105):349–354.

- [91] Kojetin, D. J. and Burris, T. P. (2014). REV-ERB and ROR nuclear receptors as drug targets. *Nature Reviews. Drug Discovery*, 13(3):197–216.
- [92] Konopka, R. J. and Benzer, S. (1971). Clock mutants of *Drosophila melanogaster*. *Proceedings of the National Academy of Sciences of the United States of America*, 68(9):2112–2116.
- [93] Korenčič, A., Bordyugov, G., Košir, R., Rozman, D., Goličnik, M., and Herzel, H. (2012). The interplay of cis-regulatory elements rules circadian rhythms in mouse liver. *PLoS One*, 7(11):e46835.
- [94] Kornmann, B., Schaad, O., Bujard, H., Takahashi, J. S., and Schibler, U. (2007). System-driven and oscillator-dependent circadian transcription in mice with a conditionally active liver clock. *PLoS biology*, 5(2):e34.
- [95] Kume, K., Zylka, M. J., Sriram, S., Shearman, L. P., Weaver, D. R., Jin, X., Maywood, E. S., Hastings, M. H., and Reppert, S. M. (1999). mCRY1 and mCRY2 Are Essential Components of the Negative Limb of the Circadian Clock Feedback Loop. *Cell*, 98(2):193–205.
- [96] Lamia, K. A., Papp, S. J., Yu, R. T., Barish, G. D., Uhlentaut, N. H., Jonker, J. W., Downes, M., and Evans, R. M. (2011). Cryptochromes mediate rhythmic repression of the glucocorticoid receptor. *Nature*, 480(7378):552–556.
- [97] Lamia, K. A., Sachdeva, U. M., DiTacchio, L., Williams, E. C., Alvarez, J. G., Egan, D. F., Vasquez, D. S., Juguilon, H., Panda, S., Shaw, R. J., Thompson, C. B., and Evans, R. M. (2009). AMPK regulates the circadian clock by cryptochrome phosphorylation and degradation. *Science (New York, N.Y.)*, 326(5951):437–440.
- [98] Lamia, K. A., Storch, K.-F., and Weitz, C. J. (2008). Physiological significance of a peripheral tissue circadian clock. *Proceedings of the National Academy of Sciences of the United States of America*, 105(39):15172–15177.
- [99] Lan, F., Cacicedo, J. M., Ruderman, N., and Ido, Y. (2008). SIRT1 Modulation of the Acetylation Status, Cytosolic Localization, and Activity of LKB1 POSSIBLE ROLE IN AMP-ACTIVATED PROTEIN KINASE ACTIVATION. *Journal of Biological Chemistry*, 283(41):27628–27635.
- [100] Lehninger, A. L., Nelson, D. L., and Cox, M. M. (2005). *Lehninger principles of biochemistry*. W.H. Freeman, New York, 4th ed edition.
- [101] Leloup, J.-C. and Goldbeter, A. (2004). Modeling the mammalian circadian clock: sensitivity analysis and multiplicity of oscillatory mechanisms. *Journal of Theoretical Biology*, 230(4):541–562.
- [102] LeSauter, J., Hoque, N., Weintraub, M., Pfaff, D. W., and Silver, R. (2009). Stomach ghrelin-secreting cells as food-entrainable circadian clocks. *Proceedings of the National Academy of Sciences of the United States of America*, 106(32):13582–13587.

- [103] Lev Bar-Or, R., Maya, R., Segel, L. A., Alon, U., Levine, A. J., and Oren, M. (2000). Generation of oscillations by the p53-Mdm2 feedback loop: a theoretical and experimental study. *Proceedings of the National Academy of Sciences of the United States of America*, 97(21):11250–11255.
- [104] Liu, A. C., Tran, H. G., Zhang, E. E., Priest, A. A., Welsh, D. K., and Kay, S. A. (2008). Redundant function of REV-ERB α and β and non-essential role for Bmal1 cycling in transcriptional regulation of intracellular circadian rhythms. *PLoS genetics*, 4(2):e1000023.
- [105] Liu, C., Li, S., Liu, T., Borjigin, J., and Lin, J. D. (2007a). Transcriptional coactivator PGC-1 α integrates the mammalian clock and energy metabolism. *Nature*, 447(7143):477–481.
- [106] Liu, C., Li, S., Liu, T., Borjigin, J., and Lin, J. D. (2007b). Transcriptional coactivator PGC-1 α integrates the mammalian clock and energy metabolism. *Nature*, 447(7143):477–481.
- [107] Long, Y. C. and Zierath, J. R. (2006). AMP-activated protein kinase signaling in metabolic regulation. *Journal of Clinical Investigation*, 116(7):1776–1783.
- [108] Loros, J. J. and Dunlap, J. C. (2001). Genetic and molecular analysis of circadian rhythms in *Neurospora*. *Annual Review of Physiology*, 63:757–794.
- [109] Lowrey, P. L., Shimomura, K., Antoch, M. P., Yamazaki, S., Zemenides, P. D., Ralph, M. R., Menaker, M., and Takahashi, J. S. (2000). Positional Syntenic Cloning and Functional Characterization of the Mammalian Circadian Mutation tau. *Science*, 288(5465):483–491.
- [110] Lévi, F., Okyar, A., Dulong, S., Innominato, P. F., and Clairambault, J. (2010). Circadian timing in cancer treatments. *Annual Review of Pharmacology and Toxicology*, 50:377–421.
- [111] Marcheva, B., Ramsey, K. M., Affinati, A., and Bass, J. (2009). Clock genes and metabolic disease. *Journal of Applied Physiology (Bethesda, Md.: 1985)*, 107(5):1638–1646.
- [112] Marcheva, B., Ramsey, K. M., and Bass, J. (2011). Circadian genes and insulin exocytosis. *Cellular Logistics*, 1(1):32–36.
- [113] Marcheva, B., Ramsey, K. M., Buhr, E. D., Kobayashi, Y., Su, H., Ko, C. H., Ivanova, G., Omura, C., Mo, S., Vitaterna, M. H., Lopez, J. P., Philipson, L. H., Bradfield, C. A., Crosby, S. D., JeBailey, L., Wang, X., Takahashi, J. S., and Bass, J. (2010a). Disruption of the clock components CLOCK and BMAL1 leads to hypoinsulinaemia and diabetes. *Nature*, 466(7306):627–631.
- [114] Marcheva, B., Ramsey, K. M., Buhr, E. D., Kobayashi, Y., Su, H., Ko, C. H., Ivanova, G., Omura, C., Mo, S., Vitaterna, M. H., Lopez, J. P., Philipson, L. H., Bradfield, C. A., Crosby, S. D., JeBailey, L., Wang, X., Takahashi, J. S., and Bass, J. (2010b). Disruption of the clock components CLOCK and BMAL1 leads to hypoinsulinaemia and diabetes. *Nature*, 466(7306):627–631.

- [115] Meng, Q. J., McMaster, A., Beesley, S., Lu, W. Q., Gibbs, J., Parks, D., Collins, J., Farrow, S., Donn, R., Ray, D., and Loudon, A. (2008). Ligand modulation of REV-ERB α function resets the peripheral circadian clock in a phasic manner. *Journal of Cell Science*, 121(Pt 21):3629–3635.
- [116] Milo, R., Jorgensen, P., Moran, U., Weber, G., and Springer, M. (2010). BioNumbers—the database of key numbers in molecular and cell biology. *Nucleic Acids Research*, 38(Database issue):D750–D753.
- [117] Minh, N. L., Damiola, F., Tronche, F., Schütz, G., and Schibler, U. (2001). Glucocorticoid hormones inhibit food-induced phaseshifting of peripheral circadian oscillators. *The EMBO Journal*, 20(24):7128–7136.
- [118] Mirsky, H. P., Liu, A. C., Welsh, D. K., Kay, S. A., and Doyle, F. J. (2009). A model of the cell-autonomous mammalian circadian clock. *Proceedings of the National Academy of Sciences of the United States of America*, 106(27):11107–11112.
- [119] Mohawk, J. A., Green, C. B., and Takahashi, J. S. (2012). Central and Peripheral Circadian Clocks in Mammals. *Annual Review of Neuroscience*, 35(1):445–462.
- [120] Mohawk, J. A. and Takahashi, J. S. (2011). Cell autonomy and synchrony of suprachiasmatic nucleus circadian oscillators. *Trends in Neurosciences*, 34(7):349–358.
- [121] Moles, C. G., Mendes, P., and Banga, J. R. (2003). Parameter estimation in biochemical pathways: a comparison of global optimization methods. *Genome Research*, 13(11):2467–2474.
- [122] Moore, D. D. (2013). Physiology: A metabolic minuet. *Nature*, 502(7472):454–455.
- [123] Murray, R. K., editor (2003). *Harper's illustrated biochemistry*. A Lange medical book. Lange Medical Books/McGraw-Hill, New York, NY, 26. ed edition.
- [124] Nakahata, Y., Kaluzova, M., Grimaldi, B., Sahar, S., Hirayama, J., Chen, D., Guarente, L. P., and Sassone-Corsi, P. (2008). The NAD⁺-dependent deacetylase SIRT1 modulates CLOCK-mediated chromatin remodeling and circadian control. *Cell*, 134(2):329–340.
- [125] Nakamura, M. T., Yudell, B. E., and Loor, J. J. (2014). Regulation of energy metabolism by long-chain fatty acids. *Progress in Lipid Research*, 53:124–144.
- [126] Nazaret, C. and Mazat, J.-P. (2008). An old paper revisited: "a mathematical model of carbohydrate energy metabolism. Interaction between glycolysis, the Krebs cycle and the H⁺-transporting shuttles at varying ATPases load" by V.V. Dymnik, R. Heinrich and E.E. Sel'kov. *Journal of Theoretical Biology*, 252(3):520–529.
- [127] Nemoto, S., Fergusson, M. M., and Finkel, T. (2005). SIRT1 Functionally Interacts with the Metabolic Regulator and Transcriptional Coactivator PGC-1. *Journal of Biological Chemistry*, 280(16):16456–16460.
- [128] Nicolis, G. and Prigogine, I. (1977). *Self-organization in nonequilibrium systems: from dissipative structures to order through fluctuations*. Wiley, New York.

- [129] Novák, B. and Tyson, J. J. (2008). Design principles of biochemical oscillators. *Nature Reviews. Molecular Cell Biology*, 9(12):981–991.
- [130] Ouyang, Y., Andersson, C. R., Kondo, T., Golden, S. S., and Johnson, C. H. (1998). Resonating circadian clocks enhance fitness in cyanobacteria. *Proceedings of the National Academy of Sciences*, 95(15):8660–8664.
- [131] Panda, S., Antoch, M. P., Miller, B. H., Su, A. I., Schook, A. B., Straume, M., Schultz, P. G., Kay, S. A., Takahashi, J. S., and Hogenesch, J. B. (2002). Coordinated transcription of key pathways in the mouse by the circadian clock. *Cell*, 109(3):307–320.
- [132] Paranjpe, D. A. and Sharma, V. K. (2005). Evolution of temporal order in living organisms. *Journal of Circadian Rhythms*, 3(1):7.
- [133] Peek, C. B., Affinati, A. H., Ramsey, K. M., Kuo, H.-Y., Yu, W., Sena, L. A., Ilkayeva, O., Marcheva, B., Kobayashi, Y., Omura, C., Levine, D. C., Bacsik, D. J., Gius, D., Newgard, C. B., Goetzman, E., Chandel, N. S., Denu, J. M., Mrksich, M., and Bass, J. (2013a). Circadian clock NAD⁺ cycle drives mitochondrial oxidative metabolism in mice. *Science (New York, N.Y.)*, 342(6158):1243417.
- [134] Peek, C. B., Affinati, A. H., Ramsey, K. M., Kuo, H.-Y., Yu, W., Sena, L. A., Ilkayeva, O., Marcheva, B., Kobayashi, Y., Omura, C., Levine, D. C., Bacsik, D. J., Gius, D., Newgard, C. B., Goetzman, E., Chandel, N. S., Denu, J. M., Mrksich, M., and Bass, J. (2013b). Circadian clock NAD⁺ cycle drives mitochondrial oxidative metabolism in mice. *Science (New York, N.Y.)*, 342(6158):1243417.
- [135] Peek, C. B., Ramsey, K. M., Marcheva, B., and Bass, J. (2012). Nutrient sensing and the circadian clock. *Trends in endocrinology and metabolism: TEM*, 23(7):312–318.
- [136] Pittendrigh, C. S. (1993). Temporal organization: reflections of a Darwinian clock-watcher. *Annual Review of Physiology*, 55:16–54.
- [137] Preitner, N., Damiola, F., Lopez-Molina, L., Zakany, J., Duboule, D., Albrecht, U., and Schibler, U. (2002). The orphan nuclear receptor REV-ERB α controls circadian transcription within the positive limb of the mammalian circadian oscillator. *Cell*, 110(2):251–260.
- [138] Raghuram, S., Stayrook, K. R., Huang, P., Rogers, P. M., Nosie, A. K., McClure, D. B., Burris, L. L., Khorasanizadeh, S., Burris, T. P., and Rastinejad, F. (2007). Identification of heme as the ligand for the orphan nuclear receptors REV-ERB α and REV-ERB β . *Nature Structural & Molecular Biology*, 14(12):1207–1213.
- [139] Ralph, M. R., Foster, R. G., Davis, F. C., and Menaker, M. (1990). Transplanted suprachiasmatic nucleus determines circadian period. *Science (New York, N.Y.)*, 247(4945):975–978.
- [140] RAMSEY, K. and BASS, J. (2011). Circadian Clocks in Fuel Harvesting and Energy Homeostasis. *Cold Spring Harbor symposia on quantitative biology*, 76:63–72.

- [141] Ramsey, K. M., Yoshino, J., Brace, C. S., Abrassart, D., Kobayashi, Y., Marcheva, B., Hong, H.-K., Chong, J. L., Buhr, E. D., Lee, C., Takahashi, J. S., Imai, S.-I., and Bass, J. (2009). Circadian clock feedback cycle through NAMPT-mediated NAD⁺ biosynthesis. *Science (New York, N.Y.)*, 324(5927):651–654.
- [142] Relógio, A., Westermark, P. O., Wallach, T., Schellenberg, K., Kramer, A., and Herzel, H. (2011). Tuning the mammalian circadian clock: robust synergy of two loops. *PLoS computational biology*, 7(12):e1002309.
- [143] Richards, J. and Gumz, M. L. (2012). Advances in understanding the peripheral circadian clocks. *FASEB journal: official publication of the Federation of American Societies for Experimental Biology*, 26(9):3602–3613.
- [144] Richards, J. and Gumz, M. L. (2013). Mechanism of the circadian clock in physiology. *American Journal of Physiology. Regulatory, Integrative and Comparative Physiology*, 304(12):R1053–1064.
- [145] Ripperger, J. A. and Schibler, U. (2006). Rhythmic CLOCK-BMAL1 binding to multiple E-box motifs drives circadian Dbp transcription and chromatin transitions. *Nature Genetics*, 38(3):369–374.
- [146] Roenneberg, T., Daan, S., and Merrow, M. (2003). The art of entrainment. *Journal of Biological Rhythms*, 18(3):183–194.
- [147] Sabath, E., Salgado-Delgado, R., Guerrero-Vargas, N. N., Guzman-Ruiz, M. A., del Carmen Basualdo, M., Escobar, C., and Buijs, R. M. (2014). Food entrains clock genes but not metabolic genes in the liver of suprachiasmatic nucleus lesioned rats. *FEBS Letters*, 588(17):3104–3110.
- [148] Saini, C., Liani, A., Curie, T., Gos, P., Kreppel, F., Emmenegger, Y., Bonacina, L., Wolf, J.-P., Poget, Y.-A., Franken, P., and Schibler, U. (2013). Real-time recording of circadian liver gene expression in freely moving mice reveals the phase-setting behavior of hepatocyte clocks. *Genes & Development*, 27(13):1526–1536.
- [149] Sato, T. K., Panda, S., Miraglia, L. J., Reyes, T. M., Rudic, R. D., McNamara, P., Naik, K. A., FitzGerald, G. A., Kay, S. A., and Hogenesch, J. B. (2004). A functional genomics strategy reveals Rora as a component of the mammalian circadian clock. *Neuron*, 43(4):527–537.
- [150] Siepkka, S. M., Yoo, S.-H., Park, J., Song, W., Kumar, V., Hu, Y., Lee, C., and Takahashi, J. S. (2007). Circadian Mutant Overtime Reveals F-box Protein FBXL3 Regulation of Cryptochrome and Period Gene Expression. *Cell*, 129(5):1011–1023.
- [151] Smolensky, M. H., Scott, P. H., Harnett, R. B., Hiatt, P. H., Wong, T. K., Baenziger, J. C., Klank, B. J., Marbella, A., and Meltzer, A. (1987). Administration-time-dependency of the pharmacokinetic behavior and therapeutic effect of a once-a-day theophylline in asthmatic children. *Chronobiology International*, 4(3):435–447.
- [152] Solt, L. A., Wang, Y., Banerjee, S., Hughes, T., Kojetin, D. J., Lundasen, T., Shin, Y., Liu, J., Cameron, M. D., Noel, R., Yoo, S.-H., Takahashi, J. S., Butler, A. A., Kamenecka, T. M., and Burris, T. P. (2012). Regulation of circadian behaviour and metabolism by synthetic REV-ERB agonists. *Nature*, 485(7396):62–68.

- [153] Stein, L. R. and Imai, S.-i. (2012). The dynamic regulation of NAD metabolism in mitochondria. *Trends in endocrinology and metabolism: TEM*, 23(9):420–428.
- [154] Sukumaran, S., Xue, B., Jusko, W. J., Dubois, D. C., and Almon, R. R. (2010). Circadian variations in gene expression in rat abdominal adipose tissue and relationship to physiology. *Physiological Genomics*, 42A(2):141–152.
- [155] Suwa, M., Nakano, H., and Kumagai, S. (2003). Effects of chronic AICAR treatment on fiber composition, enzyme activity, UCP3, and PGC-1 in rat muscles. *Journal of Applied Physiology*, 95(3):960–968.
- [156] Takahashi, J. S. (2015). Molecular components of the circadian clock in mammals. *Diabetes, Obesity and Metabolism*, 17:6–11.
- [157] Takano, A., Isojima, Y., and Nagai, K. (2004). Identification of mPer1 Phosphorylation Sites Responsible for the Nuclear Entry. *Journal of Biological Chemistry*, 279(31):32578–32585.
- [158] Tay, S., Hughey, J. J., Lee, T. K., Lipniacki, T., Quake, S. R., and Covert, M. W. (2010). Single-cell NF- κ B dynamics reveal digital activation and analogue information processing. *Nature*, 466(7303):267–271.
- [159] Tsai, T. Y.-C., Choi, Y. S., Ma, W., Pomerening, J. R., Tang, C., and Ferrell, J. E. (2008). Robust, tunable biological oscillations from interlinked positive and negative feedback loops. *Science (New York, N.Y.)*, 321(5885):126–129.
- [160] Tsang, A. H., Barclay, J. L., and Oster, H. (2014). Interactions between endocrine and circadian systems. *Journal of Molecular Endocrinology*, 52(1):R1–16.
- [161] Turek, F. W. (1985). Circadian Neural Rhythms in Mammals. *Annual Review of Physiology*, 47(1):49–64.
- [162] Turek, F. W., Joshu, C., Kohsaka, A., Lin, E., Ivanova, G., McDearmon, E., Laposky, A., Losee-Olson, S., Easton, A., Jensen, D. R., Eckel, R. H., Takahashi, J. S., and Bass, J. (2005). Obesity and metabolic syndrome in circadian Clock mutant mice. *Science (New York, N.Y.)*, 308(5724):1043–1045.
- [163] Um, J.-H., Pendergast, J. S., Springer, D. A., Foretz, M., Viollet, B., Brown, A., Kim, M. K., Yamazaki, S., and Chung, J. H. (2011). AMPK Regulates Circadian Rhythms in a Tissue- and Isoform-Specific Manner. *PLoS ONE*, 6(3):e18450.
- [164] Um, J. H., Yang, S., Yamazaki, S., Kang, H., Viollet, B., Foretz, M., and Chung, J. H. (2007a). Activation of 5-AMP-activated Kinase with Diabetes Drug Metformin Induces Casein Kinase I (CKI)-dependent Degradation of Clock Protein mPer2. *Journal of Biological Chemistry*, 282(29):20794–20798.
- [165] Um, J. H., Yang, S., Yamazaki, S., Kang, H., Viollet, B., Foretz, M., and Chung, J. H. (2007b). Activation of 5-AMP-activated Kinase with Diabetes Drug Metformin Induces Casein Kinase I (CKI)-dependent Degradation of Clock Protein mPer2. *Journal of Biological Chemistry*, 282(29):20794–20798.

- [166] Vollmers, C., Gill, S., DiTacchio, L., Pulivarthy, S. R., Le, H. D., and Panda, S. (2009). Time of feeding and the intrinsic circadian clock drive rhythms in hepatic gene expression. *Proceedings of the National Academy of Sciences of the United States of America*, 106(50):21453–21458.
- [167] Wang, Z. Y. and Tobin, E. M. (1998). Constitutive expression of the CIRCADIAN CLOCK ASSOCIATED 1 (CCA1) gene disrupts circadian rhythms and suppresses its own expression. *Cell*, 93(7):1207–1217.
- [168] Webb, A. B., Angelo, N., Huettner, J. E., and Herzog, E. D. (2009). Intrinsic, non-deterministic circadian rhythm generation in identified mammalian neurons. *Proceedings of the National Academy of Sciences of the United States of America*, 106(38):16493–16498.
- [169] Welsh, D. K., Logothetis, D. E., Meister, M., and Reppert, S. M. (1995). Individual neurons dissociated from rat suprachiasmatic nucleus express independently phased circadian firing rhythms. *Neuron*, 14(4):697–706.
- [170] White, A. T. and Schenk, S. (2012). NAD⁺/NADH and skeletal muscle mitochondrial adaptations to exercise. *American Journal of Physiology - Endocrinology and Metabolism*, 303(3):E308–E321.
- [171] Williams, K. W. and Elmquist, J. K. (2012). From neuroanatomy to behavior: central integration of peripheral signals regulating feeding behavior. *Nature Neuroscience*, 15(10):1350–1355.
- [172] Woller, A. and Gonze, D. (2013). The Bird Circadian Clock: Insights from a Computational Model. *Journal of Biological Rhythms*, 28(6):390–402.
- [173] Woller, A., Gonze, D., and Erneux, T. (2014). The Goodwin model revisited: Hopf bifurcation, limit-cycle, and periodic entrainment. *Physical Biology*, 11(4):045002.
- [174] Yang, X., Downes, M., Yu, R. T., Bookout, A. L., He, W., Straume, M., Mangelsdorf, D. J., and Evans, R. M. (2006). Nuclear receptor expression links the circadian clock to metabolism. *Cell*, 126(4):801–810.
- [175] Yerushalmi, S. and Green, R. M. (2009). Evidence for the adaptive significance of circadian rhythms. *Ecology Letters*, 12(9):970–981.
- [176] Yin, L., Wu, N., Curtin, J. C., Qatanani, M., Szewergold, N. R., Reid, R. A., Waitt, G. M., Parks, D. J., Pearce, K. H., Wisely, G. B., and Lazar, M. A. (2007). Rev-erb, a Heme Sensor That Coordinates Metabolic and Circadian Pathways. *Science*, 318(5857):1786–1789.
- [177] Yoo, S.-H., Yamazaki, S., Lowrey, P. L., Shimomura, K., Ko, C. H., Buhr, E. D., Siepkka, S. M., Hong, H.-K., Oh, W. J., Yoo, O. J., Menaker, M., and Takahashi, J. S. (2004). PERIOD2::LUCIFERASE real-time reporting of circadian dynamics reveals persistent circadian oscillations in mouse peripheral tissues. *Proceedings of the National Academy of Sciences of the United States of America*, 101(15):5339–5346.
- [178] Yuan, H.-X., Xiong, Y., and Guan, K.-L. (2013). Nutrient sensing, metabolism, and cell growth control. *Molecular Cell*, 49(3):379–387.

- [179] Zhang, E. E., Liu, Y., Dentin, R., Pongsawakul, P. Y., Liu, A. C., Hirota, T., Nusinow, D. A., Sun, X., Landais, S., Kodama, Y., Brenner, D. A., Montminy, M., and Kay, S. A. (2010). Cryptochrome Mediates Circadian Regulation of cAMP Signaling and Hepatic Gluconeogenesis. *Nature medicine*, 16(10):1152–1156.
- [180] Zhang, R., Lahens, N. F., Ballance, H. I., Hughes, M. E., and Hogenesch, J. B. (2014). A circadian gene expression atlas in mammals: implications for biology and medicine. *Proceedings of the National Academy of Sciences of the United States of America*, 111(45):16219–16224.
- [181] Zheng, B., Albrecht, U., Kaasik, K., Sage, M., Lu, W., Vaishnav, S., Li, Q., Sun, Z. S., Eichele, G., Bradley, A., and Lee, C. C. (2001). Nonredundant roles of the mPer1 and mPer2 genes in the mammalian circadian clock. *Cell*, 105(5):683–694.
- [182] Zheng, Y. and Sriram, G. (2010). Mathematical modeling: bridging the gap between concept and realization in synthetic biology. *Journal of Biomedicine & Biotechnology*, 2010:541609.
- [183] Zylka, M. J., Shearman, L. P., Weaver, D. R., and Reppert, S. M. (1998). Three period homologs in mammals: differential light responses in the suprachiasmatic circadian clock and oscillating transcripts outside of brain. *Neuron*, 20(6):1103–1110.

